Cyclometallated platinum and iridium complexes with thiolate ligands, and novel bioimaging agents inspired by dynamic disulfide interchange reactions

William Andrew Tarran

Department of Chemistry
Durham University

A thesis submitted in part-fulfilment of the requirements for the degree of Doctor of Philosophy

28th February 2011

Abstract

The photoluminescence properties of cyclometallated second and third row transition metal complexes make them potential candidates for use in a range of applications such as triplet harvesting agents in OLEDS, as photosensitizers, and in solar cells. Also, the strong luminescence of these complexes gives them much potential for use in chemosensing applications and as bioimaging agents. This final topic is an area of increasing study as a result of the diverse and tuneable excited states of such molecules, and their advantages over conventional organic emitters such as reduced photobleaching and long luminescence lifetimes allowing time-resolved imaging to be performed.

The synthesis of cyclometallated complexes of the type [Pt(N^C^N)Cl], $[Ir(N^C)_2(L)Cl]$, and $[Ir(N^C^N)(N^X)Cl]^{n+}$ (where N^C^N and N^C are terdentate and bidentate cyclometallating aromatic ligands; L = monodentate pyridine ligand; X = heterocyclic N or cyclometallated aryl C; n = 0,1) is described and their reactions with thiolates are explored with the aim of producing new classes of thiol sensors. Thus, novel monometallic complexes of the type [Pt(N^C^N)(thiolate)] and [Ir(N^C^N)(N^C)(thiolate)] are reported as well as a novel series of dimers with the general structure $[Ir(N^C)_2(\mu\text{-thiolate})]_2$ and one example of a $[Ir(N^C^N)(\mu\text{-thiolate})(thiolate)]_2$ dimer. The effect of the introduction of a thiolate ligand on the excited states of the Pt(N^C^N) complexes is also described.

In addition, a series of luminescent compounds based on the dansyl group or iridium complexes are reported for use as bioimaging agents and their utility in cellular assays has been investigated. These probes incorporate molecular structures inspired by the ability of small molecules to mimic the activity of certain redox active proteins and hence have the potential to engage in disulfide exchange processes *in vivo*. These compounds have been shown to display acceptable uptake into cells without excessive cytotoxicity and have been used to obtain fluorescence microscopy images of live CHO cells.

Declaration

The work described herein was carried out in the Department of Chemistry at Durham University between October 2005 and May 2009. This thesis is the work of the author, unless otherwise stated, and no part of it has been submitted for a degree at this or any other university.

Statement of Copyright

Acknowledgements

Firstly, and most importantly, I would like to give thanks to my supervisor Dr. J. A. Gareth Williams for his help, support and patience throughout the project for which I will be eternally grateful.

In addition I must acknowledge ONE North East and Durham University, whose financial support made this PhD possible, as well as Dr. Adam Benham and Dr. Ritu Kataky for their help in securing funding.

There are, of course, many people within the Department of Chemistry without whom this project would have been much more difficult, if not impossible, so I would also like to express my thanks to the following:

Dr. Alan Kenwright, Catherine Heffernan and Ian McKeag for NMR spectroscopy; Dr. Mike Jones, Lara Turner, Dr. Jackie Mosely and Dr. Dave Parker for mass spectrometry; Jarika Dostal and Judith Magee for elemental analysis.

All of the staff involved in Stores, the glass-blowers, the workshop staff, the lab technicians and administrative staff. I feel I should mention, in particular, Jean Eccleston for her patience and gentle encouragement towards submission.

My co-workers from the beginning to the end for their help, support and friendship – it seems a very long time; In particular Drs. Dave Rochester, Victoria Whittle and Pierpaolo Brulatti, but also Kathryn, Louise, Lisa, Gemma, Stephanie and all our project students.

From ‘the dark half’ of the lab; my good friend Dr. Tom Woods, as well as Nick, Marie, Marvis, Pete ‘Big Bear’, Matt, Michal, Kathryn, John, John and Jon

Finally, for those people who provide a relief from chemistry, I would like to acknowledge Olley for his philosophy and Jenny for her company during climbing sessions, and also both for their hospitality and floor/sofa space.
And, of course… Mum, Dad and Duncan.

Contents

Abbreviations

Ac	acyl
acac	acetylacetonate
ATP	adenosine-5'-triphosphate
ATR	attenuated total reflectance
BMC	(±)-*trans*-1,2-*bis*(2-mercapto-acetamido)cyclohexane
BOC	*tert*-butoxycarbonyl
bpy	2,2'-bipyridine
Bu	butyl
CHO	chinese hamster ovary
cmbpy	4-carboxy-4'-methyl-2,2'-bipyridine
COSY	correlation spectroscopy
CV	cyclic voltammetry
DCC	1,3-dicyclohexylcarbodiimide
DCM	dichloromethane
DFT	Density Functional Theory
DMAP	4-(N,N-dimethylamino)pyridine
DME	1,2-dimethoxyethane
DMSO	dimethylsulfoxide
dcbpy	4,4'-dicarboxy-2,2'-bipyridine
dfpyH	2-(2,4-difluorophenyl)pyridine
dmpybza	N,N-dimethyl-3-(2-pyridyl)benzylamine
dppf	1,1'-bis(diphenylphosphino)ferrocene
$dppyH_2$	2,6-diphenylpyridine
dppm	bis(diphenylphosphino)methane
dpybH	1,3-di(2-pyridyl)benzene
dpytH	1,3-di(2-pyridyl)-5-methylbenzene
dpyxH	4,6-di(2-pyridyl)-*meta*-xylene
DTT	dithiothreitol
ECP	effective core potential
EDCI	1-ethyl-3-(3-dimethylaminopropyl)carbodiimide hydrochloride
EDU	1-ethyl-3-(3-dimethylaminopropyl)urea
EI	electron ionisation

ER	endoplasmic reticulum
ES	electrospray
Et	ethyl
Et_2O	diethyl ether
EtOAc	ethyl acetate
EtOH	ethanol
FAD	flavin adenine dinucleotide
FBS	foetal bovine serum
Fc	ferrocene
FLIM	fluorescence lifetime imaging microscopy
FRET	Förster resonance energy transfer
GFP	green fluorescent protein
HATU	2-(7-aza-1H-benzotriazole-1-yl)-1,1,3,3-tetramethyluronium hexafluorophosphate
HMBC	heteronuclear multiple bond correlation
HOBt	hydroxybenzotriazole
HPLC	high performance liquid chromatography
HSA	human serum albumin
HSQC	heteronuclear single quantum correlation
IC	internal conversion
IC_{50}	half maximal inhibitory concentration
IgG	immunoglobulin G
ILCT	intraligand charge transfer
IR	infrared
ISC	intersystem crossing
GCMS	gas chromatography-mass spectrometry
GFP	green fluorescent protein
LC	ligand-centred (excited state)
LLCT	ligand-to-ligand charge transfer
MALDI	matrix assisted laser desorption ionisation
mdpybzH	methyl-3,5-di(2-pyridyl)benzoate
Me	methyl
MeCN	acetonitrile
MC	metal-centred (excited state)

MLCT	metal-to-ligand charge transfer
MMLCT	metal–metal-to-ligand charge transfer
Mp	melting point
MS	Mass Spectrometry
mt	methanethiolate
mtpH	4-methylthiophenol
MTT	3-(4,5-dimethythiazol-2-yl)-2,5-diphenyltetrazolium bromide
neo	neopentylglycolate
NHS	N-hydroxysuccinamide
NMA	N-methylmercaptoacetamide
NMR	Nuclear Magnetic Resonance
ntpH	4-nitrothiophenol
PBS	phosphate buffered saline
PDI	Protein Disulfide Isomerase
PEG	polyethylene glycol
Ph	phenyl
phbpyH	6-phenyl-2,2'-bipyridine
phen	1,10-phenanthroline
ppy	2-phenylpyridine
pin	pinacolate
PMT	photomultiplier tube
pybaH	4-(2-pyridyl)benzaldehyde
pybzaH	3-(2-pyridyl)benzylamine
pybzbiH	N-(3-(2-pyridyl)benzyl)benzylimine
pybzpipH	ethyl 1-(3-(2-pyridyl)benzyl)piperidin-2-yl acetate
RNase	ribonuclease
S_n	singlet excited state
TCE	1,1,2,2-tetrachloroethane
TCEP	tris(2-carboxyethyl)phosphine
THF	tetrahydrofuran
T_n	triplet excited state
tpH	thiophenol
ttpy	4'-tolyl-2,2':6'2''-terpyridine
tpy	2,2':6'2''-terpyridine

TREM	time-resolved emission imaging microscopy
Trx	thioredoxin

Amino Acid abbreviations

Alanine	Ala	A
Arginine	Arg	R
Asparagine	Asn	N
Aspartic acid	Asp	D
Cysteine	Cys	C
Glutamic acid	Glu	E
Glutamine	Gln	Q
Glycine	Gly	G
Histidine	His	H
Isoleucine	Ile	I
Leucine	Leu	L
Lysine	Lys	K
Methionine	Met	M
Phenylalanine	Phe	F
Proline	Pro	P
Serine	Ser	S
Threonine	Thr	T
Tryptophan	Trp	W
Tyrosine	Tyr	Y
Valine	Val	V

Chapter 1

Introduction

1 Introduction

The ability of certain compounds to emit light provides a vital tool in chemistry since in many cases the characteristics of the emitted radiation are sensitive to the molecular environment. Emissive molecules, therefore, are widely used as reporters for many processes.[1,2] The diverse photophysical properties of transition metals with aromatic chelating ligands such as polypyridyls or their cyclometallated analogues have led to their use in many areas involving the absorption and emission of light.[3,4,5] Such compounds often display strong, long-lived emission and thus are well suited to roles in sensing. More recently, in addition to their use in chemosensing applications, these metal complexes are becoming more common in cellular studies and bioimaging.[6,7]

1.1 Luminescence in chemistry

Luminescence in chemistry is the result of the relaxation of a molecule from some electronically excited state back to the ground state by the emission of a photon. The source of energy to form this excited state can be the result of various processes, for example the application of an electric current to a material leads to electroluminescence or, more commonly, excitation by the absorption of a photon of light leads to the processes of fluorescence and phosphorescence.

The majority of molecules in their ground state exist with all their electrons paired leading to a total spin value S = 0 for the molecule, which is known as a singlet ground state, termed S_0. Molecules can also exist in a series of excited states where an electron has been promoted to a higher energy molecular orbital. Since two electrons now occupy different orbitals, these may adopt 'parallel' or 'opposed' spins leading to total spin values of S = 1 or S = 0 for the system. This pairing leads to triplet or singlet excited states which are numbered T_1, T_2, T_3 etc. and S_1, S_2, S_3 etc. in order of increasing energy. In general, any given triplet state T_n will be lower in energy than its singlet counterpart S_n due to spin correlation.[8]

The absorption of a photon by the ground state causes the excitation of the molecule into an excited state, S_n, from where it relaxes rapidly to the lowest singlet excited state, S_1, by processes of vibrational relaxation and internal conversion (IC) between states of the same multiplicity. From this state the molecule may emit a photon causing relaxation to the ground state in the process known as fluorescence, or relax by some other non-radiative pathway. It is also possible for a molecule in the S_1 excited state to undergo intersystem crossing (ISC) to the T_1 excited state and subsequent relaxation from this state is termed phosphorescence. Formally transitions of the type $T_n \leftarrow S_0$ are disallowed by the $\Delta S = 0$ selection rule for electronic transitions and are very rarely observed in absorption. Population of the T_1 state is therefore almost entirely due to ISC. Equally, the formally forbidden nature of phosphorescence leads to much longer luminescence lifetimes, of the order of μs to s, compared to fluorescence which generally has lifetimes in the ns range. In fact, in the majority of organic molecules, phosphorescence is not observed due to much faster competitive non-radiative decay processes. All the processes in the relaxation of excited states such as non-radiative relaxation, IC, ISC and radiative decay have associated rate constants, and it is the balance of these rate constants in a particular molecule that determines its photophysical properties.

In molecules containing heavy atoms such as second or third row transition metals, the high spin-orbit coupling of these atoms leads to a breakdown of the $\Delta S = 0$ selection rule, increasing rate constants for the formally spin-forbidden processes of ISC and phosphorescence. The presence of such heavy elements can therefore lead to long-lived phosphorescence being observed. Figure 1.1 shows a Jablonski Diagram which illustrates the described processes.

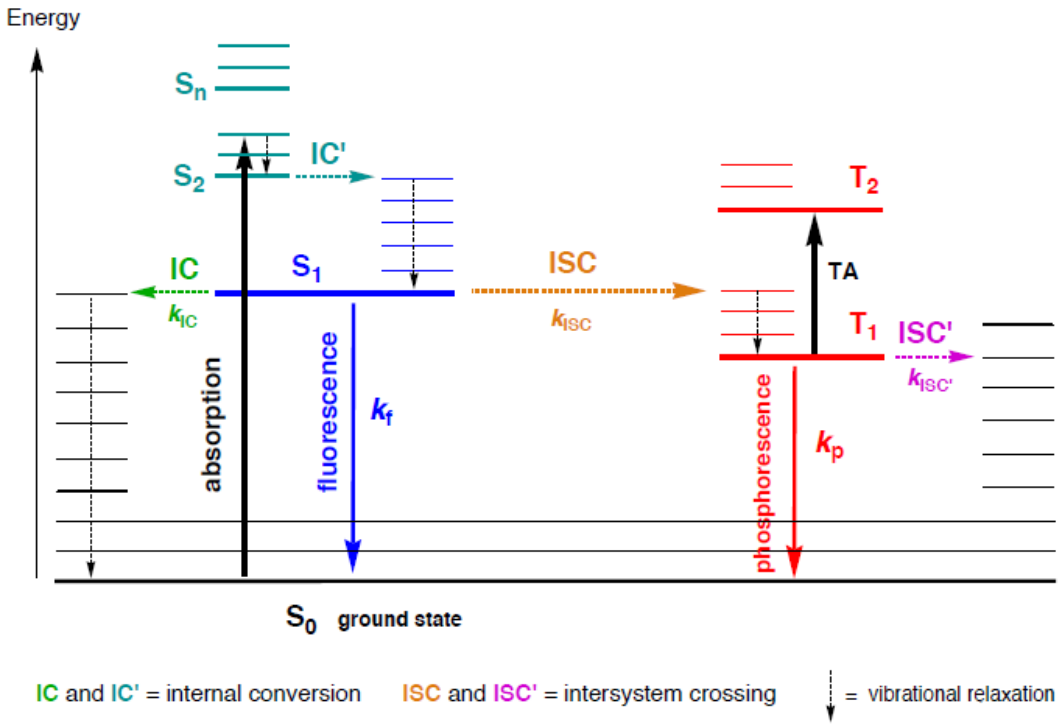

Figure 1.1 Jablonski Diagram.

Another important factor in luminescence results from the Franck-Condon principle. This states that electronic transitions occur on a much faster timescale than molecular reorientation. This generally results in vibrationally excited electronic states upon excitation, after which the molecule relaxes to the vibrational ground state of S_1 or T_1 before emission. The overall result of this is that the emitted radiation is universally red shifted with respect to the absorbed frequency, with the gap between the lowest energy absorption band and highest emission band being known as the Stokes' shift. It is therefore the case that molecules with larger differences between ground state and excited state geometries tend to show much larger Stokes' shifts than those with very little molecular reorganisation.

1.1.1 Luminescence of metal complexes with polypyridyl type ligands

Aromatic molecules such as 2,2'-bipyridine (bpy) are, in themselves, quite unremarkable in their photophysical properties. In general they display strong absorption in the UV region of the spectrum due to π-π^* excitation in the delocalised aromatic system. However, by using these compounds as ligands for second and third row transition metals, a wealth of varied excited states can

be unlocked, many with useful emissive properties. The first such compound to be discovered was the octahedral metal complex ruthenium(II) tris-bipyridine dichloride $[Ru(bpy)_3]Cl_2$ and it and its derivatives have been the subject of intensive study.[9] In this particular case, significant π backbonding between the Ru(II) and the bipyridine ligands[10] allows the latter to act as a π acceptor in a low energy metal-to-ligand charge transfer (MLCT) excited state. This, in combination with the spin-orbit coupling of ruthenium, results in emission from a ^{3}MLCT state.

The key to the versatility of this and related metal complexes is the variety in the types of excited states that can be achieved by changing the metal centre and the ligands around it. The combination of metal centred orbitals and ligand π and π^* orbitals can lead to a host of excited states in these complexes including metal-centred (MC), metal-to-ligand charge transfer (MLCT), ligand-centred (LC) and intraligand charge transfer (ILCT) states. The high spin-orbit coupling of the metal in these complexes may, then, lead to ^{3}MLCT phosphorescence or emission from metal-perturbed ^{3}LC or ^{3}ILCT states. In addition, the mixing of metal and ligand orbitals can lead to the formation of states which are predominantly ligand-to-ligand charge transfer (LLCT) in character which would not normally form due to poor orbital overlap leading to low oscillator strengths in the transition. Figure 1.2 shows a representation of the available excited states from transitions in a metal complex.

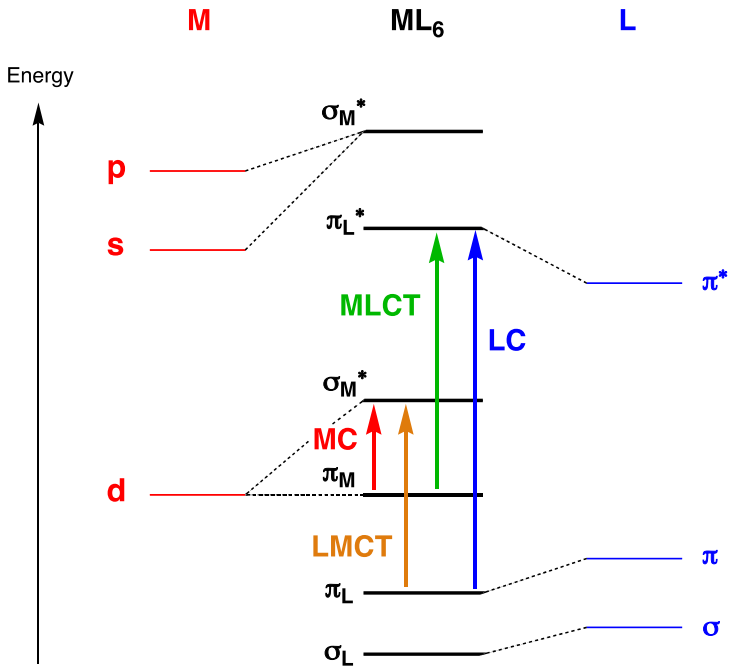

Figure 1.2 Schematic energy level diagram showing possible excited states in metal complexes.

In multimetallic clusters and in square planar complexes, orbital interactions between metals can lead to metal–metal-to-ligand charge transfer (MMLCT) or other more complex excited states that can be tuned to a specific function.

1.1.2 Complexes of Iridium(III)

Iridium(III) is isoelectronic with ruthenium(II), but studies into the use of the former metal in polypyridyl and related compounds were slower to take off than for the latter, in part due to the harsher reaction conditions required to substitute the ligands occupying the coordination sphere of the third row, more highly charged Ir^{3+} ion.[11]

1.1.2.1 Iridium(III) complexes with bipyridine-type ligands

As a third row transition metal, iridium(III) has lower lying d states than ruthenium(II) and thus the Ir(III) centre is more difficult to oxidise leading to differences in the observed emissive excited states. $[Ir(bpy)_3]^{3+}$ complexes, for example, show predominantly LC type emission[12] which contrasts with the MLCT emission of the pseudo-isoelectronic analogue $[Ru(bpy)_3]^{2+}$ reflecting the lower energy of the d orbitals in Ir(III). The introduction of negatively charged

ligands, for example in complexes such as $[Ir(bpy)_2Cl_2]PF_6$, leads to a situation where dual emission is observed at low temperatures from non-equilibrated ^{3}LC and ^{3}MLCT states.[13,14] This is the result of an increase in energy of the metal d orbitals, such that they reach a level similar to the highest occupied ligand based orbitals. In addition to dual emission, this situation leads to non-radiative deactivation through the d-d* excited states.[15] Similar compounds with diimine ligands such as 2,2'-bipyrimidine, 2,3-bis(2-pyridyl)pyrazine, 2,3-bis(2-pyridyl)quinoxaline and 2,3-bis(2-pyridyl)benzoquinoxaline (Figure 1.3), which have more extended π systems, tend to display emissive states with increased MLCT character since this state is lower in energy than in the corresponding bpy complexes.[16]

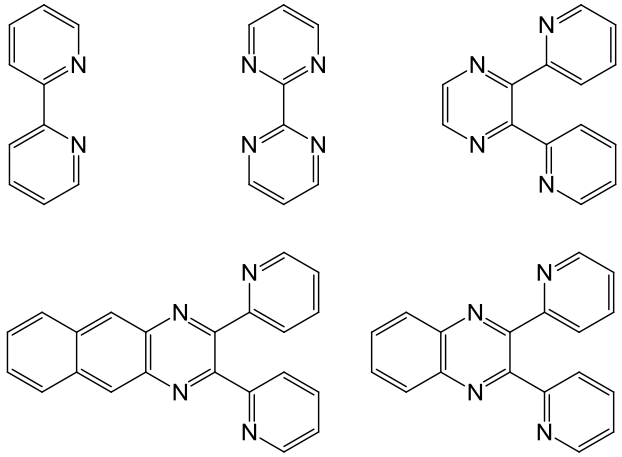

Figure 1.3 Diimine ligands in complexes of the type $[Ir(N\hat{}N)_2Cl_2]^+$ lead to ^{3}MLCT emission.

As a result of its kinetic inertness, many early syntheses attempting to introduce bpy ligands into the coordination sphere of iridium(III) relied on relatively harsh conditions. In one study, the reaction of $IrCl_3$ with bpy was carried out at high temperature (~180 °C) in glycerol.[17] The resulting compound contained three bipyridine ligands yet had different photophysical properties from a different sample of $[Ir(bpy)_3]^{3+}$ and was erroneously reported as the complex $[Ir(bpy\text{-}N,N')_2(bpy\text{-}N)(H_2O)]^{3+}$ (Figure 1.4a). Later studies showed that, in fact, the complex was the N-protonated cyclometallated analogue of $[Ir(bpy)_3]^{3+}$, $[Ir(bpy\text{-}N,N')_2(Hbpy\text{-}C^3,N')]^{2+}$ (Figure 1.4b).[18]

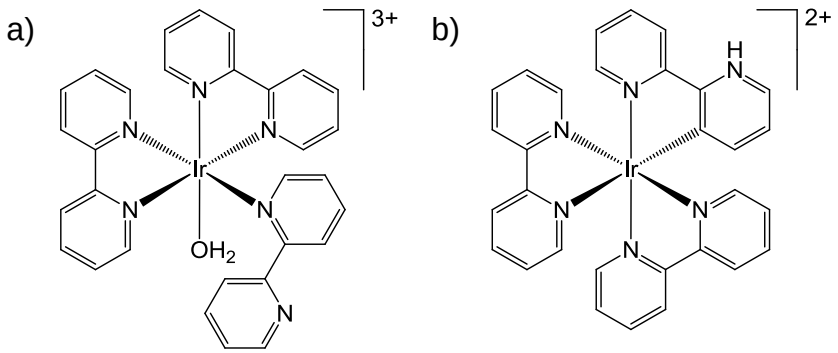

Figure 1.4 a) reported $[Ir(bpy\text{-}N,N')_2(bpy\text{-}N)(H_2O)]^{3+}$ structure and b) structure of $[Ir(bpy\text{-}N,N')_2(Hbpy\text{-}C^3,N')]^{2+}$ solved by X-ray crystallography.

The emission from this cyclometallated variant was assigned to an LC state with increased MLCT character compared to the emission of $[Ir(bpy)_3]^{3+}$ owing to the presence of one Ir-C bond. In addition, as a result of the protonated pyridine fragment, the photophysics of this complex were shown to be pH dependent.[17] The observation of this cyclometallation, however, led to investigations involving cyclometallating ligands with structures similar to bpy such as 2-phenylpyridine (ppy).

1.1.2.2 Iridium(III) complexes with N^C bidentate cyclometallating ligands

The reaction of $IrCl_3$ with 2-phenylpyridine yields the bis N^C coordinated dimer $[Ir(ppy\text{-}N,C^2)_2Cl]_2$[19] shown in Figure 1.5. The structure of this dimer was reported as having the cyclometallating carbons mutually *cis* due to their relatively high trans effect and reported crystal structures have confirmed that, in general, related complexes of iridium(III) and rhodium(III) with two bidentate N^C cyclometallating ligands do adopt this configuration.[20,21,22,23] The relatively large *trans* influence of the carbon in such ligands has also been observed by its effect on the vibrational frequency of *trans* Ir-Cl bonds.[24]

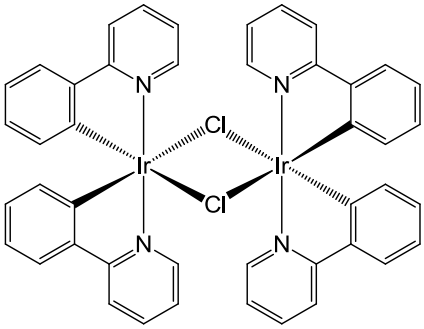

Figure 1.5 $[Ir(ppy\text{-}N,C^2)_2Cl]_2$

This family of bis-bidentate N^C bound dimers are cleaved readily by a variety of ligands giving monometallic complexes. It has been shown that bidentate chelating ligands such as bpy and 1,10-phenanthroline (phen) can be used to cleave the bis N^C dimer structure yielding cationic complexes such as $[Ir(ppy)_2(bpy)]^+$, in which the *cis* disposition of the cyclometallating carbon atoms is retained.[25]

Cleavage using monoanionic, bidentate β-diketonate ligands such as acetylacetonate (acac) likewise gives a series of highly phosphorescent charge neutral complexes of the form $[Ir(N^C)_2(O^O)]$ with quantum yields in solution of up to 0.6 and microsecond lifetimes.[26] The emission maxima of these compounds can also be readily tuned by variation of the N^C ligand.

Another important class of compounds are homoleptic *tris* cyclometallated Ir(III) complexes using similar N^C bidentate ligands, with $Ir(ppy)_3$ first being reported as a by-product in the synthesis of $[Ir(ppy)_2Cl]_2$.[27] This type of compound, again, can be synthesised with a variety of N^C binding ligands and can exist either as *fac* or *mer* isomers (as shown in Figure 1.6). It is possible, by varying the reaction conditions, to selectively synthesise these isomers[23,28] which is important since they display distinct photophysical properties resulting from their structural differences. While the *fac* isomer has C_3 symmetry, with all Ir-C bonds being *trans* to Ir-N bonds, the *mer* isomer shows noticeable distortion with mutally *trans* Ir-N bonds being relatively shorter and mutually *trans* Ir-C bonds being lengthened. This is due to the much higher *trans* influence of the cyclometallating carbon over the pyridine nitrogen. A larger Stokes' Shift in the emission of the *mer* isomer results from more pronounced geometrical changes

in the excited state, a reflection of the weaker bonds. In addition, the *mer* isomer tends to display shorter lifetimes and lower phosphorescence quantum yields due to non-radiative decay processes associated with photoisomerisation.[28]

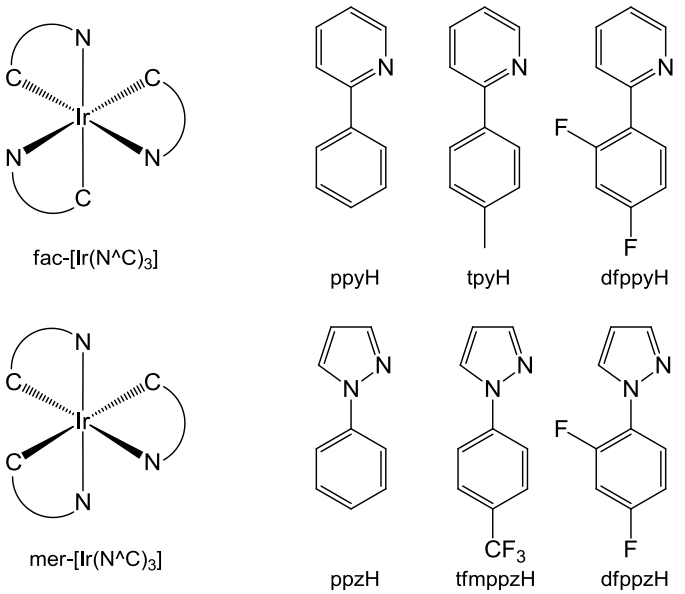

Figure 1.6 The possible *fac* and *mer* configurations of $Ir(N^C)_3$ complexes and the ligands used in ref. 28.

With the additional electron density at the metal centre provided by two or three strongly σ-donating cyclometallating carbons in bis or tris cyclometallated iridium(III) complexes, the highly efficient phosphorescence exhibited by these compounds is almost universally from ^{3}MLCT states.

While ^{3}MLCT emission is common in tris-bidentate complexes with two or three cyclometallating carbons, the nature of the ligands can alter the orbitals which are involved in this state. In the case of $[Ir(ppy)_2(acac)]$ type complexes, the ppy ligand is the acceptor in the lowest energy MLCT excited state, but the replacement of the acac by a diimine can lead to a change in the emissive state. It has been reported that in the case of $[Ir(ppy)_2(bpy)]^+$, dual emission is observed from non-equilibrated ^{3}MLCT states at 77 K, corresponding to charge transfer to a ppy ligand or the bpy as the energies of the two ligands are similar in this case.[25] In related complexes containing diimine ligands with more extended π systems, this ligand's π^* orbital is sufficiently lower than the

corresponding ppy orbitals leading to phosphorescence from a d→π*(diimine) ^{3}MLCT state.

The highly tuneable photophysical properties of these N^C cyclometallated Ir(III) complexes and the observed high quantum efficiencies have led to wide ranging potential of these compounds in areas such as photocatalysis,[27] singlet oxygen sensitizers,[29] oxygen sensing[30] and, in particular, triplet harvesting agents in OLEDS.[26,31,32,33,34]

1.1.2.3 Iridium(III) complexes with terdentate ligands

Developments in the chemistry of iridium(III) complexes with terdentate polypyridyl ligands began significantly later than the corresponding bidentate complexes. The terdentate ligand 2,2':6',2''-terpyridine (tpy) was first successfully incorporated into the homoleptic complex $[Ir(tpy)_2]^{3+}$ in 1990 by Demas *et al.* using harsh conditions and with only a poor yield.[35] An improved stepwise synthesis *via* $Ir(tpy)Cl_3$ was reported several years later which also allowed a series of similar heteroleptic complexes to be made[36] (Figure 1.7). These complexes tend to show phosphorescent emission from ^{3}LC excited states with lifetimes of a few microseconds with relatively low oxygen quenching. These properties led to the exploration of such compounds as potential sensors with elaboration at the 4' position on the central pyridine leading to reports of pH sensitive emission[37,38] and chloride ion sensing.[39]

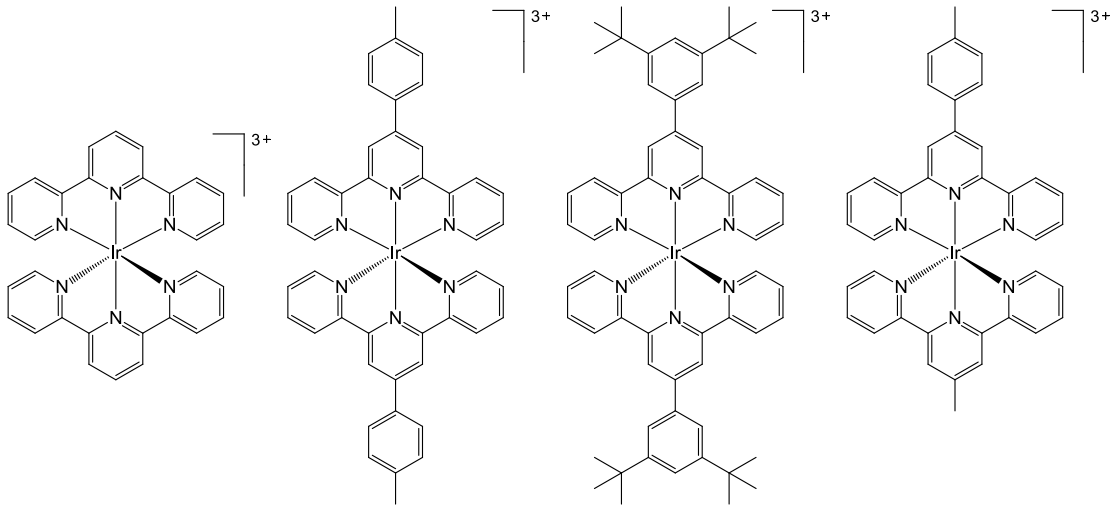

Figure 1.7 Homoleptic and heteroleptic complexes of iridium(III) with terpyridyl ligands.

In addition to the use of terpyridine ligands, the effects of cyclometallation in these bis-terdentate systems have also been of interest. Ligands such as 6-phenyl-2,2'-bipyridine (phbpyH), 2,6-diphenylpyridine ($dppyH_2$) and 1,3-di(2-pyridyl)benzene (dpybH) have the potential to bind as anionic analogues of tpy with N^N^C, C^N^C and N^C^N binding modes respectively (Figure 1.8).

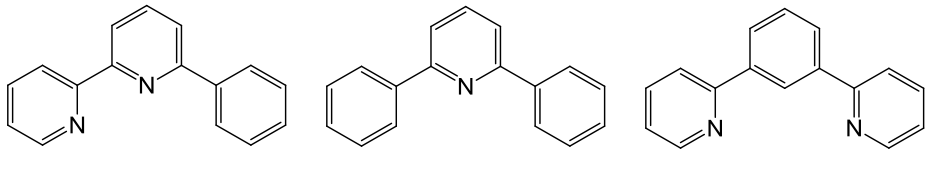

phbpyH $dppyH_2$ dpybH

Figure 1.8 The terdentate bicyclometallating ligands phbpyH, $dppyH_2$ and dpybH.

The synthesis of transition metal complexes with the N^N^C binding terpyridine analogue phbpy was first reported for palladium and platinum.[40] Similar use was soon reported with ruthenium(II) in a heteroleptic complex with 4'-tolyl-2,2':6'2''-terpyridine (ttpy), $[Ru(phbpy)(ttpy)]^+$, which gave significant enhancement in emissive properties compared to $[Ru(tpy)_2]^{2+}$.[41] The use of the N^C^N binding analogue dpyb was also reported with ruthenium(II) around the same time.[42]

The first report of cyclometallated analogues of tpy in iridium complexes made use of the ligand 2,6-bis(7'-methyl-4'-phenyl-2'-quinolyl)pyridine where a bis terdentate complex can be formed either with both ligands bound in an N^N^C mode or with one ligand instead bound in an N^N^N coordination mode[43] (see Figure 1.9).

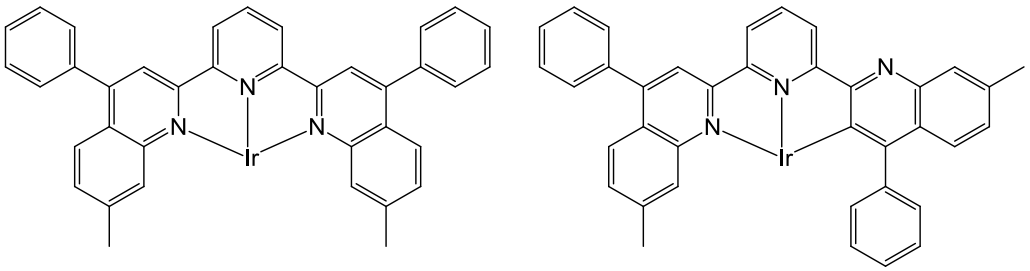

Figure 1.9 N^N^N and N^N^C binding modes with a bis-quinolylpyridine ligand giving rise to $[Ir(N^N^N)(N^N^C)]^{2+}$ and $[Ir(N^N^C)_2]^+$ complexes.

The use of dianionic tpy analogues with C^N^C bound ligands is also reported[44] in heteroleptic complexes of the type $[Ir(C^N^C)(N^N^N)]^+$ which show microsecond lifetime red emission in room temperature solutions.[44,45]

During investigations into potential N^C^N bound ligands, it was discovered that the simplest ligand of this type, dpyb, does not adopt the desired configuration. Unlike with ruthenium(II), it was discovered that the preferred site of metallation of iridium(III) is at the C^4 position of the central benzene ring rather than the desired C^2 position as shown in Figure 1.10. This problem was initially overcome through the use of the dimethyl substituted ligand 4,6-di(2-pyridyl)-*meta*-xylene (dpyxH), where the C^4 position is blocked, in the synthesis of the complex [Ir(dpyx)(dppy)].[46] This complex is particularly interesting in that it is a bis-terdentate analogue of the highly phosphorescent complex $Ir(ppy)_3$ with three cyclometallating carbon atoms.

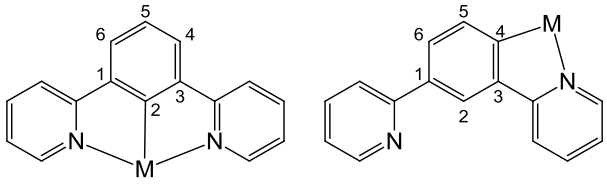

Figure 1.10 Competitive binding displayed by iridium(III) with dpyb.

The number of cyclometallating carbons present in these bis-terdentate complexes with iridium(III) appears to govern the observed emissive excited states. While $[Ir(tpy)_2]^{3+}$ shows long lived ^{3}LC emission in room temperature solutions, $[Ir(dpyx)(ttpy)]^{2+}$ is a poor emitter[47]. This is due to poor orbital overlap in the lowest excited state which is in this case a dpyx→ttpy ligand-to-ligand charge transfer. The incorporation of a second cyclometallating carbon for example in $[Ir(dpyx)(phbpy)]^+$, however, raises the energy of the metal centred orbitals leading to increased metal character in the excited state and improved emission[48]. The metal centred orbitals are further increased by the addition of a third carbon in the ligand system leading to strong ^{3}MLCT phosphorescence.[46] The effect of increasing cyclometallation in these complexes is illustrated in Figure 1.11.

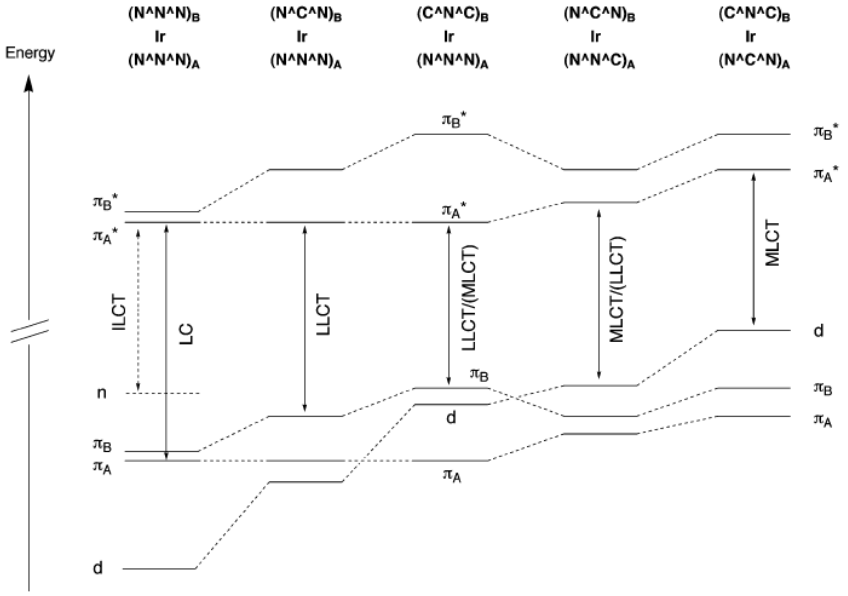

Figure 1.11 Simplified schematic energy level diagram showing the influence of cyclometallation on the frontier orbitals in bis-terdentate Ir(III) complexes, leading to excited states of different character.[49] Reprinted from J. A. G. Williams *et al.*, *Dalton Trans.*, 2008, 2081, Copyright 2008, with permission from RSC Publishing.

A particular advantage of bis-terdentate complexes over their tris-bidentate counterparts is in the formation of multimetallic assemblies. The latter, having D_3 symmetry exist as racemic mixtures, and thus when two complexes are linked diastereoisomers may form which have subtly different photophysical properties. This problem is not suffered by bis-terdentate complexes, and in addition, they allow linear assemblies to be built which display well defined directional electron transfer. These structural advantages have led to a predominant focus upon these compounds for use in multimetallic assemblies, electron transfer processes and photoinduced charge separation.[48,50,51]

In summary, the complexes of iridium(III) with bidentate and terdentate cyclometallating ligands provide a wealth of options in terms of the tuning of excited states in both cationic and neutral complexes, as well as a structural diversity making them ideal for use in monometallic roles or multimetallic assemblies.

1.1.3 Complexes of Platinum(II)

The first reported compound of platinum(II) with the cyclometallating ligand 2-phenylpyridine was the simple complex *cis*-bis(2-phenylpyridine)platinum(II),[52] synthesised by the treatment of *trans*-$PtCl_2(SEt_2)_2$ with ortholithiated ppyH. The *cis* product was the result of sequential binding of the ppy ligand, with the pyridine N of the second ligand being directed *trans* to the first cyclometallated carbon followed by subsequent ring closure to form the bis-cyclometallated species. This complex displayed a solvatochromic absorption band in the visible region assigned to an MLCT transition and, while it is non-emissive in solution, the solid displays strong emission around 600 nm which was reported to be the result of a dimeric species in the solid state.[53]

Similar compounds with ppy type ligands were shown to also display emission from ^{3}MLCT states in low temperature glasses and in the solid state,[54] however the majority of compounds of this type are essentially non-emissive in room temperature solutions.

1.1.3.1 Platinum with terdentate cyclometallating ligands

Constable *et al.* first demonstrated the use of an N^N^C bound terdentate ligand with platinum(II)[55,56] (Figure 1.12) and compounds using this type of ligand were demonstrated to show emission in both low temperature glasses and in solution at room temperature.[57] Similarly to complexes with ppy, the planar nature of these Pt(N^N^C) complexes causes the photophysical properties to be strongly influenced by Pt-Pt interactions at low temperature, with emission from ^{3}MMLCT states common in these systems. In solution most complexes of this type show ^{3}MLCT emission, however with the use of a bridging bis(diphenylphosphino)methane (dppm) ligand, ^{3}MMLCT emission can also be observed in solution.

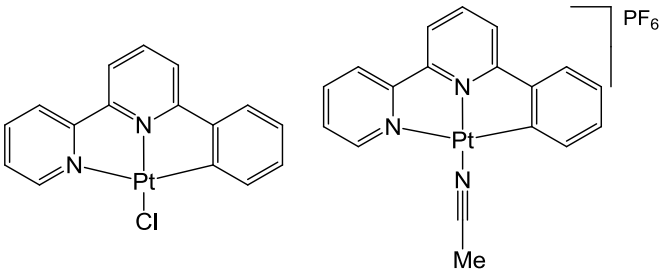

Figure 1.12 Some platinum(II) complexes with N^N^C ligands.

The use of terdentate C^N^C binding motifs has also been reported[58,59] and again, the emissive properties of these compounds are affected by stacking interactions in the solid state. However unlike the interactions in Pt(N^N^C) complexes, the C^N^C ligand leads to head-to-tail π stacking in the solid state with minimal Pt-Pt interactions.[60] This leads to the concentration dependent formation of $\pi\pi^*$ excimer formation in low temperature glasses. These compounds, like many with ppy ligands, prove to be non-emissive under ambient conditions.

In contrast to many other cyclometallated complexes of platinum(II), the complex with an N^C^N coordinating ligand [Pt(dpyb)Cl] (Figure 1.13), first reported by Cardenas,[61] is highly emissive in room temperature solutions (Φ = 0.6 τ = 7.2 µs in degassed DCM).[62] The emission wavelength of similar compounds can also be widely tuned by substituent effects on the dpyb ligand.[63] The emission of these compounds is of $^3\pi$-π^* character, although a significant contribution from a d-π^* component is suggested by DFT calculations which is consistent with high rates of triplet emission induced by the spin-orbit coupling of the metal.[64]

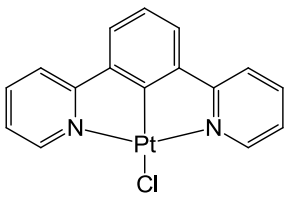

Figure 1.13 [Pt(dpyb)Cl]

The high efficiency of phosphorescence in these complexes is in part attributed to a shorter Pt-C bond in comparison to complexes with N^N^C ligands leading

to an increase in energy of MC excited states. This in turn leads to a decrease in non radiative decay through these metal-centred states. In addition, the rigidity of the terdentate ligand reduces excited state relaxation through distortion as is observed in analogous compounds with bidentate ligands such as [Pt(ppy)(ppyH)Cl].[54]

The varied properties of cyclometallated platinum complexes, particularly the highly emissive Pt(N^C^N) systems, has led to such compounds being investigated for use as phosphorescent dopants in OLEDS,[65] emissive liquid crystals,[66] and bioimaging agents.[67]

1.2 Disulfide bond formation in protein biosynthesis

The endoplasmic reticulum (ER) is an organelle that resides around the nucleus in eukaryotic cells. It is in the ER (specifically, the rough ER) that the translation and folding of trans-membrane and secretory proteins is performed. Many of these proteins rely on disulfide bonds for their structural integrity or function, unlike those destined for roles in the cytosol which generally do not. The electrochemical potential of the cytosol in most cells will disfavour the stability of disulfide bonds as it is more reducing than the conditions in the extra-cellular space. The ER, therefore, provides safe passage for proteins destined for secretion or trans-membrane roles which rely on these disulfide bonds, and as part of this function it maintains a more oxidising environment than the surrounding cytosol. After biosynthesis in the ER, proteins are transported in vesicles to their necessary destinations. The structure of a general eukaryotic cell is shown in Figure 1.14.

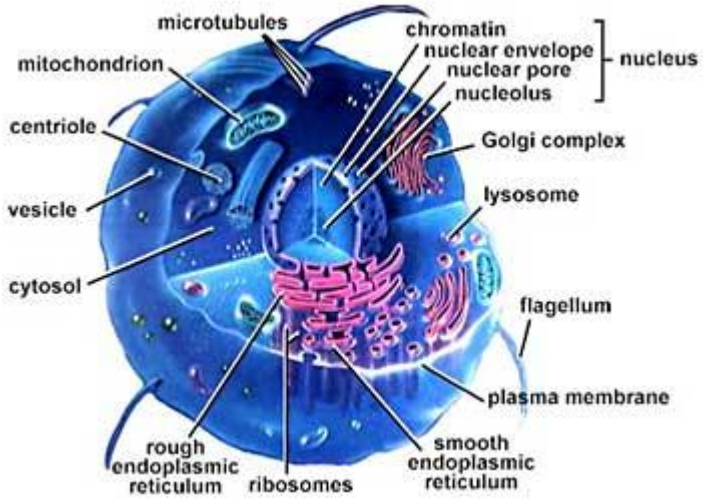

Figure 1.14 The general structure of a eukaryotic cell.[68]

Transcription of DNA in the nucleus followed by translation in the ER gives an unfolded protein. Any thiols present on cysteine residues will be in their reduced form when the protein is translated. If the protein is required to form disulfide bonds between these thiols to achieve its functional structure then an oxidative pathway must be present. Under aerobic conditions, many thiols will spontaneously form disulfide bonds depending on their precise oxidation potential, however, indiscriminate disulfide bond formation in protein folding can lead to aggregates of many separate proteins and non-native structures which do not show the required function. As is the case in many biological systems, a large number of enzymes and chaperones are present in the ER to aid correct protein folding. The identity and action of some of the key enzymes in protein folding in the ER have been discovered and the current understanding of these processes is discussed.

1.2.1 Protein Disulfide Isomerase

During investigations into the folding of reduced bovine pancreatic ribonuclease (RNase) upon reoxidation of the sulfhydryl groups to disulfide bonds *in vitro*, it was found that the protein will spontaneously adopt its native configuration.[69,70] In order to establish whether systems were present *in vivo* to accelerate re-oxidation, the reactivation of RNase activity was studied in the presence of homogenised rat liver cells.[71] It was discovered that certain microsomal fractions did indeed greatly accelerate the regeneration of the native RNase

from its reduced form. Further study indicated that the system was not only involved in the oxidation of sulfhydryl groups but also in the isomerisation of non-native disulfide bonds.[72]

This, in essence, was the first discovery of protein disulfide isomerase (PDI), which was successfully purified from bovine liver and partly characterised in 1966.[73] Refinements to the purification and a more detailed molecular characterisation classified PDI as a 57 kDa protein which resides in the endoplasmic reticulum.[74]

1.2.1.1 Structure and activity of PDI

Analysis of complementary DNA cloned from rat liver indicated a protein structure with domains homologous to that of the single domain protein thioredoxin (Trx), a known cofactor in redox reactions in prokaryotes such as *Escherichia coli*.[75] Comparison between PDI amino acid sequences from bovine, rat and human sources revealed two regions homologous to Trx in all three, with rat and bovine PDI being identical within these regions[76] (Figure 1.15).

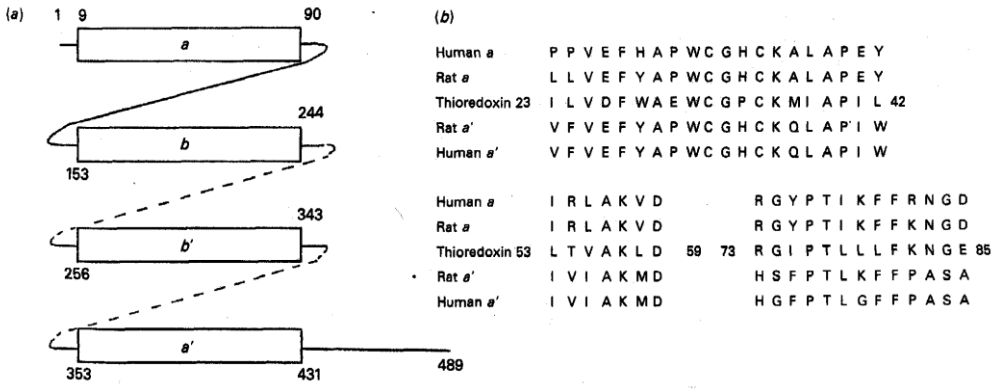

Figure 1.15 (a) Schematic domain Structure of PDI. (b) Homology between PDI and Trx.[76] Reprinted from R. B. Freedman *et al.*, *Biochem. Soc. Trans.*, 1987, **16**, 96, Copyright 1987, with permission from Portland Press Ltd.

From this information it was deduced that PDI has two active sites with the amino acid sequence WCGHCK, differing only from Trx in the substitution of a histidine residue for proline. The gene for encoding PDI in *Saccharomyces*

cerevisiae (yeast) was also identified and predicted a protein with the same homologous regions and active sites with 30% overall similarity to mammalian PDI.[77] In this study it was also found by gene disruption experiments that *S. cerevisiae* cells are inviable without PDI production.

Bearing in mind the function of PDI as an oxidase for sulfhydryl groups and an isomerase for non-native disulfide bonds, it is evident that the two cysteine residues are of importance. Various studies of mutant PDIs where one or both cysteine residues was substituted for serine have shown that the N- and C-terminal cysteines are inequivalent in properties and function.[78] Removal of the N-terminal residue causes a significant decrease in the rate of reactivation in reduced, denatured RNase while an inactivated C-terminal mutant shows no appreciable loss of activity. This mutation did appear, however, to reduce the steady-state binding constant K_m between enzyme and substrate.

Further analysis of these mutants confirmed that only the N-terminal cysteine is necessary for catalysis of isomerisation while both cysteine residues are needed for activity in the oxidation of reduced, denatured RNase.[79] This investigation also noted the accumulation of covalent PDI-RNase complex for the Cys-Gly-His-Ser active site mutant which does not occur with the wild-type PDI. It was suggested that, as well as allowing catalytic oxidation, the presence of two cysteine residues allows the enzyme an escape in the event of a geometrical barrier to rapid formation of the native structure (Scheme 1.1).

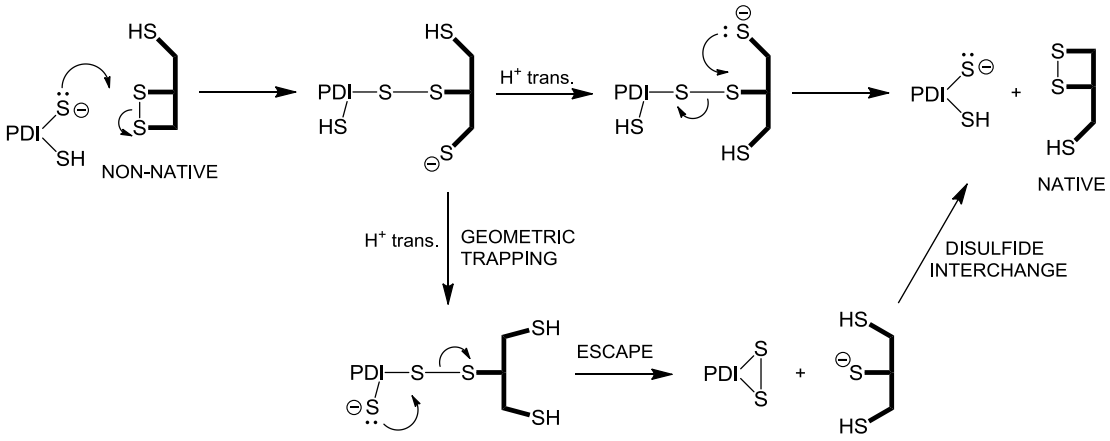

Scheme 1.1 Action of PDI in isomerisation of disulfide bonds showing escape from geometrically trapped arrangement.[79]

Microbiological studies have also revealed that in *S. cerevisiae* with chromosomal deletion of the *pdi1* gene, the inviable cells can be complemented with a wild-type rat gene. This is also possible with a CGHS mutant gene coding, but cells with a mutant SGHC coding remain inviable.[80] This indicates that the primary function of PDI in yeast is as an isomerase since the lack of oxidase activity of the CGHS mutant PDI does not affect viability.

There has been some disagreement over these results since in studies of PDI variants and individual PDI domains it was found that a significant reduction in isomerase activity still allows viability in *pdi1*Δ* *S. cerevisiae*, provided the variant has high oxidase activity.[81,82,83] This may suggest that isomerisation to the native structure could proceed by reduction and re-oxidation of disulfide bonds in systems with low isomerase activity. It has been shown, however, that isomerase activity in homogeneous conditions can be fully retained in variants without redox capabilities.[84]

In any case it is certain that wild type PDI performs both isomerase and oxidase functions, even though its exact roles and those of its homologues in redox cycles and isomerisation *in vivo* are not fully understood.

The structure of PDI proposed from initial determination of the amino acid sequence[76] was of two homologous domains, *a* and *a'*, separated by two segments (*b* and *b'*) which were recognised as being internal repeats. The limits of these domains (see Figure 1.15) and their structures have since been studied in more depth.[85,86,87] The full structure consists of 5 domains designated *a, b, b', a'* and *c* with a C-terminal endoplasmic reticulum retention signal.[88] The first four domains have been found to have Trx-like folds although *b* and *b'* are without an active site. A fragment containing the first 120 amino acids (the *a* domain) has been directly characterised by multidimensional heteronuclear NMR[85] and is shown in Figure 1.16.

* *pdi1*Δ indicates the deletion of the *pdi1* gene which is responsible for coding the protein PDI.

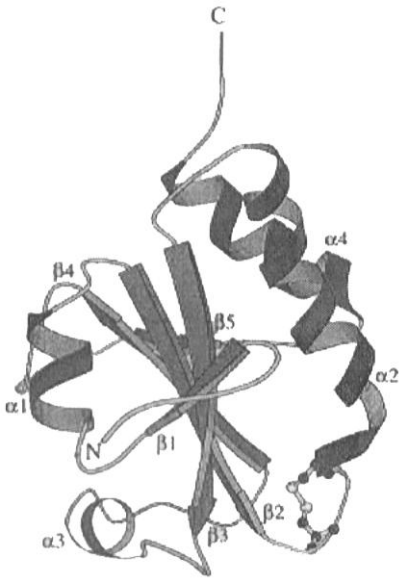

Figure 1.16 PDI *a* domain.[85] Reprinted from J. Kemmink *et al.*, *Biochemistry*, 1996, **35**, 7684, Copyright 1996, with permission from ACS Publications.

The full domain structure of PDI is shown in Figure 1.17. The numbering system shown is for rat PDI. Domain sizes vary slightly between different mammals but all retain the C-terminal Lys-Asp-Glu-Leu (KDEL) ER retention signal while *S. cerevisiae* PDI has the yeast ER retention signal His-Asp-Glu-Leu (HDEL).

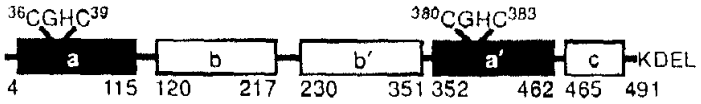

Figure 1.17 Numbered domain sequence for rat PDI.[89] Reprinted from E. A. Kersteen *et al.*, *Antioxid. Redox Signalling*, 2003, **5**, 413, Copyright 2003, with permission from Mary Ann Liebert, Inc.

It should also be noted that as well as individual activity as an isomerase/oxidase, PDI has been identified as a subunit of the multimeric enzyme assemblies prolyl-4-hydroxylase[90] and microsomal triglyceride transfer protein.[91] Interestingly, there is also evidence that PDI chaperones the folding of proteins without disulfide bonds while preventing aggregation.[92]

1.2.1.2 PDI mimics

As discussed previously, PDI is a protein with five domains, two of which contain an active site homologous to that of the well classified[93,94] *Escherichia coli* thioredoxin (Trx), a 12 kDa polypeptide (Figure 1.18). Despite the similarity in structure, Trx is not able to replicate the function of PDI in yeast cells as only a fraction have a reduced, deprotonated thiolate group necessary for activity under the pH and electrochemical conditions of the ER.[95] Modified Trx with a lower thiol pK_a on the other hand will show PDI activity[96] indicating that small analogues can mimic the behaviour of PDI.

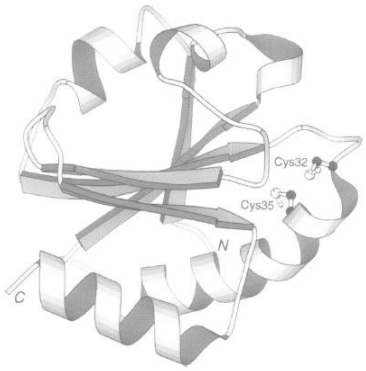

Figure 1.18 Thioredoxin structure.[96] Reprinted from P. T. Chivers *et al.*, *EMBO J.*, 1996, **15**, 2659, Copyright 1996, with permission from Nature Publishing Group.

It was found that as well as homologues with a CXXC active site, the tripeptide Cys-Gly-Cys-NH_2 and a mutant Trx with the P34 residue absent giving it a CXC active site will mimic PDI activity.[97]

It has now been shown that as well as small proteins and polypeptides, even small molecules can also mimic PDI activity. The molecule (±)-*trans*-1,2-*bis*(2-mercapto-acetamido)cyclohexane (BMC) (Figure 1.19), which has been studied for use as a technetium ligand[98] and as a reducing agent,[99] will catalyse the reactivation of scrambled RNase A *in vitro*.[95] This study also showed that BMC added to the growth medium of *S. cerevisiae* cells increased secretion of *Schizosaccharomyces pombe* acid phosphatase, a side effect normally associated with PDI overproduction indicating *in vivo* PDI activity.

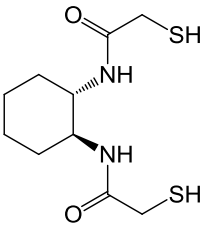

Figure 1.19 *trans*-1,2-*bis*(2-mercaptoacetamido)cyclohexane (BMC).

Although this small molecule does mimic PDI, its activity is only a fraction of that of the wild-type protein. This was attributed to lack of peptide binding sites possessed by PDI to form enzyme-substrate complexes, non-ideal thiol pK_a and E^0 and also to loss of BMC through formation of mixed disulfides with the redox buffer.[95]

Similar small-molecule approaches have been used in studies regarding the acceleration of reduced protein refolding *in vitro*. The usual standard for the re-formation of disulfide bonds in the production of native proteins *in vitro* is a mixture of oxidised and reduced glutathione.[100] Systems similar to the glutathione buffer have been used to enhance the rate of folding and isomerisation. An aromatic thiol/disulfide buffer gives a 5-fold rate enhancement over glutathione.[101] Other strategies, more similar to the dithiol nature of BMC, have produced dithiol moieties immobilised on various supports.[102] The effectiveness of the system is dependent upon the support used but, of those studied, the most effective gave a 17-fold increase in the yield of native protein. The major advantage of this approach is the drastic simplification of purification once the native proteins have been produced.

Since, on this evidence, small molecules can be made to mimic PDI activity, an investigation into similar small molecules containing fluorescent or phosphorescent tags would prove highly advantageous in the development of knowledge concerning the action and localisation of PDI *in vitro* and *in vivo*.

1.2.2 Endoplasmic Reticulum Oxidoreductase

As previously discussed, PDI is intimately involved in oxidative protein folding in the endoplasmic reticulum. PDI in its oxidised state can form disulfide bonds in

newly synthesised proteins by dithiol-disulfide exchange reactions. Any non-native bonds produced can then be isomerised by PDI in its reduced, deprotonated form. In this state, however, PDI can no longer provide any oxidase activity. There must, therefore, be a system in place *in vivo* to maintain the correct ER environment which will give the right balance of PDI in its disulfide and dithiol forms.

Genetic studies in *Saccharomyces cerevisiae* revealed the existence of a protein that is essential to oxidative folding in the ER.[103,104] It was concluded that this protein, named Ero1p in yeast, was involved in oxidative pathways for the maintenance of active PDI. During these studies, comparison of Ero1p to sequence databases indicated the existence of homologues in mammals. Two homologues have since been identified in human cells and have been named Ero1α[105] and Ero1β.[106]

1.2.2.1 The role of ERO proteins in the action of PDI

Further investigations have revealed more details of the oxidative pathways involved in protein folding. The dependence of Ero1p upon the cofactor flavin adenine dinucleotide (FAD) for oxidase activity has been demonstrated[107] as well as the importance of the reduced and oxidised glutathione levels *in vivo*, both within the ER and in the surrounding cytosol.[108,109] It has also been shown that Ero1p transfers electrons from the reduced PDI directly to molecular oxygen.[110] The likely mechanism for oxidative protein folding based on these findings is shown in Scheme 1.2. Interestingly, despite the presence of definite oxidative pathways for PDI involving Ero1 proteins in both yeast and mammalian cells, it has been noted that the while PDI at steady state in yeast is mostly oxidised,[111] it appears to be mostly in its reduced form in mammals.[112]

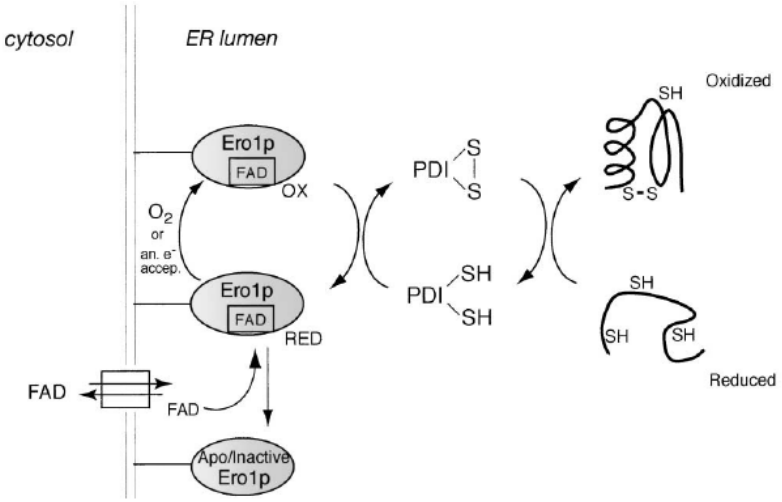

Scheme 1.2 A model for the transfer of oxidative equivalents from O_2 or an e^- acceptor to folding proteins in the ER of yeast. Ero1p activity is dependent on weakly associated free FAD as well as bound FAD. Apo Ero1p refers to a state where weakly associated FAD is absent.[110] Reprinted from B. P. Tu *et al.*, *Mol. Cell*, 2002, **10**, 983, Copyright 2002, with permission from Cell Press

Another factor relating to protein folding is that of 'quality control'. An excess of unfolded protein in the ER induces increased transcription of various genes. In general the genes activated by this Unfolded Protein Response (UPR) are ER specific proteins.[113,114] Ero1p in yeast is one of the proteins up-regulated by the UPR[104] but in mammalian cells only Ero1β expression is increased by this response.[106] Despite the fact that Ero1α is homologous, up-regulation is stimulated by hypoxia[115] not UPR indicating that although they are related, Ero1α and Ero1β have separate specialised functions. This is supported by reports that Ero1β exhibits tissue specific expression.[116] It is also becoming apparent that Ero proteins and Ero-Ero dimers may be involved in processes unrelated to PDI since in certain tissues Ero1β expression is inversely correlated with that of PDI.[116]

1.2.2.2 Structural features of ERO proteins

Unsurprisingly, Ero1 proteins contain several cysteine residues, some of which form redox active or structural disulfide bonds. The functions of conserved cysteine-containing motifs have been investigated[117,118] and the absolute structure of Ero1p has been determined by X-ray crystallography[119] (Figure 1.20).

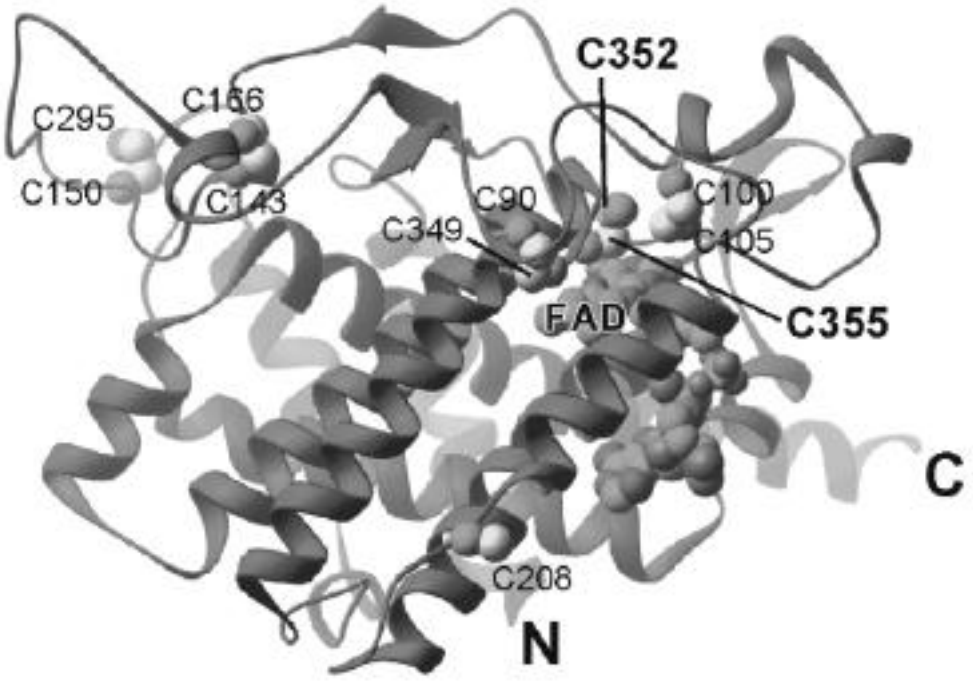

Figure 1.20 Structure of Ero1p showing cysteine residues and FAD positions.[119] Reprinted from E. Gross *et al.*, *Cell*, 2004, **117**, 601, Copyright 2004, with permission from Cell Press.

The Ero1p structure contains two relevant conserved motifs with the structures CXXXXC and CXXCXXC. Amino acid substitution studies indicate that the $C_{100}XXXXC_{105}$ site is needed in the binding of Ero1p to PDI and the necessary dithiol-disulfide exchange. Removal of C_{352} or C_{355} (the two cysteine residues closer to the C-terminus in CXXCXXC) also impairs Ero1p activity indicating that these are also involved in the process, most likely their role being in reoxidising the CXXXXC dithiol.[118] This is consistent with the determined structure as the N-terminal C_{349} of this motif is involved in a structural disulfide bond. It is also apparent from the X-ray structure that the CXXXXC motif resides on a flexible chain section which facilitates shuttling between an exposed position for interaction with PDI and the CXXCXXC active site, adjacent to the FAD cofactor.

While it is likely that there are a many more enzymes and chaperones involved in oxidative protein folding, both PDI and the ERO proteins are clearly key species in this process. The ability to further target these enzymes for study would therefore provide more insight into the function of the endoplasmic reticulum as a factory for secretory and trans-membrane proteins.

1.3 Detection of biological thiols

The detection of biological thiols has been extensively researched, initially in the context of detecting levels of free amino acids such as cysteine and homocysteine.[120] Elevated or depressed concentrations of these substances in plasma can be indicators of various diseases such as cardiovascular disease[121] and Alzheimer's disease.[122] Deficiencies in these amino acids can also be responsible for health problems including slowed growth, muscle and fat loss, lethargy and many others.[123] Many of these early methods, however, rely on derivatisation and separation prior to analysis and are useful only in the determination of concentration with respect to free cysteine, homocysteine and glutathione.

Approaches of this nature, while suited to roles in medical analysis and diagnosis, are less useful for probing the structure and action of larger biological species such as polypeptides and proteins.

1.3.1 Organic fluorophores as sulfhydryl labels

There have been two general approaches to the detection of thiol-containing molecules in biological systems using organic fluorophores. These are direct, normally irreversible reactions of a thiol group with a suitable label or the use of a "chemosensing ensemble"[124] where non-covalent interactions between a receptor and the analyte and fluorophore induce changes in fluorescence.

The direct labelling approach has been successfully employed in the selective detection of the amino acids cysteine and homocysteine. One investigation[125] developed a labelling system based on the selective reaction of N-terminal cysteine residues with aldehydes to form thiazolidines[126] (Scheme **1.3**).

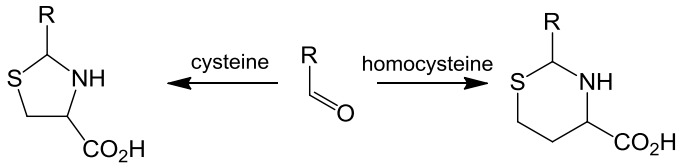

Scheme 1.3 Reaction of N-terminal cysteine with an aldehyde.

This reactivity is also displayed by free cysteine and homocysteine, forming 5 and 6 membered rings respectively, since the required functionality is a thiol group and a neighbouring primary amine. The necessity for both these groups allowed the development of a colorimetric sensor with specificity for cysteine and homocysteine over other biological thiols such as glutathione or non-terminal cysteine residues in proteins.[125] The reactivity of the aldehyde group with cysteine has also been used to label proteins synthesised with additional N-terminal cysteine residues.[126,127]

Another novel sensor system based on squaraine derivatives was found to show selectivity for thiol groups when tested with various amino acids.[128] The quenching of luminescence in the sensor has been proposed to be a result of the reaction shown in Scheme **1.4**.

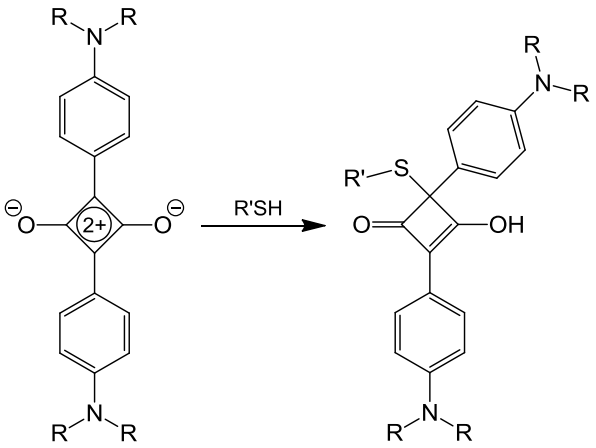

Scheme 1.4 Proposed reaction between squaraine derivatives and biological thiols causing bleaching of the sensor and quenching of fluorescence.[128]

As well as detection of small biological molecules, direct labelling has also been used in the study of proteins, often in conjunction with protein modification. Common functionalities for labelling the thiol side chains of cysteine residues are maleimides[129] and haloacetamides.[130] A good example of the use of these

labels was in a study of adenosine-5'-triphosphate (ATP) hydrolysis by actomyosin subfragment 1 ATPase.[131] Here, to measure the release of phosphate upon ATP hydrolysis, an A197C mutant of the *Escherichia coli* phosphate binding protein was labelled via the unnatural cysteine with a fluorescent maleimide. The labelled mutant showed a ~50 nm shift in emission maxima with a 5-fold increase in intensity upon the binding of phosphate allowing the kinetics of ATP hydrolysis to be studied in depth.

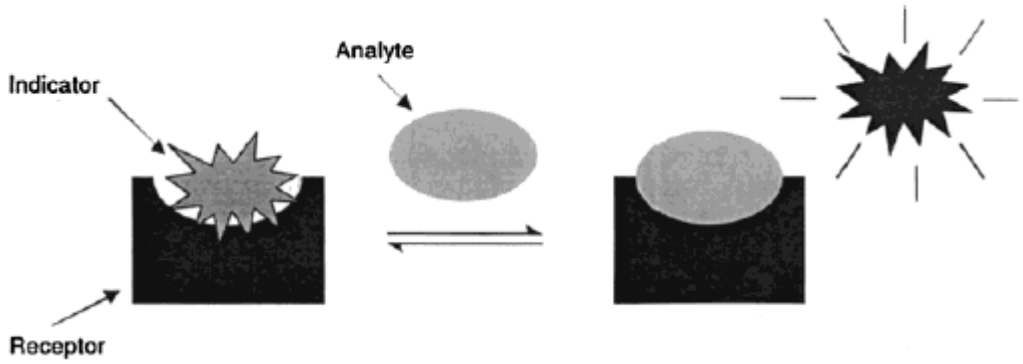

Scheme 1.5 A chemosensing ensemble. Displacement of the fluorophore by the analyte causes a change in its photochemical response.[124] Reprinted from S. L. Whiskur *et al.*, *Acc. Chem. Res.*, 2001, **34**, 963, Copyright 2001, with permission from ACS Publishing.

The alternate "chemosensing ensemble" approach has been shown to be successful in the detection of biological molecules including citrate, tartrate and also inorganic species such as nitrate.[124] There has also been some success in selective detection of histidine over other amino acids.[132] The general scheme for the action of a chemosensing ensemble is shown in Scheme **1.5**. One such sensor developed using this approach which has the ability to selectively detect cysteine, homocysteine and peptides with thiol groups using Cu^{2+} has been demonstrated.[133] In this ensemble Cu^{2+} was used as the receptor since thiol groups have a strong affinity for this ion. The fluorophore used was the anthracene derivative shown in Figure 1.21.

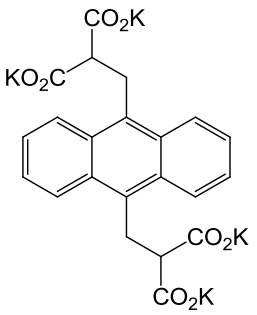

Figure 1.21 Fluorescent indicator for Cu^{2+}.

The addition of Cu^{2+} to the indicator causes quenching of fluorescence from the anthracene moiety by this ion as it is held in proximity by the complexation of the carboxylate groups. While the addition of most amino acids to a solution of the receptor and indicator had very little effect, cysteine, homocysteine and glutathione resulted in almost complete recovery of fluorescence.

As well as organic emitters, there has also been a report of a novel chemosensing ensemble approach using luminescence in metal complexes.[134] A trinuclear heterobimetallic complex of Ru and Pt was synthesised with bridging cyano groups between the metals. Upon the addition of thiol-containing peptides, the affinity of platinum for these side chains causes the release of the mononuclear ruthenium fragment producing a marked change in luminescence (Scheme 1.6).

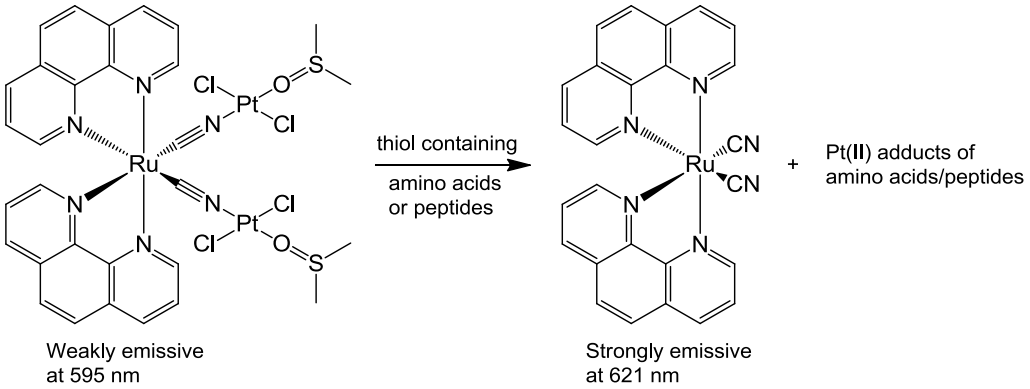

Scheme 1.6 Action of trimetallic Ru/Pt complex in thiol detection.[134]

The use of metal complexes has become more common in biological sensing, however most are externally functionalised complexes for use in bioconjugation. This approach is discussed in the following section.

1.3.2 Luminescent metal complexes for bioconjugation

Initial research into transition metal complexes for use as thiol labelling agents was mainly centered on ruthenium[135] and rhenium.[136,137] Complexes of these metals with polypyridyl or diimine ligands such as phenanthroline, display relatively long-lived ^{3}MLCT emission[138,139,140] and so were deemed useful in fluorescent labelling. In general maleimide,[137] or haloacetamide[135,136] units were attached to one of the ligands as a sulfhydryl specific linker.

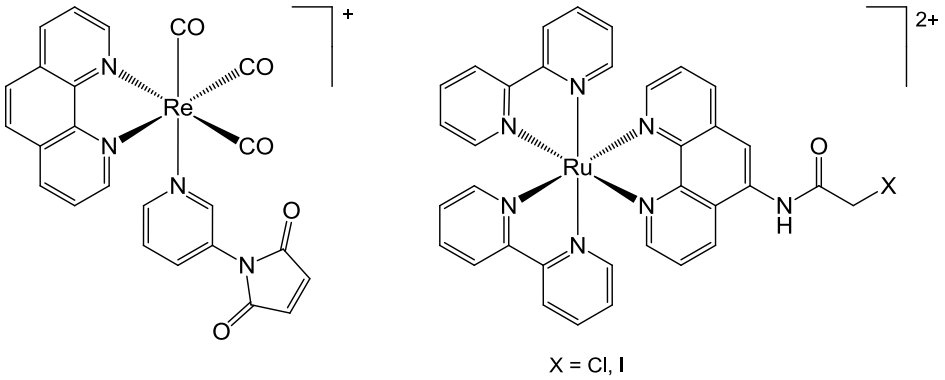

Figure 1.22 Luminescent complexes with a) maleimide linker[137] and b) haloacetamide[135]

Although osmium complexes with these ligands generally display lower quantum yields than Re and Ru analogues,[141] these have also been explored as possible bioconjugates. Initial studies reported an osmium complex with 5-amino-1,10-phenanthroline which could be converted to the isothiocyanate derivative for attachment to amine side chains of peptides.[142] Unsurprisingly, similar osmium complexes have now been used for labelling via thiol containing side chains using the well established iodoacetamide linker.[143]

Iridium complexes with polypyridyl and cyclometallating ligands have also received significant attention due to their useful photochemical properties.[144,145,146,147] The first reported iridium bioconjugate was a complex with two cyclometallating phenylpyridines and a functionalised phenanthroline as ligands[148] (Figure 1.23).

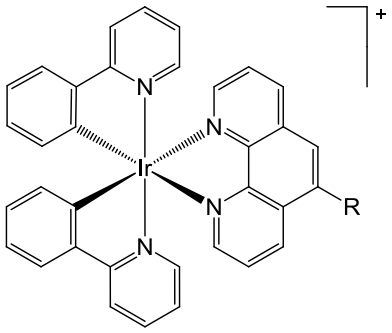

R = NCS, $NHCOCH_2I$

Figure 1.23 Iridium complex for conjugation to amine or thiol side chains.

A set of iridium bis-terpyridine complexes has also been synthesised. In this study the terpy ligands were functionalised, one with an isothiocyanatophenyl group and the other with various groups to tune the photochemical properties.[149] Further work has resulted in the publication of a series of thirty iridium complexes with bidentate ligands of the form $[Ir(N^C)_2(N^N)]PF_6$ where the N^N ligand is functionalised for bioconjugation[150] (Figure 1.24). This included ten complexes specifically targeted at cysteine residues.

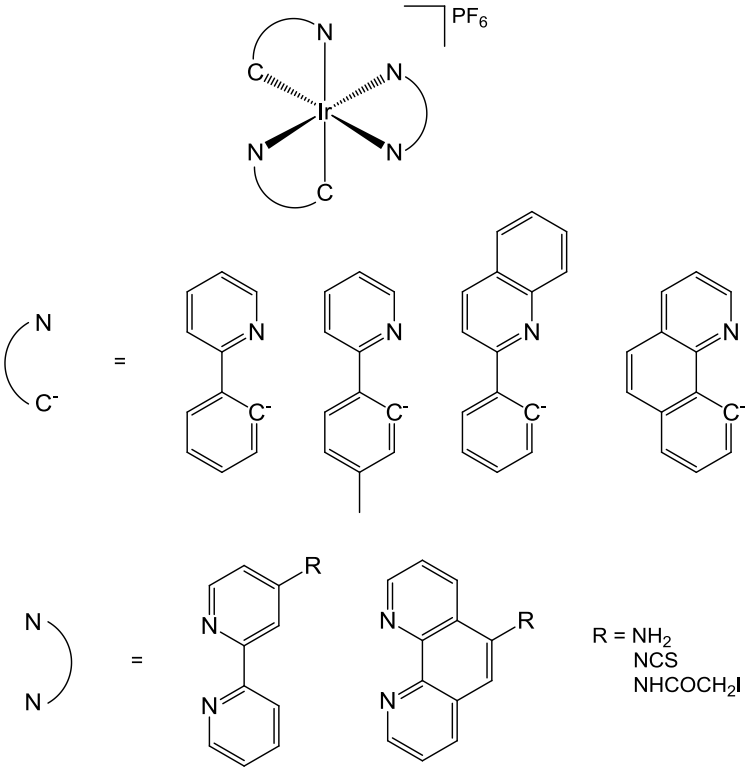

Figure 1.24 Series of Iridium bioconjugating complexes.[150]

The majority of thiol targeted labels discussed above have been proven to be effective in labelling human serum albumin (HSA) and also, in one case,[135] human immunoglobulin G (IgG) via their free cysteine residues.

More recently, functionalised iridium complexes have been shown to display selective reactivity with cysteine and homocysteine with a concurrent change in emission maximum.[151,152] This uses an analogous approach to that discussed above in Scheme **1.3**, where the aldehyde functional group of iridium complexes with 4-(2-pyridyl)benzaldehyde (pybaH) reacts with the thiol and amine functional groups of cysteine and homocysteine to form a 5 or 6 membered ring respectively (Figure 1.25).

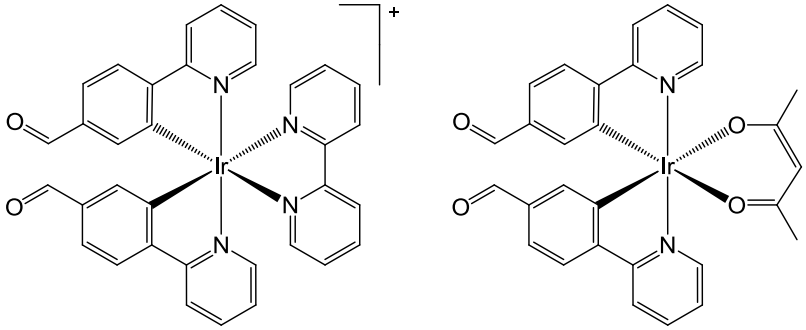

Figure 1.25 Functionalised iridium complexes $[Ir(pba)_2(bpy)]^+$ and $[Ir(pba)_2(acac)]$ which show selectivity for cysteine and homocysteine.

These compounds have been successfully employed as ratiometric sensors for these amino acids *in vivo*.[152]

So far, all labelling strategies discussed, with the exception of a chemosensing ensemble, have relied upon covalent binding to sulfur. As mentioned previously, methods of this nature are unsuitable for the study of dynamic processes involving cysteine residues in biological redox cycles. In order to produce effective probes for these processes, a system must be found which shows fully reversible binding to cysteine thiol groups with a concomitant change in photochemistry while also being soluble in aqueous media. Direct coordination of an analyte to transition metals as a ligand is in many cases reversible and thus seems an effective approach to explore.

1.3.3 Metal coordination in sensory systems

There are several general methods for using coordination of an analyte to metals in sensing applications. This technique is in many ways related to the well established detection of transition metal ions[153] through ligation or chelation by fluorescent organic species, except the roles of ligand and metal are reversed. Here, a metal with some fixed ligand system is perturbed by the binding of a new ligand (the analyte) and a change in the photochemical properties of the sensor occurs. Also, while the use of transition metal and lanthanide complexes in general has become common in sensing applications[154,155], the approach using direct analyte-metal interactions is relatively recent.

There has been very little use of this technique in the selective detection of cysteine residues but there has been a significant body of work towards sensors of anions, small molecules such as water, and ammonia as well as other gases. The methods used in these sensors are ideal for adaptation to cysteine sensors since the systems are designed to show fast, fully reversible binding to the analyte.

There are various approaches to molecular sensing via direct metal coordination that have been explored. Firstly, coordination of the analyte can take place by substitution of a weakly bound ligand or coordination to a vacant site. Secondly, the metal can either be simply a binding receptor attached to a separate luminophore or can alternatively perform both of these roles.

Where the metal is used as both the receptor and luminophore, it is easy to appreciate how a change in photochemical properties occurs. Direct perturbation of the metal orbitals by the analyte causes a shift in energy of the emissive state or may even change the nature of the lowest energy state. The modular approach to this method with a separate luminophore can require more consideration. Often in these systems the metal acts as an electron transfer quencher for the luminophore which can be modulated by anayte binding, either by altering the electron transfer ability of the metal or the separation between the metal and luminophore.

A common approach to sensing via a vacant coordination site is the use of porphyrin or other related planar ring systems (Figure 1.26) and is analogous to the function of haemoglobin in the body which shows reversible binding to O_2. This type of complex has been demonstrated for use in the detection of nucleobases[156] and has also been used extensively in the production of O_2 sensors.[157,158,159] The incorporation of binding pockets around the vacant coordination site has also been used to produce selective sensors for a wide range of analytes.[160]

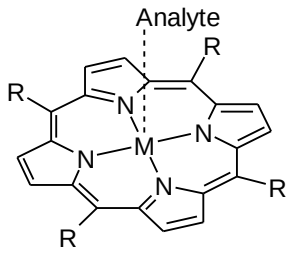

Figure 1.26 A porphyrin based sensor.

A similar approach has been used in anion sensing except using the chelating ligand cyclen with a pendant organic fluorophore.[161] This sensor (Figure 1.27) was found to detect pyrophosphate and citrate anions in neutral aqueous solution, as well as the biological anions ATP and ADP. The success of this sensor in aqueous solution is important since many fluorescent species are subject to quenching by H_2O.

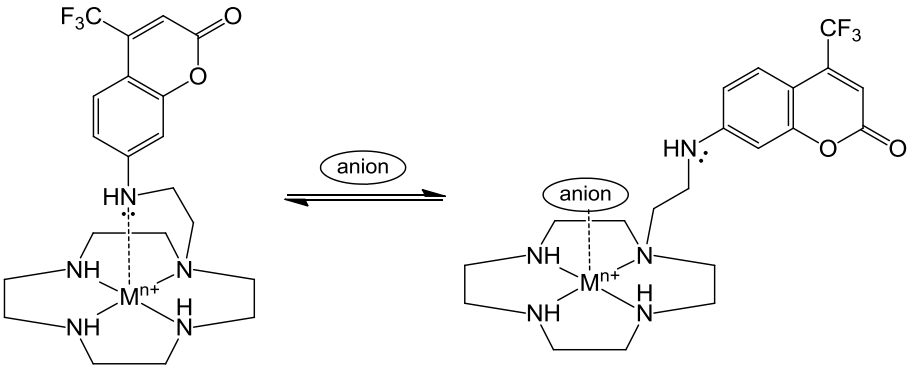

Figure 1.27 Anion sensor based on displacement of the organic fluorophore.

In sensors where the metal provides both photochemical activity and the binding site by substitution of a weakly bound ligand, reversibility of the process is often problematic since there is no thermodynamic drive for the replacement of the analyte by the weak ligand. It has been discovered that a system in which the displaceable ligand is covalently attached to a fixed ligand, keeping it in the vicinity of the metal, can enhance the reversibility of an analyte response. This was demonstrated in the sensing of CO[162] and has been referred to as the 'hemilabile ligand' approach. A system with more relevance to cysteine sensing has also been reported using this approach. A luminescent ruthenium bipyridyl complex with a hemilabile ligand has shown affinity for sulfur donors such as DMSO, thiols and sulfides[163] (Scheme 1.7). This complex has limitations however: the luminescence is only observed in low temperature glasses and it is also sensitive to binding of H_2O, making it unsuitable for use in aqueous media.

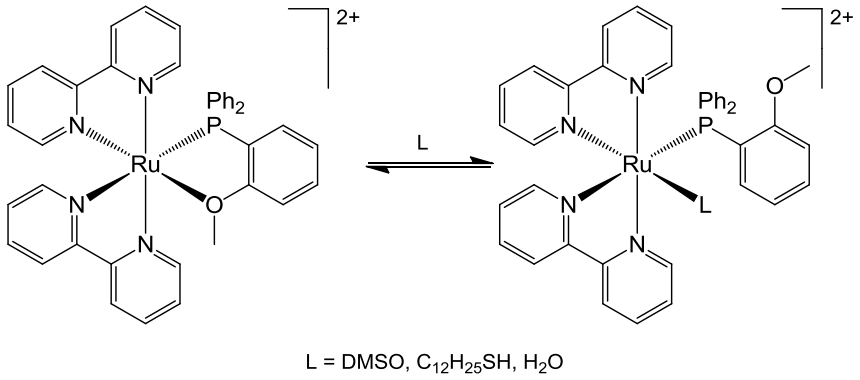

L = DMSO, $C_{12}H_{25}SH$, H_2O

Scheme 1.7 Reversible binding of S donors to ruthenium.

It has also been discovered that cyclometallated complexes of platinum with diamine pincer ligands provide very useful colorimetric sensors for sulfur dioxide gas.[164] This Pt(N^C^N) motif has been now incorporated into dendritic and quartz microbalance systems for the detection of sulfur dioxide at very low levels.[165] The action of this platinum unit is shown in Scheme 1.8. It is worth noting, however, that upon changing the amine substituents from methyl to ethyl the binding of sulfur dioxide no longer occurs, most likely due to steric considerations.

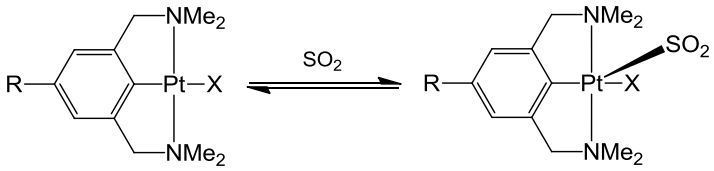

Scheme 1.8 Reversible binding of SO_2 to platinum.

As a final note, although not studied in the context of sensing, it has been found that platinum complexes with a bidentate diimine and the 1,4,7-trithiacyclononane ligand display a square pyramidal structure with a very long apical Pt-S interaction as shown in Figure 1.28.[166] It has been discovered that, by variation of the σ-donor and π-acceptor strength of the diimine ligands, the apical Pt-S interaction can, to some extent, be modified.[166,167] This provides further indication that interaction between thiol groups and the vacant site of square planar platinum compounds can be controlled.

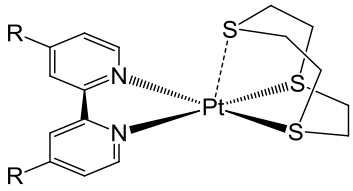

Figure 1.28 Platinum complex with apical Pt-S interaction

1.4 The role of luminescence in cellular studies

Microscopy is well established in studies of the cellular environment and as a non-invasive technique is vital in exploring the behaviour of cells without disturbing their function. The introduction of fluorescent cellular probes and the associated use of fluorescence microscopy can provide the opportunity to study in more detail specific sub-cellular structures by using probes which display specific cellular localisation. It is also possible, through the design of fluorescent probes that are responsive to their environment, to investigate the biological processes at work within the cell.

1.4.1 Fluorescence microscopy

In fluorescence microscopy a light source, in combination with an appropriate filter, is used to irradiate the sample through the objective lens of the

microscope. Emitted light from the sample passes back through the objective and on to a detector, in many cases a digital camera. A dichroic mirror is used to reflect the excitation beam towards the sample while allowing the emitted light to pass through to the detector. Using this set-up, known strictly as epifluorescence microscopy, most of the excitation beam passes through the sample and only a small proportion reflected by the sample passes through towards the detector with the emitted light. The addition of an emission filter leads to a very good signal-to-noise ratio using this method. A schematic diagram of an epifluorescence microscope is shown in Figure 1.29.

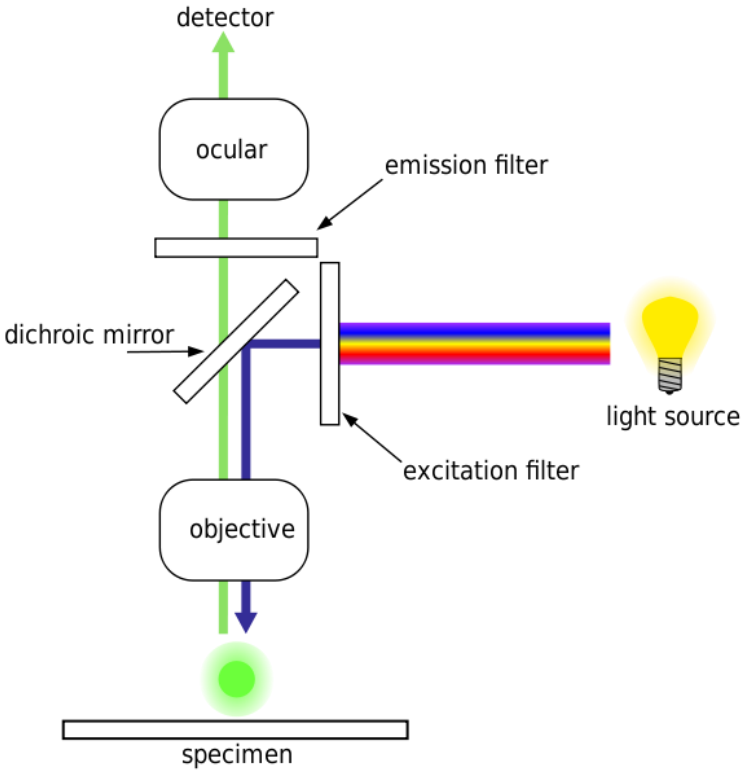

Figure 1.29 Schematic representation of a fluorescence microscope.[168]

In addition to standard epifluorescence microscopy, the use of confocal fluorescence microscopy is becoming more common where focused 'point illumination' is used to excite only part of the sample in the focal plane. By scanning over the sample in the *xy* plane as well as adjusting the depth of focus, a 3D image of the sample can be acquired with high spatial resolution.

1.4.1.1 Desired properties of probes for fluorescence microscopy

There are several requirements for luminescent probes for use in bioimaging in addition to the obvious need for an acceptable intensity of emission. These include low cytotoxicity, good cell uptake properties, high chemical stability and photostability as well as good localisation properties.

There are also several considerations specific to the photophysical properties of the probe that can lead to limitations in its use. Ultraviolet light shows poor tissue penetration and UV irradiation can lead to cell damage; therefore it is preferred for a luminophore to display absorption bands in the visible region of the spectrum. Compounds with small Stokes' shifts will tend to be affected by self-quenching where emitted light is reabsorbed by the sample. A larger Stokes' shift also allows much easier separation of the excitation beam and the luminescence of the sample.

1.4.1.2 Organic and biological probes for bioimaging

The vast majority of probes currently in use are based on organic fluorophores.[169] Also, more recently, developments in cloning techniques and genetic engineering have led to an increased use of fluorescent proteins, in particular green fluorescent protein (GFP) from jellyfish as the fluorescent unit in a variety of studies.[170] In general, these systems display only small Stokes' shifts and are often prone to photobleaching.

1.4.1.3 Inorganic species as cellular probes

Nanoparticles of semiconducting materials, or 'Quantum Dots', show high quantum yields as well as longer lifetimes than organic emitters and have also been used for biological imaging studies.[171] While these are advantageous in that they do not suffer from photobleaching or excited state reactivity, the materials used tend to show very high cytotoxicity. This can be mitigated by coating the dots with organic layers, however this can lead to expensive synthetic procedures.

The lanthanide series has also received attention as luminophores as they display very long-lived emission at specific energies, however these ions also display high cytotoxicity and must be used in complexes of very high stability, in many cases using macrocyclic ligands.[172,173,174] The direct excitation of lanthanides is also problematic due to the forbidden nature of f-f transitions leading to the need for further functionalisation of the ligands with antennae units.[174]

1.4.1.4 Transition metal complexes in bioimaging

Recently, phosphorescent transition metal complexes have become more common in cellular imaging applications.[6,7] As discussed earlier, complexes of second and third row transition metals with cyclometallating ligands can display a wide range of excited states which can be easily tuned to a particular function. The versatile properties of such compounds have led to their use as imaging agents for live cells with a common approach being the functionalisation of emissive complexes with biological molecules. Examples of this include the attachment of biotin to complexes of rhenium[175] and iridium[176] and functionalisation of ruthenium complexes with estradiol.[177] The conjugation to biotin provides a wide range of uses for these emitters since the affinity of biotin for the protein avidin is already the basis for a wide variety of biochemical assays.[178,179,180] Equally, conjugation to hormones such as estradiol provides the opportunity to study the binding of these biomolecules to protein receptors.

Since the localisation of cellular probes is so important in determining their applications, this is a particular area that has received much interest. It has been found that the structural variety in luminescent transition metal complexes can lead to noticeably different intracellular localisation.

Compounds of ruthenium(II),[181] iridium(III)[176,182] and rhodium(III)[183] with polypyridyl and cyclometallating ligands have been shown to localise in the cytoplasm. Additionally, Coogan *et al.* have shown that rhenium(I) complexes containing long chain ester functional groups tend to localise in membranes

within the cytoplasm.[184] Figure 1.30 shows a selection of these compounds observed as showing cytoplasmic localisation.

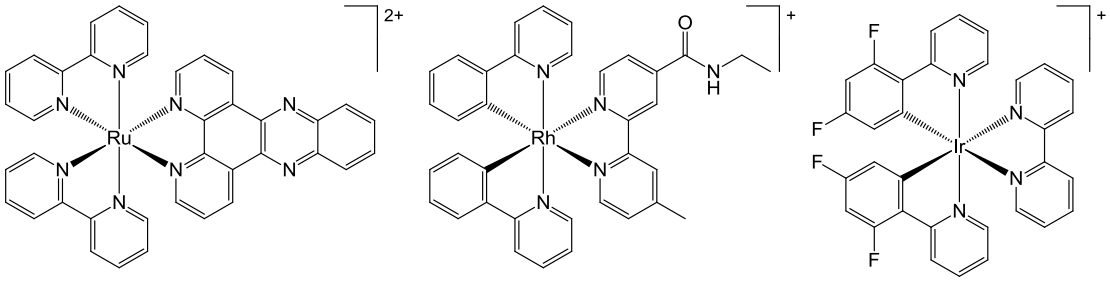

Figure 1.30 Some luminescent complexes of Ru(II), Ir(III) and Rh(III) which localise in the cytosol.

In addition, while some platinum(II) complexes with an N^N^C ligand have also been shown to localise in the cell cytoplasm[185,186] similar compounds with an N^C^N coordinating ligand instead show localisation in the nucleoli.[67] The localisation properties of complexes can also be altered by functionalization of the ligands. For example the incorporation of a triphenylphosphonium-functionalised unit into a platinum N^N^C complex results in staining of the nucleoli[187] rather than the cytoplasm. These two compounds are shown in Figure 1.31.

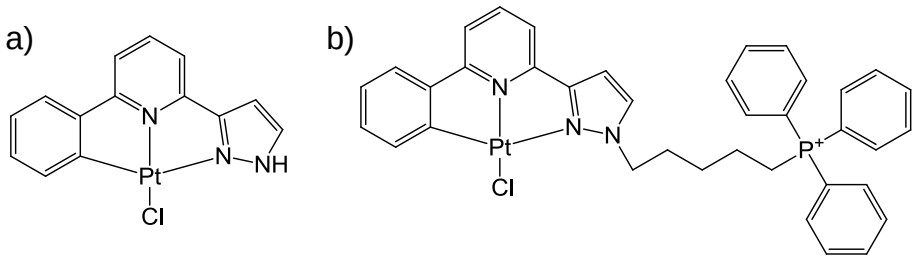

Figure 1.31 Complex a) shows cytoplasmic localisation[186] while the functionalised analogue b) stains the nucleoli.[187]

The varied cellular localisation properties of these complexes, coupled with their tuneable emission makes the exploration of such complexes as bioimaging agents of particular interest. It certainly seems likely that the recent interest is justified and likely to continue for some time.

A potential problem, however, in the use of these phosphorescent complexes is that many commonly suffer from quenching in aerated solution via $^1O_2$ sensitization mechanisms. In addition to the loss of quantum yield, this creates problems with phototoxicity in their use in cellular studies due to the production of singlet oxygen *in vivo*. Complexes that show high levels of oxygen quenching therefore may not be ideal for use as intracellular probes.

1.4.2 Lifetime based fluorescence microscopy techniques

Intensity based measurements are inherently affected by, for example, wavelength dependence in the output of a light source or the response of a detector as well as being dependent on the local concentration of the emissive species. Luminescence lifetimes, on the other hand, can be measured absolutely, independent of concentration, and are often sensitive to the local environment. This has led to the development of fluorescence lifetime imaging microscopy (FLIM) which allows the measurement of environment effects such as pH and O_2 concentrations as well as processes such as Förster resonance energy transfer (FRET) *in vivo*.[188] In addition, polarisation-resolved FLIM can be used to measure the rotational mobility of a fluorophore indicating the viscosity of its surroundings.[189] FLIM has mainly been used in the analysis of organic emitters and other fluorescent species with short, nanosecond lifetimes[190,191] and thus requires fast gated excitation and measurement techniques.

The use of bioimaging agents which show much longer lifetimes *in vivo*, such as lanthanide complexes and transition metal complexes with low levels of oxygen quenching, low cytotoxicity and high photochemical stability, has allowed the development of time-resolved emission imaging microscopy (TREM).[192] This technique employs the use of a pulsed laser as the excitation source while a time-gated CCD camera is used as the detector. It has been shown that TREM is especially useful in removing interference from short-lived background autofluorescence.[67] Autofluorescence occurs in all cells as a result of endogenous fluorescent molecules such as the amino acids tyrosine and tryptophan as well as various fluorescent proteins. This can lead to high signal-

to-noise ratios in fluorescence microscopy methods and can cause particular interference in FLIM measurements due to the similarity in lifetimes between fluorescent probes and this background autofluorescence. The advantage of TREM as a technique for overcoming this interference is illustrated in Figure 1.32.

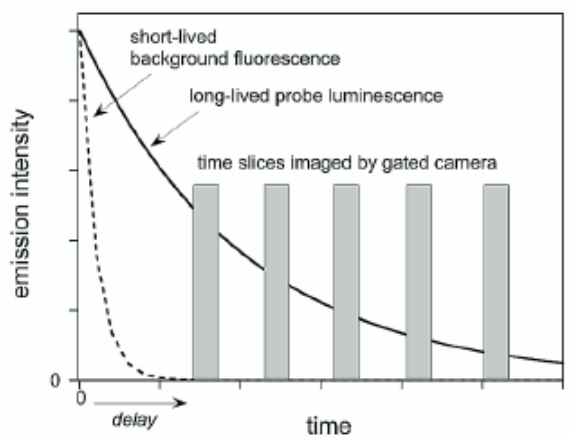

Figure 1.32 Illustration of time gating to eliminate short-lived background fluorescence. Reprinted from S. W. Botchway *et al.*, *Proc. Natl. Acad. Sci. U. S. A*., 2008, **105**, 16071, Copyright 2008, with permission from the National Academy of Sciences.

The availability of this technique provides an additional advantage in the development of bioimaging agents based on transition metal emitters which will have the appropriate long-lived phosphorescent emission.

1.4.3 Flow cytometry

Another important tool in the study of emissive bioimaging agents is flow cytometry which can be used as a method of counting fluorescently or phosphorescently labelled cells. This technique involves the injection of cells into a hydrodynamically focused stream of carrier fluid which forces the cells into 'single file' within the stream. The cells are analysed one at a time by directing a beam of light at the stream and both reflected and emitted light are analysed by a series of detectors. Detectors in line with the incident beam and at 90° to it measure the forward and side scattering of all cells which gives information on their size and composition, while fluorescence detectors count cells which have been successfully labelled with an emissive compound. This

gives a rapid method for counting the proportion of labelled cells in a sample. Figure 1.33 shows a schematic representation of the operation of a flow cytometer.

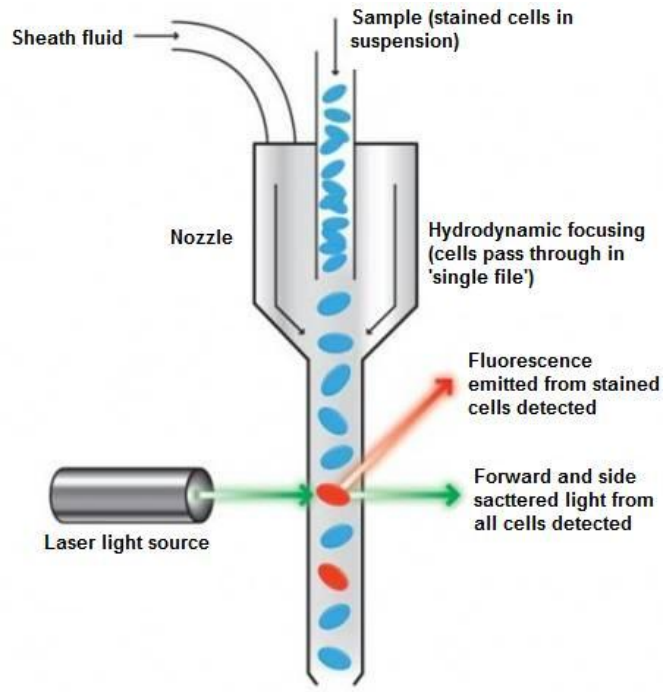

Figure 1.33 Schematic of the function of a flow cytometer.

Some flow cytometers are also able to perform fluorescence-activated cell sorting where a vibrating mechanism causes the flow to break into droplets. These will generally each contain a maximum of one cell per droplet. The stream in this type of machine also passes through an electrical charging ring which can apply a charge to individual droplets. After measurement, the stream passes through an electrostatic deflector and using this set-up, a droplet conforming to some measured criteria, e.g. successful fluorescent labelling, can be diverted from the main stream into a collection vessel.

1.5 Concluding remarks

A brief overview has been given of the role of second and third row transition metals in photochemical and photophysical applications, with particular reference to complexes containing cyclometallating ligands. The utility and tenability of such complexes has been discussed

The role of particular proteins which mediate cellular processes involving thiols has also been explored, as well as developments in the detection of sulfur containing molecules. It is evident that much of the oxidoreductase machinery in the endoplasmic reticulum is controlled by dithiol-disulfide exchange reactions. Although there is a significant body of research into fluorescent probes for cysteine residues, the vast majority of those currently available are unsuitable for studying these dynamic processes. The direct labelling of cysteine residues through covalent linkages will seriously disrupt, if not remove, any processes performed by the labelled site. If, on the other hand, a set of fluorescent labels could be produced with transient associations to cysteine residues this would provide a very useful tool in monitoring disulfide bond formation and reduction *in situ* while minimising interference with the processes involved.

Furthermore, the application of techniques such as fluorescence microscopy and flow cytometry in the study of cellular environments has been discussed, with emphasis on the growing role of luminescent metal complexes in this field.

1.6 Aims

The primary aim of this project is to synthesise fluorescent compounds which are functionalised in such a way as to show potential activity as PDI mimics. If successful, this will provide a series of novel compounds which could be used to elucidate the mechanisms of oxidative protein folding and disulfide isomerisation processes *in vivo* through the use of fluorescence microscopy. As a result of functionalisation it is hoped that such compounds will display particular intracellular localisation properties, ideally being taken into cellular compartments particularly associated with disulfide oxidation and isomerisation, for example the endoplasmic reticulum.

In addition, the substitution chemistry of sulfur with cyclometallated complexes of platinum(II) and iridium(III) will be explored. It is hoped that this will provide potential for luminescent sensors that show affinity for sulfur and, especially, reversible binding to sulfur containing species, allowing the study of dynamic processes involving thiol/disulfide interchange without inhibiting them.

Chapter 2

Cyclometallated platinum complexes with thiolate ligands

2 Cyclometallated platinum complexes with thiolate ligands

As discussed in the introduction, complexes of platinum have received much attention as luminescent reporters for a variety of applications due to their varied excited state properties. In particular, complexes related to 1,3-di(2-pyridyl)benzene platinum(II) chloride are highly emissive, with long phosphorescence lifetimes. In addition, complexes of platinum(II) are of particular interest due to their tendency to display square-planar geometries, allowing axial interactions with the metal centre leading to excited state modification through metal-metal or transient ligand-metal interactions. The utility of such compounds will therefore be explored in the hope of producing novel luminescent sensors for sulfur-containing analytes.

2.1 Complexes of platinum designed for axial thiol interactions

The initial approach explored in this section is modelled on the SO_2 sensors reported by Van Koten.[165] The ability of the amine pincer ligand complex (Figure 2.1a) to form an axial interaction with SO_2 suggests that interaction with thiols may also be possible. This complex, however, does not display any luminescence in fluid solutions. It was hoped that replacing one aliphatic amine with a pyridyl substituent will activate radiative decay from charge-transfer or ligand-centred excited states involving the new phenylpyridine moiety whilst maintaining the ability to reversibly bind to sulfur (Figure 2.1). It is certainly the case that many platinum complexes with the phenylpyridine ligand display bright luminescence in fluid solutions.[193,194]

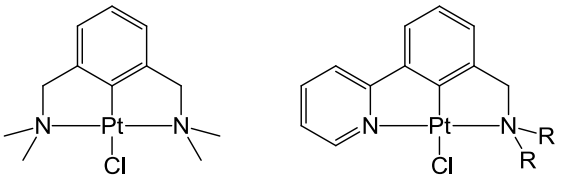

Figure 2.1 a) Known SO_2 sensor b) Proposed general structure for new sensors.

2.1.1 N^C^N binding ligands with inequivalent nitrogen donors

In the design of a potential terdentate ligand which can bind in an N^C^N mode containing both a phenylpyridine fragment and an amine, possibly the simplest structure would be 3-(2-pyridyl)benzylamine (pybzaH), shown in Figure 2.2.

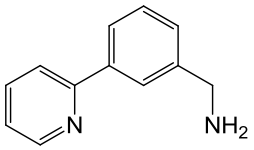

Figure 2.2 3-(2-pyridyl)benzylamine (pybzaH).

The synthesis of this ligand was carried out using the Stille reaction which provides a convenient method for C-C bond-forming reactions between aryl rings. This reaction is one of a range of palladium-catalysed cross-coupling reactions which are commonly used to link aryl or vinyl halides to a variety of functionalised molecules including aryl-boronic acids (Suzuki coupling), alkenes (Heck reaction) and alkynes (Sonogashira coupling). In the case of the Stille reaction, an aryl stannane is used and the mechanism for this reaction is shown in Scheme 2.1.

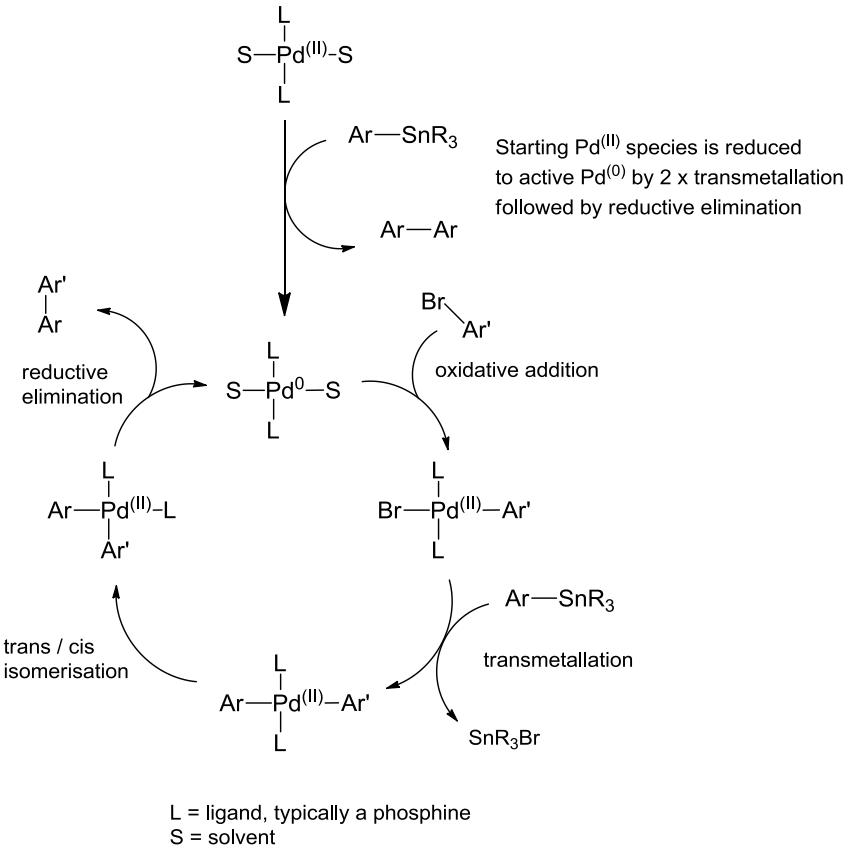

Scheme 2.1 Mechanism of the Stille reaction. When a Pd(II) catalyst is used, an equivalent molar amount of the homo-coupled stannane is produced in the reduction of the catalyst to Pd(0).

Scheme 2.2 shows the synthesis of pybzaH by a Stille reaction between 3-bromobenzonitrile and 2-(tri-n-butylstannyl)pyridine followed by reduction of the nitrile to the primary amine using borane in THF.

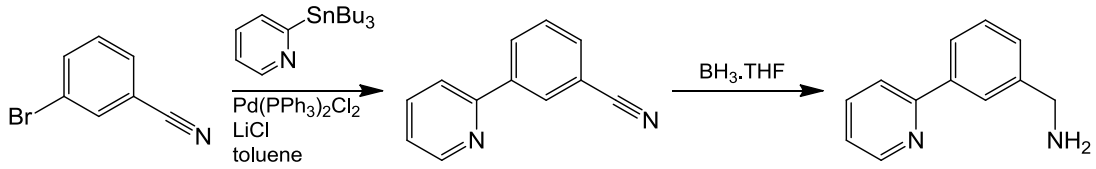

Scheme 2.2 Stille cross-coupling reaction between 3-bromobenzonitrile and 2-(tri-n-butylstannyl)pyridine followed by reduction with borane in THF.

With a quantity of this ligand available, various modified analogues could also be synthesised by reactions with the amine group. Firstly, the synthesis of a tertiary amine would be a useful structure to complement pybzaH, and would also avoid potential problems with the reactivity of the primary amine upon complexation with platinum. As noted in Section 1.3.3, the utility of

cyclometallated amine pincer complexes as SO_2 sensors is impaired by nitrogen substituents larger than a methyl group so the potential ligand N,N-dimethyl-3-(2-pyridyl)benzylamine (dmpybzaH) was regarded as the most suitable structure. While primary amines will readily react with methyl iodide to give methyl substituted amines, this reaction generally leads to quaternary amine salts. Instead, the Eschweiler-Clarke reaction was used which provides a simple route to methyl-substituted tertiary amines by successive reductive amination steps.[195] This method conveniently yielded the desired dmpybzaH ligand as shown in Scheme 2.3.

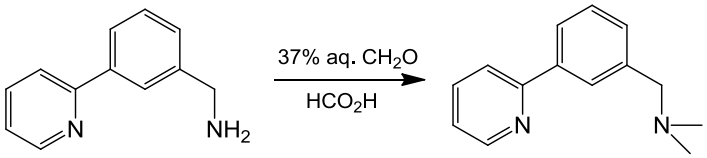

Scheme 2.3 Reductive amination using formaldehyde and formic acid to give dmpybzaH (Eschweiler-Clarke reaction).

It was also considered to be of interest to explore other 'mixed nitrogen donor' N^C^N ligands and so, in addition to the pyridine-amine ligands, other potential ligands were synthesised. The reaction of pybzaH with benzaldehyde provided a simple method for the synthesis of a potential N^C^N ligand with one pyridine donor and a substituted imine as shown in Scheme 2.4.

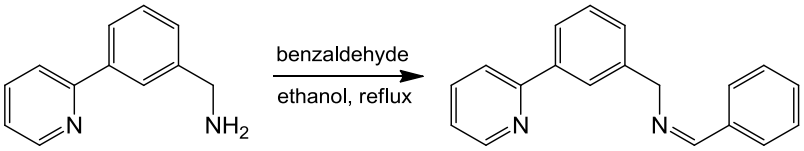

Scheme 2.4 Synthesis of N-(3-(2-pyridyl)benzyl)benzylimine (pybzbiH).

A novel piperidine containing structure was also synthesised using a tandem S_N2-Michael addition analogous to a procedure reported by Bunce *et al.* for the synthesis of N or S containing heterocycles.[196] This required the preparation of an an iodo-enone compound via a Wittig-type reaction and a halide exchange. The reaction of this compound with pybzaH gave the new potential ligand ethyl 1-(3-(2-pyridyl)benzyl)piperidin-2-yl acetate (pybzpipH) as shown in Scheme 2.5. This ligand is particularly of interest due to the ester pendant on the

piperidine ring; if this ester were to be hydrolysed to the carboxylic acid this could provide a ligand with the potential to chelate the platinum centre in an N^C^N^O binding mode (Figure 2.3).

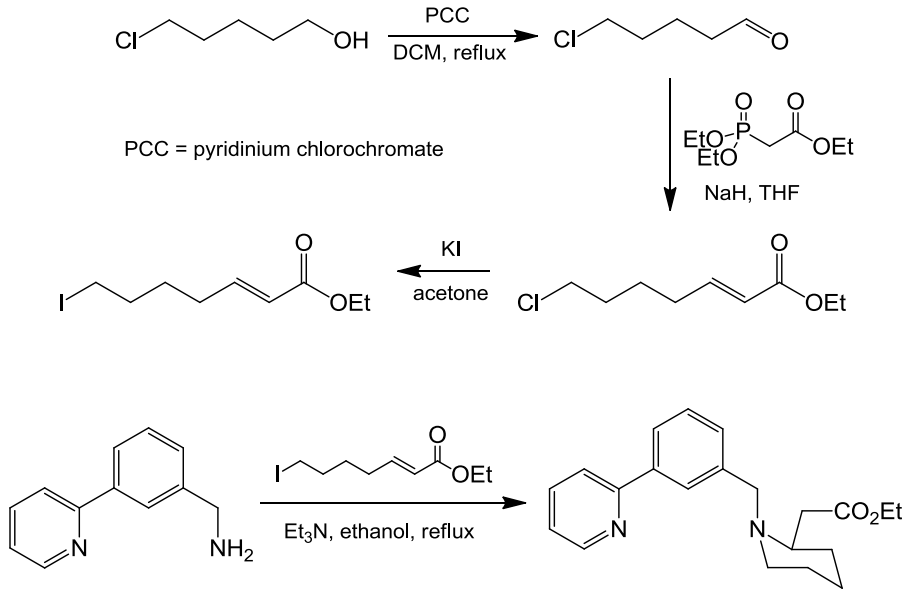

Scheme 2.5 Preparation of iodo-enoate and tandem S_N2-Michael addition to give pybzpipH.

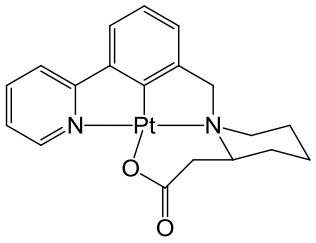

Figure 2.3 Potential N^C^N^O binding of hydrolysed pybzpip.

2.1.2 Attempted complexation of N^C^N ligands with platinum

N^C^N bound complexes with platinum(II) are commonly synthesised by heating K_2PtCl_4 with the appropriate ligand in degassed acetic acid as reported for the original synthesis of [Pt(dpyb)Cl].[61] For certain ligands, the reaction has been carried out in mixtures of acetonitrile and water, in some cases without the need for oxygen-free conditions.[62,197]

The complexation of the four ligands was attempted using these two methods, however all reactions attempted resulted in complicated mixtures. While it did appear from the consumption of the red $PtCl_4^{2-}$ and the precipitation of

yellow/brown solids that some complexation was occurring, the clean reaction to a single product observed in the synthesis of other Pt(N^C^N) complexes did not occur. Further evidence for the partial success of the reactions was observed in the ^{1}H NMR spectra of the products where some signals at high δ, corresponding to the pyridine H^{6} signal, displayed satellite peaks arising from ^{3}J coupling to ^{195}Pt which has nuclear spin = ½ and comprises ~33% naturally occurring platinum. Extraction or washing of the crude products with solvents such as ethanol or DCM in some cases yielded products of slightly increased purity, however no pure complexes could be obtained by these methods. In addition, the purification of such complexes by column chromatography is generally unsuitable as many are poorly soluble and suffer from instability with respect to oxidation when in solution. Also, dissociation of chloride in solution leads to immobilisation of the resulting cationic species on the chromatography support.

The best sample obtained was from the reaction of the dimethylamino ligand (dmpybzaH) with K_2PtCl_4 in 3:1 MeCN:H_2O at reflux, followed by extraction of the crude product with ethanol after washing with water. In the first attempt this gave only a trace of sparingly soluble yellow solid which showed a ^{1}H NMR spectrum consistent with the desired complex [Pt(dmpybza)Cl]. The spectrum clearly shows ^{195}Pt satellites on one low field aromatic doublet, H^{6} on the pyridine, and two aliphatic signals, the CH_2 and methyl groups (Figure 2.4). This is consistent with the ligand in an N^C^N bound pincer configuration.

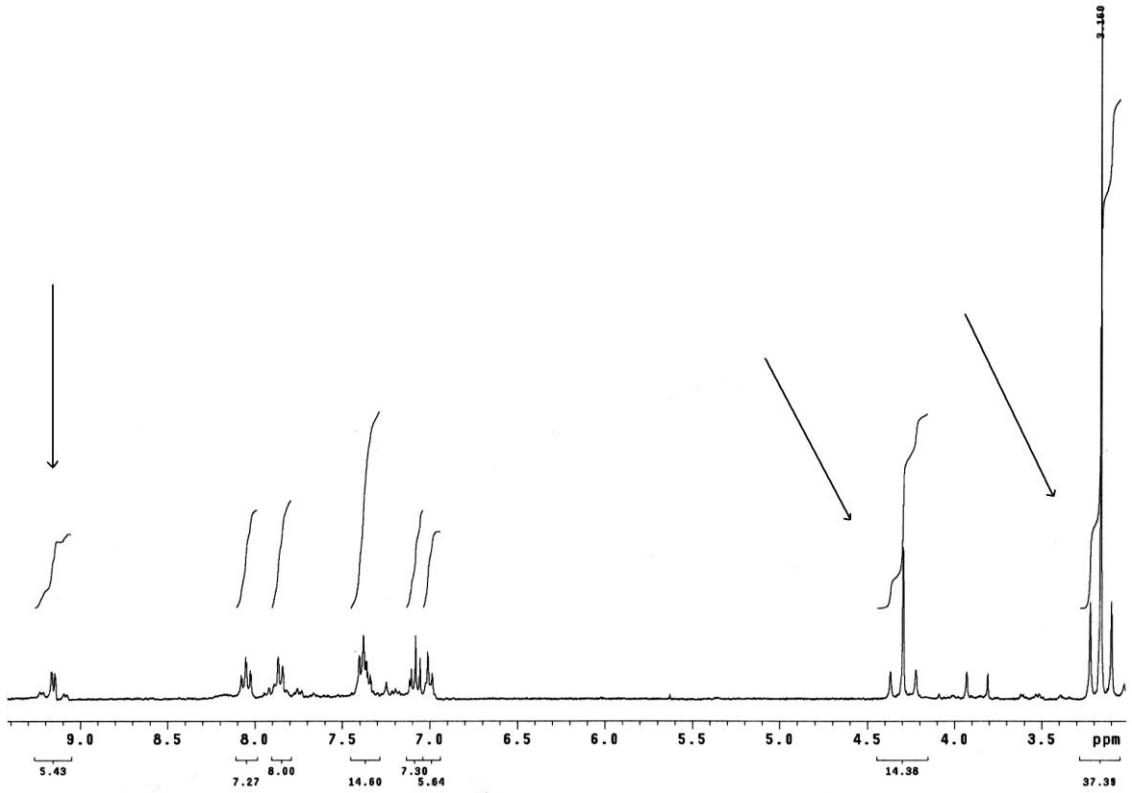

Figure 2.4 300 MHz ^{1}H NMR spectrum of [Pt(dmpybza)Cl] in d_6-acetone. Arrows indicate signals with ^{195}Pt satellites.

The NMR also showed traces of at least one other Pt complex indicated by another H^6-py signal at δ ~ 9.6 (not shown in Figure 2.4). There was also a significant amount of this complex remaining in the residual solid after extraction. Attempts to repeat the complexation on a larger scale gave a very impure sample.

The complexation of pybzaH was also attempted using a method analogous to that used in the synthesis of the dimer *bis*(2-phenylpyridine-N,C)(μ-dichloride)diplatinum[198] as shown in Scheme 2.6. It was hoped that the use of this method would encourage the formation of a platinum dimer with the phenylpyridine fragment of dmpybzaH followed by either spontaneous cleavage by the pendant amine or cleavage by a subsequent reaction. This procedure, however, also failed to yield a pure complex for study.

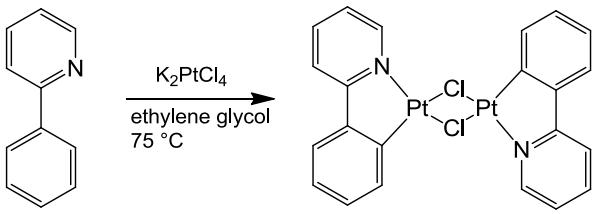

Scheme 2.6 Reaction of ppy with K_2PtCl_4 in 2-ethoxyethanol gives the dichloro-bridged dimer.[198]

It was evident from these results that complexation of these ligands is less specific than that of 1,3-di(2-pyridyl)benzene and its derivatives.[62] This may be a result of weaker coordination of the platinum between the two nitrogen donors prior to cleavage of the C–H bond. Aromatic nitrogen donors have significant π acceptor abilities which leads to stronger bonding interactions with ligands such as pyridine compared to aliphatic amines. Therefore, while there is sufficient interaction to induce C-H activation in dpybH, this may not be the case with these new ligands. It is also possible that alternate complexes are formed in the reactions since with these ligands there are three sites where cyclometallation can occur which give distinct complexes, thus leading to the observed mixtures (Figure 2.5).

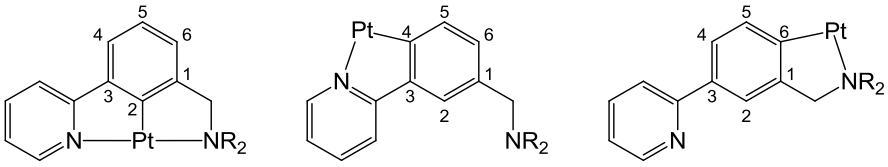

Figure 2.5 Possible binding modes in mixed nitrogen N^C^N ligands.

Since complexation of the new N^C^N ligands could not be achieved by direct reaction with K_2PtCl_4, an approach similar to that used by Soro *et al*[199] in overcoming competitive binding modes of palladium with dpybH was attempted. In this report, reaction of the N^C^N ligand was first carried out with mercury(II) acetate in the presence of LiCl giving a [Hg(dpyb)Cl] complex with metallation only observed at the 2 position of the benzene. This was then transmetallated using $Pd(OAc)_2$ to give the required palladium complex.

It was hoped that the reaction of $Hg(OAc)_2$ with the new N^C^N ligands would also give selective metallation at the desired 2 position and the resulting

complex could be transmetallated with $Pt(PPh_3)_4$. Unfortunately, here, as was the case with the direct reaction of the novel N^C^N ligands with platinum, no mercury complexes were successfully isolated and so the transmetallation with platinum could not be attempted.

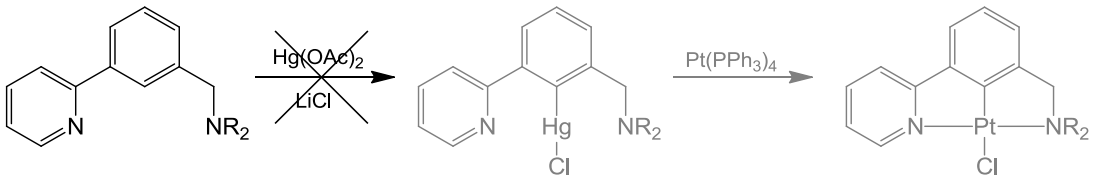

Scheme 2.7 Attempted synthesis of a mercury complex followed by transmetallation with $Pt(PPh_3)_4$.

It appears that, while these 'mixed nitrogen' N^C^N ligands could be of particular interest in the design of new platinum N^C^N complexes, there are particular problems associated with their use. It seems the case that poorer binding prior to cyclometallation and the asymmetric nature of the ligands leads to significant problems in the isolation of platinum complexes with these ligands. This is unfortunate, since the properties of such complexes would likely be distinct from both Pt(N^C) complexes and Pt(N^C^N) complexes with fully aromatic ligands.

2.2 Platinum N^C^N complexes with thiolate ligands

In addition to the attempted synthesis of novel Pt(N^C^N) complexes with mixed nitrogen donors, the effects of the introduction of thiolate ligands into the coordination sphere of platinum were explored. As discussed previously, the complex [Pt(dpyb)Cl] is highly phosphorescent and it was hoped that the substitution of the relatively labile chloride ligand with thiols or thiolates in this and related complexes would lead to new excited-state properties.

2.2.1 Synthesis of complexes

Two starting complexes were synthesised using the ligands 1,3-di(2-pyridyl)benzene (dpybH) and methyl-3,5-di(2-pyridyl)benzoate (mdpybzH) to give the complexes [Pt(dpyb)Cl] and [Pt(mdpybz)Cl] using reported methods[62]

(Scheme 2.8). For simplicity, the coordinated ligands dpyb and mdpybz will be referred to as L^1 and L^2 respectively.

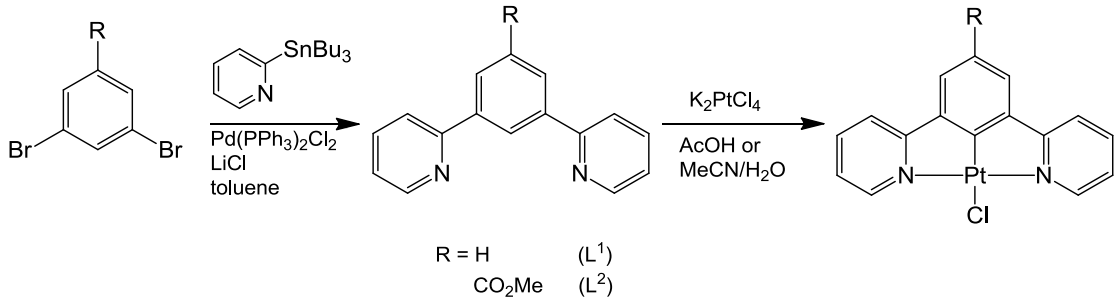

Scheme 2.8 Synthesis of $[PtL^1Cl]$ and $[PtL^2Cl]$.

With these two complexes in hand, substitution reactions were carried out with the thiols sodium methanethiolate (mtNa), thiophenol (tpH), 4-methylthiophenol (mtpH), 4-methoxythiophenol (motpH) and 4-nitrothiophenol (ntpH).

Initially, substitutions with the aryl thiols were attempted without the use of base in both degassed and aerated methanol solutions at room temperature. While this led to some substitution of chloride by thiolate, in most cases no more than 30% conversion was achieved using these methods. Instead, it was discovered that reaction of the complexes with a degassed solution of thiolate prepared by treatment of the thiol with potassium *tert*-butoxide led to precipitation of the desired complexes at room temperature. The resulting yellow, orange or red compounds were purified by successive washings with H_2O, methanol and diethyl ether giving the complexes $[PtL^n(tp)]$, $[PtL^n(mtp)]$, $[PtL^n(motp)]$ and $[PtL^n(ntp)]$.

The complexes $[PtL^1(mt)]$ and $[PtL^2(mt)]$ were prepared by the treatment of the corresponding chloride complexes with aqueous sodium methanethiolate suspended in methanol, also at room temperature. The synthesis of these thiolate containing complexes is summarised in Scheme 2.9.

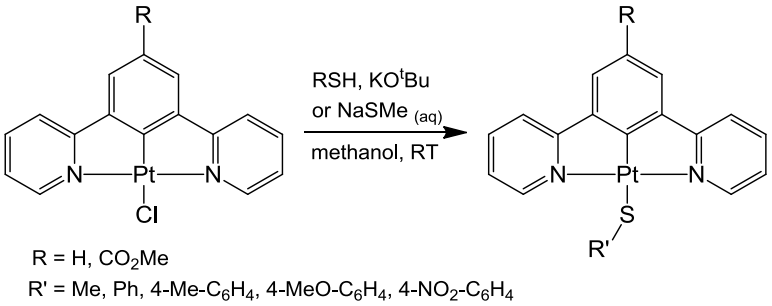

Scheme 2.9 Synthesis of [PtL^n(thiolate)] complexes.

2.2.1.1 Characterisation of the complexes

The newly synthesised complexes showed ^{1}H NMR spectra similar to those of their parent chloride complexes with the addition of peaks expected from the aromatic thiolates or from the methyl group in [PtL^n(mt)]. When the characterisation of these complexes was attempted by electrospray mass spectrometry, however, no peaks relating to the expected molecular ion were observed. Instead, a number of dimetallic clusters were indicated by isotopic patterns in the spectra, with the species $[(Pt(N\hat{}C\hat{}N))_2(SAr)]^+$ and $[(Pt(N\hat{}C\hat{}N))_2(S)(SAr)]^+$ being the most commonly observed in the case of the complexes containing aromatic thiolates. Presumably these species involve bridging sulfur atoms between platinum centres, since the tendency of sulfur to bridge between metals is known. In fact, in related complexes with terpyridine ligands, a solid state structure of $\{[Pt(tpy)]_3S\}$ has been reported by X-ray crystallography.[200] The ES mass spectra of the complexes with an mt ligand instead tended to show trimetallic clusters of the form $[3M]^+$, $[3M\text{-}Me]^+$, $[3M\text{-}2Me]^+$ and $[3M\text{-}3Me]^+$. The likely structure of these, again, features bridging sulfur atoms, with or without methyl substituents, possibly a ring-type structure such as that shown in Figure 2.6.

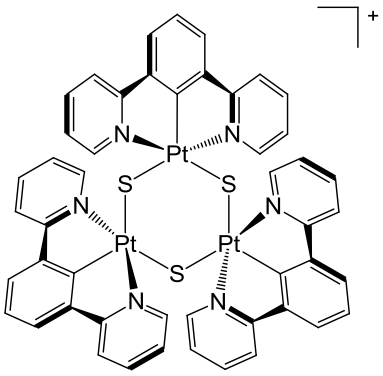

Figure 2.6 Possible gas phase structure observed in ES MS. Similar ions were also observed with 1, 2 or 3 methyl substituents on the sulfurs.

In contrast, electron ionisation mass spectrometry showed the expected molecular ion peaks and molecular ion fragments such as $[M\text{-thiolate}]^+$. In addition, commonly observed features of EI MS were observed such as the tropylium ion, $[C_7H_7]^+$, in complexes with the tolyl thiolate.

2.2.1.2 Stability of the complexes

While it appears that all the complexes are stable indefinitely in the solid state, data from NMR spectra suggest that the complexes tend to decompose over time when left in solution. This is most noticeable in complexes with the motp ligand and, in general, the complexes containing L^1 are less stable than their counterparts with L^2. This is evident from the appearance of signals in the ^{1}H NMR spectrum which apparently correspond to new species containing the Pt(N^C^N) fragment. It is likely, therefore, that the thiolate ligands are prone to dissociation, being replaced by a solvent molecule, possibly with concurrent oxidation to disulfides in air making re-coordination of this ligand impossible. This is supported by the observation that $[PtL^n(motp)]$ are the least stable complexes since these will be the most electron-rich thiolates and thus most prone to dissociation.

2.2.2 Photophysical and electrochemical properties of $[PtL^n(thiolate)]$ complexes

It was immediately obvious upon synthesis that the introduction of the thiolate ligand led to a significant change in the absorption properties of the Pt(N^C^N)

complexes from their colour. While the starting chloride complexes are pale yellow in colour, the precipitated products showed strong colouring from yellow to red depending upon the thiolate.

The photochemical and electrochemical properties of these ten new complexes were therefore studied in order to determine what changes in the observed excited states had occurred by the introduction of these new ligands.

2.2.2.1 Absorption spectra

The absorption spectra were measured at room temperature in dichloromethane solution and all show strong absorption bands in the far UV region similar to those observed in the chloride complexes arising from π-π^* transitions in the aromatic ligand systems.[62] In the near UV and visible region the complexes display moderately intense absorption up to around 500 nm. Absorbance data for the complexes are summarised in Table 2.1 and absorption spectra from 350 nm to 700 nm for the two series, [PtL^1(thiolate)] and [PtL^2(thiolate)] are shown in Figures 2.7 and 2.8.

Complex	Absorption λ_{max} / nm (ε / $dm^3mol^{-1}cm^{-1}$)[(a)]
[PtL^1(mt)]	332 (7490), 365 (5660), 377 (5980), 465 sh (2210)
[PtL^1(tp)]	363 (6420), 376 (6510), 452 sh (2040)
[PtL^1(mtp)]	363 (5700), 377 (5990), 460 sh (1820)
[PtL^1(motp)]	365 (7490), 377 (7580), 463 sh (2450)
[PtL^1(ntp)]	305 (15500), 335 (8950), 376 sh (11000), 415 (17100), 455 sh (13600)
[PtL^2(mt)]	307 (19800), 330 sh (11600), 369 (6690), 468 (3250)
[PtL^2(tp)]	330 sh (12200), 360 (7350), 373 (7780), 465 (2890)
[PtL^2(mtp)]	332 sh (11100), 362 (7380), 375 (7820), 469 (2720)
[PtL^2(motp)]	332 sh (11600), 362 (7490), 376 (7660), 472 (3150)
[PtL^2(ntp)]	305 (17000), 333 sh (8030), 378 (11500), 415 (17800), 455 sh (13800)

Table 2.1 Absorption maxima at λ > 300 nm for [Pt(N^C^N)(thiolate)] complexes in CH_2Cl_2 at room temperature. (a) all bands in the observed range obey the Beer-Lambert law up to ca. 7 × 10^{-4} mol dm^{-3}.

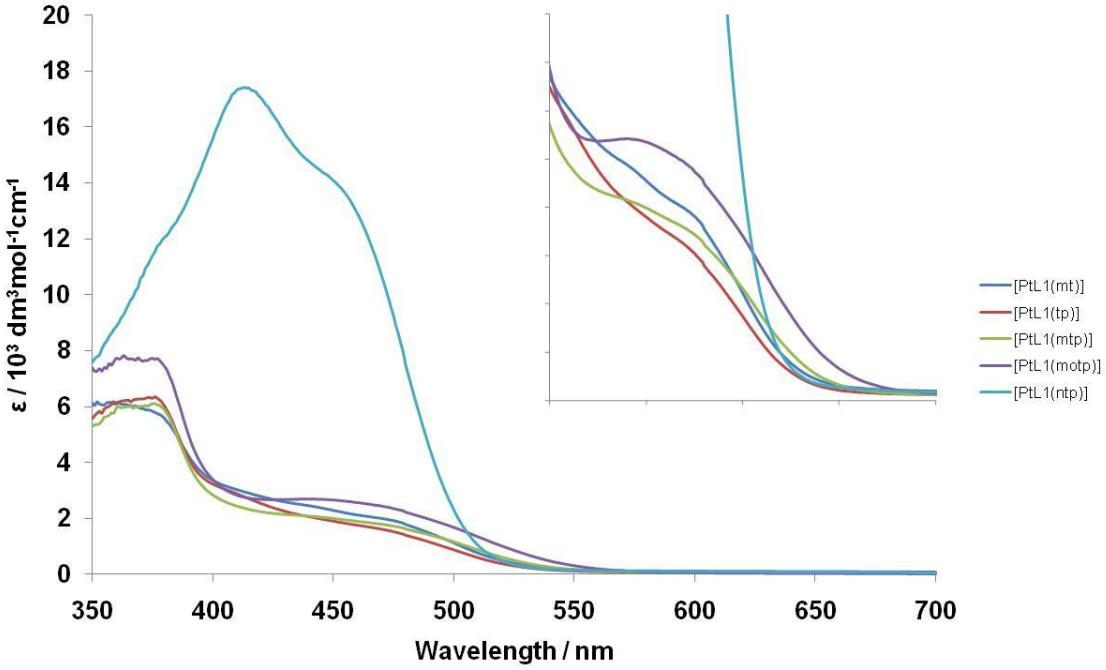

Figure 2.7 Absorption spectra of [PtL^1(thiolate)] complexes in CH_2Cl_2 at room temperature.

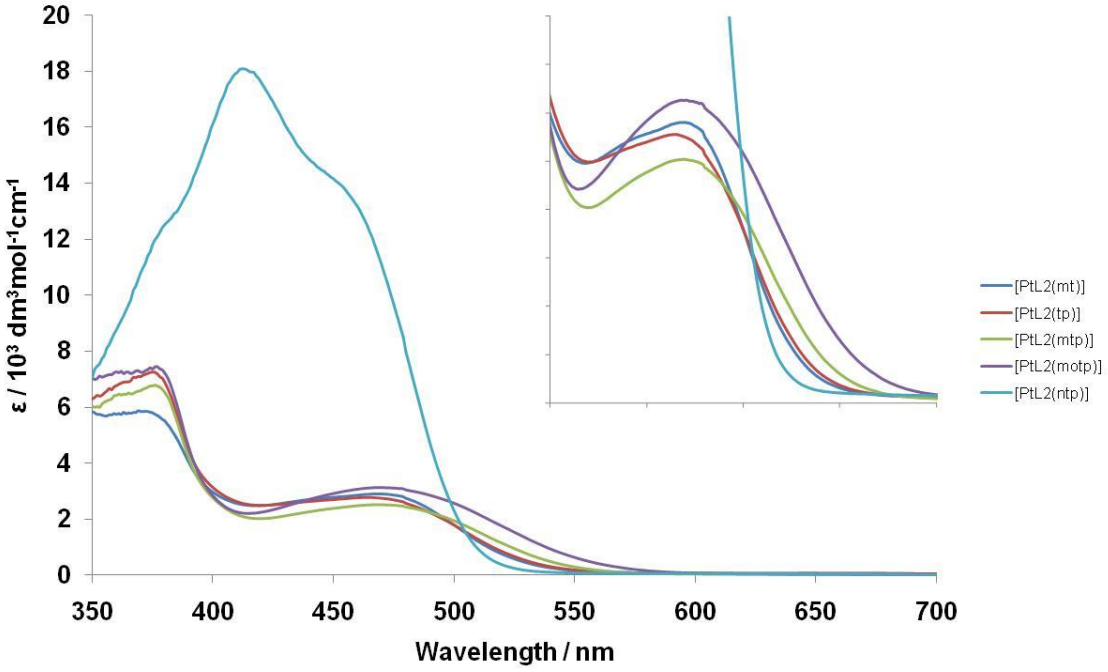

Figure 2.8 Absorption spectra of [PtL^2(thiolate)] complexes in CH_2Cl_2 at room temperature.

The lower energy band structure in the [PtL^n(thiolate)] complexes is similar throughout the series with the noticeable exception of [PtL^1(ntp)] and [PtL^2(ntp)]. In all complexes, excluding those containing the ntp ligand, in addition to the band at ~375 nm corresponding to the parent complex, these complexes display a broad absorption whose position is dependent on the thiolate ligand. For the aromatic thiolates with either L^1 or L^2 this band is red shifted in the order tp <mtp <motp within the series, while the complexes of L^1 appear blue shifted in comparison to their L^2 counterparts. As a result of these shifts this lowest energy band displayed by, for example [PtL^2(motp)], is distinct from the higher energy band at ~375 nm while in more blue-shifted examples such as [PtL^1(tp)] overlap of this band with those at higher energy make it appear as more of a shoulder. The non-aromatic thiol complexes [PtL^1(mt)] and [PtL^2(mt)] show very similar profiles to the corresponding [PtL^1(tp)] and [PtL^2(tp)] complexes.

In the case of the complexes with the ntp ligand, the low energy band structure is dominated by an intense absorption (ε ~ 17000 dm^{3}mol^{-1}cm^{-1}) at 415 nm in both complexes. This band displays shoulders at both the higher and lower energy which correspond to the two lowest energy bands observed in the other complexes. This strong feature is undoubtedly related to π-π^* absorption in the

thiolate ligand appearing at low energy due to conjugation with the nitro-substituent, while the shoulders are likely to be related to the more general band structure present throughout the series.

2.2.2.2 Absorption solvatochromism in the complexes

The effect of solvent polarity on the absorption of the complexes was also investigated. In addition to the above spectra recorded in dichloromethane, spectra were also run in acetonitrile, tetrahydrofuran and toluene. Absorption spectra for a selection of the complexes in these solvents are shown in Figure 2.9. In the UV region, the bands show very little solvatachromic shift, as expected for transitions of π-π^* character. Equally, in the complexes [PtL^1(ntp)] and [PtL^2(ntp)], the intense band at 415 nm also shows very little change with the solvent polarity. The bands between 350 nm and 400 nm show a small negative solvatochromic shift, however the most striking change is a large negative solvatochromic shift in the lowest energy band/shoulder. In most cases, this band shows a blue shift of up to 50 nm between the non-polar toluene and more polar acetonitrile. This indicates a relatively large change in dipole moment between the ground state and the lowest energy excited state, indicative of some type of charge-transfer state.

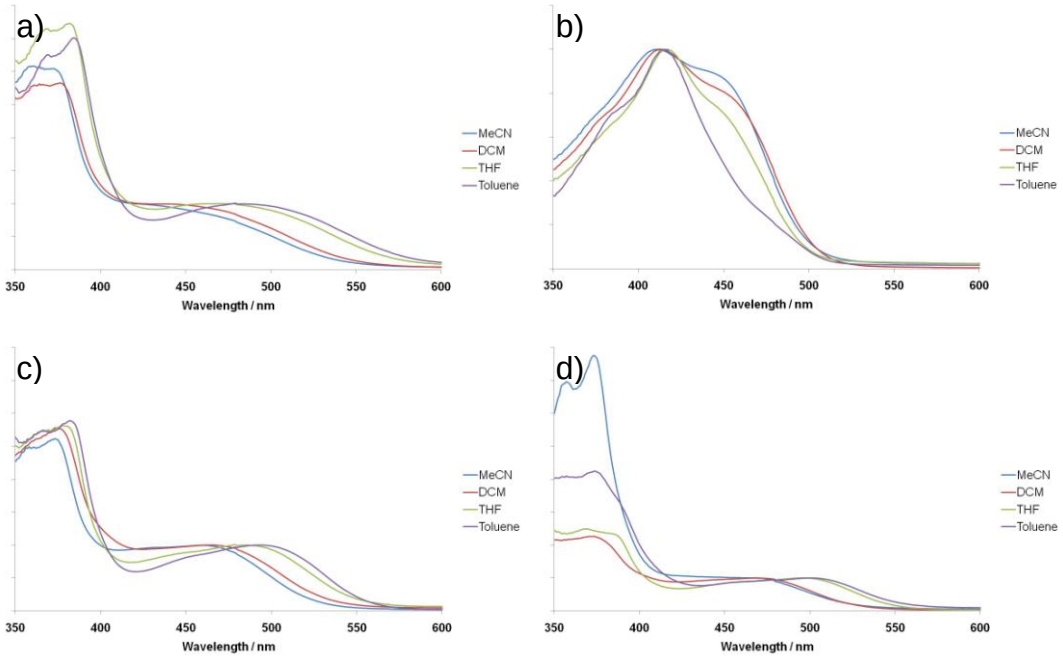

Figure 2.9 Normalised absorption spectra of a) [PtL^1(motp)], b) [PtL^1(ntp)], c) [PtL^2(tp)] and d) [PtL^2(mt)] in various solvents at room temperature.

2.2.2.3 Electrochemical properties

The redox potentials for the new complexes in dichloromethane solution were measured using cyclic voltammetry (CV) with Bu_4NPF_6 as the supporting electrolyte. The resulting data are recorded in Table 2.2.

The first reduction wave of the complexes occurs at around – 1.4 V and in most cases is partially reversible at high scan rates. When using scan rates of less than 100 mVs^{-1}, the return wave becomes poorly defined. The first oxidation wave, however, while being well defined is irreversible for all complexes and varies noticeably depending upon the structure of the thiolate ligand. The most readily oxidised complexes are [PtL^1(mt)] and [PtL^2(mt)], both with E_p^{ox} ~ –0.35 V. The values for the remaining aryl thiolate complexes appear in the region –0.3 V to +0.3 V, with the ease of oxidation relating qualitatively to the electron donating ability of the para-substituent of the thiolate ligand, e.g. OMe > Me > H > NO_2.

Complex	E_p^{ox} / V *(a)*	$E_{1/2}^{red}$ / V *(a)* (Δ / mV)	$E_p^{ox} - E_{1/2}^{red}$
[PtL^1(mt)]	–0.36	–1.36	1.72
[PtL^1(tp)]	–0.03	–1.39 (240)	1.36
[PtL^1(mtp)]	–0.10	–1.36 (220)	1.26
[PtL^1(motp)]	–0.12	*(b)*	
[PtL^1(ntp)]	+0.26	–1.36	1.62
		–1.73 (160)	
[PtL^2(mt)]	–0.35	*(b)*	
[PtL^2(tp)]	–0.07	–1.44 (290)	1.37
[PtL^2(mtp)]	–0.11	–1.38 (280)	1.27
[PtL^2(motp)]	–0.22	–1.43 (250)	1.21
[PtL^2(ntp)]	+0.13	–1.45 (200)	1.58
		–1.87 (90)	

Table 2.2 Electrochemical data for [PtL^n(thiolate)] complexes, recorded in CH_2Cl_2 at room temperature using Bu_4NPF_6 (0.1 M) as the supporting electrolyte. Scan rate 100 mVs^{-1}. Peaks quoted relative to Fc+ | Fc. (a) Peak potentials are given for the oxidations, all of which were irreversible, and for those reductions where the return wave was ill-defined. For reductions showing return waves, the quoted values refer to $E_{½}$ and the peak-to-peak separation is given in parentheses. (b) The reduction wave was poorly defined for this complex.

2.2.2.4 Photoluminescence of the complexes

All ten complexes with thiolate ligands are luminescent in dilute room temperature solutions upon excitation in the UV or blue regions of the spectrum and display broad, structureless emission bands with maxima in the region of 600-750 nm. The emission spectra, luminescence lifetimes and quantum yields of the complexes were measured in room temperature degassed solutions, while the spectra and lifetimes were also recorded at 77 K in 2:2:1 diethylether / isopentane / ethanol (EPA). The data from these measurements, as well as the calculated rate constants for both radiative and non-radiative decay, are given in Table 2.3. This table also includes the rate of quenching by oxygen in room temperature solutions.

The normalised emission spectra for the complexes at room temperature are shown in Figure 2.10 and Figure 2.11. In terms of the position and band-shape, the emission profiles of the two complexes with a methane thiolate ligand are essentially identical to those of the corresponding complexes containing thiophenolate ligands which appear at the highest energy. The emission of the aromatic thiolate complexes are red shifted in the order tp < mtp < motp < ntp for the series with the L^1 ligand while the pattern in the series with L^2 is similar with tp < mtp < motp ~ ntp. This sequence at first inspection seems unrelated to the electronic properties of the thiolate ligand substituents.

A similar discontinuity is observed in the data obtained for the lifetimes and quantum yield. While the complexes show a decrease in luminescence lifetime in line with decreasing emission energy in the sequence tp > mtp > motp, the complexes [PtL^n(ntp)] show much longer lifetimes, in the order of microseconds, rather than nanoseconds. Equally, the quantum yields for the ntp complexes are discontinuous with the other aromatic thiolate complexes which again, decrease with decreasing emission energy.

Another notable feature is that while the [PtL^1(thiolate)] complexes are predominantly blue shifted compared to the [PtL^2(thiolate)] analogues, again, the two ntp complexes do not meet with this trend, instead showing a small red shift in the emission of [PtL^1(ntp)] compared to [PtL^2(ntp)].

Complex	Emission λ_{max} / nm	Φ_{lum} $\times 10^2$	τ / ns degassed	k^Q_{O2} / 10^8 $M^{-1}s^{-1}$ *(a)*	k_r / 10^3 s^{-1} *(b)*	$\sum k_{nr}$ / 10^4 s^{-1} *(b)*	Emission 77 K λ_{max} / nm	Emission 77 K τ / μs
[PtL^{1}Cl]	*491, 524, 562*	*60*	*7200*	*9.1*	*83*	*5.5*	*486, 516, 548*	*6.4*
[PtL^1(mt)]	636	2.6	430	54	60	230	538	6.6
[PtL^1(tp)]	634	17	770	65	220	110	539	6.8
[PtL^1(mtp)]	661	6.9	510	53	140	180	548	7.4
[PtL^1(motp)]	691	1.4	48	110	290	2100	570	8.2
[PtL^1(ntp)]	714	0.21	7400	2.6	0.28	13	574, 610	760
[PtL^{2}Cl]	*481, 513, 550*	*58*	*8.0*	*4.4*	*72*	*5.3*		
[PtL^2(mt)]	642	3.8	510	90	75	190	558	6.6
[PtL^2(tp)]	643	16	880		180	95	550	7.8
[PtL^2(mtp)]	668	6.0	370		160	250	581	8.9
[PtL^2(motp)]	701	0.35	29		120	3400	597	9.5
[PtL^2(ntp)]	703	0.64	11300	8.0	0.57	8.8	567, 603	470

Table 2.3 Luminescence data for the platinum complexes in CH_2Cl_2 solution at 298 K and in EPA at 77 K (EPA = diethylether / isopentane / ethanol, 2:2:1 v/v.) *(a)* k^Q_{O2} is the bimolecular rate constant for quenching by molecular oxygen at 298 K, estimated from the relative emission intensities in degassed and aerated solutions, assuming $[O_2]$ at 1 atm pressure of air = 2.2 mmol dm^{-3}. *(b)* k_r and $\sum k_{nr}$ are the radiative and non-radiative rate constants estimated from the quantum yield and lifetime at 298 K. [PtL^{1}Cl] and [PtL^{2}Cl] are included for comparison.

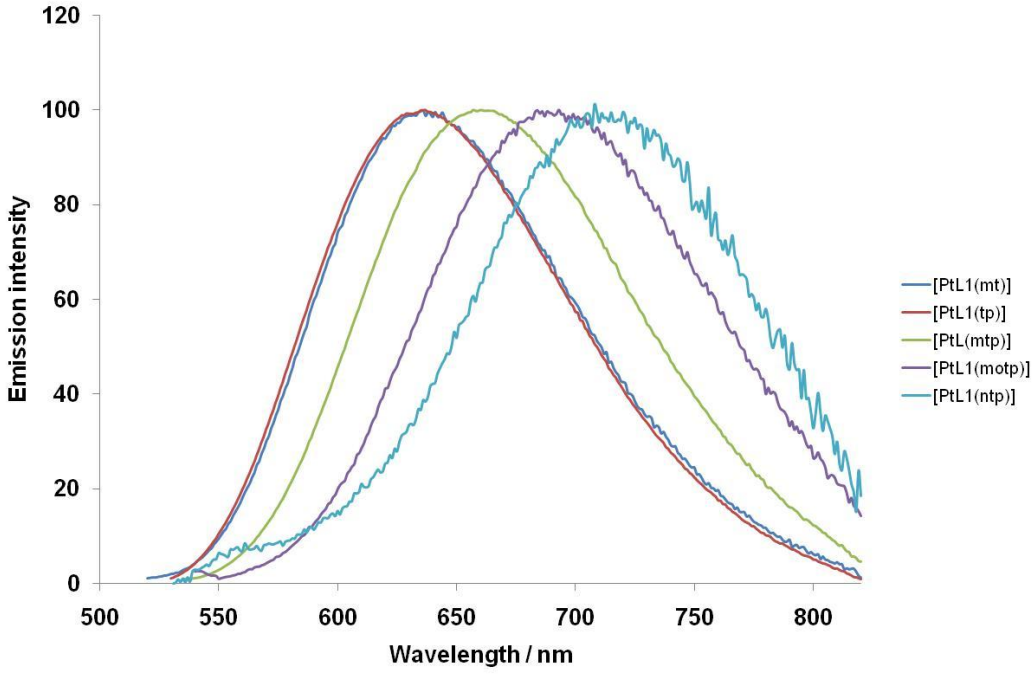

Figure 2.10 Normalised emission spectra of [PtL^1(thiolate)] complexes. Emission intensity in arbitrary units.

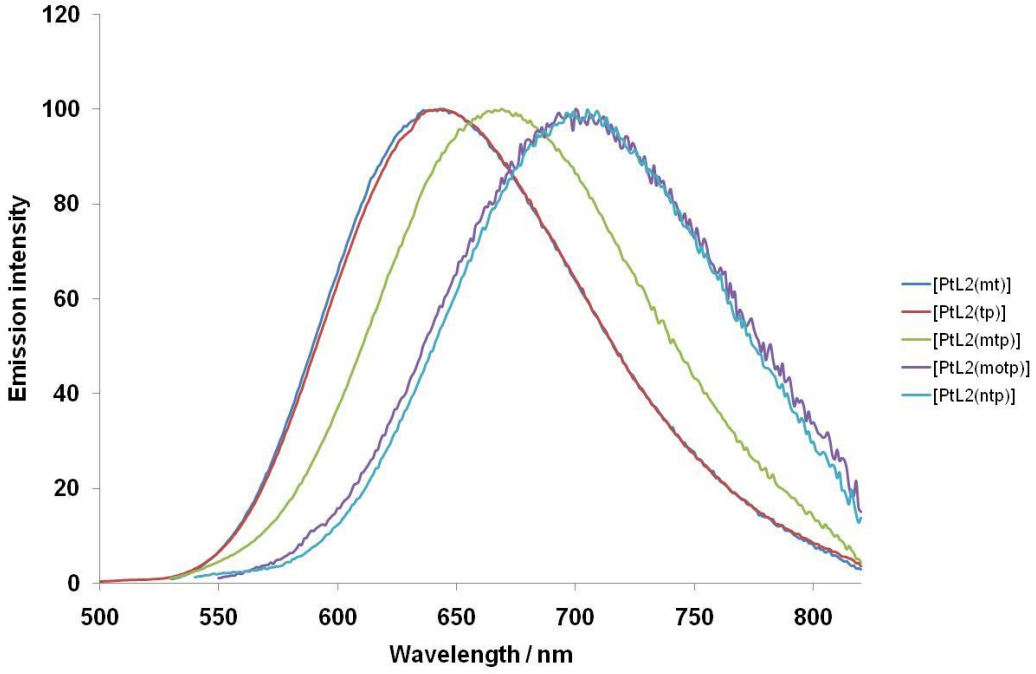

Figure 2.11 Normalised emission spectra of [PtL^2(thiolate)] complexes. Emission intensity in arbitrary units.

At low temperature, the complexes show blue shifted emission as would be expected for charge transfer excited states due to decreased molecular re-orientation at low temperature leading to a smaller Stokes' shift. The spectra of the complexes at 77 K in EPA are shown in Figure 2.12 and Figure 2.13.

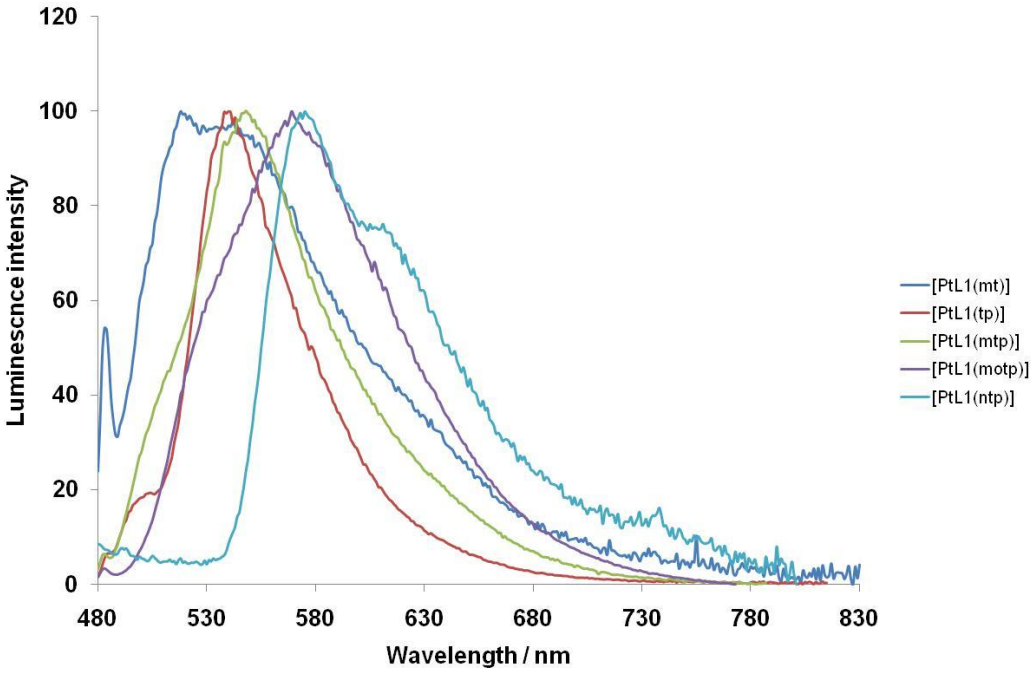

Figure 2.12 Normalised emission spectra of [PtL^1(thiolate)] complexes at 77 K in EPA. Emission intensity in arbitrary units.

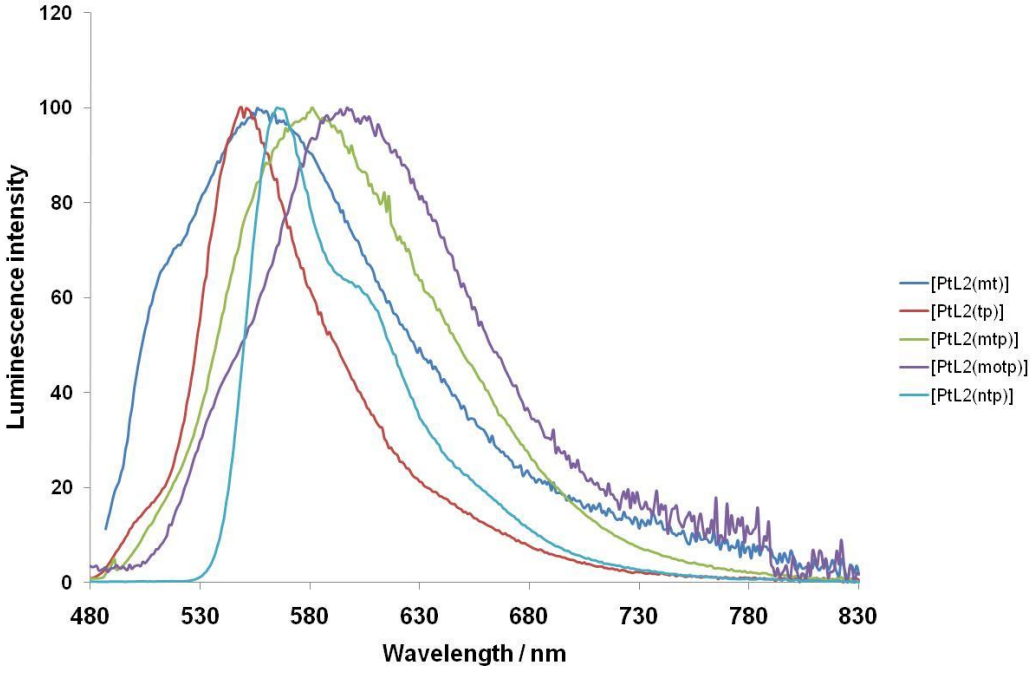

Figure 2.13 Normalised emission spectra of [PtL^2(thiolate)] complexes at 77 K in EPA. Emission intensity in arbitrary units.

The complexes [PtL^n(tp)], [PtL^n(mtp)] and [PtL^n(motp)] all show structureless bands and, in line with the trend observed at room temperature, the emission wavelength increases in the sequence tp < mtp < motp. Emission from the two [PtL^n(mt)] complexes is, again, at similar energy to the corresponding tp

complex, however the emission profile of these appears noticeably broader than the aromatic thiolate complexes. While the emission of the complexes L^2 are, again, red-shifted compared to the corresponding L^1 analogues in most cases, [PtL^1(ntp)] and [PtL^2(ntp)] show the opposite trend, as observed in the room temperature data. In addition, the emission of these two complexes at low temperature is structured, unlike that of the other eight complexes. This band structure appears to be vibrational in character and implies that the emissive state in these two complexes may be ligand-centred in character.

2.2.3 Discussion of photophysical and electrochemical results

The introduction of thiolate ligands, particularly dithiolates, into platinum diimine complexes commonly results in the observation of new low energy excited states which have been variously assigned to thiolate→diimine LLCT,[201,202] Pt→thiolate MLCT[203] and mixed Pt/thiolate→diimine charge transfer[204,205] states. It is apparent from the observed data in the synthesised class of [Pt(N^C^N)(thiolate)] complexes that the substitution of chloride with a thiolate ligand has similarly led to new excited states. Figure 2.14 shows a comparison between the absorption and emission spectra for Pt(N^C^N) complexes with a chloride or a thiolate ligands.

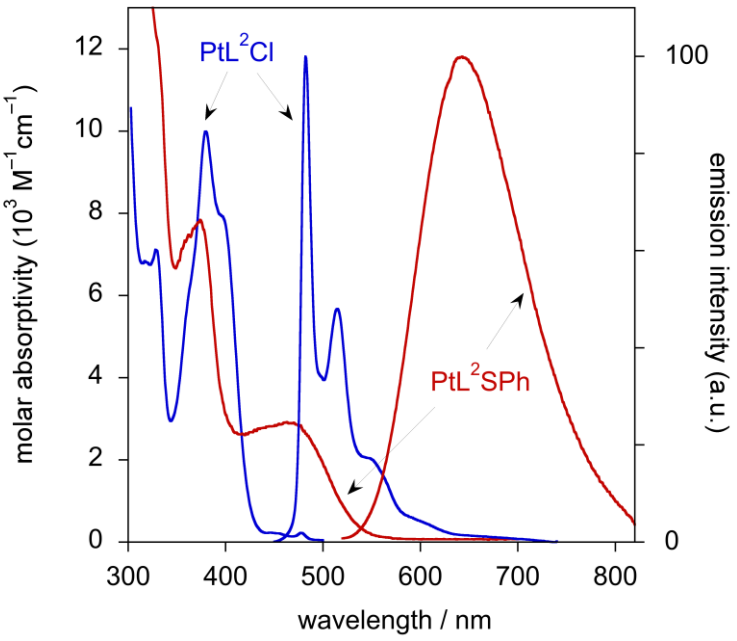

Figure 2.14 Comparison of absorption and emission spectra for [PtL^2Cl] and [PtL^2(tp)].

In absorption, while the high energy features are similar between the thiolate and chloride complexes, in the near UV and visible range (λ > 300 nm) there is a marked contrast between the new compounds and the previously reported chloride complexes. [PtL^{1}Cl] and [PtL^{2}Cl] display relatively intense absorption at around 375 nm and the lowest energy feature is a shoulder at around 400 nm (excluding weak spin-disallowed transitions which are observed in these complexes at ~480-490 nm). As discussed above, the introduction of thiolate ligands leads to lower energy absorption bands resulting from charge-transfer transitions.

The change in emission properties is equally clear from the comparison. While the parent complexes [PtL^{1}Cl] and [PtL^{2}Cl] both show strong, long-lived, vibrationally structured phosphorescence from a $^3\pi$-π^* excited state,[62] the emission of the new thiolate complexes is significantly red-shifted and structureless. Again, this is indicative of new low energy charge transfer states.

2.2.3.1 Consequences of thiolate substitution on the ground state

The electrochemical data indicate that, while the oxidation of the complexes is largely affected by the substituents of the thiolate ligand, the first reduction is largely unaffected by these changes. The trend in these data is consistent with the HOMO being either localised on the thiolate ligand or the metal centre where an increase in the electron donating properties of the para-substituent leads to more facile oxidation. The relative invariance of the reduction potential indicates that the LUMO is most likely localised on the N^C^N ligand. This would imply that the lowest energy absorption arises from transitions of MLCT or LLCT character.

These possible assignments are also indicated by the trends in absorption maxima for the lowest energy band. Stronger electron withdrawing groups on the N^C^N ligand lead to a red-shift, consistent with lowering the LUMO energy, while more strongly electron donating groups on the thiolate also result in a red-shift by increasing the energy of the HOMO. The solvatochromic effect observed for the lowest energy absorption band indicates a transition with a

large change in dipole moment, giving weight to an assignment of MLCT, LLCT or a mixed metal-thiolate to N^C^N charge transfer.

2.2.3.2 The effect of thiolate substitution on the emissive state

The results from studies of the emission of these complexes is complicated somewhat by noticeable discontinuities in the data with respect to the complexes [PtL^1(ntp)] and [PtL^2(ntp)]. If these two complexes are discounted, the trends in the data show that an assignment of ^{3}MLCT, ^{3}LLCT or a mixed metal-thiolate to N^C^N CT state is justified. Again, the observed trends in emission maxima in relation to the ligand substituents follow those observed in absorption which would be expected for excited states of this character.

2.2.3.3 Adherence to the energy gap law

The energy gap law states that for related excited states, the non-radiative decay constant is related to the energy of emission from these states. While the precise mathematical expression is quite complex, it can be reduced to the relatively simple expression shown in Equation 2.1.[206,207]

$$\ln(k_{nr}) = a - \left(\frac{\gamma_0}{\hbar\omega_m}\right)E_{00}$$

Equation 2.1

Where k_{nr} is the rate of non-radiative decay, a is a constant resulting from the simplification, $\hbar\omega_m$ is the average medium-frequency acceptor mode coupled to the excited state, E_{00} is the energy of the zero-zero transition and γ_0 is given by

$$\gamma_0 = \ln\left(\frac{E_{00}}{\hbar\omega_m S_m}\right) - 1$$

Equation 2.2

S_m is the Huang-Rhys factor (electron-vibration coupling constant).

This indicates that for a series of complexes with the same excited state, a plot of $ln(k_{nr})$ vs emission energy should give a straight line. The data for the ten [PtL^n(thiolate)] complexes, treated in this manner is shown in Figure 2.15

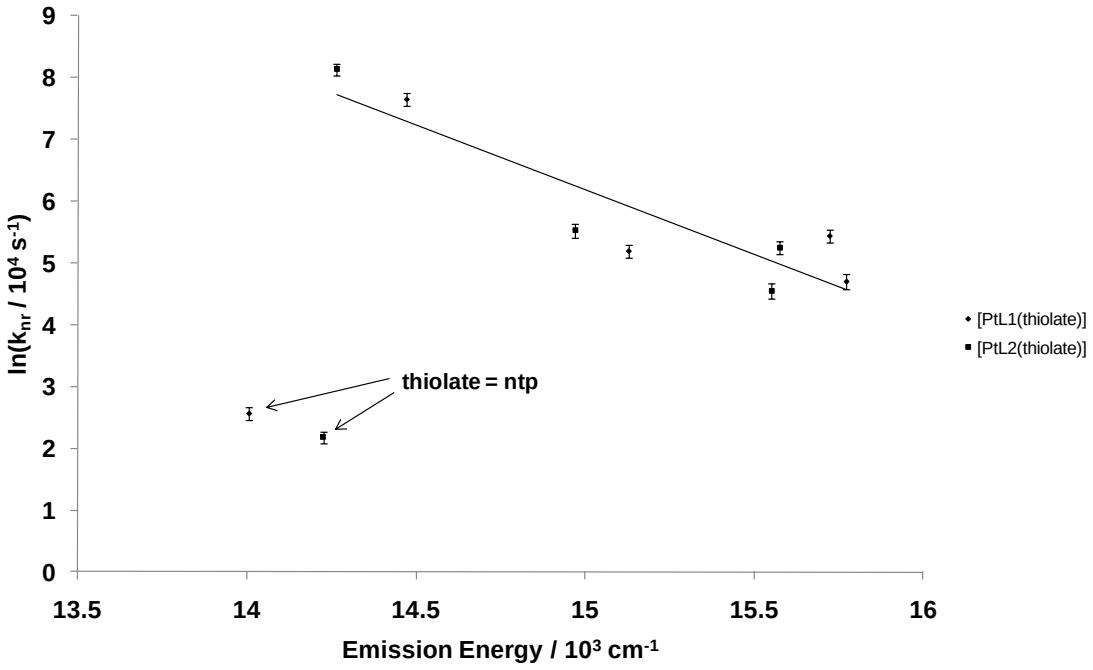

Figure 2.15 Plot of $\ln(k_{nr})$ vs emission energy showing linear best fit for all complexes except those with 4-nitrothiophenolate ligands. Error bars indicate calculated error based on 10% uncertainty in measured τ and Φ values.

The plot of $\ln(k_{nr})$ shows a reasonable fit for all the complexes with the exception of [PtL^1(ntp)] and [PtL^2(ntp)]. A linear fit to the data excluding these two complexes gives a value of $R^2 = 0.82$. In this case, a relatively large variation from a perfect linear fit is not unexpected due the simplification of the mathematical expression, which does not account for variation in vibrational mode frequencies and other excited state properties which affect the measured data. These data clearly indicate that while eight complexes from the series obey the energy gap law, the emission displayed by complexes with the ntp ligand must be from a different type of excited state. This observation is supported by the noticeably different excited state properties, particularly the long luminescence lifetime. One final point of note from these data is that the complexes with methanethiolate ligands lie within the fit of the aromatic thiolate complexes indicating that these share a similar excited state. This makes an assignment of a thiolate(π)→N^C^N(π^*) ^{3}LLCT phosphorescence unlikely since the [PtL^n(mt)] complexes do not possess the required delocalised π system. An assignment of S(p)→N^C^N(π^*) LLCT is still feasible although it is likely that

such a state will have a large amount of MLCT character due to Pt-S bonding interactions.

2.2.3.4 Excited state assignment for [PtL^n(thiolate)] complexes

Despite the difference in emission in the ntp complexes, when comparing absorption data with that from electrochemical studies, the absorption energy of the lowest energy band and the band-gap between oxidation and reduction waves show a strong linear correlation for all four aromatic thiolates, particularly within the series with the ligand L^2 (Figure 2.16). This correlation, however, is not repeated with the emission energies with [PtL^2(ntp)] lying considerably away from the co-linearity of the other three complexes.

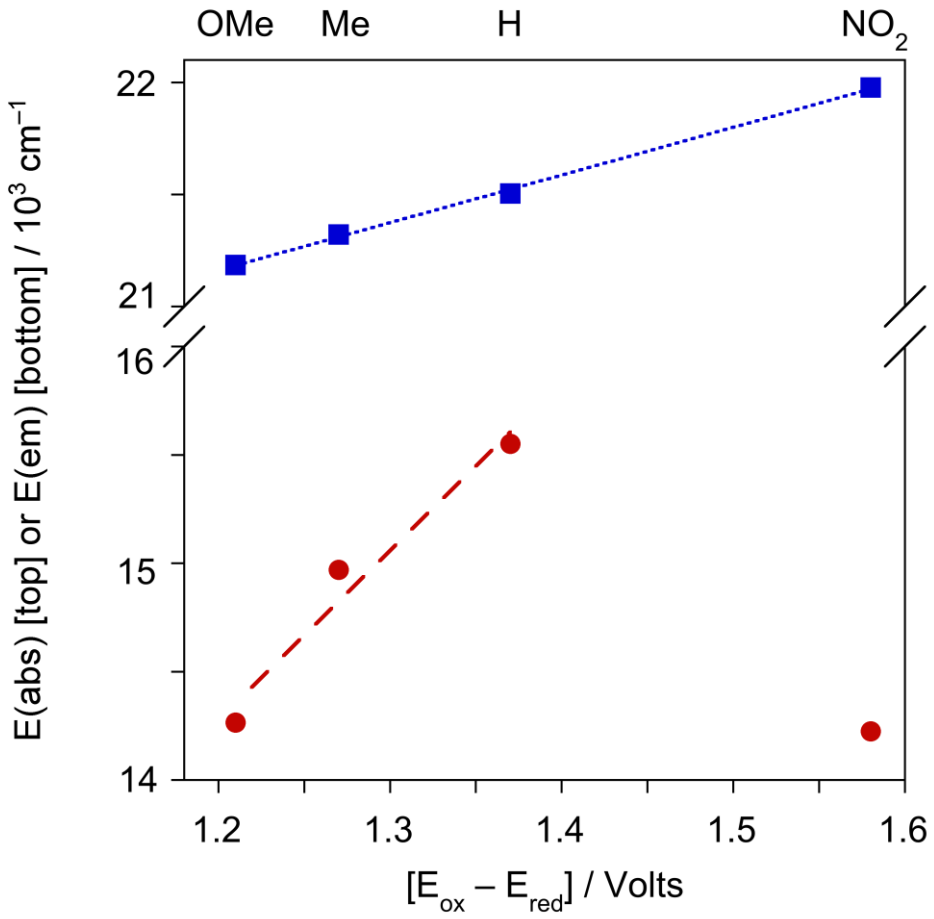

Figure 2.16 Plot of lowest energy absorption maxima (squares) and emission maxima (circles) vs. electrochemical bandgap for PtL^2 complexes with aromatic thiolates.

This supports the notion that while in the singlet manifold, the first excited state is of the same type throughout the whole series, in the triplet manifold, the

lowest excited state is indeed of a different character, as indicated by the study of the energy-gap law.

Given the data that have been discussed, it seems that the most likely assignment for the phosphorescence from the majority of the new complexes is of Pt-S(π)→N^C^N(π^*) charge transfer character since it is strongly affected by the para-substituent of the aromatic thiolates while a pure ^{3}LLCT excited state is ruled out by the aliphatic thiolate complexes. It has been confirmed that the emission from this state obeys the energy gap law with increased k_{nr} upon decreasing emission energy leading to lower quantum yields and shorter observed lifetimes. The radiative decay constants for the eight complexes exhibiting this emissive state are also relatively similar.

In contrast, the introduction of a nitro group into the thiolate ligand leads to a new, lower energy triplet excited state from which phosphorescence is observed. The observation of vibrational structure in the low-temperature emission, coupled with a luminescence lifetime of the order of microseconds, indicate a predominantly ligand-centred or intra-ligand excited state localised on the 4-nitrothiophenolate ligand. A similar effect has been observed in the study of platinum diimine acetylide complexes, where the use of a nitro group on the acetylide ligand causes a switch from ^{3}MLCT to acetylide $^3\pi$-π^* phosphorescence.[207]

The proposed energy level structure and the effect of the nitro group on the emissive state are shown in Figure 2.17. This structure accounts for a mixed metal-sulfur HOMO giving charge transfer to N^C^N(π^*) in the majority of the complexes and to thiolate(π^*) in complexes with ntp. The proposed structure also accounts for the blue shift of [PtL^2(ntp)] compared to [PtL^1(ntp)] since the inductive effect of the ester will reduce the ligand field effect of the cyclometallated carbon. This results in a decrease in energy of the metal centred orbitals which, in turn, will reduce the energy of the Pt-S filled orbital interaction.

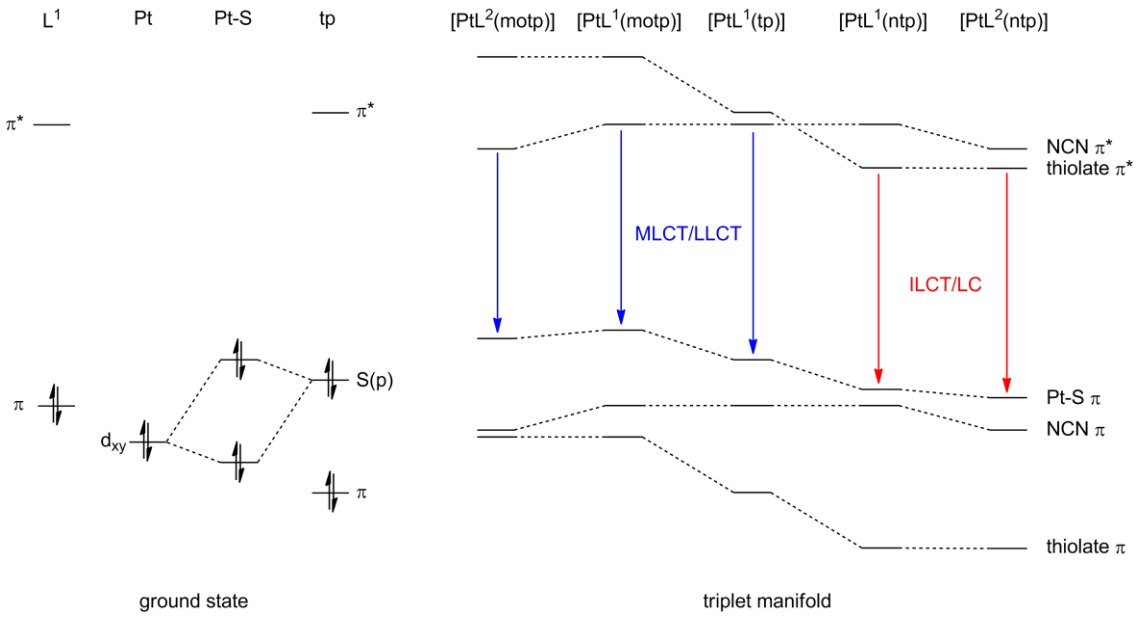

Figure 2.17 Schematic diagram of proposed energy level structure in [PtL^n(thiolate)] complexes. A Pt-S(π) filled orbital interaction accounts for mixed MLCT/LLCT character and the observed effect of the N^C^N substituent on [PtL^n(ntp)] LC state.

2.2.4 DFT calculations on [Pt(N^C^N)(thiolate)] complexes

In order to further investigate the excited states of these complexes, some preliminary DFT calculations were performed using these structures. Firstly, geometry optimisations were carried out to ensure the structures were in their lowest energy conformation and from these coordinates the ground state electronic states were calculated. This gave an indication of the localisation of the HOMO and LUMO in these systems. Representations of these orbitals for some of the [Pt(N^C^N)(thiolate)] complexes are shown in Figure 2.18 and Figure 2.19.

The data from these calculations show that in all cases the HOMO contains a large contribution from the sulfur orbitals as well as involvement of the metal and the aromatic substituent, where present. Meanwhile the LUMO is located on the N^C^N ligand, also with a small amount of metal involvement. This is consistent with the model inferred from the absorption and electrochemical data that the lowest energy singlet state is primarily of mixed metal/thiolate to N^C^N charge transfer character. It is also the case that there are only very small observed differences upon the change from L^1 to L^2.

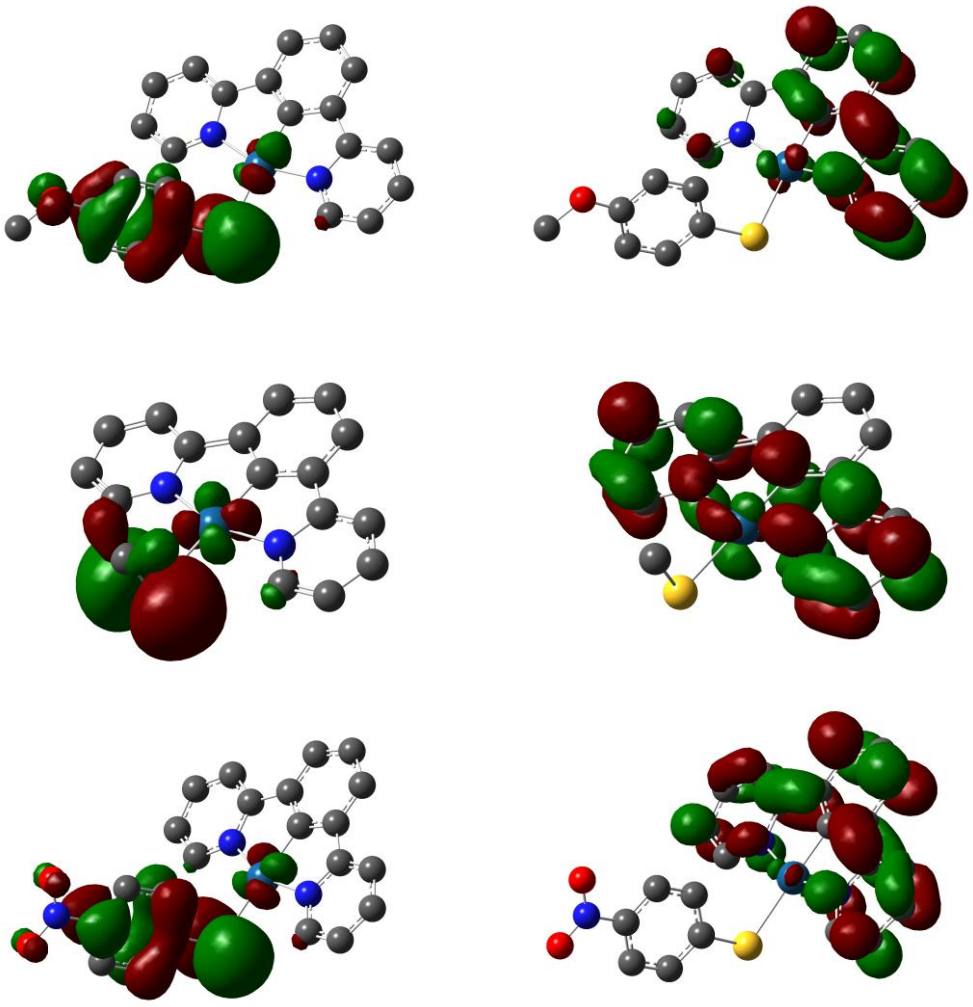

Figure 2.18 HOMO and LUMO plots for [PtL^1(motp)], [PtL^1(mt)] and [PtL^1(ntp)] calculated using the B3LYP hybrid functional with LanL2DZ and 6-31G basis sets.

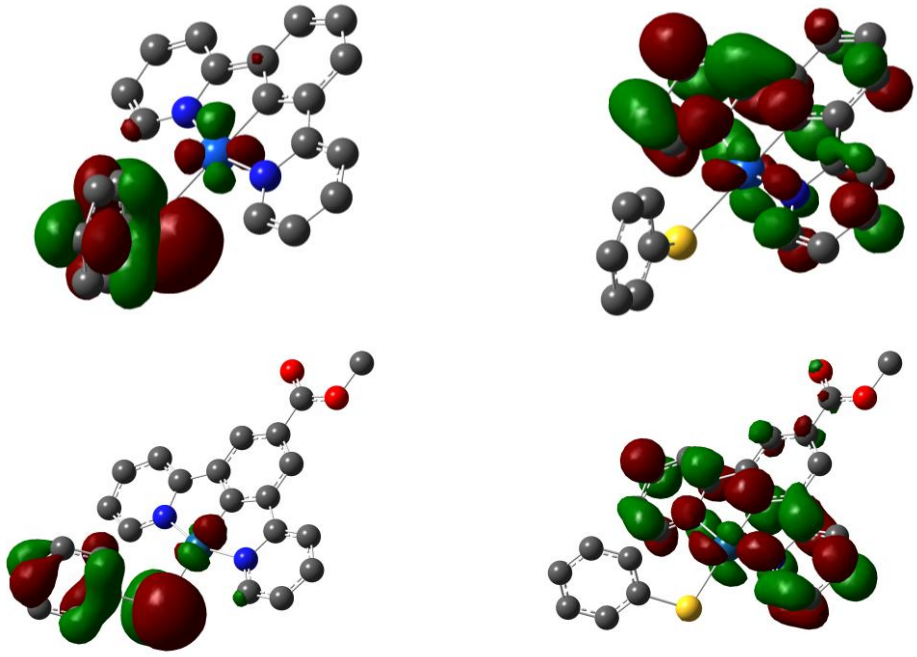

Figure 2.19 Comparison of [PtL^1(tp)] and [PtL^2(tp)] HOMO and LUMO plots calculated using the B3LYP hybrid functional with LanL2DZ and 6-31G basis sets.

As the calculated data is for the singlet manifold, these results are not representative of the emissive behaviour of the complexes. Recent, more detailed work within the group carried out by Gemma Freeman on these systems indicates that for the complexes excluding those with ntp ligands, the calculations for the triplet states confirm the assignment of emission from triplet states of the same character as the lowest singlet state. The situation with [PtL^1(ntp)] and [PtL^2(ntp)] is found to be more complicated with various orbital contributions to the lowest energy transition.[208] This, again, is consistent with the observation that introduction of a nitro group leads to a change in the emissive state.

2.3 Concluding remarks

A series of potential N^C^N coordinating ligands have been synthesised in the hope that when complexed to platinum, these will lead to both luminescence under ambient conditions as well as potential axial interactions with sulfur-containing analytes. These ligands, therefore, contained one pyridyl substituent as part of a ppy moity to activate luminescence while also containing alternate nitrogen donors. The formation of complexes with these ligands was unsuccessful, most likely due to poor chelation prior to cyclometallation and multiple binding modes.

In addition, a series of platinum complexes have been synthesised containing a fully aromatic N^C^N ligand and a thiolate ligand. The effect of the introduction of these thiolate ligands into the coordination sphere of platinum has been investigated. In contrast to the 'parent' [Pt(N^C^N)Cl] complexes which show vibrationally structured ^{3}LC emission, these novel complexes instead, show predominantly mixed metal/thiolate to N^C^N charge transfer emission, with the exception of complexes containing 4-nitro-phenylthiolate ligands, where the electronic properties of this particular ligand lead to a new, low lying ^{3}LC(thiolate) or ^{3}ILCT(thiolate) emissive state.

Chapter 3

Cyclometallated iridium complexes with thiolate ligands

3 Cyclometallated iridium complexes with thiolate ligands

Complexes of iridium with polypyridyl and cyclometallating ligands are becoming more common in studies involving photoluminescence as discussed in the introduction. Complexes containing bidentate N^C bound and terdentate N^C^N bound ligands often show particularly bright phosphorescence. However the studies on the introduction of alternate ligands in these systems still lag behind other, more heavily studied, second and third row transition metals. In this chapter the interactions of cyclometallated complexes of iridium with thiolate ligands are discussed.

3.1 Bis(2-phenylpyridine)iridium complexes

As discussed in the introduction, the complex $[Ir(ppy)_3]$ displays strong phosphorescent emission from ^{3}MLCT excited states. Related heteroleptic compounds with only two cyclometallating ppy ligands can be utilised in a variety of applications depending on the ancillary ligands used. In many cases, these complexes can be synthesised through the intermediacy of the dimer $[Ir(ppy)_2(\mu\text{-}Cl)]_2$, formed by the treatment of $IrCl_3$ with two equivalents of ppy, and its subsequent cleavage with the desired ancillary ligand. In much of the reported work on such compounds, any aromatic ligands used to form such complexes are bidentate species such as 2,2'-bipyridine (bpy). Conversely, there have been very few reports of cleavage with monodentate aromatic ligands to give mixed systems of the type $[Ir(ppy)_2(L)(X)]$ where L and X are neutral and anionic ligands respectively.

The results of one study show that cleavage of the $[Ir(ppy)_2(\mu\text{-}Cl)]_2$ dimer with various neutral ligands to give $[Ir(ppy)_2(L)Cl]$ complexes is possible and subsequent reactions using AgOTf will yield mixed complexes of the type $[Ir(ppy)_2(L)(L')]^+$.[209] In addition using AgOTf in the initial reaction with the dimer leads to $[Ir(ppy)_2(L)_2]^+$ species, including the bis-pyridine complex $[Ir(ppy)_2(py)_2]^+$.

It was therefore decided, in the first instance, to explore the cleavage of this dimer with a neutral monodentate ligand, giving a monometallic complex with a monodentate chloride ligand that could potentially be displaced by a thiolate as shown in Scheme 3.1.

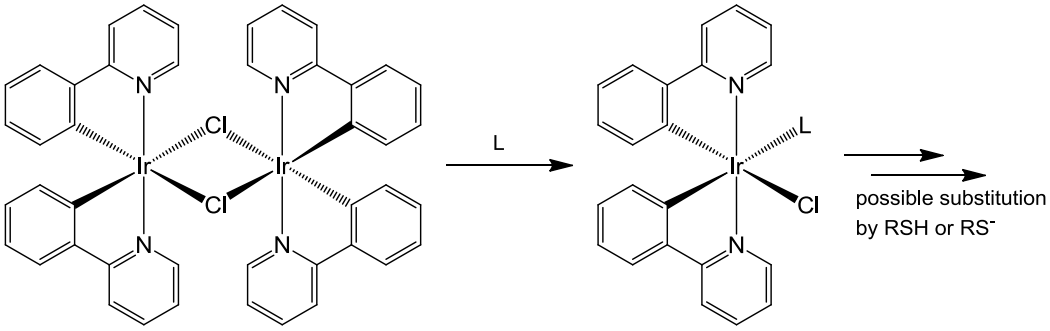

Scheme 3.1 Cleavage of iridium phenylpyridine dimer with a neutral monodentate ligand.

3.1.1 Cleavage of $[Ir(ppy)_2(\mu\text{-}Cl)]_2$ with neutral ligands

Initially, cleavage of the dimer was attempted using pyridine as the neutral ligand in refluxing dichloromethane. This gave a yellow product that could not immediately be identified. It appeared that the resulting material was a single component by TLC and the yielded mass of product after work-up was equivalent to that which would be expected by the stoichiometric addition of pyridine to the dimer. However, the expected product did not appear in either electrospray or MALDI mass spectrometry, which instead showed m/z = 542, 583 or m/z = 536 respectively. These correspond to acetonitrile adducts of an $Ir(ppy)_2^+$ fragment in the electrospray spectrum (i.e. $Ir(ppy)_2(MeCN)^+$ and $Ir(ppy)_2(MeCN)_2^+$) and an $Ir(ppy)_2Cl^+$ fragment in MALDI. ^{1}H NMR, however, clearly showed that the symmetry of the 2-phenylpyridine ligands had been broken as these presented 16 signals indicating that the 5th and 6th coordination sites contained inequivalent species. In addition to the ppy signals, the ^{1}H NMR integrals showed only an additional three proton signals in the form of a broad 2H signal and a 1H signal overlapped by a ppy multiplet, both in the aromatic region. If the product was indeed the expected $[Ir(ppy)_2(py)Cl]$ complex then there should have been another aromatic signal integrating to two protons which was not visible. The aromatic region of the ^{1}H NMR spectrum of the product is shown in Figure 3.1.

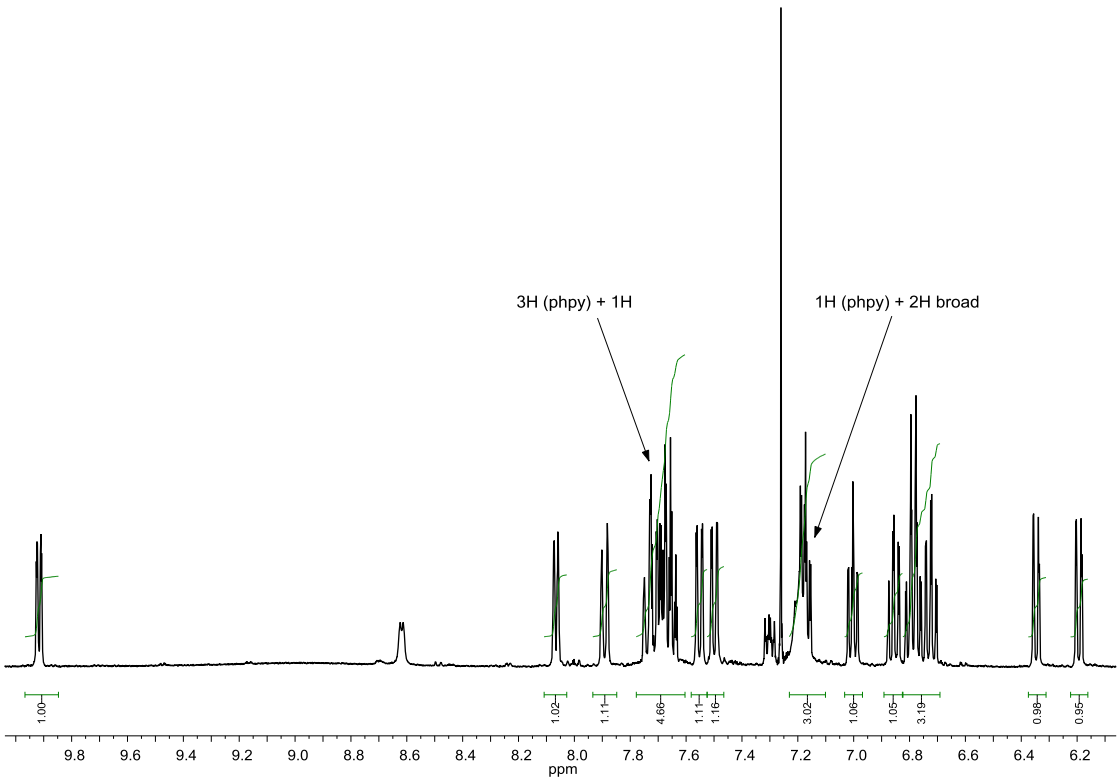

Figure 3.1 ^{1}H NMR (400 MHz) spectrum (aromatic region) of possible [Ir(ppy)$_2$(py)Cl] complex. Smaller impurity signals are free pyridine (also contributing approx 0.6 to integral of 3H (ppy) + 1H multiplet).

The solution to the identification of this unusual product came when, in a second reaction, it was decided to attempt to cleave the dimer using N,N-dimethylaminopyridine (DMAP), rather than pyridine. This reaction, like the first, gave a single product in relatively high yield. In this case, however, the MALDI mass spectrum showed a peak for the expected product at m/z = 623 as well as the fragments corresponding to $(M\text{-}Cl)^+$ and $(M\text{-}DMAP)^+$. With this product as well, however, the ^{1}H NMR spectrum again showed some unusual characteristics. There were, again, 16 separate aromatic signals corresponding to two inequivalent ppy ligands, but in this case there was only one additional broadened signal in the aromatic region with an integral corresponding to two protons. As expected there was also a singlet in the aliphatic region integrating to six protons representing the two methyl groups of the DMAP ligand. Again, there was one signal corresponding to two protons missing compared to what would be expected. One final notable feature of this spectrum, though, was a noticeable symmetrical non-linearity in the baseline between $\delta = 9.5 - 7.5$, which could be viewed as an extremely broadened signal. If this feature was, in fact, a broadened signal corresponding to 2H then this would make the

spectrum consistent with the expected product that had been detected by mass spectrometry.

Looking back at the NMR data for the previous reaction with pyridine it was noticed that this spectrum also contained a similar feature in the aromatic region that could be viewed as an extremely broadened signal, again suggesting that this could be the desired product. It was possible, therefore, that the cleavage of $[Ir(ppy)_2(py)Cl]$ with both py and DMAP had been successful giving the products shown in Figure 3.2 but ^1H NMR signals relating to the ancillary ligand were significantly broadened.

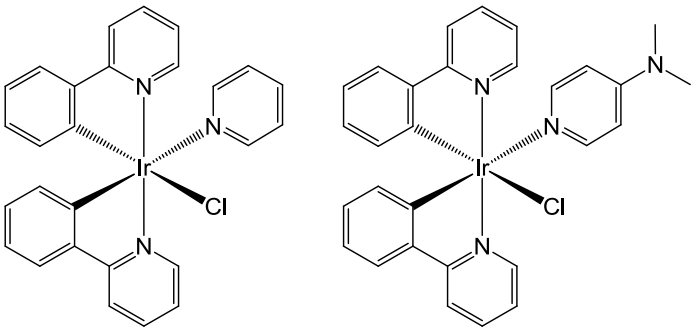

Figure 3.2 $[Ir(ppy)_2(py)Cl]$ and $[Ir(ppy)_2(DMAP)Cl]$.

It was theorised that hindered rotation around the Ir-N bond due to a steric interaction between $H^{2/6}$ of the pyridine ligand and H^6 of the neighbouring ppy could lead to broadening on the NMR timescale (Figure 3.3). If the rotation were entirely blocked, H^2 and H^6 of the pyridine would be expected to have relatively different δ values and to a lesser extent H^3 and H^5 due to proximity to the chloride ligand. Some level of hindered rotation could lead, therefore to broadening and/or splitting of these signals in the complex.

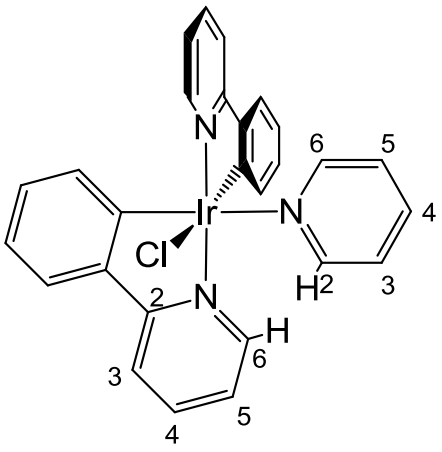

Figure 3.3 Steric hindrance to rotation in anciliary pyridine ligand.

To discover whether this was indeed the case, variable temperature NMR experiments were conducted on the [Ir(ppy)$_2$(DMAP)Cl] complex. If this effect were a result of hindered rotation, it would be expected that at higher temperatures, rotation would be increased and the peaks relating to the DMAP protons should sharpen. Conversely, at lower temperatures, it would be expected that the peaks would appear broader or, if the rotational motion were reduced sufficiently, would split into non-degenerate signals. In addition to the original spectra taken at room temperature in $CDCl_3$, experiments were performed at -50 °C in $CDCl_3$ and at 90 °C in d_4-tetrachloroethane (TCE). The resulting spectra are shown in Figure 3.4 and it can be seen that while the signals relating to the ppy ligands are largely unaffected, the proposed ancillary ligand signals show a significant sharpening at higher temperature, with the appearance of a broad, 2H integral signal in the centre of the originally observed non-linear baseline feature. In addition, it appears that at -50 °C the sample is below the thermal barrier to rotation as four distinct broad, single integral signals are seen. This evidence confirms that the product is, indeed, the [Ir(ppy)$_2$(DMAP)Cl] complex but some signals in the ambient temperature ^{1}H NMR spectrum are broadened to the extent that they are scarcely visible.

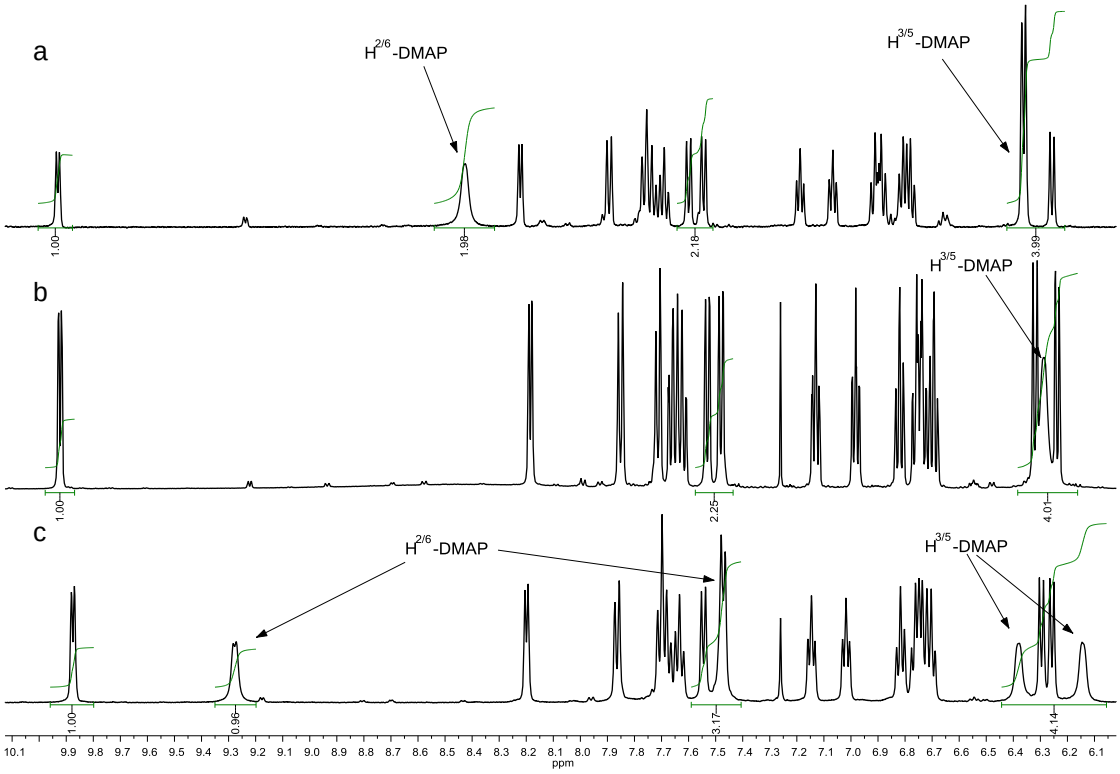

Figure 3.4 ^{1}H NMR (500 MHz) spectra of [Ir(ppy)$_2$(DMAP)Cl] at 90 °C in d$_4$-TCE (a), ambient temperature in CDCl$_3$ (b) and -50 °C in CDCl$_3$ (c). Broadening and splitting of the DMAP signals at δ 8.4 and 6.35 is clearly observed with decreasing temperature.

3.1.2 Unexpected reactivity of monometallic complexes with aromatic thiols

With the products of the cleavage reactions now confirmed as the complexes [Ir(ppy)$_2$(py)Cl] and [Ir(ppy)$_2$(DMAP)Cl], the behaviour of these new compounds when treated with thiols could be explored. It was proposed that a series of thiolates could be substituted in place of the chloride ligand giving a series of charge neutral complexes of the type shown in Scheme 3.2.

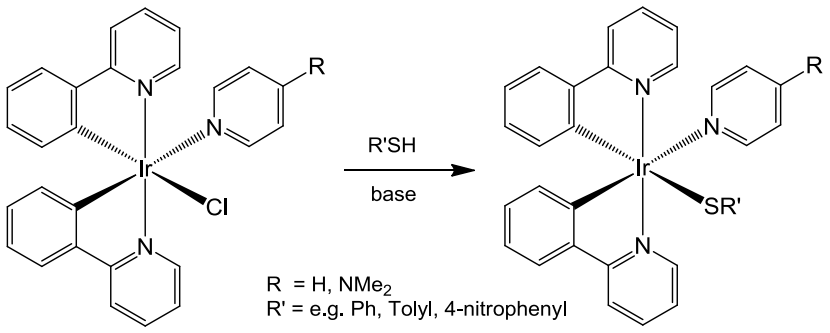

Scheme 3.2 Possible substitution reactions of [Ir(ppy)$_2$(Rpy)Cl] complexes.

The first approach was to investigate whether substitutions could occur at room temperature with aromatic thiolates and so in the first reaction, a solution of $[Ir(ppy)_2(DMAP)Cl]$ was treated with a stoichiometric amount of 4-methylthiophenol and potassium tert-butoxide in methanol. After work-up to remove any excess butanol or remaining thiol the resulting yellow product was shown to contain two components by TLC. These components were separated by column chromatography and analysed by mass spectrometry and NMR spectroscopy. It was immediately obvious that neither of these products were the result of chloride substitution by a thiolate since the ^1H NMR spectrum of both showed that the 2-phenylpyridine ligands were now equivalent giving only 8 aromatic signals, rather than 16. In fact, the spectrum of the minor product was identical to that of the dimer $[Ir(ppy)_2(\mu\text{-}Cl)]_2$, showing only these 8 aromatic signals. In the major product there were three signals in addition to those of the ppy ligands – two aromatic doublets* and one aliphatic singlet with integral ratios of 2:2:3, consistent with a 4-methylthiophenol fragment. The relation of integrals between the ppy ligands and thiol indicated that these fragments were present in a 2:1 ratio of ppy:thiol. Structurally, this ratio could be rationalised in a number of ways, as shown in Figure 3.5. Possibilities are: substitution of DMAP by thiol (A), substitution of chloride by thiolate with replacement of DMAP by some labile species (e.g. solvent) (B), or a five coordinate species where the thiolate has replaced both chloride and DMAP (C).

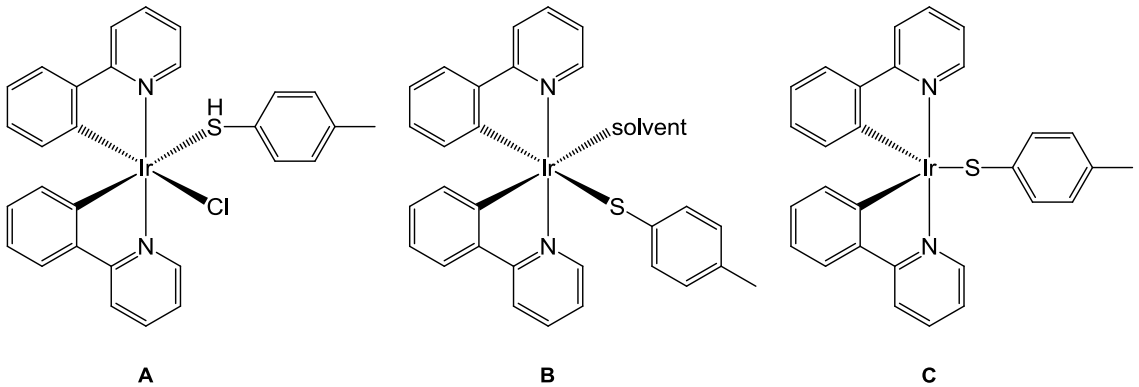

Figure 3.5 Possible product structures containing 2:1 ratio of ppy to thiol and no DMAP ligand.

All these structures, however present problems when compared to the data. Structures A and B would lead to a degeneracy in the ppy ligands in the ^1H

* These 'doublets' showed the classic a,a'-x,x' coupling pattern seen in para-substituted benzenes.

NMR spectrum as there are different units in the 5th and 6th coordination sites. As mentioned above, this does not fit with the observed spectrum. While structure C could meet the criteria for degenerate ppy ligands, a 5-coordinate complex with iridium is unlikely and none are reported in related structures with ppy ligands. The identity of the product became clearer when studying the MALDI mass spectrometry results which showed a peak at m/z = 1246, equal to twice the mass of structure C. It appears, therefore that both the products isolated from the reaction with this thiol were dimers, the minor product being $[Ir(ppy)_2(\mu\text{-}Cl)]_2$ and the major product, a dimer with two bridging thiolate ligands as shown in Figure 3.6.

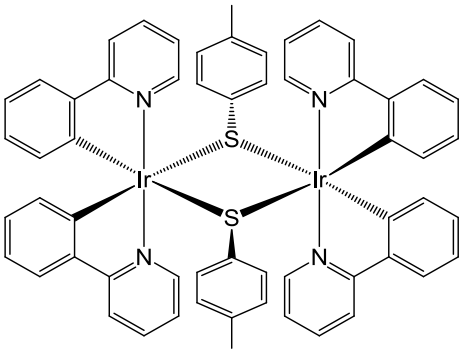

Figure 3.6 $[Ir(ppy)_2(\mu\text{-}mtp)]_2$

This result is not surprising, given the tendency of sulfur to form bridging compounds with a variety of metals, either as a sulfur atom or as part of a thiolate. Recent examples with iridium include bridging by 2-mercaptobenzimidazole,[210] perfluorothiophenol[211] and also a diiridium species with bipyridine ligands bridged with 4-methylthiophenol.[212]

3.1.3 Direct reaction of $[Ir(ppy)_2(\mu\text{-}Cl)]_2$ with thiolates

Since the reaction of a monometallic complex with a thiolate gave a dimer in this manner, it was of interest to explore what effect addition of a thiolate directly to the chloride bridged dimer would have. Given that 4-methylthiophenol displaces both the chloride and DMAP ligands to form a dimer, it is possible that this product could instead be formed by direct chloride substitution in $[Ir(ppy)_2(\mu\text{-}Cl)]_2$ making cleavage with a neutral ligand and subsequent reforming of a dimeric species superfluous.

3.1.3.1 Diastereoisomerism resulting from the direct reaction with $[Ir(ppy)_2(\mu\text{-}Cl)]_2$

Again, the first reaction attempted was addition of a solution of 4-methylthiophenol and KO^tBu in methanol to a solution of $[Ir(ppy)_2(\mu\text{-}Cl)]_2$ in DCM. This addition caused the immediate precipitation of a yellow, semi-crystalline solid, which was collected and analysed by NMR spectroscopy. Although the ^1H spectrum initially appeared quite complicated (Figure 3.7), on closer inspection, half of the signals present were consistent with the spectrum of the dimer $[Ir(ppy)_2(\mu\text{-}mtp)]_2$ obtained in the previous work from the mononuclear iridium complex. With these signals discounted, what remained was another set of signals, also consistent with a structure containing a 2:1 ratio of ppy:mtp. Data from MALDI mass spectrometry, on the other hand, indicated only a single product, consistent with that of the thiolate bridged dimer.

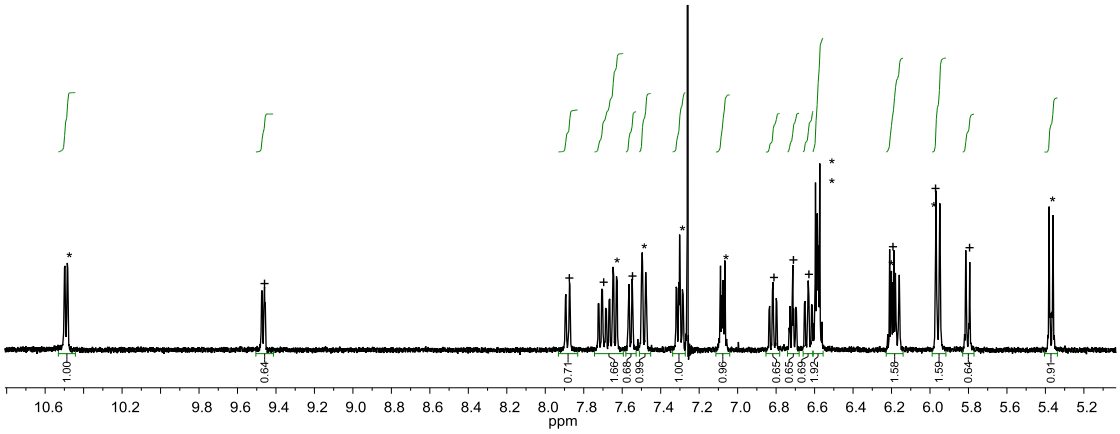

Figure 3.7 ^1H NMR (400 MHz) spectrum of initial precipitate from reaction of $[Ir(ppy)_2(DMAP)Cl]$ with mtpH/KO^tBu. + marks peaks consistent with previous $[Ir(ppy)_2(\mu\text{-}mtp)]_2$ sample.

It appeared that this reaction had resulted in a pair of diastereoisomers, where the two $Ir(ppy)_2$ units are arranged differently with respect to each other. It is possible for the phenylpyridine ligands on the same side of the plane formed by the bridging bonds to be arranged either parallel or perpendicular to one another (Figure 3.8). These diastereoisomers result from different combinations of iridium centres with either Λ or Δ symmetry. In all, the possible combinations are Λ,Δ (meso), Λ,Λ and Δ,Δ, the last two being a pair of enantiomers. This is unusual in complexes of this type with the overwhelming majority of previously reported dimers adopting only a racemic mixture of Λ,Λ and Δ,Δ isomers.[14-17]

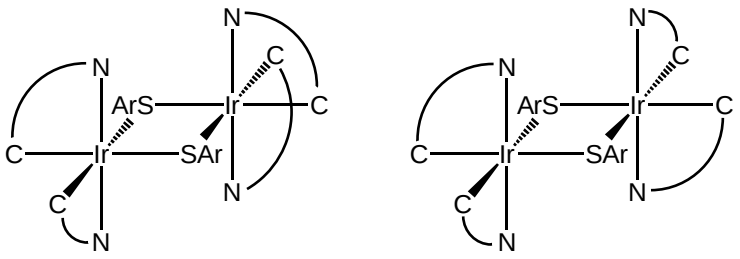

Figure 3.8 Λ,Λ and Λ,Δ diastereoisomers of $[Ir(ppy)_2(\mu\text{-mtp})]_2$

From the NMR spectrum it was possible to determine that the ratio of isomers in the initial sample was 1:1.5 with the smaller proportion being the isomer similar to that resulting from the reaction with $[Ir(ppy)_2(DMAP)Cl]$. It was also noted that the isomeric ratio changed over time when the mixture was left in solution. The same NMR sample, having been left at room temperature for approximately 20 h showed an increase in the proportion of the originally discovered isomer up to a ratio of 1:1. The proportion of this isomer was increased further to 1:0.5 after the sample was heated at reflux for 45 min in chloroform. It seems, therefore that the new isomer, formed initially in larger proportion, is likely to be the kinetically favoured product of the thiolate substitution while the alternate isomer (and sole product of reaction with $[Ir(ppy)_2(DMAP)Cl]$) is more thermodynamically stable. Additional reactions were carried out at different temperatures to discover whether these isomers could be synthesised independently. The substitution was performed at -78 °C to favour the new isomer and another reaction was refluxed for 7 h to produce the original isomer. These reactions, however, gave mixtures in ratios 1:1.5 and 1:1 respectively.

The diastereoisomers did show a slight separation in TLC and so separation by column chromatography was attempted. The column was carried out as quickly as possible to try to minimise interconversion of the isomers while on the column and in solution. This separation was to some extent successful as a large proportion of the new isomer was obtained, but there was a small amount of the original isomer in the ^1H NMR spectrum of the sample.

A similar substitution was also attempted using thiophenol (tpH), 4-nitrothiophenol (ntpH) and sodium methanethiolate (mtNa) in place of 4-methylthiophenol on $[Ir(ppy)_2(\mu\text{-Cl})]_2$ with reflux for approximately 16 h. While the reaction with sodium methanethiolate was unsuccessful, with only starting

materials recovered, the reactions with tpH and ntpH both gave thiolate-bridged dimers analogous to the result of the reaction with mtpH. In these two cases no evidence of diastereoisomers was seen in the products and, based on the tendency of similar dimers to adopt the chiral Λ,Λ or Δ,Δ structure, it is expected that this is also the case for $[Ir(ppy)_2(\mu\text{-tp})]_2$ and $[Ir(ppy)_2(\mu\text{-ntp})]_2$. However, in light of the observed isomerism in $[Ir(ppy)_2(\mu\text{-mtp})]_2$ this assignment is tentative. The synthesised dimers are shown in Figure 3.9.

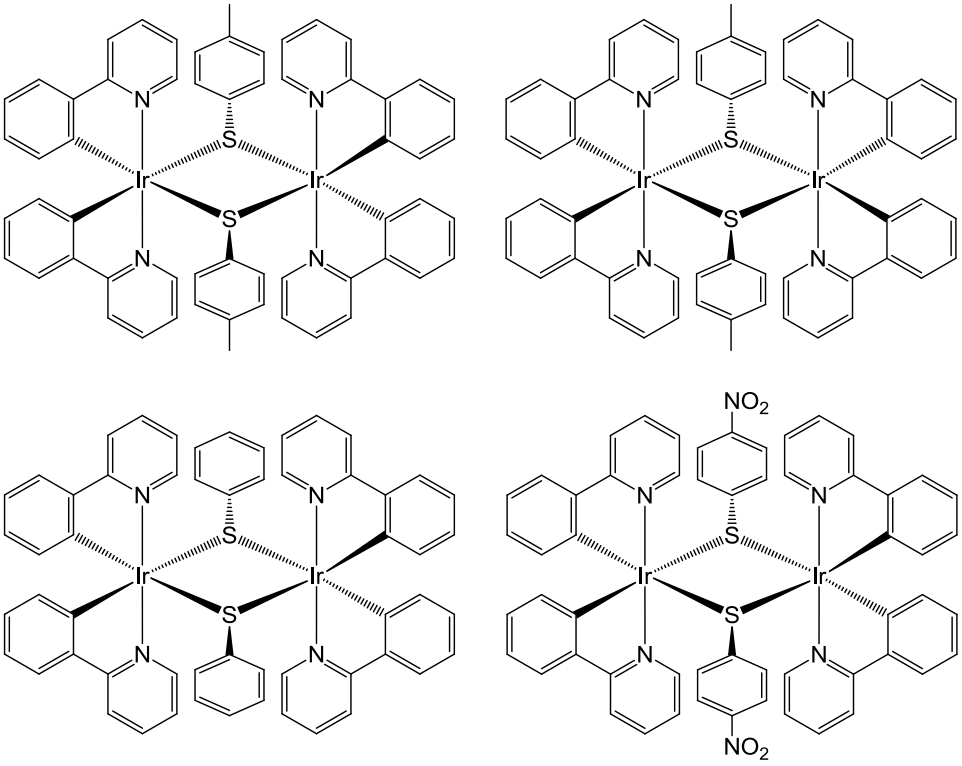

Figure 3.9 $[Ir(ppy)_2(\mu\text{-mtp})]_2$ (racemic and meso), $[Ir(ppy)_2(\mu\text{-tp})]_2$ and $[Ir(ppy)_2(\mu\text{-ntp})]_2$

3.1.3.2 Assignment of $[Ir(ppy)_2(\mu\text{-mtp})]_2$ isomers from NMR data

Although the two isomers of $[Ir(ppy)_2(\mu\text{-mtp})]_2$ can readily be distinguished by ^1H NMR, it is not possible to assign which set of signals correspond to which isomer simply by inspection. Attempts to produce crystals for single crystal X-ray structural analysis, which would provide the definitive solution, were unsuccessful but some evidence can be inferred from NMR data.

By comparison of the ^1H NMR spectra of the dimers shown in Figure 3.9, it seems clear that the isomerically pure samples of $[Ir(ppy)_2(\mu\text{-tp})]_2$ and $[Ir(ppy)_2(\mu\text{-ntp})]_2$ are likely to have the same stereochemistry as the

thermodynamically favoured isomer of $[Ir(ppy)_2(\mu\text{-mtp})]_2$. The most deshielded protons of these three compounds are the H^6 and H^3 protons of the pyridine ring and appear at around δ 9.5 and 7.9 respectively, similar to the spectrum of $[Ir(ppy)_2(\mu\text{-Cl})]_2$, whereas these two signals in the alternate isomer (referred to above as the kinetic product) are quite different, at δ 10.49 and 7.49. In fact, the comparatively more shielded position of the H^3 signal has put this at a lower δ than H^4 which in this isomer is now the second highest signal at δ 7.65. A comparison of the ^{1}H NMR spectra of the synthesised dimers is shown in Figure 3.10 and the distinct pattern of the novel isomer can clearly be seen.

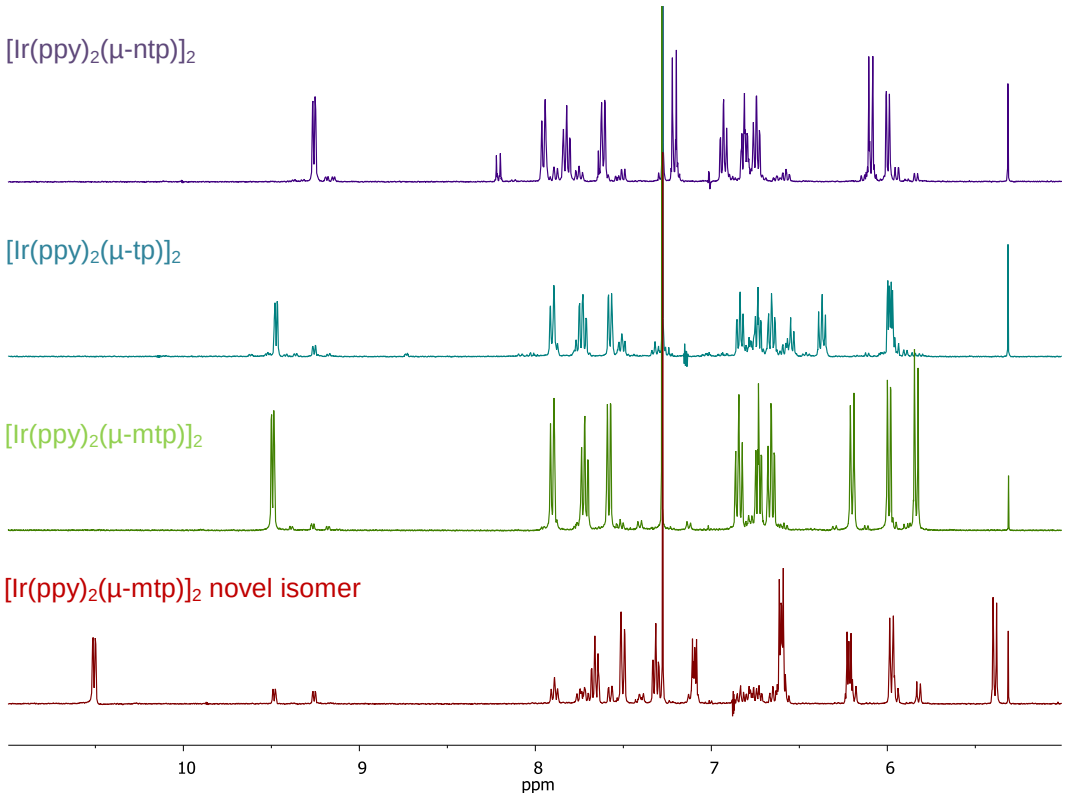

Figure 3.10 ^{1}H NMR spectra (aromatic region) of thiolate-bridged dimers showing distinctive peak distribution in the new isomer of $[Ir(ppy)_2(\mu\text{-ntp})]_2$.

As discussed in the introduction, X-ray crystallography has shown that compounds related to $[Ir(ppy)_2(\mu\text{-Cl})]_2$ generally exist as a mixture of Λ,Λ and Δ,Δ isomers and, given the similarity in the ^{1}H NMR spectra, it can be tentatively expected that these new dimers exist in the racemic Λ,Λ and Δ,Δ forms. This would imply that the kinetically favoured isomer produced in the case of $[Ir(ppy)_2(\mu\text{-mtp})]_2$ is the meso isomer with mixed Λ and Δ metal centres. While these data do suggest an assignment of Λ,Δ stereochemistry to the additional

isomer, this evidence is somewhat circumstantial so other methods were explored to try to confirm this assignment.

3.1.3.3 Use of Density Functional Theory to confirm assignment

Density Functional Theory (DFT) has a wide variety of uses in chemistry, most commonly in the examination of the electronic structure of molecules and their excited states. This can be useful in areas such as determining reaction dynamics as well as helping to characterise the excited state properties of emissive molecules. It is also possible, using DFT, to calculate NMR spectra by virtue of the relationship between the electronic energy levels and the nuclear shielding constant. The shielding constant of a nucleus σ defines the effective magnetic field at the nucleus in relation to the applied field B_0 and is given by the mixed second derivative of the energy with respect to the magnetic moment of the nucleus μ and the magnetic field B as shown in Equation 3.1.

$$B = B_0(1-\sigma)$$

$$\sigma = \frac{\partial^2 E}{\partial \mu \partial B}$$

Equation 3.1

It was therefore decided to explore the effect of the observed isomerism upon the calculated ^{1}H NMR spectra using this method. With the observed NMR spectra of the two isomers for comparison it was hoped that these could be matched to the results of calculations run on the two structures. Assuming the theoretical and observed spectra were sufficiently matched, this would confirm or refute the initial assignment since the input structure for the theoretical spectra is known.

Before performing calculations to produce shielding values, it is first necessary to perform a geometry optimisation on the two structures to ensure they are in their lowest energy conformation. Since the Δ,Δ and Λ,Λ isomers are enantiomers of one another, in terms of DFT calculations they are identical and so the calculations were performed only on the Δ,Δ and Λ,Δ isomers. The results of these optimisations are shown in Figure 3.11 and, as expected, show that in the Δ,Δ isomer the pairs of phenylpyridine ligands on the same side of

the iridium-sulfur plane are aligned approximately parallel, while in the Λ,Δ isomer they lie perpendicular. It is also worth noting that the final molecular energies resulting from these calculations showed a difference of 3.91×10^{-3} Hartrees, with the meso isomer being slightly higher in energy. This is equivalent to 10.3 $kJmol^{-1}$ and gives credit to the earlier assumption that the Δ,Δ and Λ,Λ isomers are more thermodynamically stable than the Λ,Δ meso isomer.

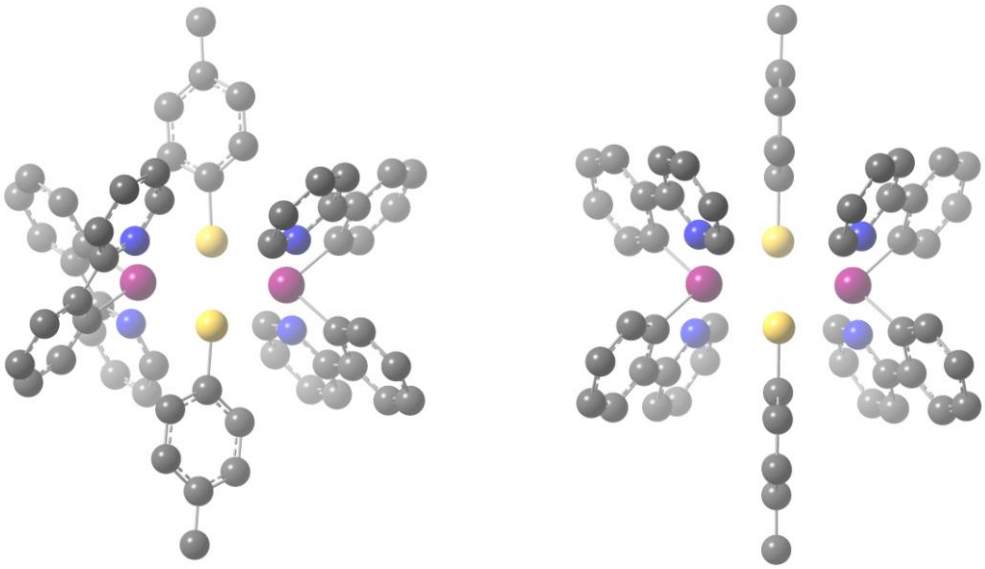

Figure 3.11 Geometry optimised structures of Δ,Δ (left) and Λ,Δ (right) diastereoisomers of $[Ir(ppy)(\mu\text{-mtp})]_2$. Calculations performed with Gaussian03 using the B3LYP hybrid functional with basis sets 6-31G* and LanL2DZ. Hydrogen atoms are omitted for clarity.

Using the atomic coordinates from the geometry optimisations, the NMR shielding constants could then be calculated. The calculated shielding values for the Λ,Δ (meso) isomer show, as expected, a fourfold degeneracy in signals relating to the phenylpyridine ligands since these four ligands are equivalent in this structure. This leads to eight distinct signals for the protons in these ligands as is observed in the solution NMR spectrum. For signals from the bridging thiolate ligands, while in the observed NMR spectrum these appear as two distinct signals each with a fourfold degeneracy, the calculated spectrum shows four signals of twofold degeneracy for these protons. This is due to the fact that the calculated values are for the rigid structure of the optimised geometry making, for example, H^2 and H^6 symmetrically inequivalent, while in the observed spectrum these signals are equilibrated by rotation of this ligand faster than the NMR timescale.

The calculated results for the Δ,Δ isomer are slightly more complex. In this case, the results do not show the observed fourfold degeneracy for signals relating to the phenylpyridine ligands. This, again, is due to the lack of rotational equilibration in the calculated spectrum. The non-degeneracy in the ppy ligands arises from the relative orientation of the mtp phenyl rings making the two ppy on the same side of the iridium-sulfur plane symmetrically inequivalent. The signals calculated for the mtp ligands themselves show a similar result to the meso isomer with four separate values for each aromatic ring position and the two mtp fragments remaining equivalent.

Essentially, the difference in degeneracy between the calculated spectra is a result of the positioning of the bridging ligands. Both complexes possess a single C_2 axis passing through the two iridium centres making the ppy ligands around the same metal centre symmetrically equivalent. However, in the optimised structure of the Λ,Δ isomer, the aromatic rings of the mtp ligands are aligned perpendicular to this C_2 axis and this, in addition to the meso arrangement of the ppy ligands gives this isomer a mirror plane, σ_h, resulting in a centre of inversion as it belongs to the point group C_{2h} rather than C_2. As discussed above, these particular symmetry arguments only apply to the calculated spectra since they are rigid, while in the solution NMR spectra, intramolecular motion, primarily rotation of the mtp ligands leads to increased degeneracy. Table 3.1 shows the calculated and observed δ values with their proton assignments, numbered as shown in Figure 3.12.

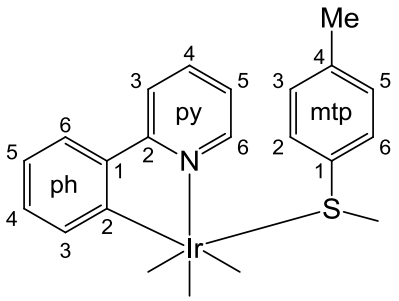

Figure 3.12 Proton numbering in $[Ir(ppy)_2(\mu\text{-mtp})]_2$ for NMR assignment.

Δ,Δ isomer calculated ^{1}H δ values / ppm (assignment)	Λ,Δ isomer calculated ^{1}H δ values / ppm (assignment)	Initial isomer observed ^{1}H δ values / ppm (assignment)	Secondary isomer observed ^{1}H δ values / ppm (assignment)
10.1 (H^6-py)[a]	11.0 (H^6-py)	9.47 (H^6-py)	10.49 (H^6-py)
8.50 (H^6-py')[a]			
7.43 (H^3-py)[a]	7.85 (H^4-py)	7.88 (H^3-py)	7.65 (H^4-py)
7.35 (H^3-py')[a]			
7.30 (H^6-ph)[a]	7.75 (H^3-py)	7.70 (H^4-py)	7.49 (H^3-py)
7.24 (H^6-ph')[a]			
7.24 (H^4-py)[a]	7.66 (H^5-py)	7.56 (H^6-ph)	7.30 (H^5-py)
7.10 (H^4-py')[a]			
6.54 (H^5-py)[a]	7.38 (H^6-ph)	6.82 (H^5-ph)	7.08 (H^6-ph)
6.25 (H^5-py')[a]			
6.25 (H^5-ph)[a]	7.21 (H^2-mtp)[a]	6.71 (H^5-py)	6.58 (H^4-ph)
6.25 (H^5-ph')[a]			
6.25 (H^4-ph)[a]	7.06 (H^3-ph)	6.64 (H^4-ph)	6.58 (H^5-ph)
6.25 (H^4-ph')[a]			
6.25 (H^3-ph)[a]	6.84 (H^4-ph)	6.18 ($H^{2/6 \text{ or } 3/5}$-mtp)	6.20 (H^3-ph)
6.06 (H^3-ph')[a]			
6.06 (H^2-mtp)[a]	6.84 (H^3-mtp)[a]	5.97 (H^3-ph)	5.96 ($H^{2/6 \text{ or } 3/5}$-mtp)
5.90 (H^3-mtp)[a]	6.63 (H^5-ph)	5.82 ($H^{2/6 \text{ or } 3/5}$-mtp)	5.27 ($H^{2/6 \text{ or } 3/5}$-mtp)
5.82 (H^5-mtp)[a]	6.33 (H^5-mtp)[a]	1.92 (Me)	1.99 (Me)
5.51 (H^6-mtp)[a]	5.35 (H^6-mtp)[a]		
1.74, 1.49, 1.21 (Me)[a]	2.56, 2.35, 1.93 (Me)[a]		

Table 3.1 Calculated and observed ^{1}H NMR δ values for the two isomers of $[Ir(ppy)_2(\mu\text{-mtp})]_2$. Overlapping signals are listed separately at the same δ for clarity. (a) These signals appear non-degenerate in the calculated spectra due to the lack of rotational equilibration.

As discussed in Section 3.1.3.2, the most notable difference in the observed NMR spectra of the two isomers is firstly the order of the peaks at high δ and secondly the difference in δ between the two most deshielded protons. It has been inferred from comparisons with other dimers that the kinetically favoured isomer in the reaction of mtp with $[Ir(ppy)_2(\mu\text{-Cl})]_2$ was the Λ,Δ isomer. When the data calculated for a Λ,Δ structure is compared to the observed spectrum of this alternate isomer it can be seen that the predicted sequence follows the

observed spectrum for the five most deshielded protons. In addition, the gap between the H^6-py and H^4-py signals is also relatively large at 3.15 ppm in the calculated spectrum compared to 2.84 ppm in the solution NMR spectrum.

The correlation between the more thermodynamically stable isomer and the calculated values for a Δ,Δ isomer are complicated slightly by the non-degeneracy in signals from the ppy. However, for the most part the separated signals appear at similar δ to one another and so a crude comparison with the observed data can still be made. In this case, the calculation correctly places H^3-py as the second most deshielded proton rather than H^4-py as in the alternate isomer. The next two highest signals in the calculated spectrum, H^6-ph and H^4-py, are very close together and partially overlapped due to the issue of non-degeneracy and while these are indeed the next two signals in the observed data, the peak order is reversed. In terms of the gap between the two most deshielded protons in this isomer, if averaged values for the non-degenerate signals with the same assignment are taken this gives a gap of 1.91 ppm in the calculated values compared to 1.59 ppm in the observed solution NMR.

While in both the spectra obtained by DFT calculations the δ values are somewhat different from the observed data, with the variation in many cases being up to 0.5 ppm, the overall patterns of the spectra in terms of peak ordering and position do show similar variation to the difference in the observed spectra. In trying to match the calculated spectra to those observed from solution NMR, there is a clear similarity between the 'alternate' isomer and the calculation for the Λ,Δ structure, while the calculation for the Δ,Δ structure has more in common with the originally synthesised isomer. This seems to confirm the previous assignment that the more common structures displayed in the new $[Ir(ppy)_2(\mu\text{-thiolate})]_2$ dimers is a racemic Δ,Δ and Λ,Λ mixture while the unusual isomer in the case of $[Ir(ppy)_2(\mu\text{-mtp})]_2$ exists as a meso Λ,Δ diastereoisomer.

3.1.4 Photophysical properties of thiolate bridged dimers

Beyond the observed isomeric changes occurring in solution with the mtp bridged dimer, in the case of all the synthesised dimers, a period of 2-3 days in

solution led to significant decomposition, with NMR samples showing up to four different components as evidenced by the differing H^6-pyridine signals at high δ.

All the dimers synthesised are slightly soluble in chlorinated solvents and acetone but insoluble in most others including alcoholic solvents such as methanol and ethanol, the ether solvents THF and Et_2O, or non-polar solvents such as hexane. $[Ir(ppy)_2(ntp)]_2$ is noticeably more soluble than the other two dimers. During the work-up following the synthesis of this compound, an intriguing effect was observed. While the other two dimers are bright yellow in colour like the chloride bridged dimer, this compound is a darker orange/yellow colour. Upon contact with methanol, however, the solid became deep red in colour, whilst a subsequent wash with diethyl ether caused another colour change to yellow. Upon drying under reduced pressure the solid returned to its original orange/yellow colour. On further investigation it was discovered that a variety of solvents produced a reversible colour change upon contact with the solid. For most, the colour change is relatively small, but methanol and diethyl ether produce marked changes towards red and yellow respectively. It was also discovered that the effect is not limited to suspension of the material in a solvent, but in addition, contact with solvent vapour induced similar changes as shown in Figure 3.13. While the colour change in contact with liquid solvent is immediate, the effect takes place over 1-2 min in the presence of a solvent vapour, a slower rate of change being expected in response to the vapour if the change results from diffusion of solvent molecules into vacant sites within the solid structure. Similarly, when removed from a vapour, the solid takes between 2 and 5 min to return to its original orange/yellow colour but can be accelerated by placing the sample under vacuum.

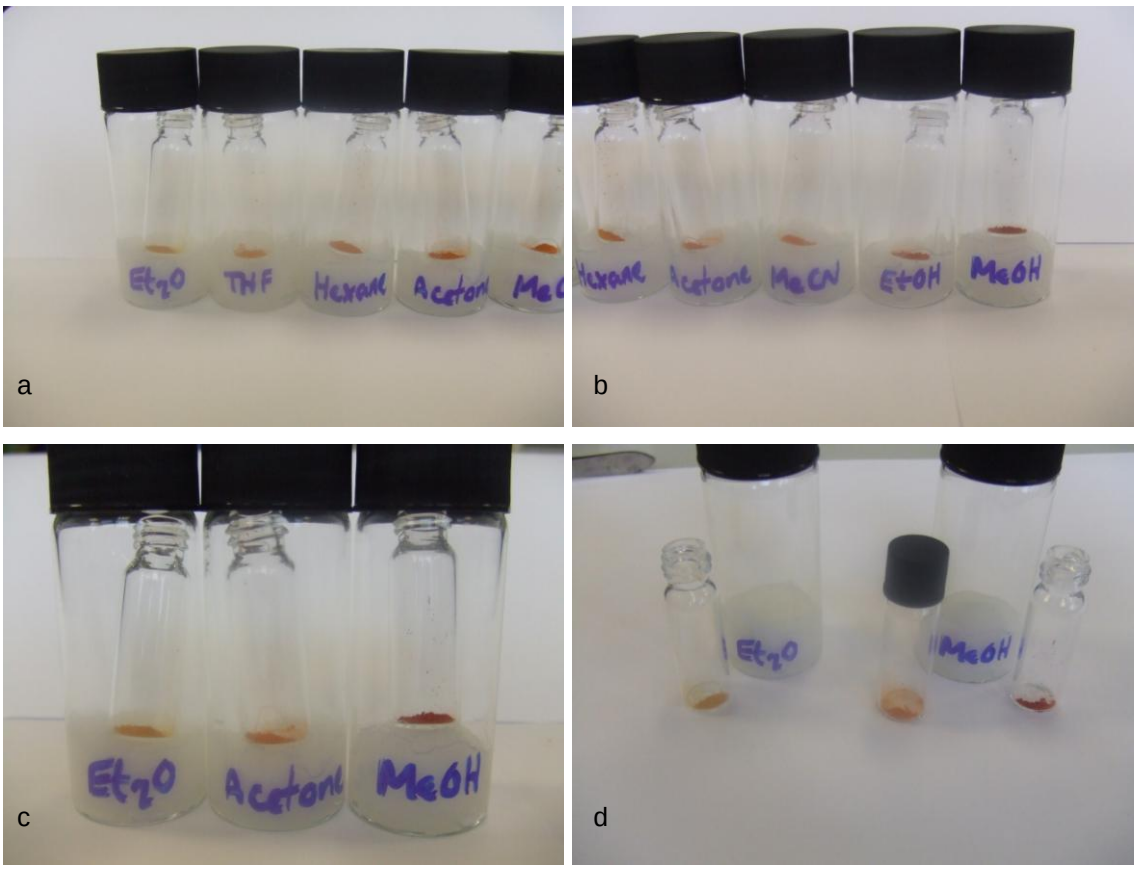

Figure 3.13 Samples of $[Ir(ppy)_2(\mu\text{-ntp})]_2$ exposed to various solvent vapours (a, b and c) and immediately after removal (d). The sealed vial in (d) is the dry sample.

It is not clear what solvent property is involved in this effect: it seems unlikely to be simply related to polarity since while ethanol and methanol produce some of the most noticeable changes, the more polar acetonitrile has very little effect. A simple rationalisation based on the presence of heteroatoms is also difficult since ether and alcohols appear to produce changes in opposite directions. It seems likely that the effect will be in some way related to the size of the solvent molecule, as it must be incorporated into holes in the solid structure.

In order to better understand this effect, the three dimers were studied by UV/visible spectroscopy. The solution absorption spectra of $[Ir(ppy)_2(\mu\text{-ntp})]_2$, $[Ir(ppy)_2(\mu\text{-tp})]_2$ and the two isomers of $[Ir(ppy)_2(\mu\text{-mtp})]_2$ in DCM are shown in Figure 3.14. As expected, these compounds all show strong UV absorption resulting from the aromatic π systems in the ligands. The dimer containing 4-nitrothiophenol has an additional distinct band at ~440 nm, whilst the others show only a weak tail in this region extending to around 520 nm. The parent dichloro-bridged dimer shows similar low energy absorptions which have been

assigned to MLCT transitions involving the ppy ligands.[19] It is therefore likely that the observed tails arise from similar transitions in these new dimers.

Another noticeable feature of these spectra is that while $[Ir(ppy)_2(\mu\text{-tp})]_2$ and the original $[Ir(ppy)_2(\mu\text{-mtp})]_2$ isomer have very similar profiles, the meso mtp isomer shows slightly increased intensity in the tail at around 350 nm and 460 nm relative to the corresponding racemate. This difference is certainly not great enough to indicate any major change in band structure in the meso isomer, but could be indicative of a slight perturbation of the ligand π systems resulting from their differing relative orientation.

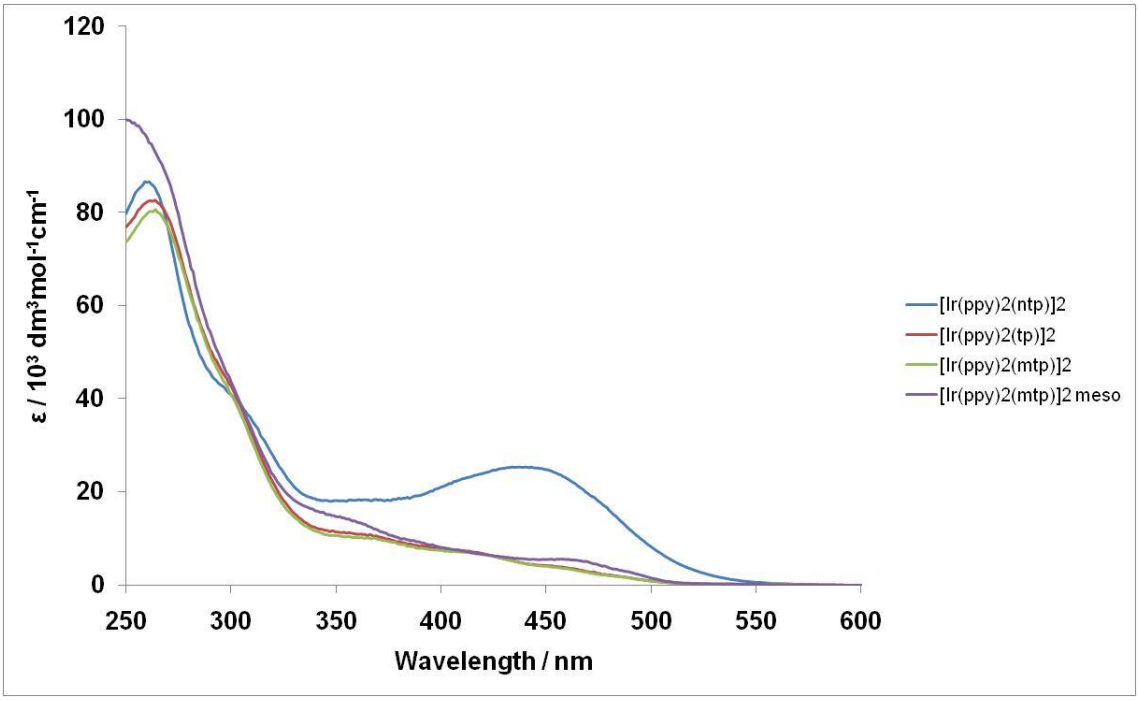

Figure 3.14 Absorption spectra of $[Ir(ppy)_2(\mu\text{-thiolate})]_2$ dimers in DCM normalised for concentration.

What is clear is that the additional band in $[Ir(ppy)_2(\mu\text{-ntp})]_2$ is due to the significantly lower energy π system of the bridging ligand resulting from conjugation with the nitro group and it is this band which contributes to the noticeable colour difference of this dimer. It is certainly the case that with other metals such as platinum, the introduction of nitro-substituted ligands can lead to noticeable differences in the orbital characteristics of a complex (See Section 2.2.2). It also seems likely that the observed vapochromism of this dimer is

related to this transition since the effect is not observed in the other synthesised dimers.

The absorption spectrum of $[Ir(ppy)_2(\mu\text{-ntp})]_2$ was therefore measured in a variety of solvents to establish whether any changes in the structure or position of this band would be observed. Due to the low solubility of the dimer in non-chlorinated solvents, samples were prepared by dilution of 0.1 mL DCM stock solution with the required solvent to a total volume of 3 mL giving 0.033% DCM in the measured sample. In this manner, absorption spectra were obtained in acetone, acetonitrile, dichloromethane, diethyl ether, ethanol, ethyl acetate, hexane, methanol and tetrahydrofuran and these are shown in Figure 3.15.

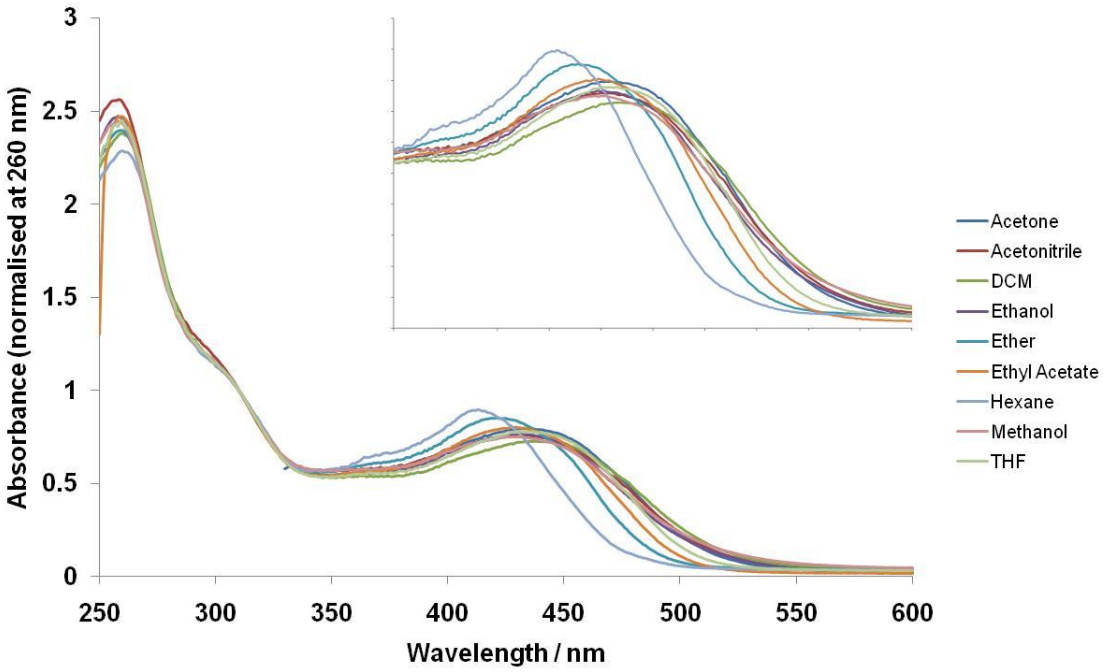

Figure 3.15 Absorption spectra of $[Ir(ppy)_2(\mu\text{-ntp})]_2$ in various solvents, normalised at 310 nm.

While a noticeable change in the low energy band does, indeed, occur in different solvents, these data appear to show a pattern consistent with positive solvatochromism of a charge transfer band indicating an increase in polarity in the excited state. Plots of the absorption maxima against the solvent dipole moment (Figure 3.16a) and dielectric constant[213] (Figure 3.16b), however, indicate a more complex situation. While the relationship with the solvent dipole moment does indicate a decrease in energy with increasing solvent polarity, the values for DCM, THF and acetonitrile lie noticeably away from a linear

correlation. Meanwhile it appears that for solvents with low dielectric constants (ε_r < 10) there is a linear relationship with the absorption maximum while for the more polar solvents, this relationship breaks down. It is clear from these results that the shift in absorption energy is not simply a result of solvent polarity indicating there may be a signifant contribution from direct solvent-complex interactions in certain solvents.

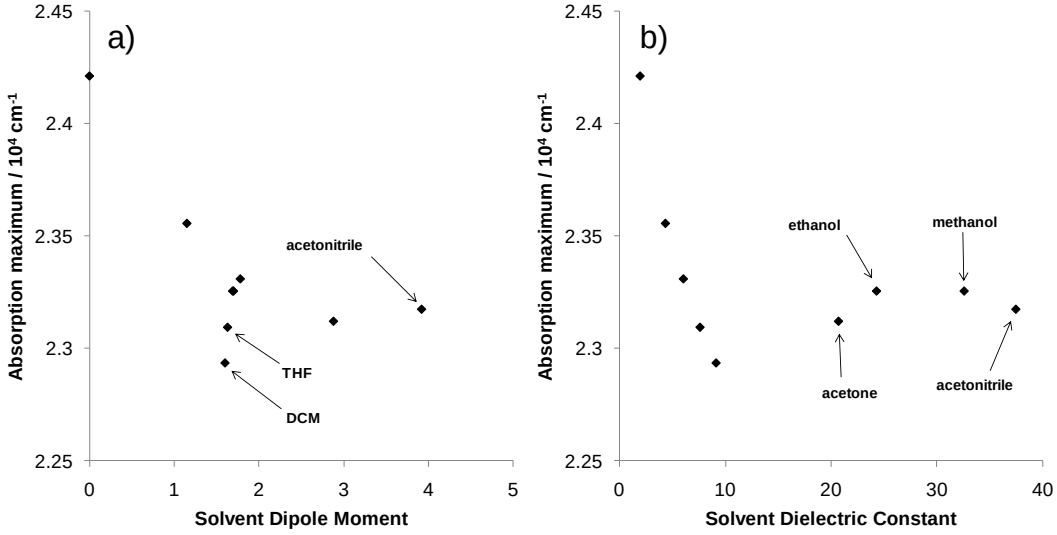

Figure 3.16 Plots of λ_{max} against a) dipole moment and b) dielectric constant for the low energy band of $[Ir(ppy)_2(\mu\text{-ntp})]_2$.

As a qualitative investigation into this effect in the solid state, microscope cover slips were taken and coated in a thin layer of the dimer by evaporation of a DCM solution. Three slides were prepared using increasing concentrations of solution to give slides with varying thicknesses of solid, as shown in Figure 3.17. The absorption spectra of these slides were then measured using the group's solution UV/visible spectrometer by placing them in the path of the sample beam in place of a cuvette. While this is not the ideal apparatus for such work, it was hoped that the results would provide some indication of the changes occurring during exposure to solvent vapours. As the coating on the slides could not be made entirely uniform, the spectrum of each slide was measured five times in various orientations. The raw data from these runs were quite varied, however after baseline correction and normalisation the results were reasonably self-consistent for each slide. There were noticeable differences between slides, however, with the relative intensity of lower energy bands appearing much higher on the more concentrated slides.

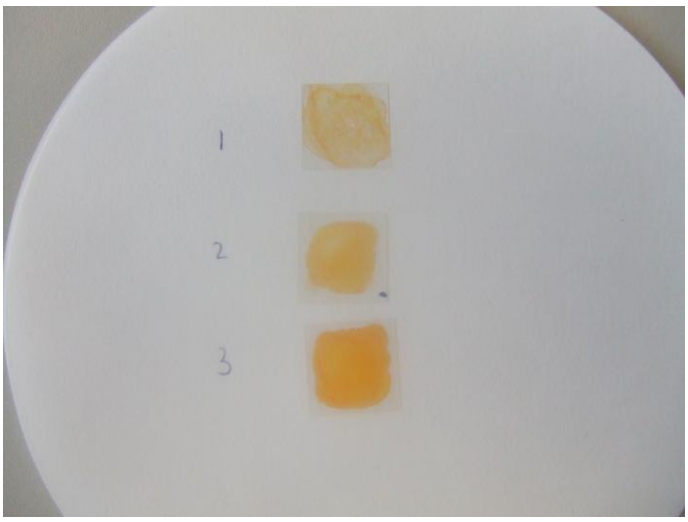

Figure 3.17 Glass slides coated with $[Ir(ppy)_2(\mu\text{-ntp})]_2$.

Each slide was then incubated for 5 min on a stand inside a sealed jar containing methanol and a new scan was performed immediately upon removal. The slide was then replaced in the solvent vapour for a further 5 min and another scan taken. This was repeated to give a total of 5 scans for each slide. Each slide was then left under reduced pressure for approximately 20 min to ensure the removal of all methanol, then the process was repeated with diethyl ether. Data from the two solvent systems was again quite varied but after baseline correction and normalisation the separate runs were more consistent. Plots of averaged data from all five runs of the dry and solvent-treated slides are shown in Figure 3.18. While there is some difference between dry and solvent-treated slides, including a slight red-shift of the charge transfer band at ~450 nm, the changes are small and there appears to be very little difference between the spectra for the two solvents. If the spectra were representative of the observed colour changes in the solid state, it would be expected that methanol and diethyl ether would have differing effects on the absorption profile since methanol produces a red colour while ether turns the solid yellow. It is therefore likely that the effects of solvent absorption into the structure are not being observed by this method, while the minor changes observed in the spectra of treated slides could be instead attributed to a slight wetting of the thin film altering its light scattering and absorption properties.

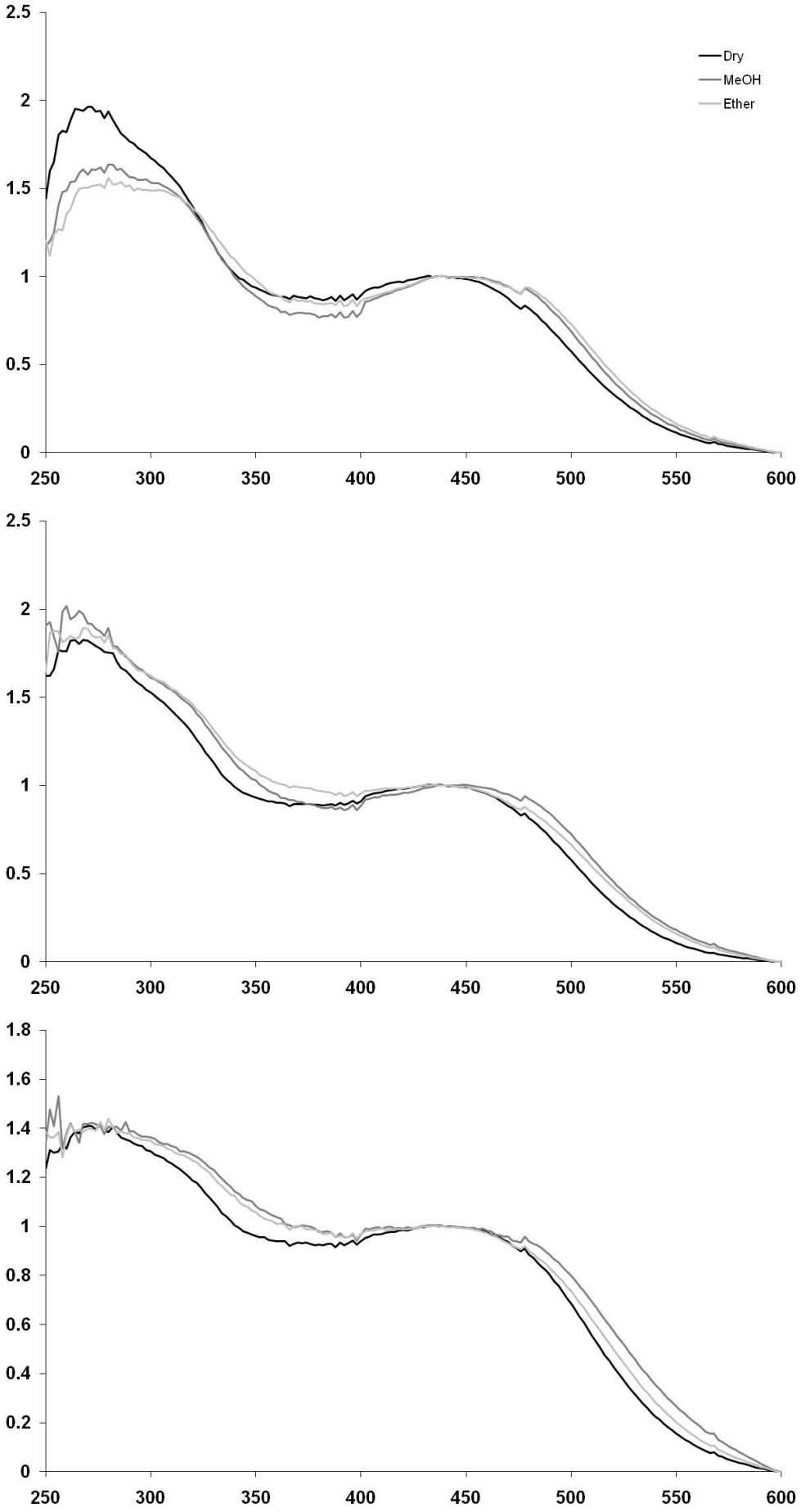

Figure 3.18 Absorption spectra of Slide 1 (top) Slide 2 (middle) and Slide 3 (bottom).

While no definitive answer has been obtained as to what particular interaction leads to the vapochromic effect in this particular compound, it is highly likely to involve orbital interactions relating to the 4-nitrothiophenolate ligands in $[Ir(ppy)_2(\mu\text{-ntp})]_2$. The observation that noticeable changes in the photophysical properties can arise from interactions with small molecules in the solid state justifies further investigation into the orbital characteristics of this, and the related dimers – in particular, what changes occur upon the introduction of the nitro group. If the precise nature of the interaction can be elucidated, this could lead to the design of useful sensing materials utilising these, or similar complexes.

3.2 Iridium complexes with terdentate N^C^N bound ligands

The reaction of iridium(III) chloride with terdentate cyclometallating ligands such as 1,3-di(2-pyridyl)-4,6-dimethylbenzene (dpyxH) gives a chloride bridged dimer which can be cleaved with various ligands to give a monometallic complex. As discussed in the introduction, both bidentate and terdentate ligands can be used, but of particular interest within the scope of this project is where the dimer is cleaved with diimine-type ligands such as bipyridine or a bidentate cyclometallating ligand such as 2-phenylpyridine thus leaving one monodentate chloride ligand as shown in Scheme 3.3. In the case of [Ir(dpyx)(ppy)Cl] it has been observed that the Ir-Cl bond is relatively labile, despite the normal kinetic inertness associated with the Ir^{3+} ion, due to the high trans effect of the trans-disposed metallated phenyl ring. This observation indicates that such complexes could be suitable for facile substitution of the chloride ligand with a thiolate.

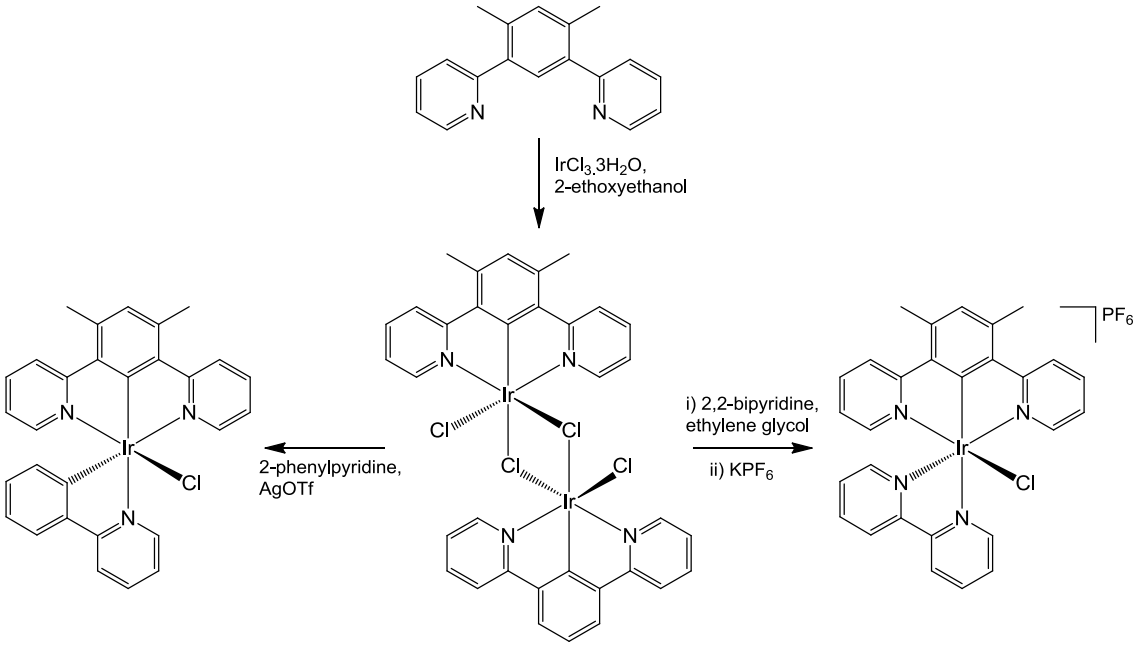

Scheme 3.3 Synthesis of Ir(N^C^N)(N^C)Cl and [Ir(N^C^N)(N^N)Cl]PF_6 complexes.

Work was undertaken, therefore, to synthesise N^C^N ligands and from there, produce the dimer required to give various monometallic complexes for study.

3.2.1 The extent of C^2/C^4 competitive binding

As discussed in Section 1.1.2.3, during the original investigations into N^C^N coordinating ligands with iridium, it was found that the formation of terdentate bound complexes with the simplest 'parent' structure, 1,3-di(2-pyridyl)benzene was not feasible due to competition with metallation at C^4 giving bidentate N^C binding, which is kinetically favoured in the case of iridium.[46] The xylene-based ligand shown above was therefore introduced, where the C^4 and C^6 positions are blocked, to enforce the desired N^C^N binding. It was decided that, concurrent with the preparation of iridium complexes containing this xylene ligand, it would be of interest to explore whether a single methyl group at the C^5 position would be sufficient in also disfavouring the bidentate binding mode. The ligand 1,3-di(2-pyridyl)-5-methylbenzene (dpytH) was prepared by a Stille coupling of 3,5-dibromotoluene with tri-n-butylstannylpyridine. DpyxH was similarly prepared from 4,6-dibromo-m-xylene, itself produced by bromination of meta-xylene catalysed by I_2 as shown in Scheme 3.4.

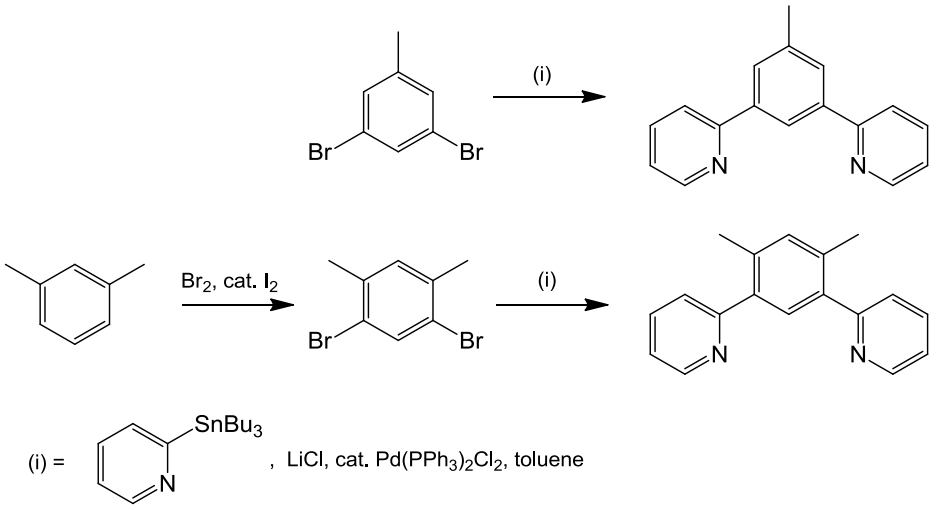

Scheme 3.4 Synthesis of N^C^N ligands dpytH and dpyxH.

The reaction of this ligand with $IrCl_3.3H_2O$ was attempted under conditions identical to those for the synthesis of $[Ir(dpyx)(\mu\text{-}Cl)Cl]_2$ by heating the metal salt and ligand at reflux in a mixture of 2-ethoxyethanol and water. Similarly to the case with dpyxH where the resulting dimer is fairly insoluble, the product of the reaction with dpytH was a yellow/orange solid which was, in fact, even less soluble. Despite its limited solubility, enough could be dissolved in d_6-DMSO to give a weak NMR spectrum which was consistent with an N^C^N bound product and given the structural similarity with dpyxH, it can be confidently assumed that the product was the dimer $[Ir(dpyt)(\mu\text{-}Cl)Cl]_2$ which is cleaved by DMSO to give $[Ir(dpyt)(DMSO)Cl_2]$.

3.2.2 Monometallic complexes for reaction with thiols

With these two dimers in hand, bridge cleaving reactions could be carried out to give monometallic complexes for subsequent reaction with thiols. The synthesis of both charge neutral and cationic complexes was carried out by cleaving the dimers with 2-phenylpyridine and 2,2'-bipyridine, respectively, under the conditions shown in Scheme 3.3. The synthesis of the highly phosphorescent complex [Ir(dpyx)(ppy)Cl] has already been reported[47] and the data in this case were consistent with those reported. The analogous procedure with $[Ir(dpyt)(\mu\text{-}Cl)Cl]_2$ resulted in a yellow product which was purified by column chromatography and showed an NMR spectrum consistent with the expected N^C^2 bound complex [Ir(dpyt)(ppy)Cl]. Cleavage of both dimers with bipyridine in ethylene glycol was also successful, so in all, the four complexes

shown in Figure 3.19 were available. Yields tended to be noticeably lower when using the methyl-substituted dipyridylbenzene than its dimethyl analogue, and the solubility of the complexes of the former ligand was slightly poorer than the corresponding complexes of a dpyx.

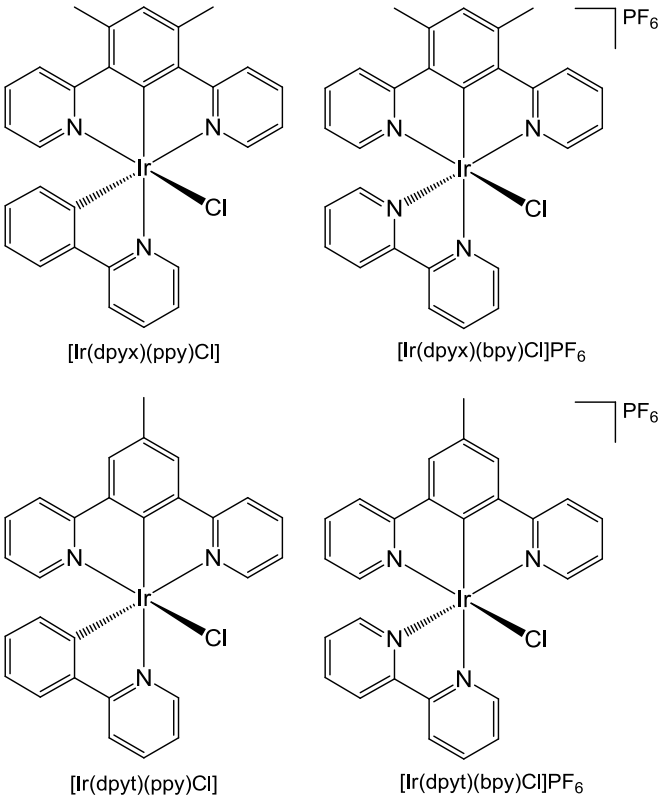

Figure 3.19 Monometallic Ir(N^C^N) complexes prepared incorporating a monodentate chloride ligand.

With these complexes, substitution reactions were attempted using three different aromatic thiols as well as the ethyl ester of L-cysteine under varying conditions. The latter was selected in place of cysteine itself in order to aid solubility and rule out possible competitive binding of the carboxylate group. Two general approaches were taken to investigate whether these various ligands would substitute the chloride ligand in the 6th coordination site of the complexes.

Firstly, the complexes were reacted directly with thiolates in methanol solution, obtained by addition of potassium tert-butoxide to the thiols *in situ*. These reactions were attempted both at room temperature and at reflux. In a second approach, the complexes were treated with silver(I) triflate (AgOTf) in refluxing acetone before the addition of a thiolate solution. This approach is designed to

encourage chloride substitution through formation of insoluble AgCl and has been shown to be effective in assisting substitutions in the iridium coordination sphere.[47] The results of these substitution attempts are shown in Scheme 3.5.

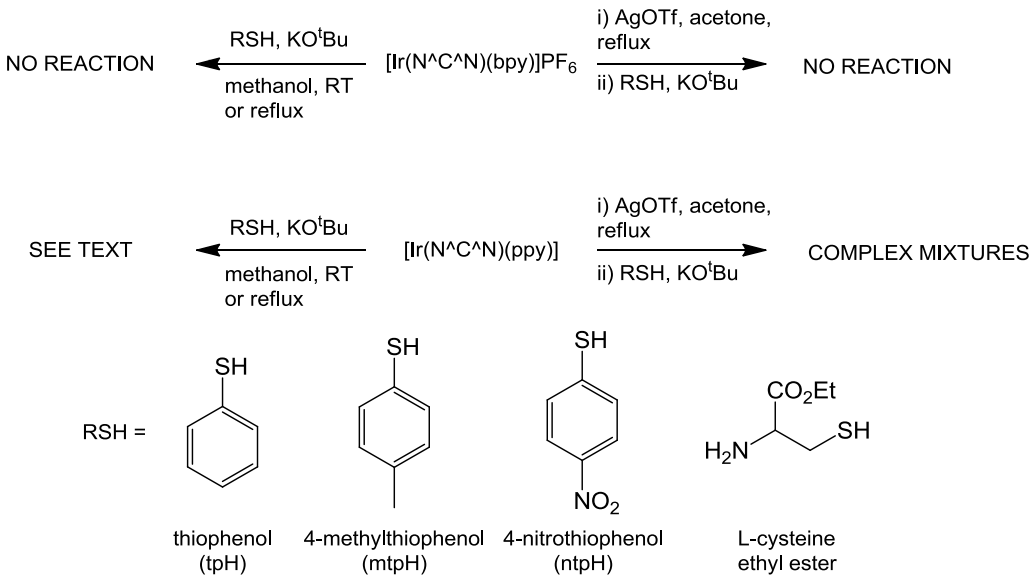

Scheme 3.5 Attempted substitutions of the chloride ligand in the [Ir(N^C^N)(N^C)Cl] and [Ir(N^C^N)(N^N)Cl]$^+$ complexes by thiolates.

NMR data from reactions of the aromatic thiolates with neutral complexes in methanol showed evidence of substitution of the chloride ligand, but the yield of substituted product was generally very low. In addition, the resulting products were relatively insoluble and difficult to separate from any residual starting material, with the exception of 4-nitrothiophenol where the product was soluble enough for isolation by column chromatography. In comparison, the use of silver(I) triflate tended to give more complex product mixtures, presenting further problems in the isolation of products. This could be a result of the affinity of Ag^+ for sulfur producing undesired side-reactions, although no direct evidence for this, e.g. the formation of black silver(I) sulfide, was observed.

In the case of the cationic complexes, in attempts at direct substitution in methanol it was clear that no reaction was taking place, with the starting material being recovered in almost quantitative yield. The chloride ligand in these systems is likely to be less labile than in the equivalent neutral complex, owing to the *trans* effect of the metallating carbon in the latter. Again, the use of AgOTf did not provide better results than the direct reaction with thiolates and the only materials isolated from these reactions appeared to be the chloride

complex and thiol. In all cases, the substitutions attempted using ethyl-L-cysteine gave complex mixtures, most likely as a result of competition between N and S bound products.

As a result of these reactions only one complex (shown in Figure 3.20), from the reaction of [Ir(dpyx)(ppy)Cl] with 4-nitrothiophenol (ntpH), was isolated at a satisfactory level of purity but in very low yield. The ^{1}H NMR spectrum is shown in Figure 3.21 and shows signals similar to the parent chloride complex with eight signals for the ppy ligand, five for the dpyx ligand and an additional two for the new ntp ligand. The reaction of the same complex with 4-methylthiophenol (mtpH) gave a product which was identifiable as the substituted complex by ^{1}H NMR but this was poorly soluble and of low purity. ^{1}H NMR also hinted at some substitution by thiophenol (tpH), however the quality of the sample and spectrum was very poor.

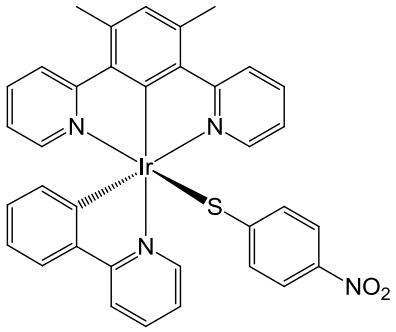

Figure 3.20 [Ir(dpyx)(ppy)(ntp)].

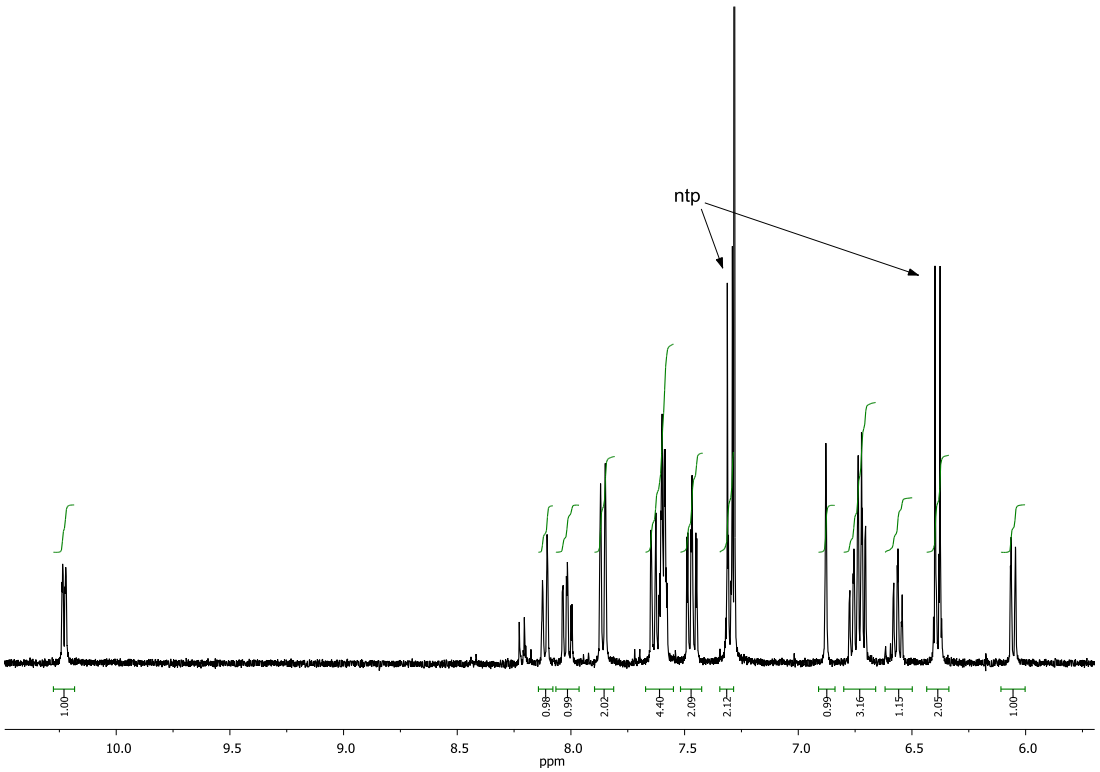

Figure 3.21 400 MHz ^{1}H NMR spectrum (aromatic region) of [Ir(dpyx)(ppy)(ntp)]. Arrows indicate signals from the ntp ligand.

It is possible that the failure in the majority of these substitutions is in part due to instability in the desired products. It is likely that an Ir-S bond in these complexes will be quite labile, particularly in the neutral complexes due to the *trans*-carbon. Any dissociation in aerated solution would lead to the loss of thiolate for re-coordination through the formation of disulfides. The fact that the only isolated complex contains the very electron withdrawing nitro group is consistent with this proposition, since the lower electron density on sulfur will reduce the rate of dissociation. It would be expected that the Ir-S bond would be less labile in [Ir(N^C^N)(N^N)(thiolate)]$^{+}$ complexes due to the increased nuclear charge on the metal centre and lower *trans* effect of the bipyridine nitrogen. It is therefore likely that in reactions with [Ir(N^C^N)(N^N)Cl]$^{+}$ complexes, substitution of the chloride is not occurring.

3.2.3 Direct reaction of Ir(N^C^N) dimers with thiolates

In addition to attempts at thiolate substitution in these [Ir(N^C^N)(N^X)] complexes, in parallel with the work on bis-bidentate cyclometallated complexes the reactivity of the chloride-bridged dimers towards thiolates was also explored. Given the observed tendency for the sulfur ligands to form bridged

species, it was of interest what would occur in terdentate dimers in which chloride ligands display both bridging and non-bridging coordination modes.

The reaction of $[Ir(dpyx)(\mu\text{-}Cl)Cl]_2$ was initially attempted with 4-nitrothiophenol in methanol at room temperature. ^{1}H NMR data indicated the formation of a new species containing both dpyx and ntp fragments, however a large amount of starting dimer remained in the sample as well as other impurities. In contrast, treatment with the thiolate, formed by addition of potassium tert-butoxide, in refluxing methanol yielded an orange product soluble enough to be purified by column chromatography. The NMR spectrum for this compound showed a set of signals consistent with a dpyx ligand as well as two sets of doublets arising from distinct ntp fragments. From the signal integrals, it appeared that these ligands were present in the complex in a 1:1:1 ratio of dpyx / ntp / ntp'. The ^{1}H NMR spectrum of the product is shown in Figure 3.22. Data from MALDI mass spectrometry showed a peak at m/z = 760, which is representative of the species $[Ir(dpyx)(ntp)_2]^+$.

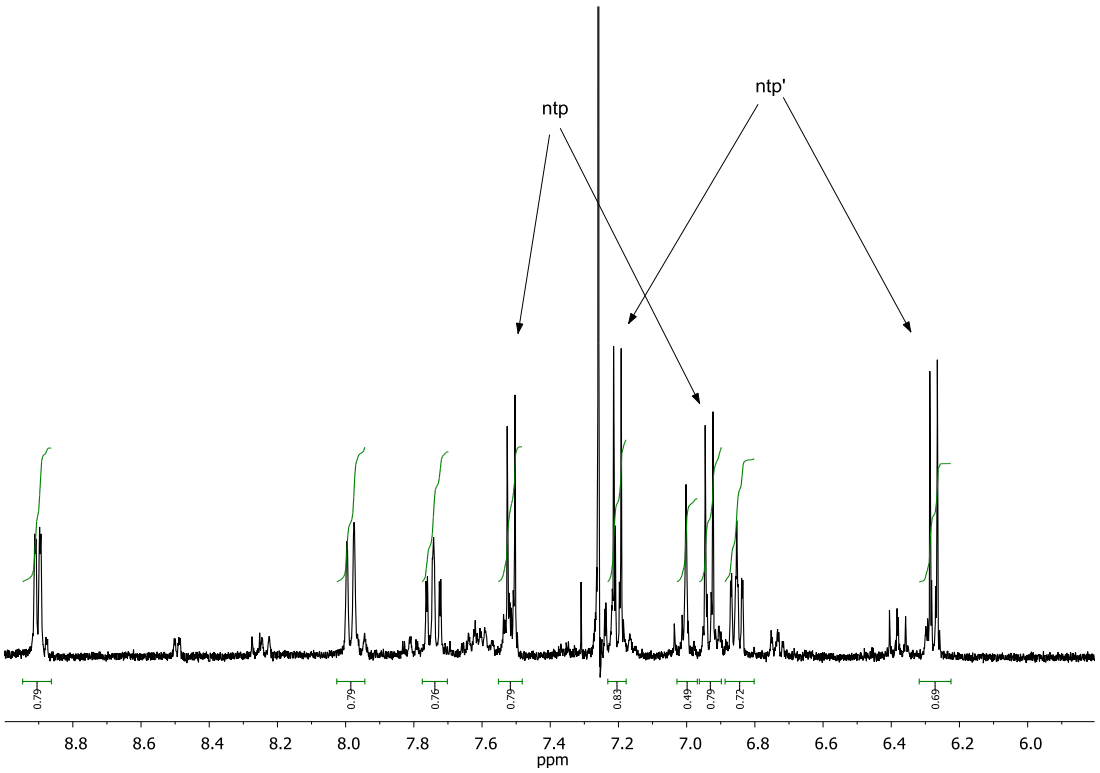

Figure 3.22 400 MHz ^{1}H NMR spectrum (aromatic region) showing the product of the treatment of $[Ir(dpyx)(\mu\text{-}Cl)Cl]_2$ with ntpH. Arrows indicate ntp fragments linked in ^{1}H COSY spectrum.

The structure of a species conforming to these data was initially difficult to rationalise, with the simplest representation consistent with the MALDI MS data requiring a 5-coordinate iridium centre. This species however, does not give the required distinction between the two ntp fragments shown in the NMR data. Instead, a dimeric structure is proposed similar to that of the starting chloride complex where two ntp ligands occupy single coordination sites while two others are found in bridging modes. The proposed structure of this [Ir(dpyx)(μ-ntp)(ntp)]$_2$ dimer is shown in Figure 3.23.

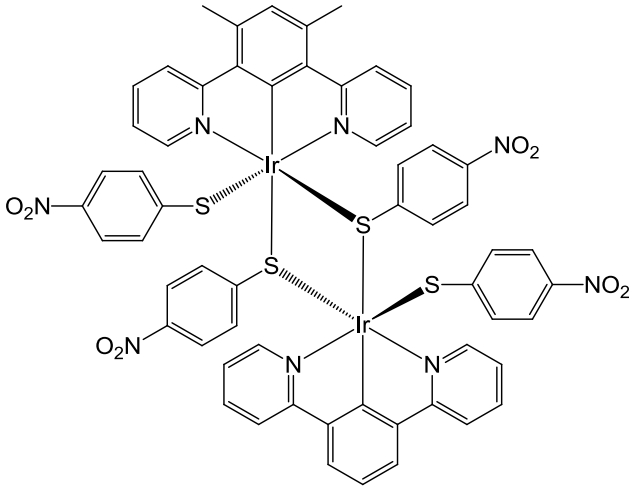

Figure 3.23 Possible structure of a [Ir(dpyx)(μ-ntp)(ntp)]$_2$ dimer

3.3 Concluding remarks

A series of iridium complexes containing both bidentate and terdentate cyclometalling ligands has been synthesised and the reactivity of these species with various sulfur-containing ligands has been explored.

In reactions with [Ir(ppy)$_2$(μ-Cl)]$_2$, two new monometallic complexes with pyridines as ancilliary monodentate ligands were synthesised. While subsequent reactions of these complexes with aromatic thiolates did not produce the desired monometallic species, a novel class of thiolate bridged dimers has been discovered. One of these, [Ir(ppy)$_2$(μ-ntp)]$_2$, displayed a remarkable solid-state vapochromic effect although the specific cause of this remains unclear. While it seems generally the case that in their synthesis these new dimers adopt a racemic mixture of Δ,Δ and Λ,Λ configurations of the iridium centres, a small amount of the kinetic Δ,Λ (or meso) isomer of [Ir(ppy)$_2$(μ-mtp)]$_2$

was also synthesised and its stereochemical assignment has been confirmed by NMR and computational data. This isomer, however, appears to undergo interconversion to the more thermodynamically stable racemic form when left in solution.

It has also been shown that in the use of terdentate N^C^N ligands, a single methyl group in the ligand 3,5-di(2-pyridyl)toluene is sufficient to overcome issues with C^2/C^4 competitive binding to iridium. While subsequent reactions of thiols with mononuclear complexes containing an N^C^N and a single bidentate ligand were mostly unsuccessful, some products were obtained and it is possible that by refining the reaction conditions, compounds of the type [Ir(N^C^N)(N^C)(thiolate)] and $[Ir(N^C^N)(N^N)(thiolate)]^+$ could be made for study. Reactions of aromatic thiolates directly with N^C^N containing dimers, however, did produce a novel compound with thiolates in both bridging and non-bridging sites.

Chapter 4

Potential luminescent PDI mimics

4 Potential luminescent PDI Mimics

One of the main aims of this project was to produce novel compounds that might mimic the activity of Protein Disulfide Isomerase while displaying some fluorescence or phosphorescence that would allow their use in probing sub-cellular sites of activity through visual assays such as fluorescence microscopy.

It is clear from the structure of the PDI active site that its isomerase activity proceeds via thiol/disulfide interchange reactions between itself and the substrate. As discussed previously, the reactivation of scrambled Rnase enzymes can be accelerated by a wide variety of thiol containing molecules, so any potential molecular mimic must therefore contain at least one thiol group that is free to engage in similar interactions. It would be preferable, though, to have two thiol groups to more accurately model the Cys-Gly-His-Cys active site, as shown in studies with (±)-*trans*-1,2-*bis*(2-mercapto-acetamido)cyclohexane (BMC) versus N-methylmercaptoacetamide (NMA)[95] (shown in Figure 4.1). The studies with BMC and NMA showed that while the mono thiol did show mimic activity, it was lower than the corresponding dithiol and the latter showed a lower tendency to become 'trapped' due to its ability to escape from a catalyst-substrate complex in the same manner as PDI (Section 1.2.1.1)

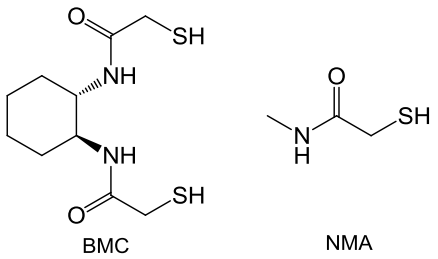

Figure 4.1 BMC and NMA.

Given that it is the expressed aim of the project to produce, in particular, fluorescent PDI mimics, two initial approaches to potential targets were envisaged. Firstly, the direct functionalisation of an appropriate fluorescent molecule, or secondly the synthesis of an independent unit with the functionality of a potential PDI mimic which could be attached covalently to a range of fluorophores using, for example, peptide coupling chemistry or a cross-coupling

reaction. It was decided that since BMC had been proven to show PDI mimic activity, its structure would provide a sensible motif for any target molecules. The synthesis of BMC is shown in Scheme 4.1, and it is clear that, potentially, any diamine can be functionalised in the same way.

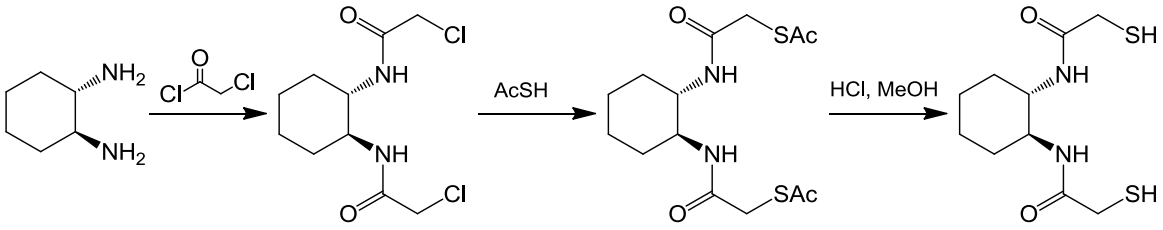

Scheme 4.1 Synthesis of BMC.[99]

With regards to the desired fluorescence in the target molecules, there are many possible options to explore ranging from simple aromatics such as anthracene, as well as other more biocompatible organic compounds common in biological fluorescence labelling such as coumarin, dansyl or fluorescein derivatives. Another possible group of emitters would be luminescent transition metal complexes. As previously discussed, complexes of metals such as ruthenium and iridium with polypyridyl or phenylpyridine ligands display stable long-lived emission in fluid solution. Such compounds could prove very useful in providing the potential for time-resolved fluorescence studies, given the possibility that in combination with the thiol/disulfide functionality there may be a significant difference in fluorescence lifetime between oxidised and reduced forms as a result of electron transfer quenching. The expected long lifetimes of transition metal phosphors would also be useful in avoiding interference from autofluorescence as discussed in Section 1.4.2. A further advantage in the use of transition metal complexes over organic emitters is the relative ease with which the colour of emission can be altered giving more flexibility in imaging applications.

Synthetically, the use of d^6 transition metal complexes with polypyridyl and cyclometallating ligands would also allow a varied approach to possible targets. It has been established that when correctly functionalised, certain complexes of this class readily undergo cross-coupling reactions to form elaborated systems or even multimetallic complexes,[48] so a similar approach could be used to attach a fluorescent complex to an appropriate mimic structure by similar

methods. Alternatively, the design of a functionalised ligand would provide the opportunity to form a complex directly.

It was anticipated that complications might arise from the easily oxidised dithiol motif of any target molecules, especially in cases where these structures would have to undergo further reactions to reach a final target – for example in a case where a mimic structure is coupled to a separate fluorophore. Fortunately, as is the case in the synthesis of BMC, thiol groups can be introduced to a molecule in a protected form and so possible synthetic routes were devised with this in mind, allowing the deprotection of the thiol groups to always be performed as a final step.

4.1 Aromatic diamines as cores for the synthesis of BMC-like units

As discussed there are potentially several approaches to the formation of a complete mimic structure, either by direct functionalisation or a coupling methodology. It was therefore decided to attempt the synthesis of different classes of diamines that could be of use in these various approaches.

4.1.1 Functionalised units for cross-coupling to a fluorophore

Initially, the synthesis of brominated aromatic analogues of BMC was attempted to provide possible mimic structures attachable by cross-coupling reactions. Both 4-bromo-1,2-phenylenediamine and 5-bromo-2,3-diaminopyridine are available as starting materials and so these were used as the starting point of synthetic routes analogous to that for BMC. The pyridine analogue, however, did not react cleanly with chloroacetyl chloride, producing a complex mixture of products. The 1,2-phenylenediamine on the other hand reacted as expected and was taken to the next stage by reaction with thioacetic acid. The product at this stage, however, was difficult to obtain to a sufficient level of purity and showed a tendency to decompose. These reactions are summarised in Scheme 4.2.

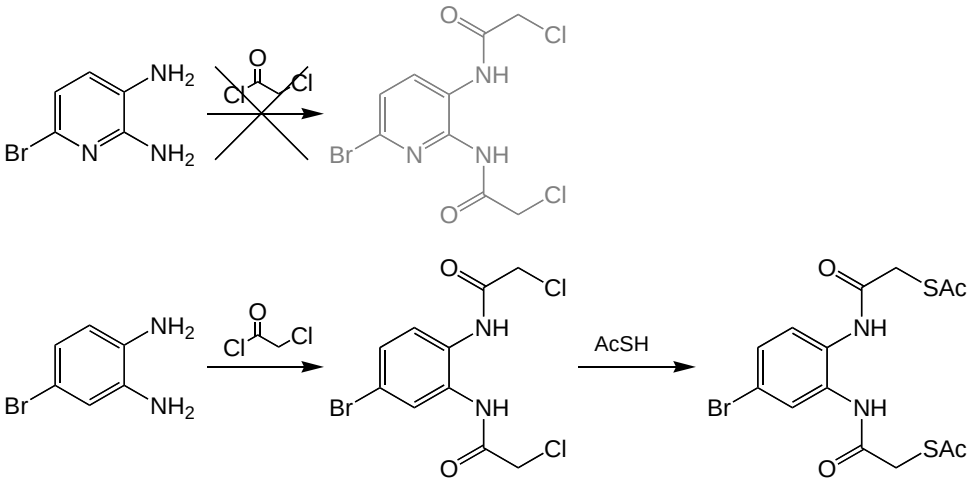

Scheme 4.2 Attempts to repeat BMC-like synthesis with aromatic bromides.

Despite this instability, a test reaction to determine whether this was a suitable aryl halide for cross-coupling reactions was carried out. A Suzuki reaction was attempted with a functionalised bipyridine in the hope that this would produce a ligand for use in a transition metal complex. The functionalised bipyridine was prepared using the Miyaura borylation reaction which is a convenient method to convert aryl bromides into boronate esters for use in Suzuki couplings.[214] This reaction follows a similar mechanism to palladium catalysed cross-coupling reactions only a C-B bond is formed, rather than a C-C bond (Scheme 4.3).

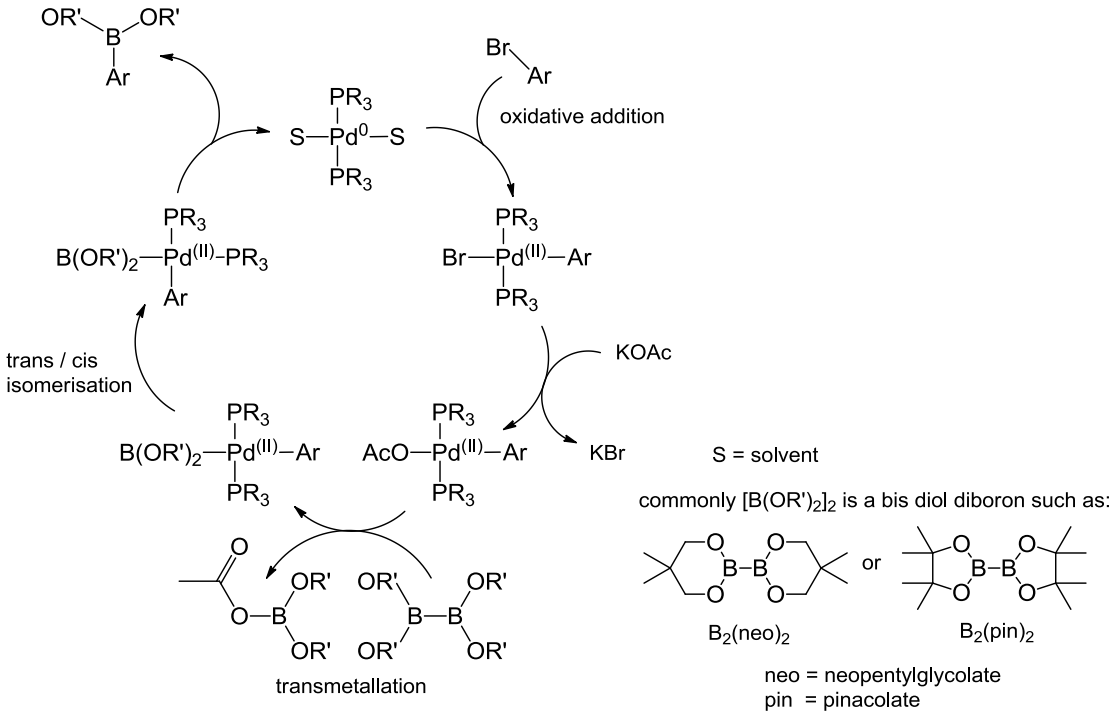

Scheme 4.3 General mechanism of a Miyaura borylation reaction.

No product could be isolated from the Suzuki coupling since the apparent instability of the bromide starting material was also observed in the product mixture with products tending to decompose during column chromatography. Scheme 4.4 shows the Miyaura coupling to produce a boronate ester substituted bipyridine ligand and the subsequent Suzuki attempt.

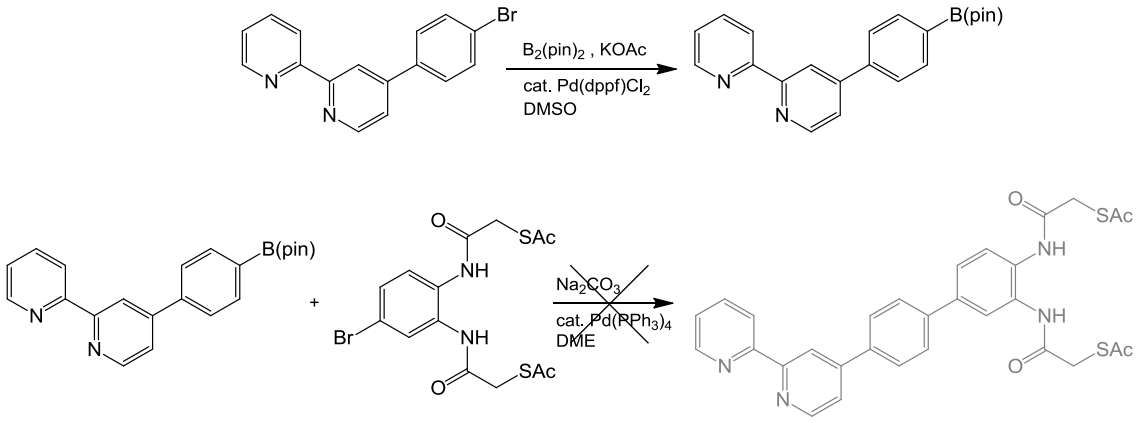

Scheme 4.4

4.1.2 A diamine functionalised N^N ligand

As well as this initial approach towards functionalised linkers, attempts were made to produce a directly functionalised diimine ligand for use with transition metals such as iridium. It has been reported that 5,6-diamino-1,10-phenanthroline (phen-diamine) can be synthesised under mild conditions from 1,10-phenanthroline-5,6-dione (phen-dione), as well as this conversion being possible with the ligand already coordinated to ruthenium[215] as shown in Scheme 4.5. This would provide two options for synthesis of a potential target with functionalisation of the diamine either before or after coordination to a metal.

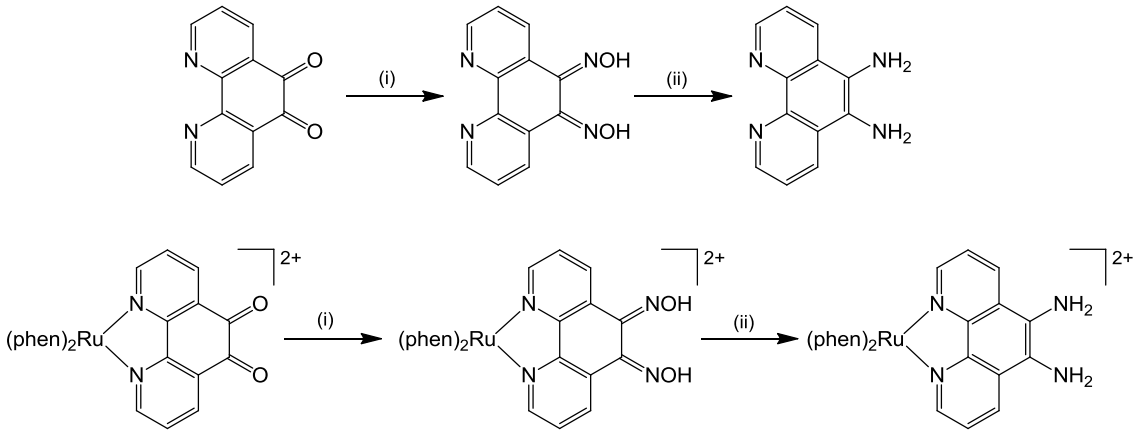

(i) $NH_2OH.HCl$, $BaCO_3$, EtOH, reflux. (ii) 10% Pd/C, N_2H_4, EtOH, reflux

Scheme 4.5 The conversion of 1,10-phenanthroline-5,6-dione to 5,6-diamino-1,10-phenanthroline as both a free and coordinated ligand.[215]

Attempts to react the uncoordinated 5,6-diamino-1,10-phenanthroline with chloroacetyl chloride were unsuccessful, with reactions tending to give complex mixtures. Any attempt to purify by column chromatography returned only starting material and it appeared that the product was unstable on the column. It is likely that this aromatic diamine, being very electron rich, is prone to oxidation which could be a factor in the complex reaction mixtures and instability of the product. No specific side-products could be identified to try and determine more specifically why this reaction was unsuccessful.

Since the functionalisation of this ligand was not possible in its uncoordinated form, it was decided to try and prepare complexes with the phenanthroline diamine or dione ligand before attempting to add the mimic structure. It is possible that by coordination to a metal, the oxidative instability of this system could be lessened, as the electron richness of the aromatic system would be attenuated by bonding to the metal.

Complexes of iridium(III) containing two 2-phenylpyridine ligands and a diimine ligand are usually easily prepared from the dimer tetrakis(2-phenylpyridine)(μ-dichloride)diiridium(III) (Figure 4.2) and the appropriate diimine ligand as discussed in Section 3.1.

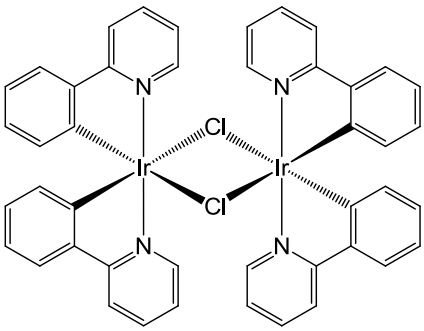

Figure 4.2 $[Ir(phpy)_2(\mu\text{-}Cl)]_2$

Initially, the synthesis of a complex with 5,6-diamino-1,10-phenanthroline was attempted but this ligand failed to react cleanly with the iridium dimer, possibly as a result of alternate binding modes introduced by the ortho-diamine structure. Instead, the ligand 1,10-phanthroline-5,6-dione was reacted with the dimer to give the corresponding mononuclear complex $[Ir(phpy)_2(phen\text{-}dione)]PF_6$. Since it has been reported that this ligand could be converted to the diamine via the hydroxyl imine while coordinated to ruthenium it was expected that a similar conversion could be carried out here. When treated with hydroxylamine, however, the only product that could be identified was the complex where only one of the two ketones had undergone the conversion to the hydroxyl imine (Scheme 4.6).

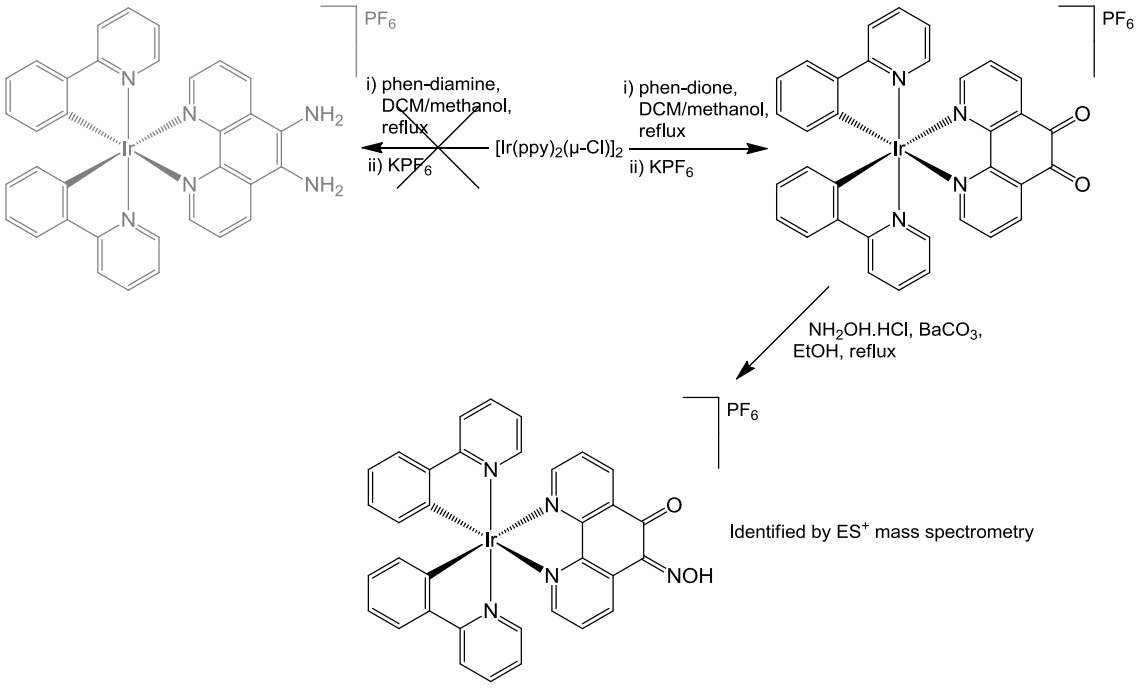

Scheme 4.6 Direct and indirect attempts to synthesise a diamine-containing iridium complex.

4.1.3 Directly functionalised organic emitters

In addition to the attempted functionalisation of phenylenediamine type compounds and the phenanthroline ligand and complex, it was also decided to explore the possibility of directly functionalising an organic fluorescent molecule and so anthracene derivatives were selected as a simple starting point. While the emissive properties of anthracene are not as tuneable and long-lived as those available from transition metal complexes, it does display relatively strong blue emission.[216] As a relatively simple system it was also expected that there should be few complications in the synthesis of potential mimics based on this structure. 2-Aminoanthracene is available and 1,8-diaminoanthracene can be obtained by the reduction of 1,8-dinitroanthraquinone.[217,218] The use of these two amines as staring materials would provide singly and doubly functionalised compounds respectively which, as well as both being potential mimics, also provide the opportunity to study the difference in activity between the two.

Attempts to repeat the one step reduction of 1,8-dinitroanthraquinone with $NaBH_4$ as reported in ref 218 were unsuccessful so instead the reduction was performed with Sn/HCl giving 1,8-diaminoanthraquinone. This was then subsequently reduced to the diamine with $NaBH_4$. Unfortunately a pure product could not be isolated from the reaction of this diamine with chloroacetyl chloride. The equivalent reaction with 2-aminoanthracene, on the other hand, did proceed as expected, as did the substitution of chloride with thioacetate, however the products throughout these steps were difficult to purify by column chromatography or recrystallisation and showed some tendency towards decomposition. All attempts to deprotect the thiol group to give the final structure gave only complex mixtures. These reactions are summarised in Scheme 4.7.

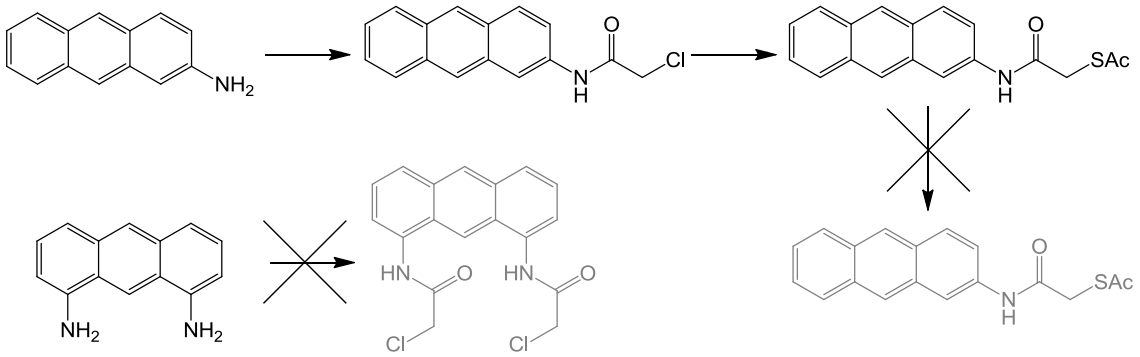

Scheme 4.7 Attempted syntheses of anthracene based mimics.

All the synthetic routes described have utilised aromatic amines, unlike the aliphatic amines in the structure of BMC. It is possible that problems encountered during the substitution reaction with chloroacetyl chloride could be the result of the lower nucleophilicity of aromatic amines compared to their aliphatic counterparts, although it would be expected that the reaction should still proceed due to the reactivity of the acyl chloride unit. It is feasible that a slower rate in the substitution at the carbonyl group could lead to an intramolecular cyclisation reaction with chloroacetyl chloride rather than two intermolecular substitutions as desired. Unfortunately, no evidence of any side reaction in particular was found to provide clues of where the problems were arising. It was the case, in fact, that the majority of compounds handled in these reaction steps showed a tendency towards decomposition, with most reactions producing complex mixtures in which it was difficult to identify any individual components or products degrading to dark insoluble matter. It may, then, be the case that, due to the very electron rich nature of the aromatic diamine structure, most of these compounds are prone to oxidation leading to the observed instability of the desired intermediate compounds.

4.2 Non-aromatic diamines

Given the lack of success with aromatic diamines it was decided to continue with a similar approach to the synthesis of a potential mimic but using aliphatic amines instead of the problematic aromatic amines.

4.2.1 Non-aromatic diamines with cross-coupling potential

With this in mind it was decided to follow a synthesis analogous to that shown in Scheme 4.4 above, but, instead of an ortho-phenylenediamine structure, to use a starting compound like that shown in Figure 4.3. Here, a CH_2 spacer has been introduced to insulate the amines from the aromatic ring. While this small molecule is not commercially available, a synthetic route, shown in Scheme 4.8, adapted from one reported for the synthesis of 4-bromophthalonitrile,[219] was devised.

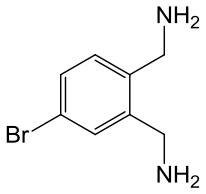

Figure 4.3

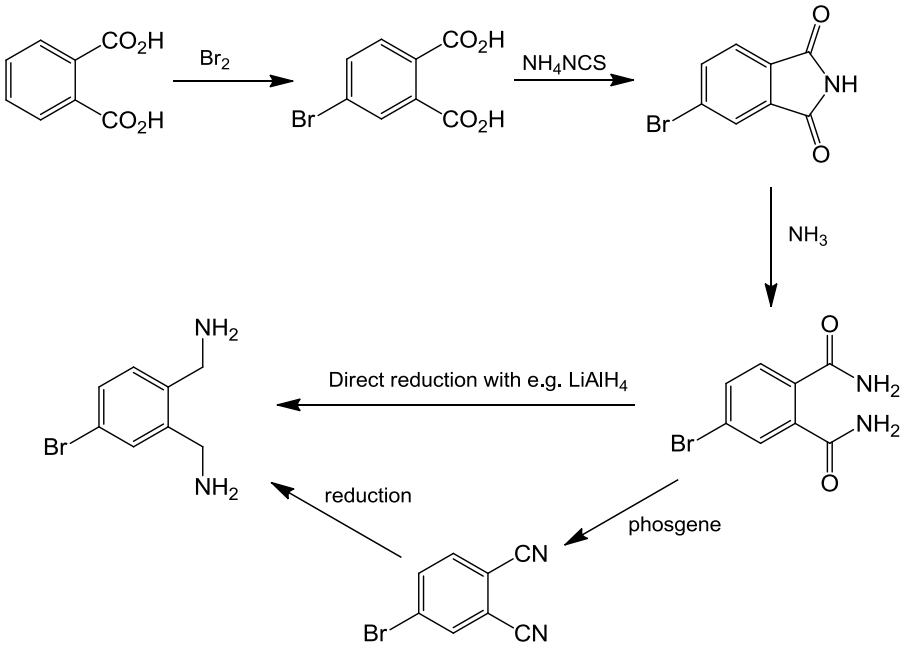

Scheme 4.8 Possible routes to 3,4-di(aminomethyl)bromobenzene.

The steps up to the synthesis of the diamide were completed successfully and several attempts were made to reduce this product directly to the diamine using $I_2/NaBH_4$.[220] While there was evidence of the desired product shown by mass spectrometry, the reaction did not proceed cleanly so it was decided instead to perform the conversion to the nitrile compound using phosgene. This approach proved advantageous in that the phthalonitrile compound could be obtained easily, in high yield and was relatively easy to purify by column

chromatography. Also, given that the intent in this approach was leading towards a cross-coupling reaction with a fluorescent moiety or possible transition metal ligand, this structure provided a useful point within the overall scheme for the cross-coupling to be carried out. The nitrile groups present at this stage would be unlikely to interfere with a cross-coupling reaction whereas, if the coupling were carried out at a later stage, the functional groups present (namely amine, amide and thioester added sequentially) would possibly cause complications with the cross-coupling reaction. It was therefore decided at this stage to couple the 4-bromophthalonitrile with a bipyridine unit using a Suzuki-Miyaura coupling as shown in Scheme 4.9.

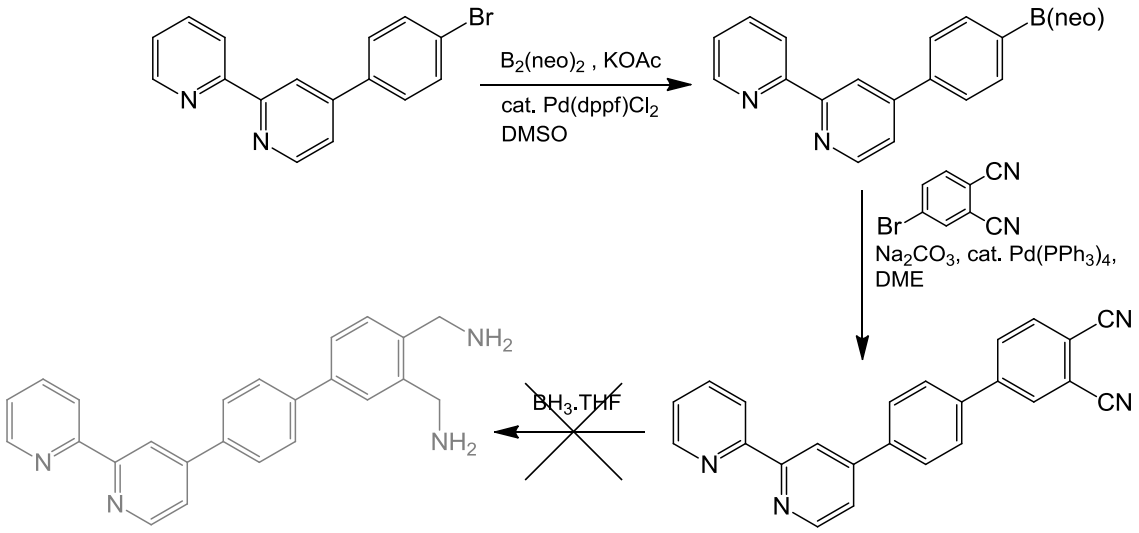

Scheme 4.9 Miyaura Borylation and Suzuki-Miyaura coupling to give a functionalised bipyridine ligand.

At this point it would be possible to use this bipyridine unit as a ligand to form a complex with iridium before subsequent functionalisation. However, since the next step in functionalisation involves the reduction of nitriles to amines, it was decided to delay the formation of the complex until a later stage to avoid exposing it to reagents such as borane or $NaBH_4$. However, upon the attempted reduction of the nitriles with BH_3.THF, a pure product could not be isolated from the reaction. Similarly, attempts to perform the reduction with $NaBH_4$ were also unsuccessful. While it seemed that some product was formed by the reaction, the components in the mixture were highly immobile or streaky in column chromatography. It was therefore not possible to purify the product by this means, and the mixture did not seem suitable for purification by recrystallisation or distillation.

4.2.2 Organic emitters with non-aromatic amine substituents

In another approach analogous to the synthetic route attempted with anthracene, the option of functionalising a different organic fluorophore with non-aromatic amines was investigated. The phenolic structures in fluorescein (shown in Figure 4.4) will undergo Mannich reactions to form amines and this approach had previously been used to synthesise fluorescent sensors for metal ions in biological systems.[221,222] These sensors were produced using the 2,7-dichlorofluorescein derivative, to ensure that substitution occurred only at the 4 and 5 positions of the molecule. While in these reports, the Mannich reactions were performed with secondary amines, giving tertiary amine products, if this reaction would proceed with ammonia the resulting primary amines could be functionalised to give a possible mimic.

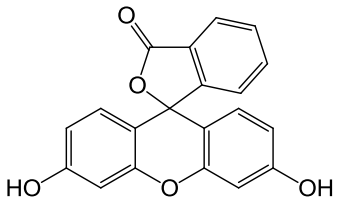

Figure 4.4 Fluorescein

Mannich reactions were therefore attempted using 2,7-dichlorofluorescein with both aqueous ammonia and ammonium chloride to give the primary amines required for functionalisation, however the products isolated from the reaction were highly insoluble and could not be positively identified as the required diamine. The only component identified was the starting material, which was detected in negative electrospray mass spectrometry. It was unclear, however, whether the material was a mixture of products including some starting material or whether there had been no reaction.

In an attempt to overcome this problem with insolubility, Mannich reactions were instead performed with benzyl amines with the intention of subsequently removing the benzyl groups by hydrogenation. These reactions were carried out using both benzylamine and dibenzylamine which would give secondary and tertiary amine products respectively. The reactions carried out with 2,7-dichlorofluorescein are summarised in Scheme 4.10.

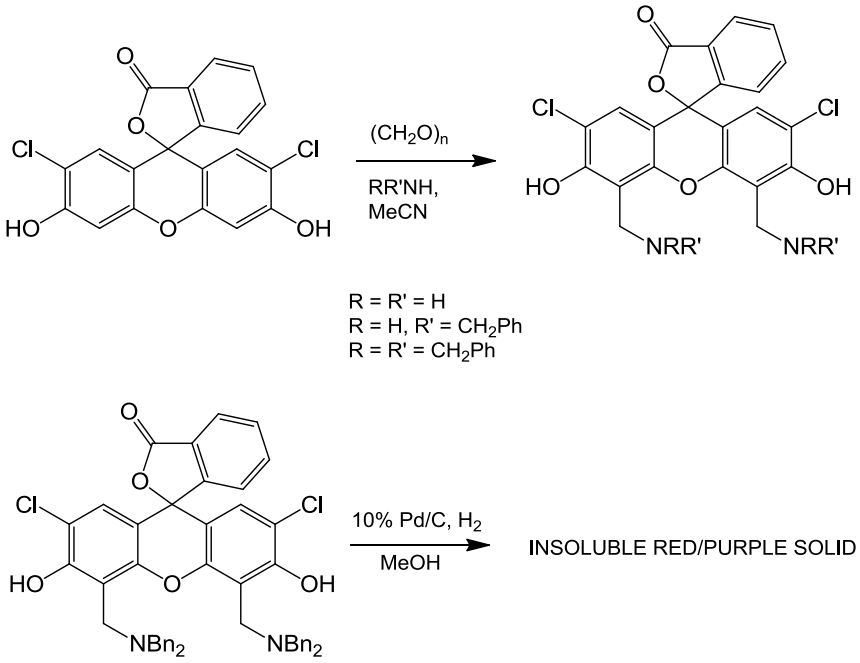

Scheme 4.10 Attempted Mannich reactions with 2,7-dichlorofluorescein and subsequent deprotection of amines.

In the reaction with benzylamine the products were, again, very insoluble and could not be identified. The reaction with dibenzylamine, on the other hand, resulted in a red solid that could be purified by column chromatography, although the yield was very low. This was identified as the expected product of a Mannich reaction by mass spectrometry, however evidence that it was the correct product was less clear using NMR spectroscopy due to the large number of overlapped benzyl aromatic signals. When this product was treated with hydrogen gas in the presence of 10% palladium on activated carbon as a catalyst in methanol, a red/purple precipitate was produced. When isolated, though, this again was too insoluble to be positively identified as the desired primary diamine.

By this point there had been very little success, for various reasons, in synthesising a potential PDI mimic structure, even without the attachment of a fluorescent unit to give a finished target molecule. As discussed previously, the reactions using aromatic amines were problematic in terms of stability, while up to this point, a system with aliphatic amines suitable for functionalisation had not yet been synthesised successfully. It was therefore decided to look into alternate strategies for the synthesis of a mimic structure that would perhaps

cause fewer complications. While it is the case that a variety of structures containing thiol groups have been shown to isomerise non-native disulfide bonds in proteins, the functional groups used by PDI itself are, of course, cysteine residues. In light of this, it seemed feasible that the amino acid cysteine could be used as the mimic part of a final target, and could be attached to a variety of structures by the formation of an amide with either an amine or a carboxylic acid.

4.3 Cysteine as a mimic structure

Amides are found in many natural molecules as well as being a common feature in many compounds with pharmaceutical relevance and as such, their synthesis has been studied in depth.[223] They are, of course, ubiquitous in biological systems given that all proteins rely on the amide functional group as the covalent link between amino acids in their primary structure. The formation of an amide between cysteine and an appropriate fluorophore or linker could provide a simple, one-step addition of a potential mimic structure. It is possible to attach cysteine to the fluorophore via either its amine or acid group as shown in Figure 4.5, however, given the lack of success so far in the synthesis of appropriate amines, it was decided to concentrate on the synthesis of carboxylic acid functionalised linkers and fluorescent molecules.

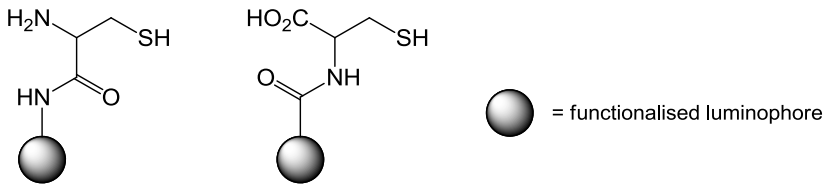

Figure 4.5

In using an amide to link cysteine to a fluorophore, the unused amine or carboxylic acid group will remain unbound. It was therefore considered that the need may arise for the use of a protecting group to mask this functional group in order to avoid possible side reactions or reactivity in the final product. Bearing this in mind, the coupling of cysteine through its amine functional group would also be advantageous in comparison to a coupling using the carboxylic acid due to the possible protecting groups for the unused functional group. The carboxylic acid can easily be protected as a relatively small ester group while

appropriate protecting groups for the amine such as FMOC or BOC groups would be much larger and could introduce steric problems to the action of a mimic.

In order to determine whether this approach was worth following, the formation of a diamide was attempted by the reaction of phthalic acid with L-cysteine ethyl ester using the peptide coupling reagent 1-ethyl-3-(3-dimethylaminopropyl)-carbodiimide hydrochloride (EDCI). This reaction did not proceed cleanly, however, possibly as a result of steric hindrance with the acid groups being ortho to one another. Instead, the reaction was attempted with 5-bromoisophthalic acid, obtained by diazotisation of 5-aminoisophthalic acid ethyl ester and subsequent copper catalysed reaction with bromide. It was expected that this would reduce these steric factors and the desired diamide was successfully isolated as shown in Scheme 4.11. Purification of this compound was not straightforward as in solution it showed a tendency to degrade, almost certainly through the formation of intra and intermolecular disulfides through oxidation. It could be stored for a few weeks under nitrogen when dry with only a small amount of apparent degradation.

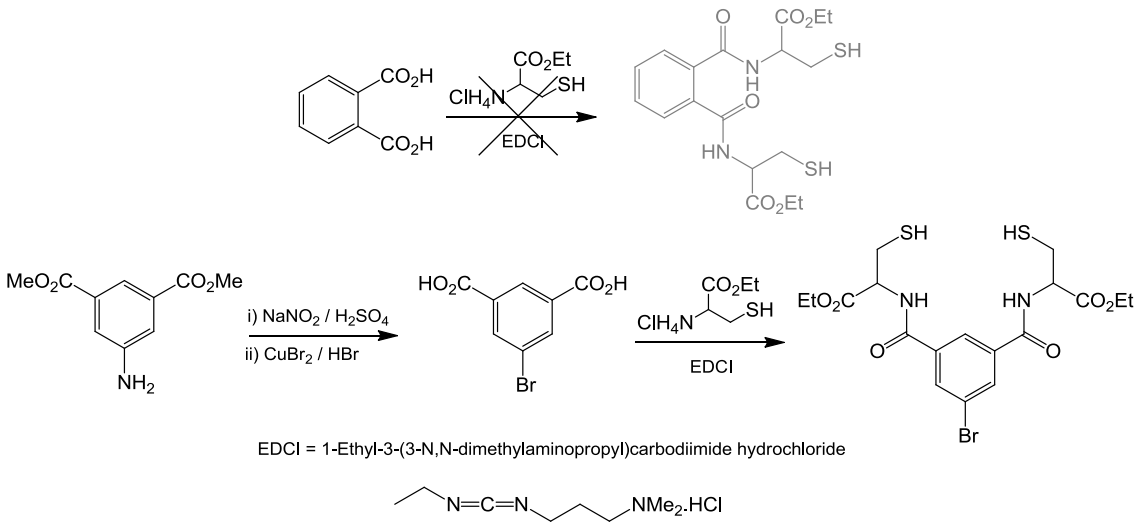

Scheme 4.11 Peptide couplings of phthalic acid derivatives with L-cysteine ethyl ester.

4.3.1 Carboxylic acid functionalised luminophores

Having established that the isophthalic acid structure could successfully be coupled to cysteine, it became necessary to devise a fluorescent probe containing this, or a similar structure.

4.3.1.1 Diacids suitable for cross-coupling reactions

The compound 5-bromoisphthalic acid which was used in the peptide coupling should in principle undergo cross-coupling reactions and so initially, attempts were made to perform a Suzuki reaction with anthracene-9-boronic acid to give a fluorescent diacid which could then be reacted with cysteine to give a potential mimic. Unusually, this reaction did not proceed as expected, with the only product identified being the result of deborylation of the anthracene starting material, i.e. anthracene itself. One possibility for the lack of reaction with the bromide is interference by the carboxylic acid groups so an alternate method was tried where these were protected as esters for the cross-coupling reaction.

In a reaction analogous to the preparation of 5-bromoisophthalic acid it is possible to react the diazotised compound with potassium iodide under milder conditions which does not give concurrent hydrolysis of the methyl esters. It was therefore decided to try the cross-coupling with dimethyl-5-iodoisophthalate, prepared in this manner. This reaction was attempted several times and while a trace amount of the required product was sometimes obtained, most of the material recovered from the reaction was, again, anthracene or the starting halide compound. It is has been shown that similar problems with deborylation in Suzuki couplings are more common with aryl boronic acids with sterically hindering ortho substituents,[224,225] however in many cases these problems can be overcome through varying the reaction conditions.[226,227] The sterically hindered position of the boronic acid on the central ring of anthracene was therefore likely to be the cause of the resulting deborylation. A highly active class of palladium catalysts with N-heterocyclic carbene (NHC) ligands for use in Suzuki[228] and Negishi[229] had recently been reported and so a further attempt at the coupling was made using one of these PEPPSI™ catalysts. The conditions used in this reaction, however, also failed to yield the desired product. The results of these attempted cross-couplings are illustrated in Scheme 4.12.

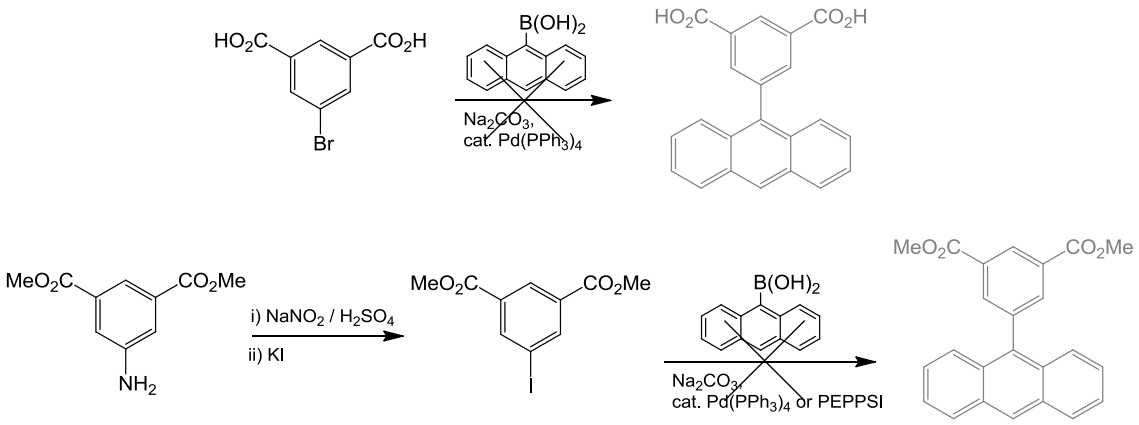

Scheme 4.12 Attempted cross-coupling reactions with anthracene-9-boronic acid.

In light of the problems associated with anthracene-9-boronic acid various other cross-coupling strategies were attempted to achieve the desired functionalised anthracene unit. If the functional groups used in the previous Suzuki coupling were reversed, i.e. with a halide substituted anthracene and a boronate ester or boronic acid funtionalised isophthalic acid, this could avoid the steric issues observed in the previous attempts. Using dimethyl-5-iodoisophthalate as a starting material, several Miyaura borylation reactions were performed to give a boronate ester which could subsequently be coupled with 9-bromoanthracene as shown in Scheme 4.13. The initial Miyaura reaction, however, did not yield the expected boronate ester but instead, the major product was the tetrasubstituted biphenyl compound tetramethyl-1,1'-biphenyl-3,5,3',5'-tetracarboxylate. It appeared that the boronate ester produced in the coupling was reacting immediately with unreacted starting material under the reaction conditions to give this homo-coupled product.

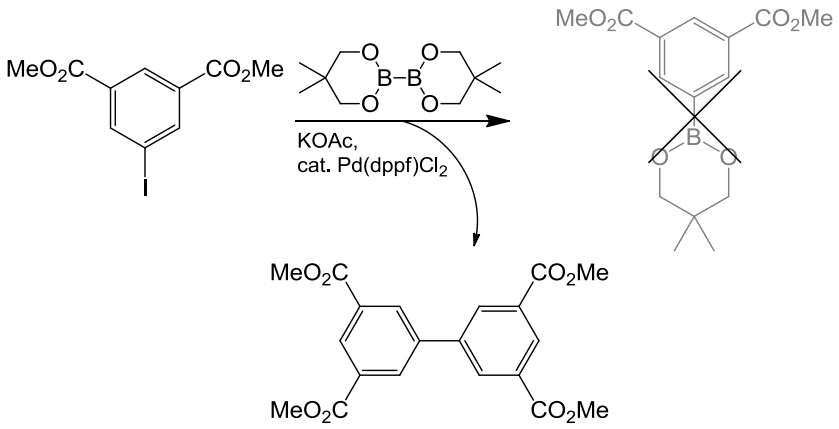

Scheme 4.13 Unexpected homo-coupled product from Miyaura coupling.

An alternative cross-coupling reaction to the Suzuki coupling is the Stille reaction where an arylstannane is used in place of an arylboronic acid or ester. Appropriate stannanes can be formed by treatment of an aryl halide with n-BuLi followed by addition of a trialkylstannyl chloride. It was therefore decided to attempt this methodology using 9-bromoanthracene with the resulting stannane used in a Stille reaction with dimethyl-5-iodoisophthalate. The formation of stannanes of anthracene was attempted using both tri-n-butylstannyl chloride and trimethyl stannyl chloride (Scheme 4.14) however reactions using both of these reagents failed to yield a functionalised anthracene compound. While lithiation of the 9-bromoanthracene appeared to occur during the reaction evidenced by a rapid colour change from colourless to yellow upon addition of n-BuLi, after quenching with the stannyl chlorides the only product that was obtained from the reaction was unsubstituted anthracene, in one case recovered in 90% yield.

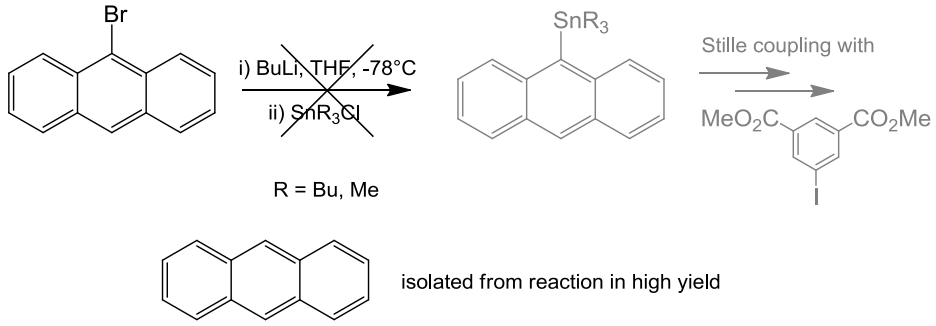

Scheme 4.14 The formation of anthracene-9-stannanes via lithiation with n-BuLi.

Finally, in addition to the cross-coupling reactions with anthracene, a Suzuki coupling was also attempted with dimethyl-5-iodoisophthalate and (4-(2,2'-bipyridin-4-yl)phenyl)(neopentyl glycolato)boron (Scheme 4.15) however no products could be isolated from this reaction.

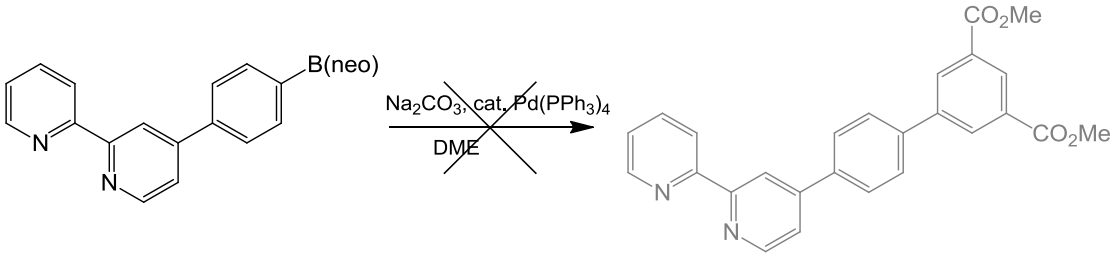

Scheme 4.15 Suzuki coupling to give a functionalised bipyridine ligand.

4.3.1.2 Functionalised dansyl compounds

Since there had been little success in using cross-coupling methods to synthesise a carboxylic acid functionalised emitter, a new approach was begun utilising the dansyl group as the fluorescent unit. Dansyl chloride has been used extensively in many sensing applications from early work in peptide and protein sequence determination through to modern chemosensing applications.[230,231,232] A distinct advantage of dansyl chloride is that it will react readily with most amines to form a relatively stable sulfonamide link, a property that led to its early use in labelling N-terminal peptide residues. Since the molecule 5-aminoisophthalic acid dimethyl ester was already being used as a starting material for the halo-isophthalates discussed above, it was thought that the formation of a sulfonamide between dansyl chloride and this amine would lead very simply to a fluorescent unit with the possibility for coupling to cysteine.

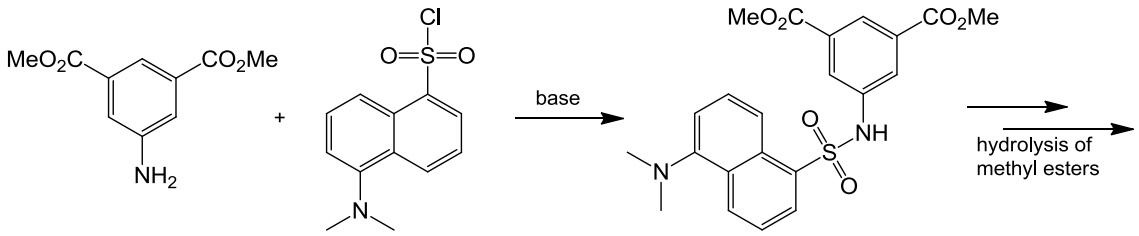

Scheme 4.16 Formation of a sulfonamide linked fluorophore and diacid species.

It was expected that the reaction of dansyl chloride with dimethyl-5-iodoisophthalate in the presence of a base would lead to a sulphonamide-coupled product, and subsequent hydrolysis of the methyl esters would then give the desired fluorescent diacid (Scheme 4.16). Initially, the reaction was performed using DMAP as the base, but it transpired that this base was in fact strong enough to allow the resulting sulfonamide to react a second time with dansyl chloride and the N,N-bis dansyl structure shown in Scheme 4.17 was the only product isolated. While this structure could be of interest, the desired mono sulfonamide would be a simpler, lower molecular weight alternative. The reaction was therefore repeated using a weaker base, pyridine, giving the required mono sulfonamide in good yield.

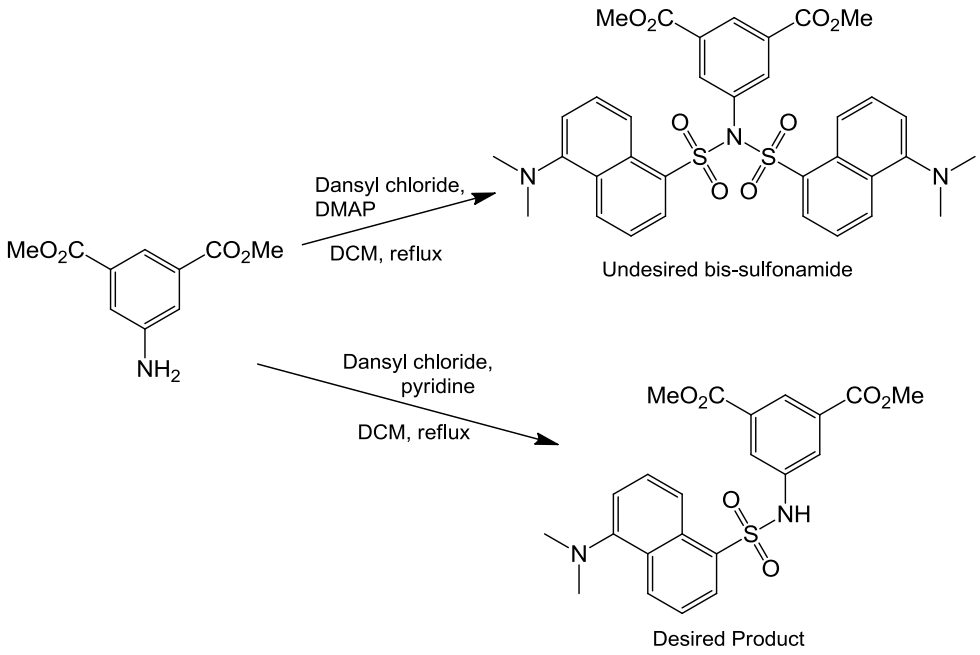

Scheme 4.17 Unexpected and desired products of the reaction of dimethyl-5-aminoisophthalate with dansyl chloride.

The methyl esters of this compound were then successfully hydrolysed under basic conditions to give the dicarboxylic acid. In addition, since 4-aminobenzoic acid is commercially available, this was also reacted with dansyl chloride to give a comparable structure which would only be singly functionalised (Scheme 4.18). As discussed previously with reference to functionalised anthracenes, this pair could provide useful comparisons between singly and doubly functionalised mimics should they lead to a successful mimic structure.

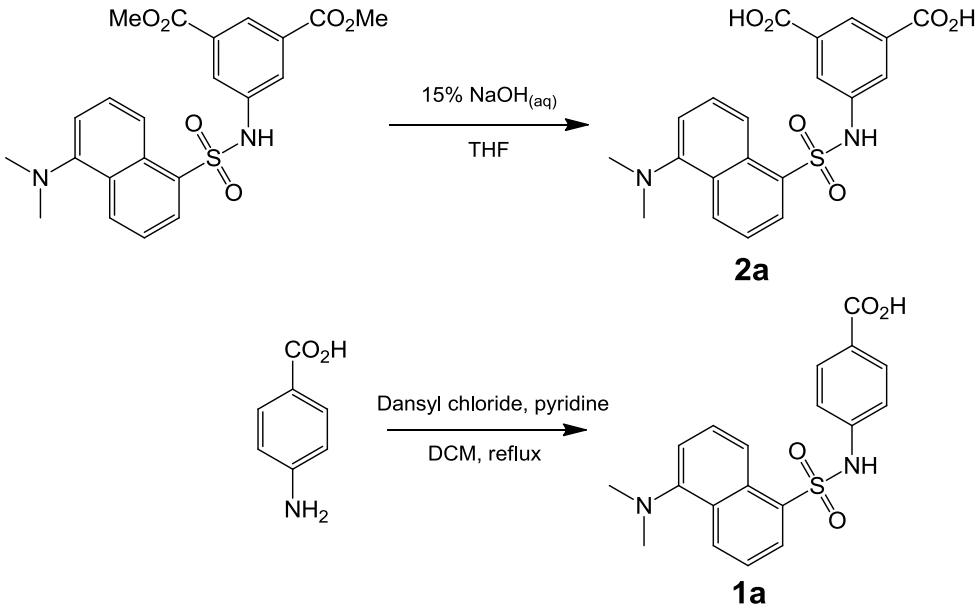

Scheme 4.18 Final steps to singly and doubly acid functionalised dansyl-based fluorophores **1a** and **2a**.

Here, then, were two acid functionalised emitters **1a** and **2a** that could be coupled to cysteine in order to give potential fluorescent PDI mimics.

4.3.1.3 Carboxylic acid functionalised iridium complexes

It was desirable to have as many structures as possible to provide a wider range of mimic structures, in particular, transition metal complexes were still of great interest given their longer luminescence lifetimes. While the first attempts to produce a bipyridine ligand by the Suzuki coupling shown above in Scheme 4.15 were unsuccessful, it was decided not to continue with this particular approach as a simpler, more compact solution presented itself. It was reported around this time that the directly functionalised bipyridines 4-carboxy-4'-methyl-2,2'-bipyridine (cmbpy) and 4,4'-dicarboxy-2,2'-bipyridine (dcbpy) could be used as ligands in complexes with iridium and rhodium[233] and such compounds are emissive at room temperature in oxygenated solution. Such complexes would be ideal for attempted couplings with cysteine to form mimic structures and so the iridium complexes shown in Figure 4.6 were synthesised according to the reported procedure. This provided two more fluorescent units, **3a** and **4a**, to be coupled with cysteine, again as a pair to compare any difference in activity between a single thiol and a dithiol.

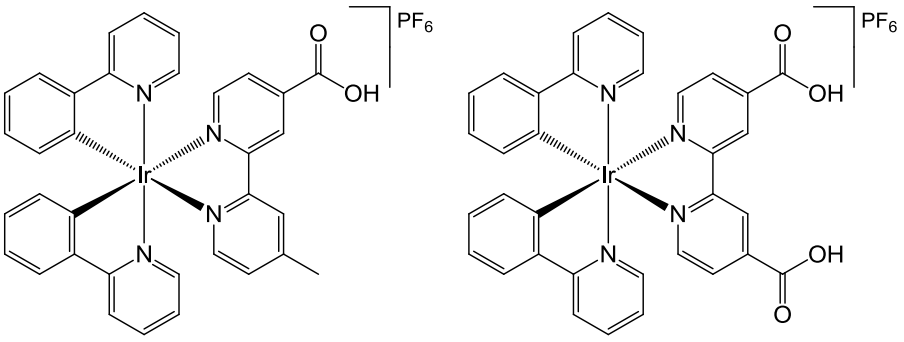

Figure 4.6 Iridium complexes $[Ir(ppy)_2(cmbpy)]PF_6$ (**3a**) and $[Ir(ppy)_2(dcbpy)]PF_6$ (**4a**) with carboxylic acid functional groups.

In addition to these two iridium complexes, the same bipyridine ligands were also used to prepare iridium complexes with a terdentate N^C^N cyclometallated structure as shown in Scheme 4.19. Synthesis of this type of $[Ir(N^C^N)(bpy)Cl]PF_6$ complexes was performed at high temperature in ethylene glycol in a method analogous to the incorporation of terpyridines into Ir(N^C^N) complexes,[47] however in this case reactions performed in this solvent tended to give glycol esters of the required product. To resolve this issue the reactions were carried out under the same conditions, only using triglyme as a solvent instead. It also transpired that in this case, silver(I) triflate was needed to encourage cleavage of the chloride bridged dimer, where normally, when these reactions are carried out at high temperature, this is not required.

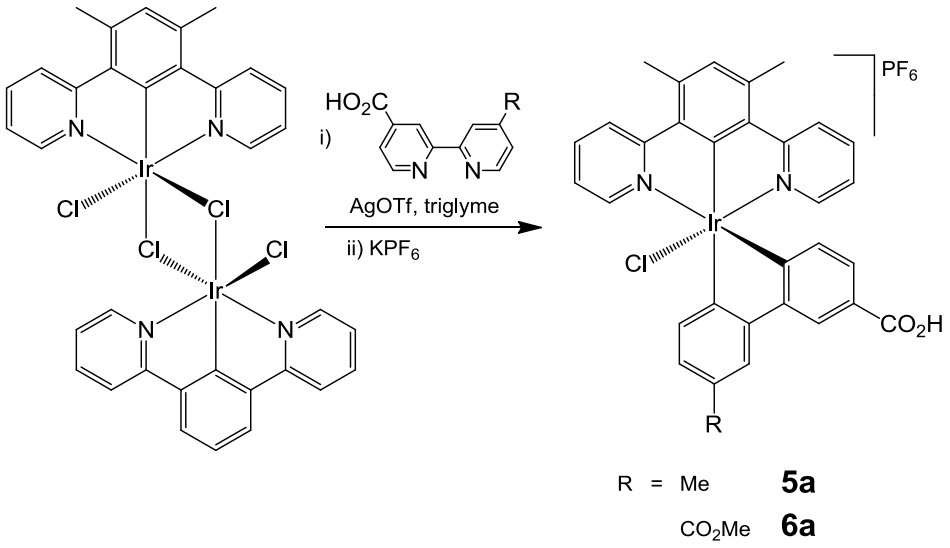

Scheme 4.19 Synthesis of carboxylate functionalised $[Ir(dpyx)(N^N)Cl]^+$ complexes **5a** and **6a**.

4.3.2 Peptide coupling reactions with cysteines

It was now required to find conditions under which these various carboxylic acids **1a-6a** could be reliably coupled to cysteine in order to give a library of potential mimics. Initially, conditions similar to those used for the synthesis of di(O-ethyl-L-cysteinyl)-5-bromoisophthalamide using EDCI as a coupling reagent were used. While in some cases the desired products were detected by mass spectrometry, invariably these reactions did not proceed cleanly or fully to completion giving mixtures of singly and doubly functionalised fluorophores. Reactions with L-cysteine ethyl ester were also attempted via the formation of acid chlorides from the respective acids. In reactions where a significant amount of product was obtained, purification of these products proved problematic. Due to the ease of oxidation of the free thiols in these products, attempts to purify these compounds by recrystallisation or column chromatography resulted in mixtures equally or more complex than the initial reaction products. Evidence from mass spectrometry suggested that oxidative disulfide formation could be responsible for some of this observed instability. In the case of the singly functionalised compounds this was necessarily intermolecular disulfide formation while the doubly functionalised mimics showed more complex mixtures of possible intermolecular and intramolecular disulfides.

It was decided to attempt the couplings with a range of S-protected cysteines that would give products stable enough to be isolated and purified which could then be deprotected when required. Various methods of amide formation were attempted with several different protected cysteines which were either obtained from commercial sources or synthesised as shown in Scheme 4.20.

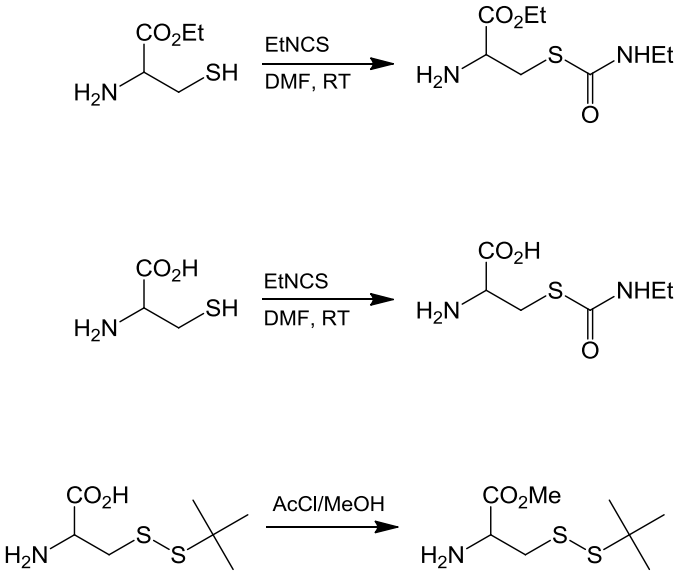

Scheme 4.20 Preparation of non-commercially available protected cysteines.

The results of the various couplings are summarised in Table 4.1. For reactions using carbodiimide coupling reagents the carboxylic acids were treated with the carbodiimide at 0 °C before addition of the cysteine derivative. Where attempts were made using either acid chlorides or N-hydrosuccinimide (NHS) active esters as intermediates, the starting acids were reacted to form the intermediate and the crude product redissolved after work-up and treated with the cysteine derivative. The majority of reactions were tested on the acids **2a** and **3a** as more of these two materials were available at the time.

Cysteine	Acids used	Conditions*	Result
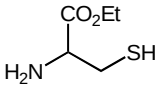	**2a**	EDCI	Incomplete
	2a	EDCI, HOBt	Incomplete
	2a	EDCI, Heat	No Product
	2a	$SOCl_2$	No Product
	2a, 3a, 4a	$(COCl)_2$	No Product. Evidence of SM for **3a**
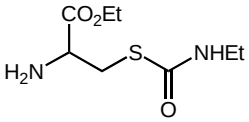	**2a**	$(COCl)_2$	No product
	2a, 3a	EDCI	Some impure product. Failure in deprotection
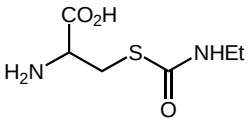	**3a**	EDCI	Acetyl transfer giving EDU† adduct
	2a	EDCI, HATU, DMAP	No Product
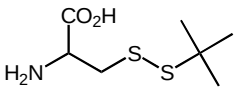	**2a**	EDCI, HATU, DMAP	No Product
	1a, 2a, 3a	NHS, DCC	No Product. Some starting materials recovered
	2a	NHS, EDCI	No Product
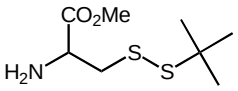	**1a-6a**	EDCI	Successful coupling. Products stable in column chromatography except N^C^N complexes

Table 4.1 Peptide coupling reactions.

There was some success in the coupling of S-(N-ethylaminocarbonyl)-cysteine ethyl ester using EDCI, where the correct products were obtained and purification was feasible using column chromatography, although the products tended to separate poorly from some impurities. Attempts to remove the carboxamide protecting groups using $NaHCO_{3\ (aq)}$, a pH 10.6 $NaHCO_3$/NaOH buffer or 0.1M NaOH were unsuccessful, with only unreacted material recovered from the reaction. However, when the deprotection was attempted on the singly functionalised iridium complex, **3a**, using 1M NaOH, the product

* Reactions were either carried out in dry THF for the organic fluorophores or a mixture of dry THF and either DCM or dry acetonitrile for iridium complexes where solubility in pure THF was poor.

† Ethyl(3-(N,N-dimethylamino)propyl)urea

isolated was not the free thiol as expected but the complex shown in Figure 4.7, identified by HRMS. It was theorised that instead of attack of hydroxide as a nucleophile at the carboxamide functional group, the hydroxide acted as a base, removing the ester α-hydrogen leading to loss of sulfur as shown in Scheme 4.21. This is unusual since the original report of the use of this protecting group found no evidence of dethiolation.[234]

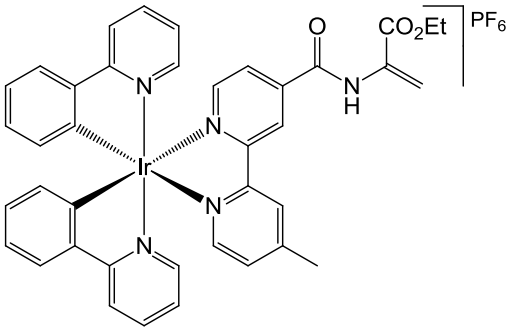

Figure 4.7 Unexpected product of deprotection.

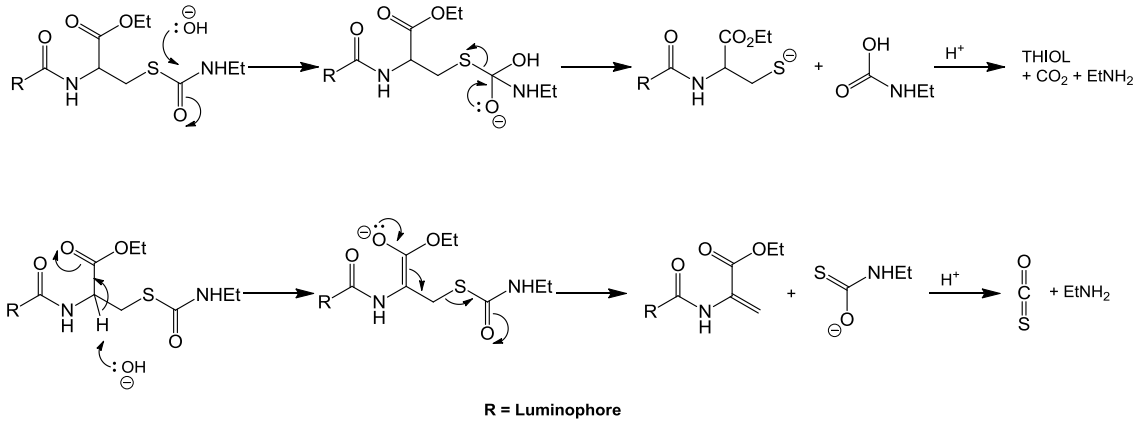

Scheme 4.21 Mechanisms for the desired removal of carboxamide protecting group (above) and the undesired dethiolation reaction (below).

It was therefore decided to attempt the coupling with the free acid equivalent, S-(ethylaminocarbonyl)-L-cysteine, since the α-hydrogen in this case would not be acidic so this side reaction could be avoided. However, as with all the coupling reactions attempted on cysteines with unprotected acid functional groups, no product was obtained.

In fact, as noted in Table 4.1, when this cysteine was reacted with **3a**, there was evidence from mass spectrometry of acetyl transfer after reaction with EDCI giving an N-acylurea species as shown in Scheme 4.22. This tends to occur in

the use of carbodiimides when reaction with the amine is very slow allowing the competing intramolecular acetyl transfer reaction to take over.

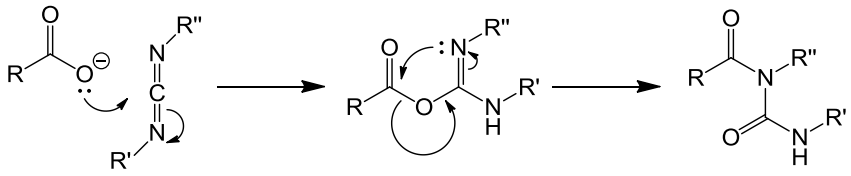

Scheme 4.22 Acetyl transfer giving N-acylurea in reactions with carbodiimides.

In the end, S-(tert-butylmercapto)-L-cysteine methyl ester was found to give reproducible results in couplings using EDCI with compounds **1a-4a** giving products stable enough to isolate and purify by column chromatography. As a result of these reactions the four compounds, **1b-4b**, shown in Figure 4.8 were available for testing as potential PDI mimics. Given the likelihood of instability with respect to oxidation after deprotection, these compounds were stored in their protected forms until required for assays.

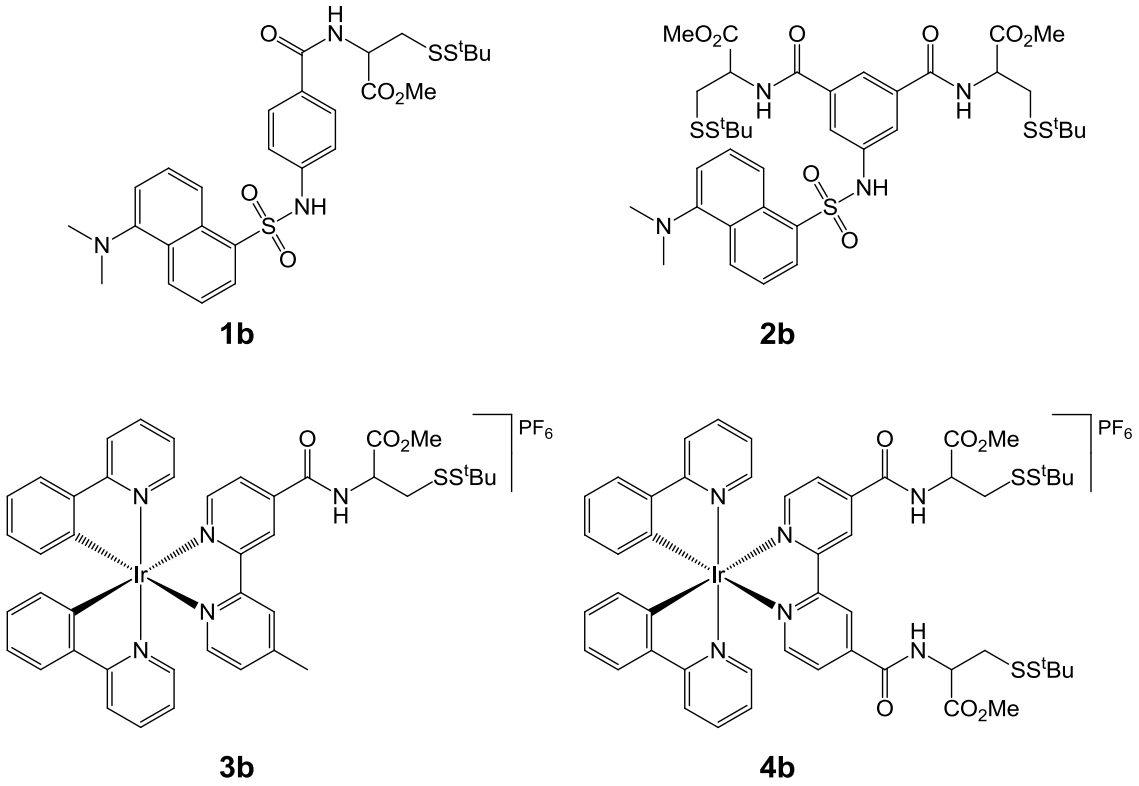

Figure 4.8 S-protected potential luminescent PDI mimics **1b**, **2b**, **3b** and **4b**.

Reactions using the two Ir(N^C^N) complexes **5a** and **6a**, however, were less successful, yielding mixtures of products. The desired compounds were

possibly isolated in low yield by column chromatography and identified by mass spectrometry, however these products were not sufficiently pure and their identity could not be confirmed by other spectroscopic methods such as NMR. In the case of the singly functionalised complex **5a**, one of the major side products isolated and identified (in approx 50% yield) was the acetyl transfer product, indicating that one possible issue with these structures is slow reactivity between the EDC activated acid and the cysteine amine. Unfortunately, despite these complexes with terdentate ligands showing promise, a lack of material and insufficient time to synthesise fresh complexes meant that the synthesis of potential mimics using these particular luminophores could not be completed.

4.3.3 Deprotection of potential mimics

With the four potential mimics in hand in their protected forms, some assays could be performed on these compounds in their own right as discussed later in the chapter. For the purposes of the project, however, it was necessary to have some samples of these compounds as free thiols. It was therefore necessary to determine conditions suitable for the removal of the *S*-*tert*-butyl protecting groups.

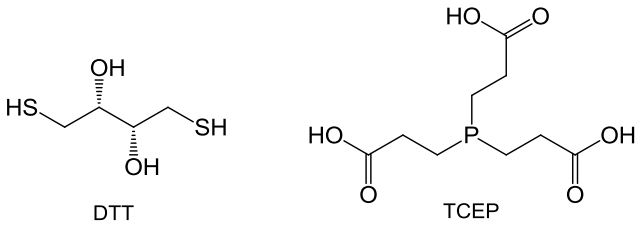

Figure 4.9 The reducing agents DTT and TCEP.

Common methods for the reduction of disulfide bonds in biological systems involve the use of thiols such as 2-mercaptoethanol, dithiothreitol (DTT)[235] or phosphines such as tris(2-carboxyethyl)phoshine (TCEP)[236], with the latter normally used in its hydrochloride salt form. It was decided, therefore, that DTT and TCEP (shown in Figure 4.9) were good candidates for the clean reduction of the disulfide bonds linking the protecting groups to the mimic structures. A series of small-scale test reactions, monitored by mass spectrometry, were carried out to determine the conditions required to achieve the reduction of

these disulfide bonds and the initial attempts are summarised in Table 4.2. The reactions were carried out on samples of **1b** in mass spectrometry vials under nitrogen. The first test was performed with DTT in acetonitrile at approx 1 mg/mL concentration of mimic, and after this various other sets of conditions were explored including higher reaction concentration and the use of mixed acetonitrile/water as a solvent. When using TCEP.HCl, since the reductive mechanism involves one molecule of H_2O, there was no need to perform these reactions in pure acetonitrile so only mixed MeCN:H_2O solvent systems were used.

Reducing Agent	**No. of equivalents**	**Solvent**	**Conditions**	**Result**
DTT	1	1 mL MeCN	RT, 30 min	No reaction. Re-run MS after 20 h, still no reaction.
DTT	1	1 mL MeCN:H_2O 4:1	RT, 30 min	Ditto
TCEP.HCl	1	1 mL MeCN:H_2O 4:1	RT, 30 min	Ditto
TCEP.HCl	1	1 mL MeCN:H_2O 1:1	RT, 30 min	No reaction
TCEP.HCl	4	0.5 mL MeCN:H_2O 1:1	RT, 2 h	No reaction
TCEP.HCl	2	0.5 mL MeCN:H_2O 1:1	Reflux, 1 h	No reaction
DTT	5	0.2 mL MeCN	RT, 30 min	No reaction
DTT	10	0.2 mL MeCN	60 °C, 1 h	No reaction
DTT	10	0.2 mL MeCN:H_2O 4:1	60 °C, 1 h	Partial reaction
DTT	10	0.2 mL MeCN:H_2O 1:1	60 °C, 1 h	Successful deprotection

Table 4.2 Mass spectrometry scale reactions of **1b** with DTT and TCEP.HCl

It appeared from these test reactions that TCEP.HCl was ineffective in this case at reducing these disulfide bonds and that for the use of DTT, a significant

excess was required as well as some heating in order to achieve deprotection. It was therefore decided to attempt the deprotection using excess DTT at reflux. While performing these reactions it became apparent that while the singly functionalised mimics **1b** and **3b** were easily deprotected under these conditions, the doubly functionalised counterparts required a higher concentration of DTT for the reaction to proceed cleanly in a short time. It was discovered that longer reaction times at reflux, in these cases, resulted in the formation of more complex mixtures of by-products, likely candidates being intramolecularly cyclised disulfides or mixed intermolecular disulfides, and therefore a higher DTT concentration was needed in order to reduce the reaction time. This gave suitable conditions for the conversion of the protected compounds **1b-4b** into the free thiols **1c-4c** (Figure 4.10).

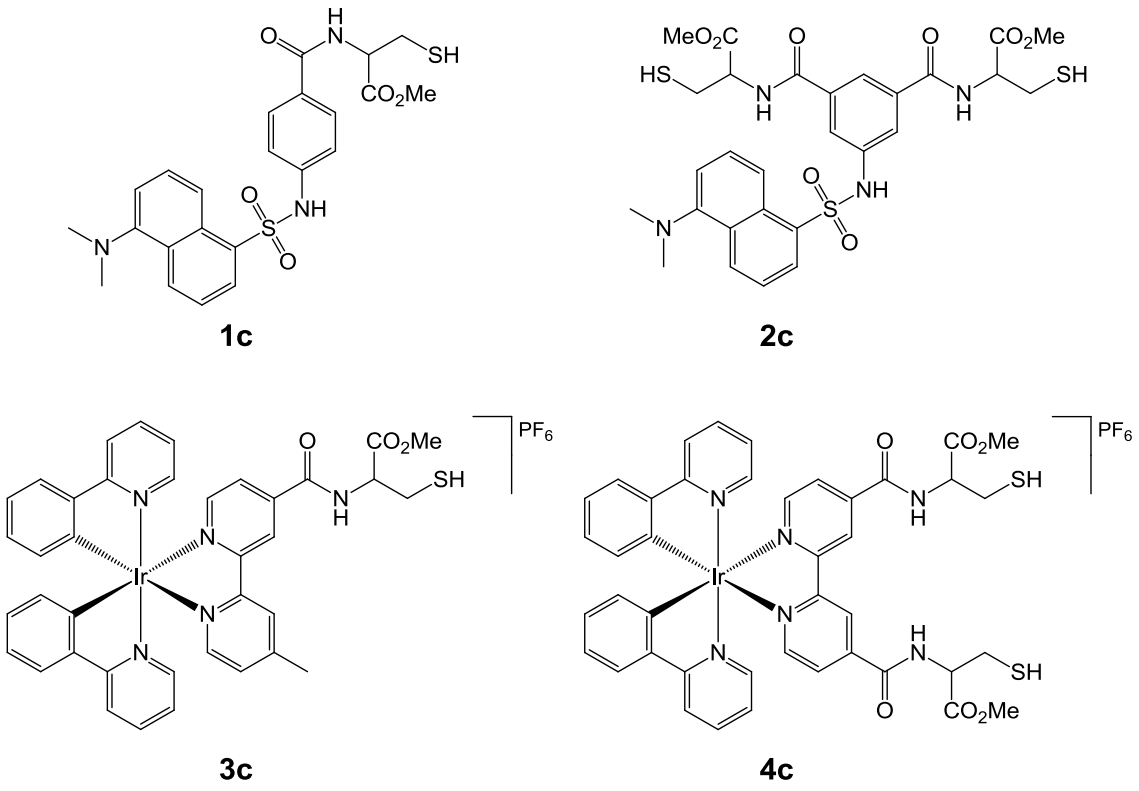

Figure 4.10 Deprotected potential mimics **1c**, **2c**, **3c** and **4c**.

4.3.4 Photophysical properties of the mimic structures

In order to understand any results from potential cellular applications involving fluorescence using the synthesised compounds, e.g. fluorescence microscopy, it is necessary to, first, assess the photophysical properties of the compounds themselves in solution. With this in mind, the absorption and emission

characteristics of the four compounds were studied. Initially, the compounds were studied in their protected forms (**1b-4b**) with the S-^{t}butylmercapto groups in place, since in this state they are unlikely to be unstable with respect to oxidation during the experiments. With the properties of the compounds in this form determined it would then be possible to determine what changes, if any, occur upon reduction to the free thiols **1c-4c**.

The absorption spectra of the compounds were measured in acetonitrile at room temperature in aerated solution and the extinction coefficients for the observed bands were determined by a dilution method according to the Beer-Lambert Law (Section 5.1.3). The data from these experiments is summarised in Table 4.3. The emission properties were also measured in acetonitrile at room temperature in both degassed and aerated solution (Table 4.4).

Compound	**Absorption λ_{max} / nm (ε / dm^{3}mol^{-1}cm^1)**
1b	205 (50900), 254 (26800), 345 (4165)
2b	215 (60900), 260sh (16100), 305 (3520), 345 (4035)
3b	252 (43050), 268 (38580), 320sh (14430), 380 (6330), 460 (845)
4b	252 (36600), 270 (30200), 295 (22550), 330sh (10540), 367 (6780), 480 (680)

Table 4.3 Absorption data for S-^{t}butylmercapto protected mimics in acetonitrile solution at 295 K.

Compound	λ_{max} / nm	τ degassed (aerated) / ns	Φ degassed (aerated) × 10^2
1b	550	20 (13)	37 (29)
2b	555	19 (16)	33 (29)
3b	652	170 (80)	3.5 (2.0)
4b	665	96 (82)	1.5 (1.6)
$[Ir(ppy)_2(cmbpy)]^+$	565	(71)	17 (3.7)
$[Ir(ppy)_2(dcbpy)]^+$	624	(70)	2.0 (1.9)

Table 4.4 Luminescence data for S-^{t}butylmercapto protected mimics in acetonitrile solution at 295 K. Data for $[Ir(ppy)_2(cmbpy)]PF_6$ and $[Ir(ppy)_2(dcbpy)]PF_6$ are included for reference.[233]

Plots of the absorption, excitation and emission profiles are shown in Figures 4.11-4.14[*]. Since the dansyl group is a purely organic fluorophore while the photophysical properties of the iridium complexes will be largely affected by the high spin-orbit coupling of this metal, the results from the two types of luminophores will be discussed separately.

4.3.4.1 Dansyl based mimics

1b and **2b** show similar absorption profiles with bands largely confined to the UV region. Both the highest and lowest energy bands are noticeably similar between the singly and doubly functionalised mimics, while the intervening bands show a slightly different structure. In the case of **2b**, two weak bands/shoulders are present between the two distinct outer bands while **1b** shows a single, stronger, more distinct band in this region. It seems likely, therefore, that these intermediate energy bands are related to transitions in the isophthalate/benzoate moieties while the retained band structure results from $^1\pi$-π^* and CT transitions within the dansyl group.

[*] The spikes visible in the excitation spectra (~320 nm) and emission spectra (~680 nm) are due to the detection scattered $½\lambda_{em}$ and $2\lambda_{ex}$ respectively.

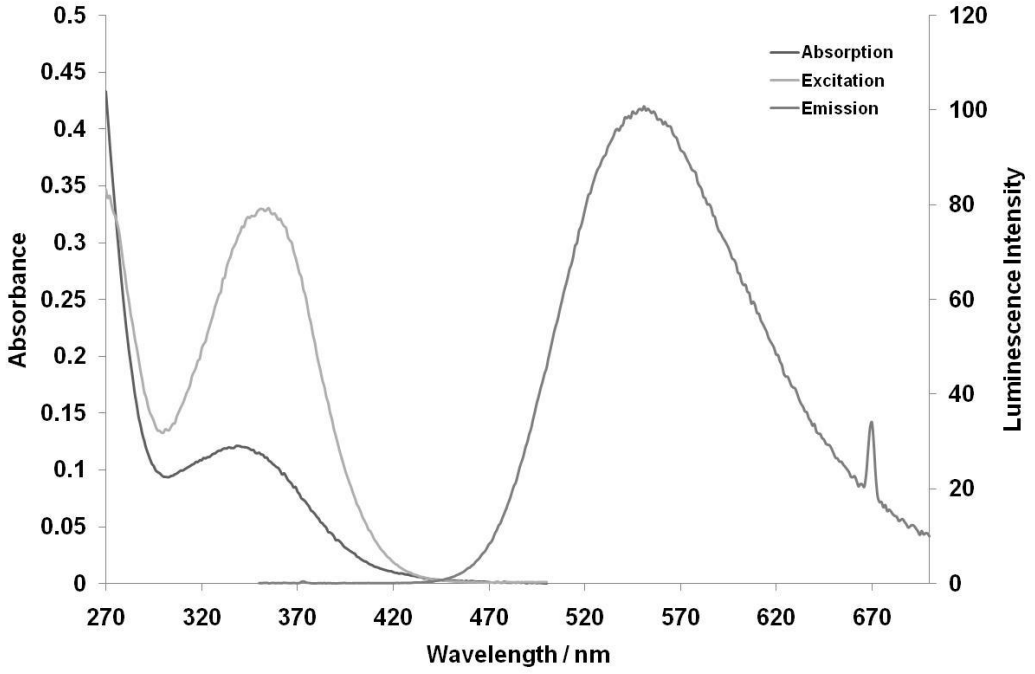

Figure 4.11 Absorption spectrum, emission spectrum (λ_{ex} = 335 nm) and excitation spectrum (λ_{em} = 537 nm) of the singly functionalised dansyl compound **1b** in MeCN at 295 K.

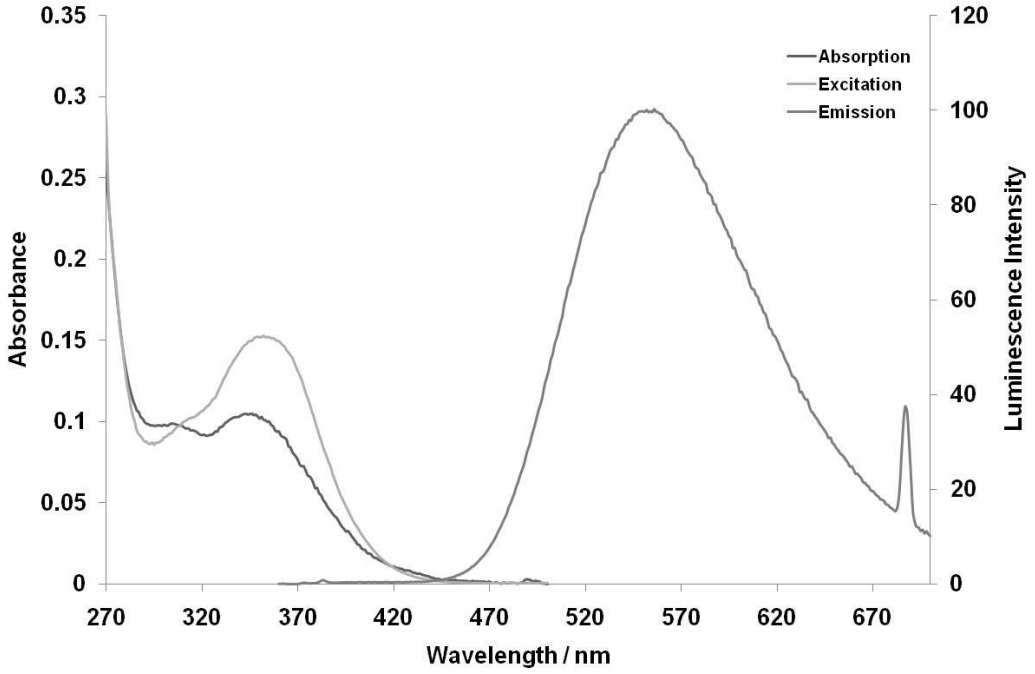

Figure 4.12 Absorption spectrum, emission spectrum (λ_{ex} = 345 nm) and excitation spectrum (λ_{em} = 537 nm) of the doubly functionalised dansyl compound **2b** in MeCN at 295 K.

Both compounds display a structureless band with a large Stokes shift, typical of dansyl amides.[237,238] There is very little difference between the two compounds in terms of the energy of this band indicating that there is little, if any, electronic communication between the dansyl moiety and the attached mimic structure.

The excited state lifetimes of the two compounds are both short, at around 20 ns as expected for fluorescence from an organic structure and as such show a low sensitivity to oxygen quenching. Both compounds also show similar quantum yields which, again, are relatively insensitive to oxygen.

In general, the photophysical properties of the dansyl group have been shown to be highly sensitive to its environment, in particular the polarity of the solvent. Studies of dansylglycine in mixtures of dioxane and water have shown an increase in quantum yield from 0.07 in pure water to 0.66 in dioxane accompanied by blue shift in emission of around 80 nm.[237] Quantum yields of up to 0.84 have also been reported for complexes with the enzyme Bovine erythrocyte carbonic anhydrase.[239] Despite this wide variation in properties of dansyl compounds, the mimics studied show similar quantum yields and emission maxima to a full series of dansyl-functionalised amino acids in solutions of acetonitrile.[238]

4.3.4.2 Iridium based mimics

In absorption these compounds also show strong bands in the UV region which can be attributed to $^{1}\pi$-π^* transitions within the aromatic ligands. However, unlike the dansyl-based mimics, these structures also show weak absorption bands extending into the visible region which most likely arise from charge transfer states common in cyclometallated complexes of this type.[25,146] The overall band structures of the two complexes are very similar which, again, is not unexpected. The only change in the photophysically active moiety is the substitution of a methyl group for second amide in the bipyridine ligand which would lead to a lowering of the π^* energies in this ligand.

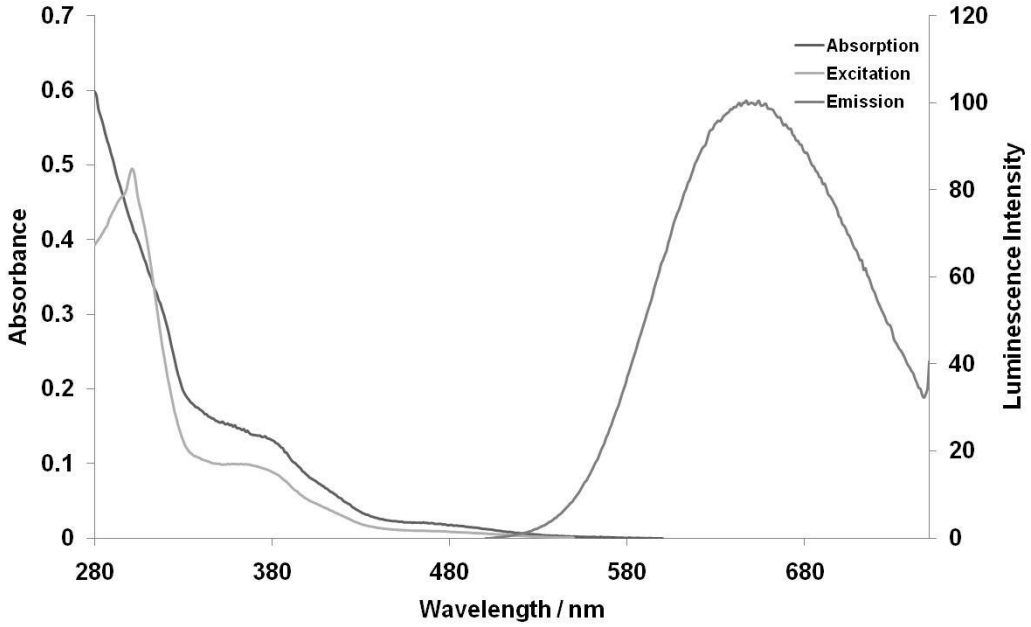

Figure 4.13 Absorption spectrum, emission spectrum (λ_{ex} = 470 nm) and excitation spectrum (λ_{em} = 600 nm) of the singly functionalised iridium complex **3b** in MeCN at 295 K.

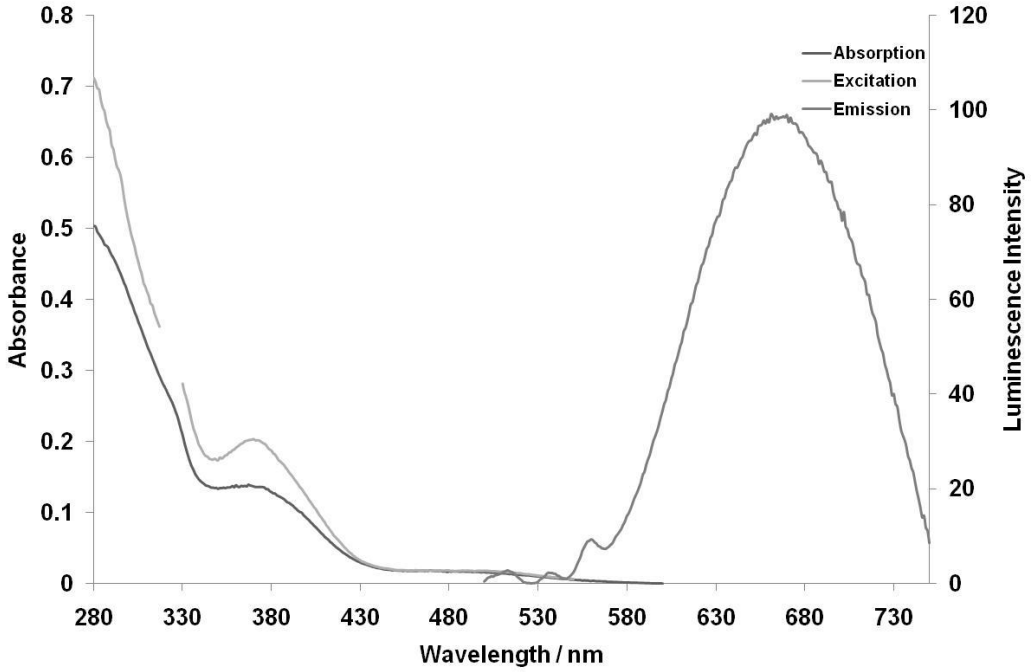

Figure 4.14 Absorption spectrum, emission spectrum (λ_{ex} = 480 nm) and excitation spectrum (λ_{em} = 645 nm) of the doubly functionalised iridium complex **4b** in MeCN at 295 K. Discontinuity at ~320 nm in excitation spectrum is due to removal of ½λ_{em} scattering peak.

The emission characteristics for the two iridium complexes are also very similar, with both displaying a structureless band at around 650 nm. Given the structural similarity of the phosphorescent moiety in these compounds to $[Ir(phpy)_2bpy]PF_6$ it would be reasonable to suppose that the emissive state would be of the same type. As discussed in Section 1.1.2.2 $[Ir(phpy)_2(bpy)]PF_6$

is known to emit from a ^{3}MLCT state involving the bipyridine ligand,[25] and the two compounds do show a similar emission profile, only significantly red-shifted, with the parent complex having λ_{max} ~ 606 nm in methanol[25] and a similar value in MeCN. This red-shift is consistent with a ^{3}MLCT excited state involving the bipyridine ligand. The electron withdrawing effect of the amide groups will significantly lower the LUMO which is located on the bpy ligand leading to the observed red-shift. This red shift is similar to that observed in the parent carboxylic acid substituted bipyridine complexes where, for example, $[Ir(ppy)_2(dcbpy)]^+$ has λ_{max} = 624 nm.[233] The luminescence lifetimes and quantum yields in aerated solution are remarkably similar between the mimics and the parent structures. In degassed solution, **3b** does show a reduced quantum yield compared to $[Ir(ppy)_2(cmbpy)]^+$ which may be a result of the comparative red-shift of the former compared to its parent structure. Also in comparison to the carboxylic acid complexes, **3b** and **4b** show very similar quantum yields to their respective parent complexes, however both show increased lifetimes compared to the carboxylic acids, particularly **3b**.

4.3.4.3 Comparison of dansyl and iridium based mimics

One notable difference between the two complexes **3b** and **4b** is in the observed luminescence lifetime, with the doubly functionalised mimic having a τ value of just over half that of its singly functionalised counterpart. It is possible that this reduction in lifetime is the result of intramolecular quenching by the pendant mimic structures which would be expected to be more pronounced with two such groups attached. This difference is not observed in the dansyl based mimics **1b** and **2b**, possibly due to their inherently much shorter lifetimes. A final point of interest is that all four compounds show little reduction in the quantum yield in aerated solutions compared to degassed solutions which qualitatively indicates a low rate of quenching by O_2. This could be of importance in bioimaging applications as these species are therefore unlikely to show phototoxicity related to singlet oxygen sensitization.

4.3.5 Effect of reduction of the S-S bond on photophysical properties

In order for these potential mimics to be useful in assays where there may be interchange between disulfide bonds and free thiols, the effect of such changes

on the photophysics of the compounds must be explored. Since the results discussed in section 4.3.4 are of the S-^{t}butylmercapto protected compounds, this data provides a model for the mimics in an oxidised disulfide form. It was therefore necessary to investigate what changes, if any, occur upon reduction of the protecting groups to give the corresponding free thiols.

Absorption and emission spectra of the four compounds were therefore recorded in acetonitrile with the addition of increasing concentration of DTT. Solutions were made up for measurements in 3 mL cuvettes from stock solutions of compound and DTT with a final concentration of 10 µM compound in all solutions and DTT concentrations of 0, 10, 20, 50, 100, 200 and 300 µM. After making up each solution, the cuvettes were shaken for 5 min before measurement. The resulting absorption and emission plots for the compounds are shown in Figure 4.15.

In the absorption spectra, all the data shows an increase in absorbance in the region between 250 – 300 nm. This correlates directly to the main absorption band of oxidised DTT which appears ~285 nm, which is not present in reduced DTT. The increase in intensity in this region during the assay shows a linear relationship with the concentration of DTT. Clearly this indicates an increasing concentration of oxidised DTT in the measured sample, although this could feasibly arise from air oxidation of DTT, rather than the reductive action of DTT on the substrate.

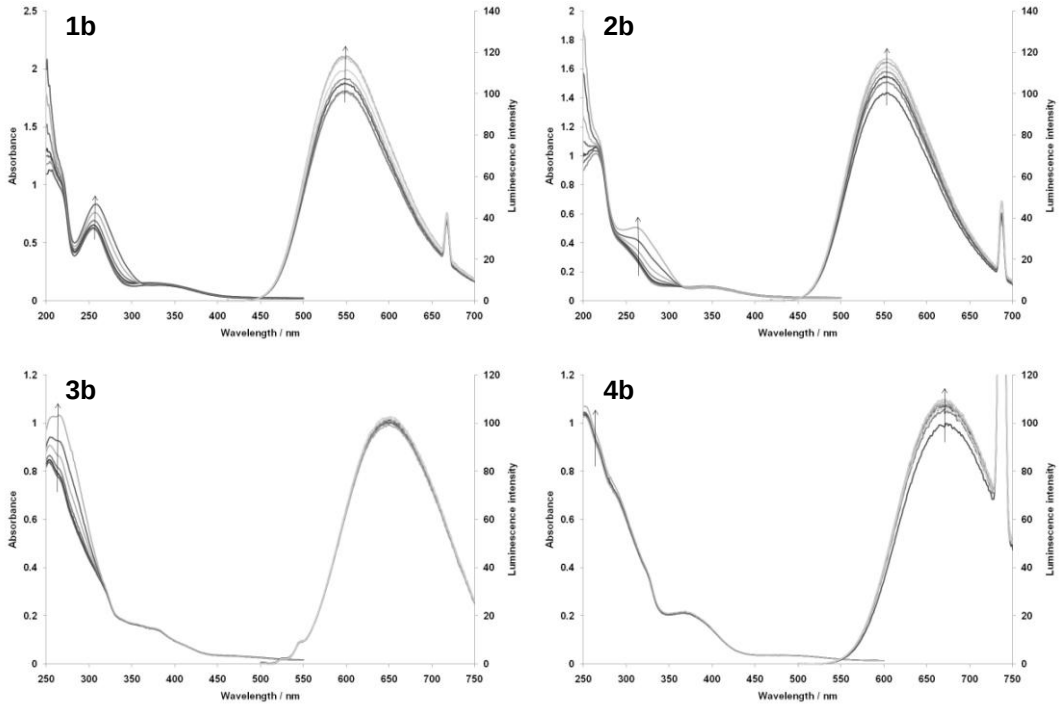

Figure 4.15 Absorption and emission profiles of 10 µM solutions of **1b**, **2b**, **3b** and **4b** with increasing DTT concentration.

Data from the emission spectra show an increase in peak intensity of emission with increasing DTT concentration for all the compounds, although the effect is much less pronounced in **3b**. Figure 4.16 shows a plot of the percentage change in the maximum emission intensity with increasing DTT concentration. This effect is unusual, in that it may be expected that the free thiols would be more effective in the quenching of luminescence than the corresponding disulfides. The reasons behind this increase are, as yet, undetermined and certainly warrant further study. In any case, despite this unusual observation, these results show that there is very little change in the emissive properties upon reduction, if, indeed, reduction is occurring under these conditions. While emission from the deprotected compounds **1c-4c** does indicate that these will still be useful as bioimaging agents, the lack of distinction between reduced and oxidised forms rules out their use as ratiometric probes of the reductive environment in cells. It is still possible however that they may show intracellular localisation properties related to an ability to participate in disulfide exchange.

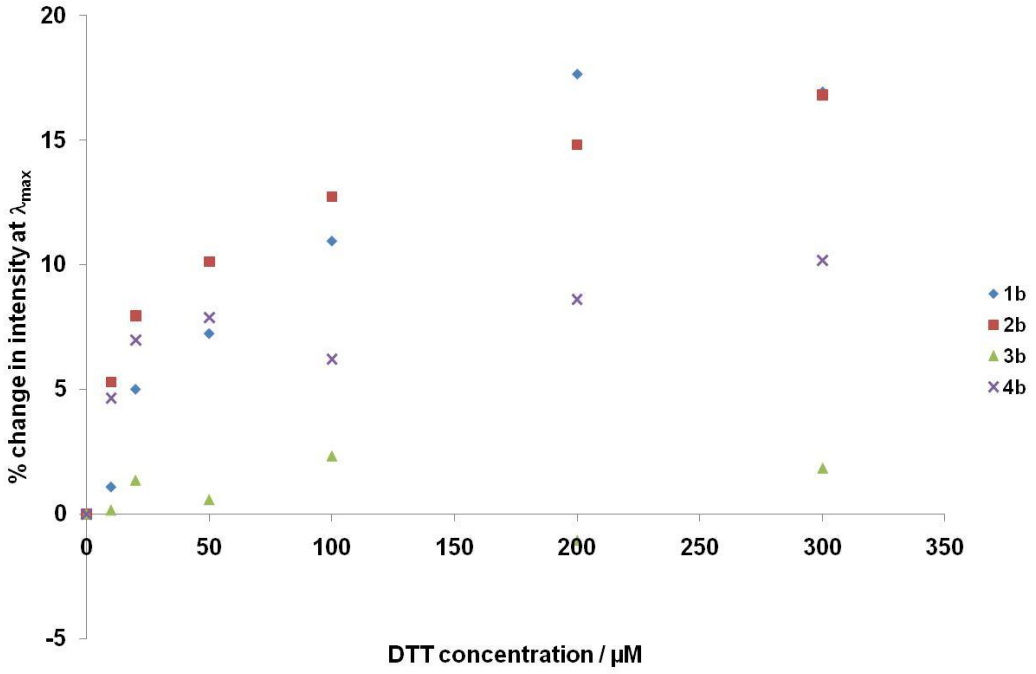

Figure 4.16 Percentage change in maximum intensity vs. DTT concentration.

4.3.6 Potential reductive activity of the mimics

As discussed in the introduction, many small molecule thiols have the capability to accelerate the reactivation of scrambled proteins such as Rnase, by catalysing isomerisation through disulfide interchange reactions. The potential of a particular thiol to engage in such processes *in vivo* can be assessed by an assay involving the cleavage of insulin. Insulin is a small protein of around 5.7 kDa in size whose structure is highly preserved in a wide range of species, being particularly similar in many mammals.[240] It is comprised of two independent peptide chains, *A* and *B*, linked by two disulfide bonds.[241] When separated, these chains have noticeably different solubility properties, with the *A* chain being highly soluble in aqueous media while the *B* chain shows a strong tendency to aggregate and precipitate from solution. The extent of cleavage can easily be measured by the apparent increase in absorbance due to light scattering induced by the precipitated *B* chain. The simplicity of this assay has led to it being used in various studies of protein aggregation where, in general, DTT has been used to induce the reductive cleavage of insulin.[242,243] This assay is also useful in the study of potential PDI mimics as the addition of thiol-containing molecules with the capability to perform disulfide interchange reactions (such as BMC and NMA) to a solution of insulin also causes cleavage of the disulfide bonds leading to aggregation and precipitation of the *B* chain.

This method was therefore attempted using bovine insulin as an initial test of the viability of the synthesised compounds as functioning PDI mimics. Samples of the four compounds were deprotected as discussed in Section 4.3.3 and taken for use in this assay. Initially, the assay was performed using DTT as the active compound to establish the criteria for a positive result while a range of blank runs were also used to determine a negative result.

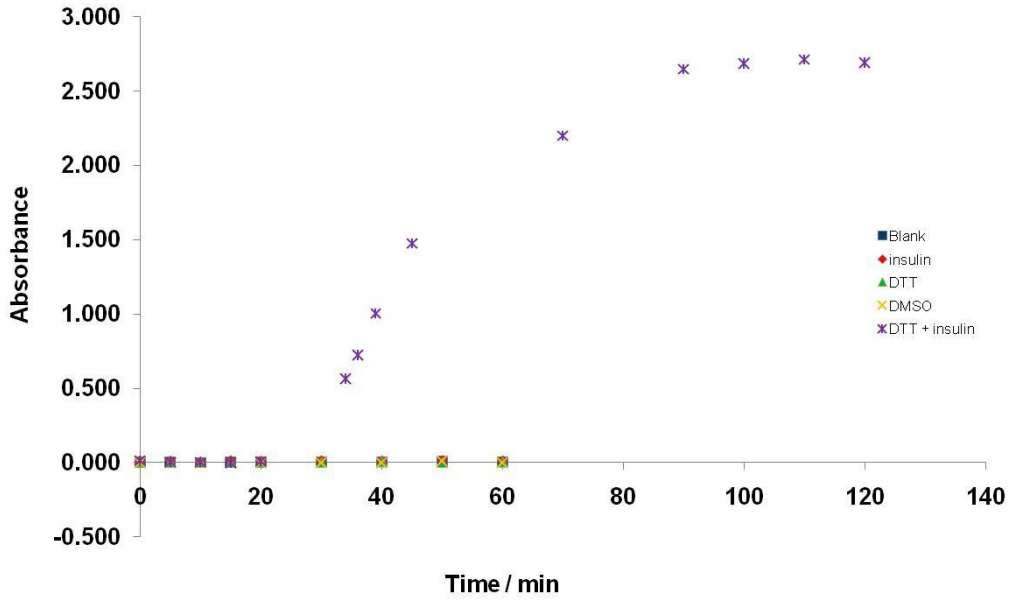

Figure 4.17 Blank runs and DTT + insulin to establish negative and positive results.

The first set of assays attempted with test compounds used 20 mM stock solutions in DMSO with the intention of running the assay at a concentration of 5 mM so, in addition to the usual blank, runs of phosphate buffered saline (PBS), insulin, DTT, test compounds, and a 1:3 DMSO:PBS blank were also run. The results of these blank runs, as well as DTT + insulin, are shown in Figure 4.17. Unfortunately, however, it transpired that addition of the stock solutions of test compounds to PBS at the required concentration when preparing the blank runs caused precipitation of the material meaning that the assay could not be performed under these conditions. It was therefore required to find a different solvent system in which to run the assays so various percentages of DMSO in PBS and several concentrations of pH 6.8 Tris buffer were tested for suitability. No system was found using these solvents in which the test compounds were soluble. Instead, acetonitrile was used for the stock

solutions of test material as it was found that 1:1 MeCN:PBS was suitable for keeping the compounds in solution.

When the assays were run using this mixture, the increase in absorbance due to the precipitation of insulin *B* chain was not observed, even with the use of DTT. The assay was repeated in this solvent system using increased concentrations of DTT to determine whether the acetonitrile was interfering with reduction of the substrate and again a negative result was observed. In addition to the assays run at higher concentration, another assay was performed using high concentration DTT in PBS followed by addition of MeCN once precipitation was complete.

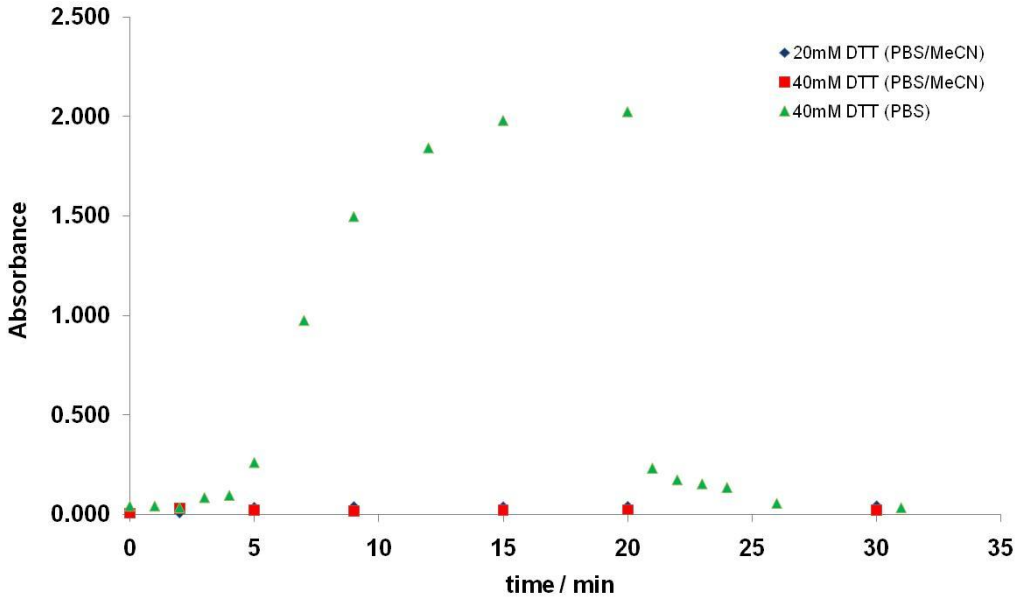

Figure 4.18 High concentration DTT assays. In 40 mM DTT in PBS, an equal volume of MeCN was added at 20 min.

The results of the assays run with 20 mM and 40 mM DTT in 1:1 MeCN:PBS and 40 mM DTT in PBS are shown in Figure 4.18 and it can be clearly seen in the latter that addition of MeCN causes the rapid dissolution of the precipitated insulin. It is unclear when using the mixed solvent system whether the cleavage of insulin is occurring without precipitation or whether the process is not occurring at all. In any case, the solubility of cleaved insulin in this solvent system unfortunately makes this assay unviable as a test of activity for the synthesised compounds.

4.3.7 Cytotoxicity of mimic compounds

For intracellular probes to be of use in assays involving live cells it is important that treatment with the probe does not lead to a significant amount of cell death. While it is possible to carry out assays using compounds with relatively high cytotoxicities, providing they enter the cells rapidly and the assay is short, the toxicity could lead to abnormal cell behaviour and so compounds with lower cytotoxicities are preferred. The toxicity of compounds can be represented by the half maximal inhibitory concentration value (IC_{50}) which represents the concentration causing 50% cell death over the length of the dose.

IC_{50} values can be measured in an assay using the compound 3-(4,5-dimethythiazol-2-yl)-2,5-diphenyltetrazolium bromide (MTT)[244] which is reduced to the purple dye formazan by the enzyme mitochondrial reductase as shown in Scheme 4.23. This process only occurs in living cells and so the intensity of absorption by the resulting formazan is proportional to the number of live cells in a sample. Therefore after dosing a batch of cells with a test compound followed by incubation with MTT, the proportion of live cells can be determined by comparison to a sample of un-dosed cells.

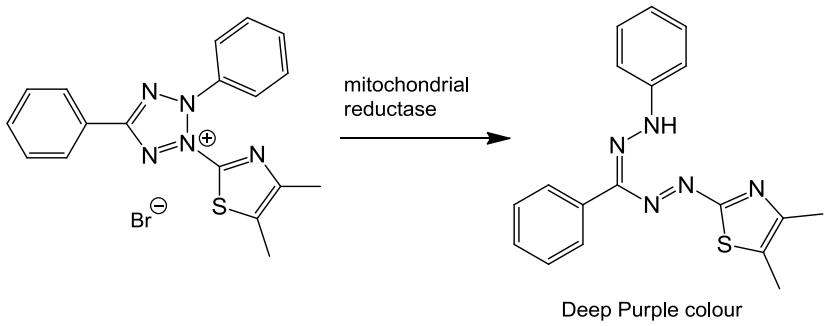

Scheme 4.23 Reduction of MTT to formazan by mitochondrial reductase.

It seems likely that the cytotoxicity of the synthesised compounds could be related strongly to the action of the mimic structure, as this has the potential to affect the oxidative balance of cellular processes involving disulfide exchange. If the potential mimics were to act as desired and assist in the isomerisation of non-native disulfide bonds then it would be expected that the viability of cells would not be greatly affected. On the other hand, high cytotoxicity could

indicate that the mimics are interfering with these processes, for example by binding to PDI or other oxidative chaperones and inhibiting their activity. However, the toxicity of these compounds could also be greatly affected by the luminophore used since the dansyl group and complexes of iridium are significantly different in their structure, charge and lipophilicity. The dansyl group is rarely associated with high levels of cytotoxicity, in fact it has been shown that capping relatively cytotoxic dendrimers with the dansyl group leads to a significant reduction in their inhibitory activity.[245] On the other hand there is a wide variation in the reported cytotoxicities of cyclometallated complexes of iridium(III). While complexes with the cyclometallating ligand 2-(2,4-difluorophenyl)pyridine (dfpyH) and a bipyridine-type ligand of the type $[Ir(dfpy)_2(N\hat{}N)]^+$ show relatively low cytotoxicity,[246] other similar $[Ir(N\hat{}C)_2(N\hat{}N)]^+$ compounds have been reported as relatively toxic with IC_{50} values in the 1-20 μM range.[247,248]

This MTT assay was carried out to determine the cytotoxicity values of the four mimic compounds **1b-4b** and the results are shown in Table 4.5. IC_{50} values were determined for a 24 h dose of the compounds.

Compound	**IC_{50} / μM**
1b	343 ± 21
2b	192 ± 18
3b	70 ± 20
4b	165 ±13

Table 4.5 IC_{50} values for CHO cells treated with S-^{t}butylmercapto protected mimics (24 h dose).

All four compounds show relatively high inhibitory concentrations, with all but one being above 100 μM. This should allow treatment of live cells with these compounds at concentrations below 100 μM without high levels of atypical behaviour or cell death. Also, it is expected that in assays such as fluorescence microscopy, the dosage times will be significantly shorter than 24 h so it is feasible that higher doses could be tolerated for short periods if necessary. One point of particular note is that the iridium complexes exhibit increased cell inhibition compared with those containing the dansyl group as a fluorophore.

As discussed, this is not unexpected due to the potential cytotoxicity of the iridium phosphor.

4.3.8 Flow cytometry

Flow cytometry is an ideal tool for monitoring the uptake of fluorescent molecules into cells as it can determine the overall proportion of labelled and unlabelled cells in a large population very quickly. This method was therefore used to investigate whether the synthesised compounds would be internalised by live cells, making them suitable for fluorescence microscopy.

The uptake of both the S-^{t}butylmercapto protected compounds **1b-4b** and the free thiols **1c-4c** was investigated over a range of concentrations. CHO cells were seeded into twelve well plates and dosed with the test compounds for 3 h at final concentrations of 0 µM, 5 µM, 25 µM, 100 µM and 500 µM. These populations were then analysed by flow cytometry with excitation using 50 mW UV excitation and measuring at 530 nm with 40 nm bandpass or 630 nm with a 30 nm bandpass for the dansyl compounds and the iridium compounds respectively. The scans were run until a total of approximately 3×10^4 events had been counted using forward scattering. Figure 4.19 and Figure 4.20 show plots of the dosage concentration versus the number of labelled cells for the dansyl and iridium compounds respectively.

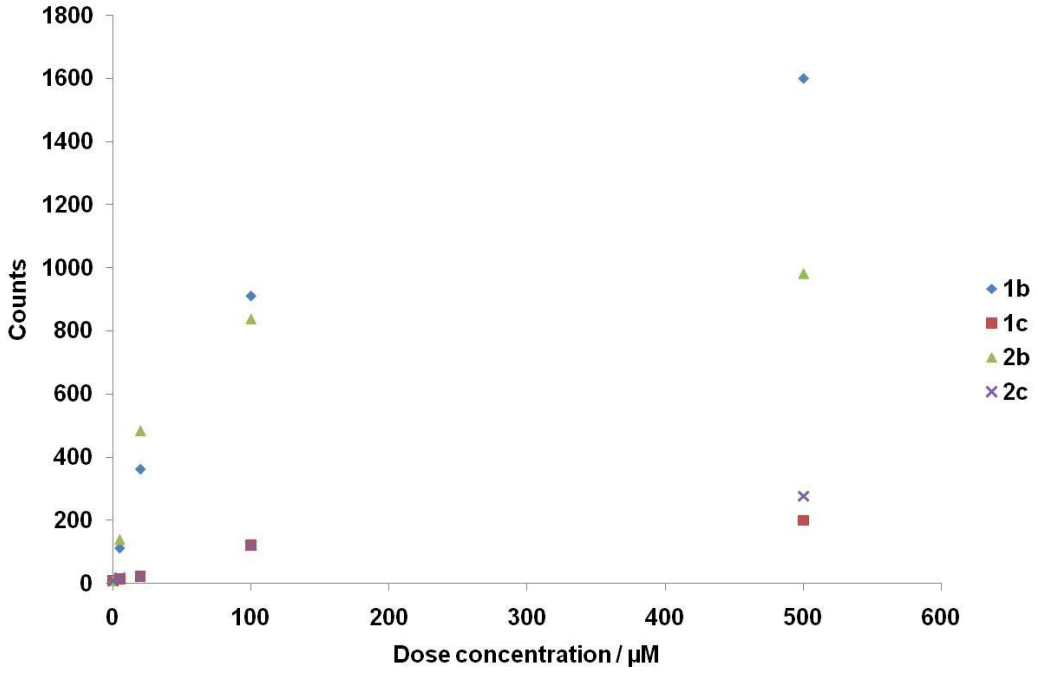

Figure 4.19 Plot of counts vs dose concentration for fluorescent population for **1b**, **1c**, **2b** and **2c**.

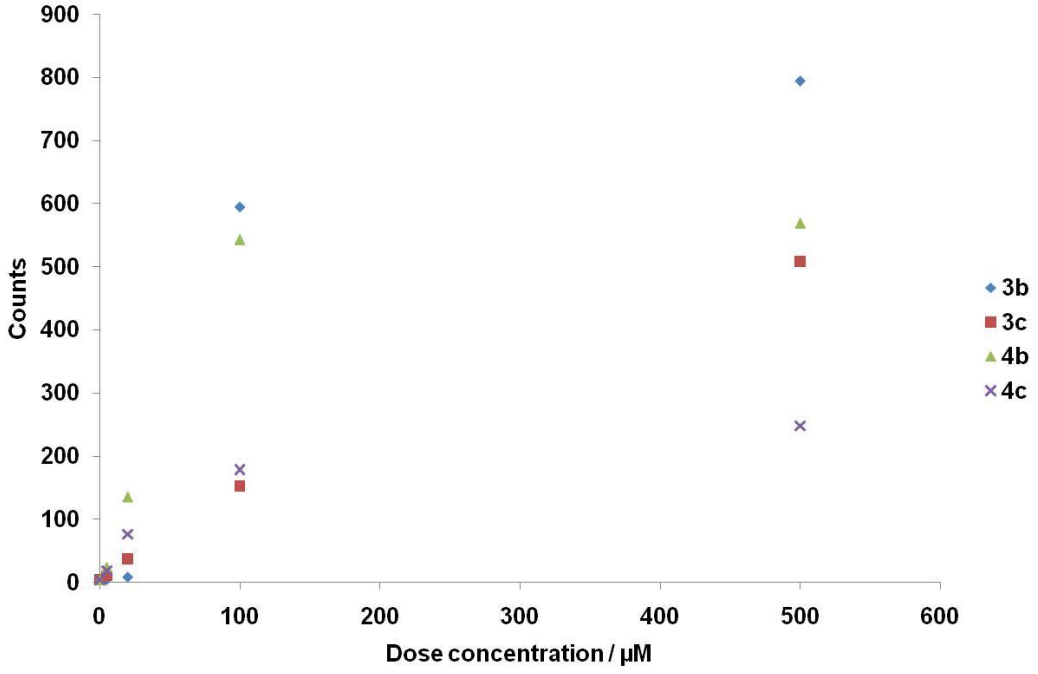

Figure 4.20 Plot of counts vs dose concentration for phosphorescent population for **3b**, **3c**, **4b** and **4c**.

The results show that all eight compounds successfully label cells during the course of the 3 h dose however it is clear that the uptake of the free thiols is considerably lower than that of the disulfide protected compounds. There are several factors that determine the cellular uptake of compounds, predominantly

size, charge and hydrophobicity. It has been found in the case of transition metal complexes that a positive charge aids in the internalisation of the compound by interaction with the negative surface charge of live cells.[6] It is possible that in the case of the deprotected compounds, deprotonation of the thiol leading to a higher negative charge inhibits uptake. In addition, in both classes of compounds, the singly functionalised mimics show slightly increased uptake when compared to the doubly functionalised analogues.

It appears that for most, a 500 µM dose is close to the saturation limit for labelling cells while a significant number of cells are still successfully labelled at 100 µM. Given the results from the cytotoxicity study, it therefore seems that concentrations of around 100 µM or below will be most suitable for fluorescence microscopy.

4.3.9 Fluorescence microscopy

With the photophysical properties of the four potential mimics known and results from the cytotoxicity assays indicating that these have the potential for the treatment of live cells, some preliminary fluorescence microscopy assays were undertaken. It was decided to investigate the intracellular properties of the compounds by dosing cells with the potential mimics in their protected disulfide forms both with and without the presence of DTT as a reducing agent. It is possible that even in the absence of DTT, the protecting groups would be removed by reductive processes *in cellulo* which would be a useful advantage in the use of the S-^{t}butylmercapto group in these compounds.

Samples of CHO cells were seeded in 12 well plates containing microscope cover slips and the cells were dosed with 100 µM final concentration of the potential mimics ± 10 mM DTT. Due to the compounds' low water solubilities, stock solutions were made up in DMSO at 20 mM concentration. While DMSO is cytotoxic at high concentrations, dilution to 100 µM gives only 0.5% DMSO in the dosage medium so there were no problems anticipated with the toxicity of this solvent. The cells were incubated in the dosed medium for 3 h and were imaged immediately after mounting on microscope slides.

All the compounds showed successful uptake into the cells over the course of the 3 h dose, as expected from the flow cytometry results, and so fluorescence microscopy images of the cells could be recorded. Figures 4.21 – 4.24 show the fluorescence microscopy images of CHO cells dosed with the four compounds incubated both with and without DTT.

All four compounds appear to localise predominantly in the cytosol with little or no staining of the nucleus. Also, in all four cases it appears that dosing with compound + DTT leads to significantly higher cytotoxicity with many of the cells becoming detached and showing a loss of membrane integrity. The cells dosed only with test compound, on the other hand, appeared mostly healthy although while imaging it was apparent that more cells were showing signs of dysfunction when treated with the iridium compounds in comparison to the dansyl compounds. This observation is consistent with the observed lower IC_{50} values of **3b** and **4b** from the MTT assays.

Also in comparison of the two types of luminophore, the iridium complexes show a slightly more punctate localisation pattern, particularly in the case of **4b**, compared to a smoother distribution in the localisation of the dansyl compounds **1b** and **2b**. This could indicate that the two luminophores convey different localisation patterns, possibly targeting discrete vesicles such as lysosomes or endosomes. Punctate cytosolic staining has recently been reported for complexes of iridium functionalised with biotin and this was attributed to endosome localisation.[176] It is also possible that this distribution pattern could be the result of aggregation of the luminophores after internalisation.

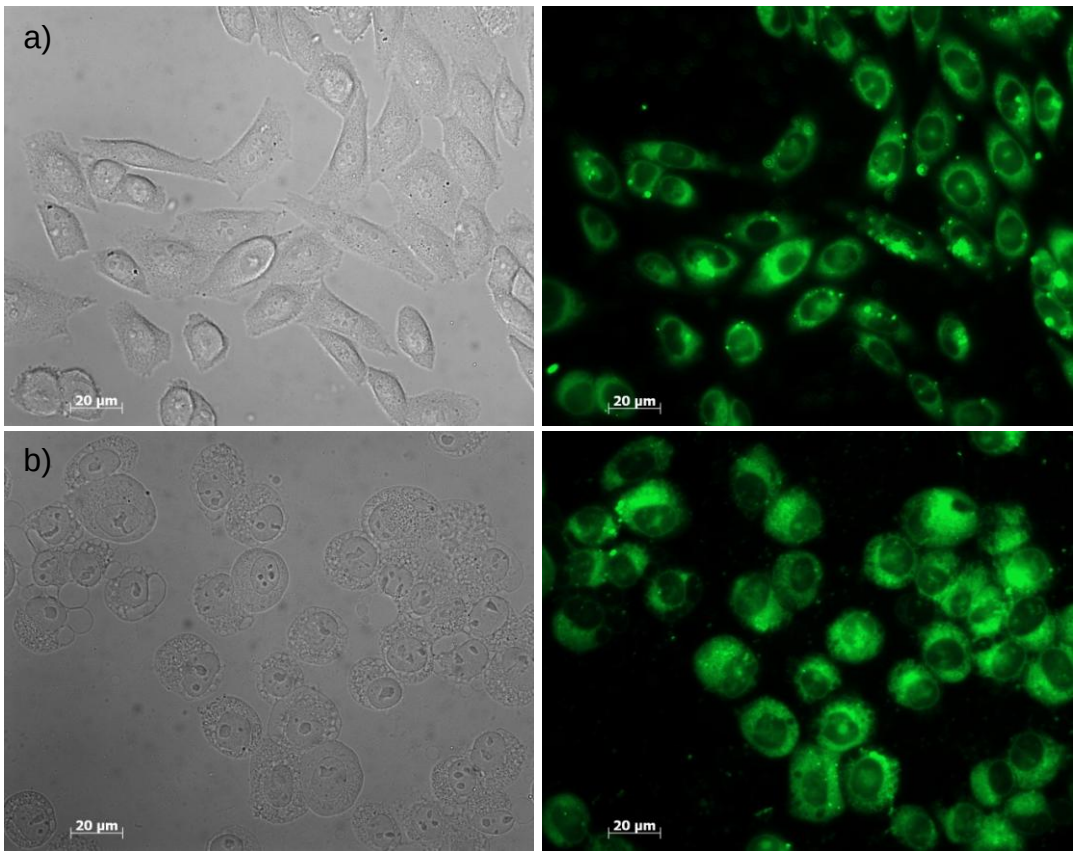

Figure 4.21 Bright field and fluorescence microscopy images of CHO cells dosed with a) 100 µM **1b** and b) 100 µM **1b** + 10 mM DTT.

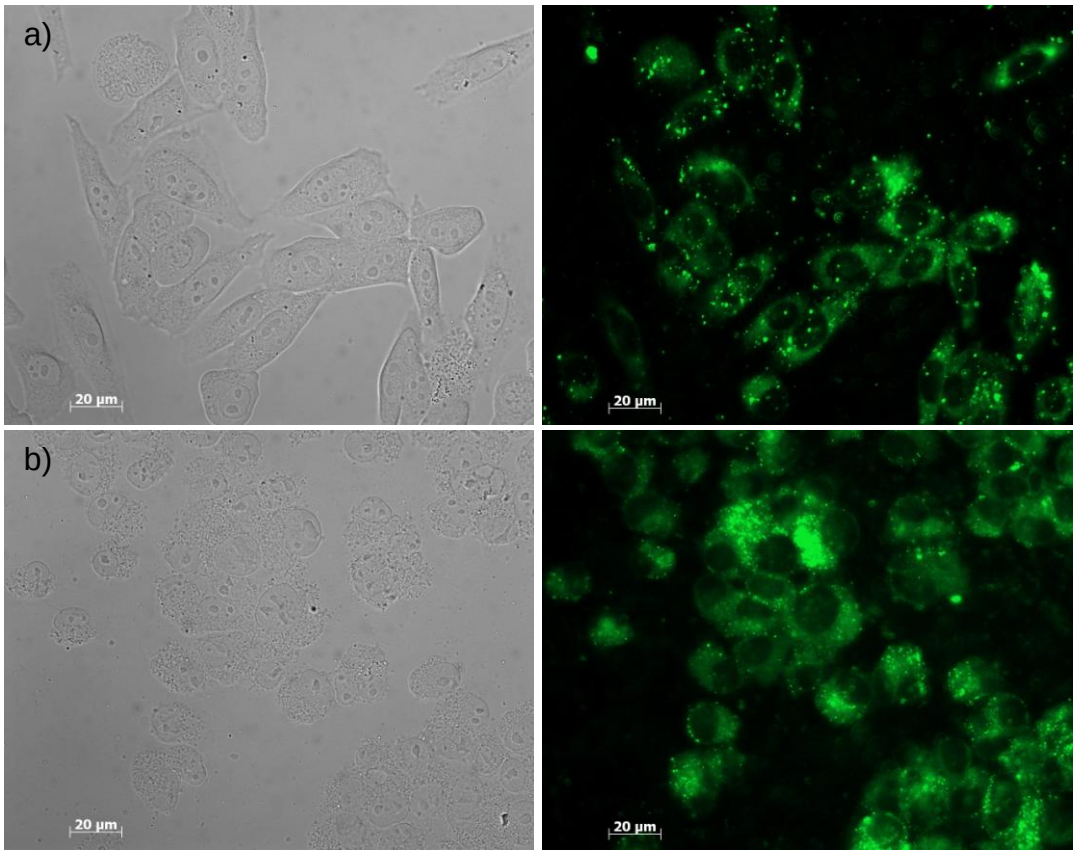

Figure 4.22 Bright field and fluorescence microscopy images of CHO cells dosed with a) 100 µM **2b** and b) 100 µM **2b** + 10 mM DTT.

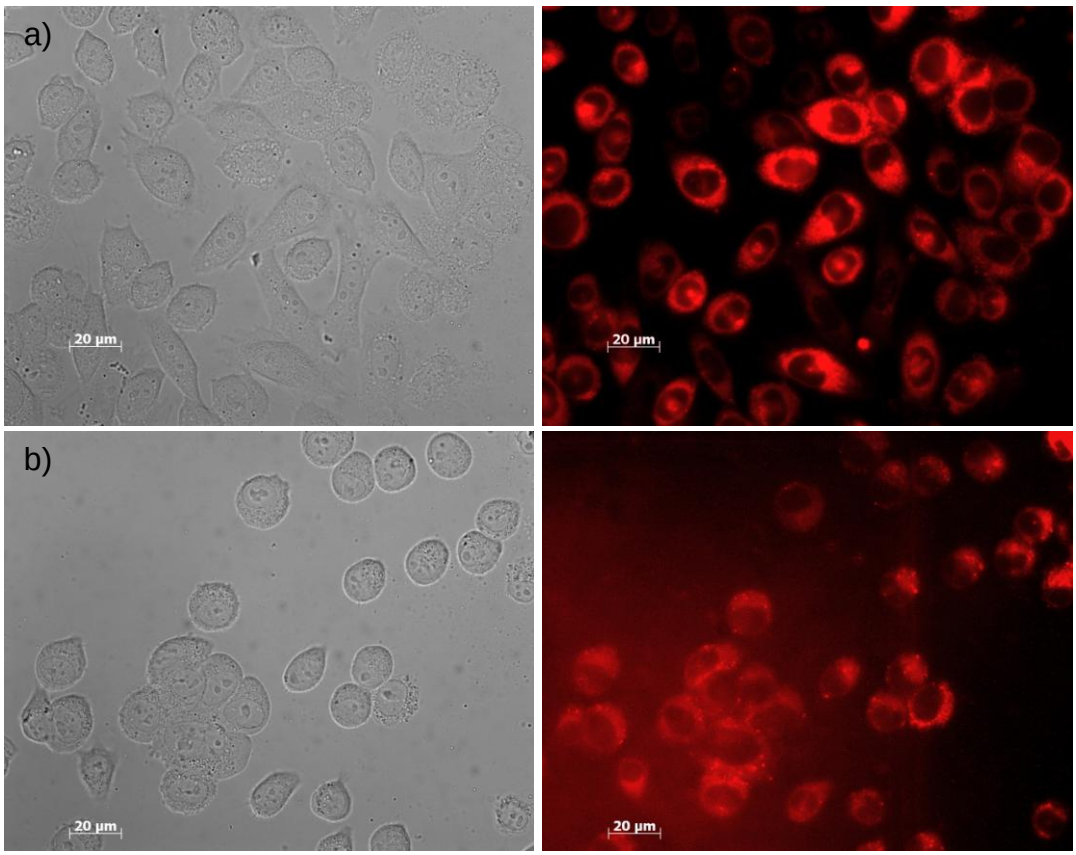

Figure 4.23 Bright field and fluorescence microscopy images of CHO cells dosed with a) 100 µM **3b** and b) 100 µM **3b** + 10 mM DTT.

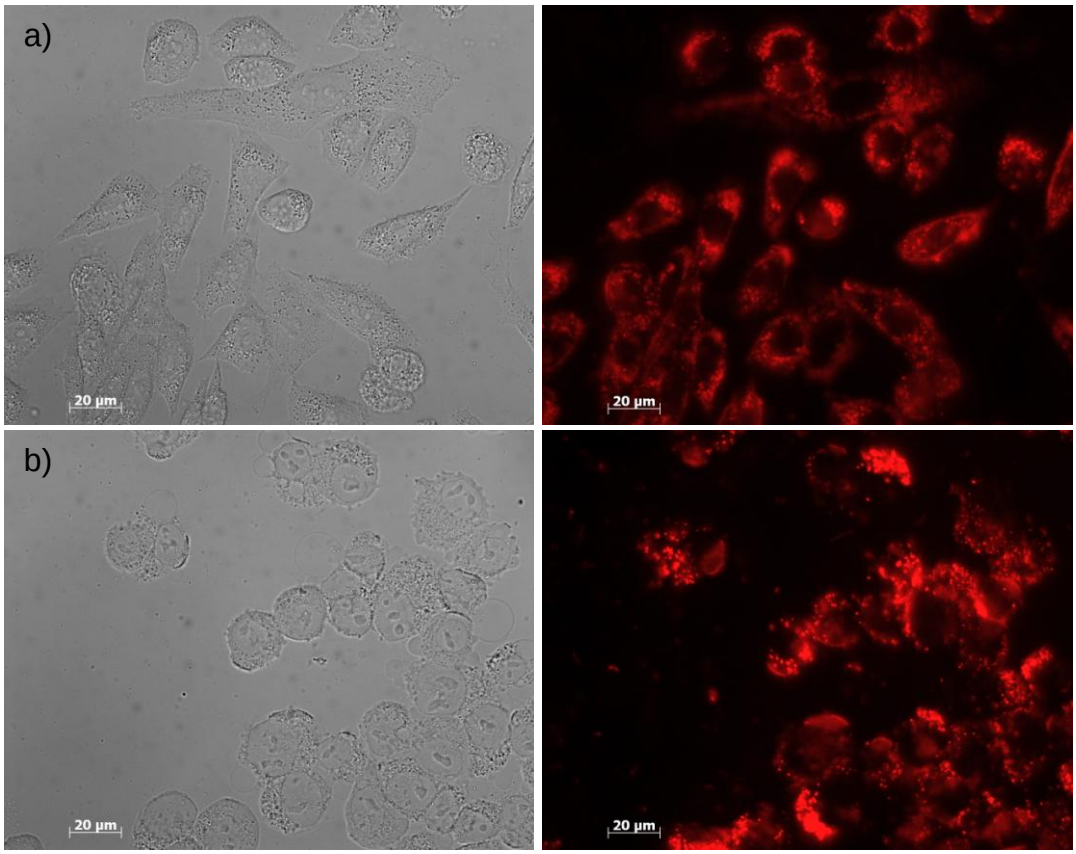

Figure 4.24 Bright field and fluorescence microscopy images of CHO cells dosed with a) 100 µM **4b** and b) 100 µM **4b** + 10 mM DTT.

One point of particular note is that in the case of **2b**, as well as cytosolic distribution similar to that of **1b**, the former also displays bright localised emission from areas both inside and outside the cells. It seems likely in this case that this is the result of aggregation both in solution and *in cellulo*, probably as a result of poor solubility in the cell medium.

4.4 Concluding remarks

The synthesis of luminescent molecules with the potential to mimic Protein Disulfide Isomerase was attempted. Initially, an approach was followed analogous to the synthesis of the known small molecule mimic BMC. This approach, however proved unsuccessful due to various complications in the attempted synthesis of amine-functionalised luminophores.

Instead, a new approach was devised leading to carboxylate functionalised emitters allowing the attachment of protected cysteine units via the use of peptide coupling methodology. This route yielded four potential mimics utilising both the dansyl group and a cyclometallated iridium complex as an organic and an inorganic luminescent moiety respectively. This synthetic route also showed potential for the synthesis of further potential mimics using different emissive structures, in particular different classes of transition metal complexes utilising a functionalised bipyridine ligand.

It was attempted to determine whether these compounds do display oxidative activity upon protein disulfide bonds by the use of an insulin cleavage assay. A positive result from this assay would be an indicator for potential mimicry, however due to the low aqueous solubility of the compounds the tests were unsuccessful.

The photophysical properties of the synthesised compounds were investigated and were found not to suffer from significant quenching by the appended mimic structures. In addition to the photophysical properties, the compounds were also tested for cytotoxicity and were shown not to significantly affect cell viability at concentrations below ~ 100 μM. Consequently, these compounds were

utilised in fluorescence microscopy imaging of live cells and showed acceptable levels of cellular uptake and cytosolic localisation upon internalisation.

It could be expected that if these compounds were to show the desired PDI mimic activity, they may show a tendency towards Endoplasmic Reticulum localisation and this, in particular, is an area which requires further investigation.

4.4.1 Scope for future work

4.4.1.1 Cellular studies

In addition to the preliminary fluorescence microscopy assays carried out it would be of great interest to further explore the intracellular localisation of these compounds as well as to better determine their uptake properties. Variable temperature studies or uptake studies with metabolic inhibitors would be of use in determining whether the compounds achieve internalisation via passive diffusion or some active transport mechanism. The localisation could be investigated through the use of co-staining in fluorescence microscopy, for example the use of stains such as ER Tracker™ Blue-White DPX[249] could be used to determine the extent of ER localisation.

The activity of these compounds as mimics should also be explored more directly. Assays involving the reactivation of reduced and randomly oxidised RNase enzymes would confirm the activity of these species as functioning disulfide isomerism catalysts in biological systems.

4.4.1.2 Structural considerations

As well as exploring a wider range of emissive species for such mimics, there is also scope for improving the properties of the synthesised compounds. As discussed, there have been particular issues relating to the water solubility of the compounds leading to problems in some biological assays. In addition, while the compounds are not highly cytotoxic, any reduction in their inhibitory properties would be of value. Both these issues could possibly be addressed in the same manner since the addition of polyethylene glycol (PEG) groups to compounds used *in cellulo* has recently been shown to reduce cytotoxicity in

compounds containing the dansyl group[250] and iridium complexes.[251] In addition, the incorporation of PEG groups in the latter study was shown to increase their solubility in water.

A modified structure such as that shown in Figure 4.25 could therefore greatly improve the properties of the iridium based mimics with regards to use in the imaging of live cells.

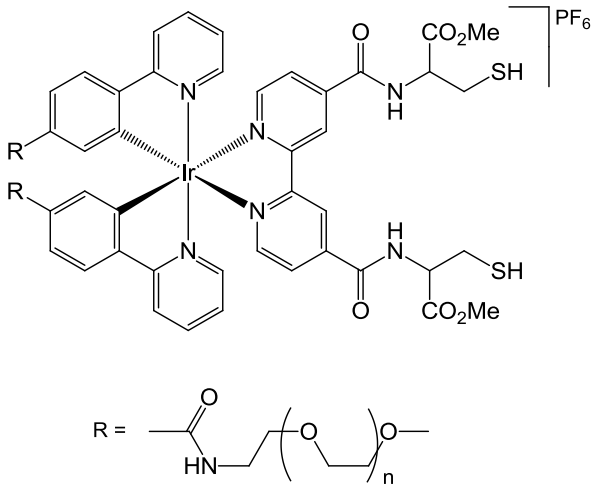

Figure 4.25 Potential iridium based mimic structure with improved solubility and reduced cytotoxicity.

Very recent work in the field of isomerase catalysts has also shown that the use of selenium in place of sulfur leads to increased performance as a disulfide isomerisation catalyst compared to the analogous sulfur compounds.[252,253] This could also be a potential area for investigation, for example coupling selenocysteine to a carboxylate functionalised luminophore (Figure 4.26).

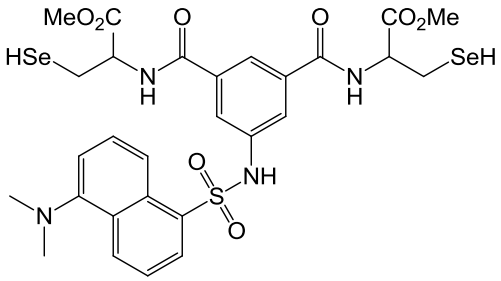

Figure 4.26 The structure of a possible selenium-based PDI mimic.

Chapter 5

Experimental

5 Experimental

5.1 Materials, equipment and methods

5.1.1 General synthetic procedures

All organic solvents used were of analytical reagent grade except MeCN which was of HPLC grade and were used as supplied unless noted as dry. Dry solvents were of HPLC grade and dried by passage through a Pure Solv 400 solvent purification system and stored under nitrogen. Water for use in reactions was purified using the 'Purite$_{STILL}$ Plus' system and had conductivity ≤ 0.04 μScm^{-1}. Reactions performed under nitrogen were carried out using Schlenk line techniques. Reagents were used as supplied by commercial sources.

Thin layer chromatography was carried out using either silica (Merck Art 5554) or aluminium oxide (Merck Art 5550) plates, both of which are fluorescent when irradiated at 254 nm. Preparative column chromatography was carried out using silica (Merck Silica Gel 60, 230-400 mesh) or neutral alumina (Merck Aluminium Oxide 90, activity I, 70-230 mesh).

5.1.2 Characterisation techniques

NMR spectra were recorded using a Varian Mercury-200 spectrometer (200 MHz for ^{1}H), Varian Mercury-400 spectrometer (400 MHz for ^{1}H, 100 MHz for ^{13}C), Bruker Avance-400 spectrometer (400 MHz for ^{1}H, 100 MHz for ^{13}C), Varian Inova-500 spectrometer (500 MHz for ^{1}H, 125 MHz for ^{13}C) or Varian VNMRS-700 spectrometer (700 MHz for ^{1}H, 175 MHz for ^{13}C). Chemical shifts are quoted in ppm relative to residual proteo-solvent resonances. ^{1}H NMR spectra assignment was assisted by ^{1}H-^{1}H COSY (correlation spectroscopy, through-bond interactions). ^{13}C NMR spectra were recorded with proton decoupling and assigned with the aid of ^{1}H-^{13}C HSQC (heteronuclear single quantum correlation) and ^{1}H-^{13}C HMBC (heteronuclear multiple bond correlation) experiments.

Low resolution electrospray mass spectra (ES MS) were recorded with a micromass LCT spectrometer or Thermo-Finnigan LTQ FT spectrometer using either acetonitrile or methanol as the carrier solvent and MALDI mass spectra were recorded using an Applied Biosystems Voyager-DE STR instrument or a Bruker Daltonics Autoflex II ToF/ToF instrument. High resolution ES mass spectra were recorded using a Micromass LCT spectrometer or a Thermo-Finnigan LTQ FT spectrometer. Electron ionisation (EI) mass spectra were recorded by the EPSRC National Mass Spectrometry Service at the University of Wales, Swansea. Gas chromatography-mass spectrometry (GCMS) was performed using a Thermo-Finnigan Trace GCMS instrument. Infrared (IR) spectra were measured using a Perkin Elmer FTIR Paragon 1000 with ATR attachment.

Elemental analysis was carried out using an Exeter Analytical E-440 elemental analyser and melting points were determined using a Gallenkamp 889339 capillary melting point apparatus.

5.1.3 Photophysical measurements

UV/Visible spectra were measured with a Biotek Instruments XS spectrometer operating with LabPower software. Samples were held in a quartz cuvette with 1 cm pathlength and measurements were performed against a reference of pure solvent in a matched cuvette. Exctinction coefficients were determined through graphical application of the Beer-Lambert law (Equation 2) using dilution techniques.[254]

$$A(\lambda) = \varepsilon(\lambda)cl$$

Equation 2

$A(\lambda)$ is the absorbance at a specific wavelength, c is the concentration of the absorbing species (mol dm^{-3}), l is the path length and ε is the extinction coefficient at the given wavelength ($dm^3mol^{-1}cm^{-1}$).

Steady state emission and excitation spectra were measured with a Jobin Yvon FluoroMax-2 spectrofluorimeter, equipped with a red-sensitive Hamamatsu

R928 photomultiplier tube (PMT) using DataMax operating software. To minimise inner filter effects, solutions being studied were sufficiently dilute as to have absorbance below 0.1 at the excitation wavelength. Samples in aerated solutions were contained in quartz cuvettes of 1 cm pathlength while samples run in degassed solution were contained in quartz cuvettes modified for attachment to a high-vacuum line. These samples were degassed with a minimum of three freeze-pump-thaw cycles leaving a final vapour pressure of $\leq 8\times10^{-2}$ mbar at 77 K. The acquired emission spectra were corrected for dark count and the spectral response of the detector, while excitation spectra were automatically corrected for lamp output through use of a beam splitter which directs 8% of the excitation light to a reference photodiode.

The quantum yields were calculated by comparison to a reference standard of ruthenium(II) tris(2,2'-bipyridine) chloride in aerated aqueous solution which has $\Phi_{st} = 0.028$.[255] The quantum yield (Φ) of the sample is calculated relative to the standard using Equation 3.

$$\Phi = \Phi_{st}\left(\frac{I}{I_{st}}\right)\left(\frac{A_{st}}{A}\right)\left(\frac{n}{n_{st}}\right)^2$$

Equation 3

Where I is the integrated emission intensity, A is the absorbance at the wavelength of excitation and n is the refractive index of the solvent. Subscript 'st' refers to the respective values of the standard.

Excited state lifetimes were measured using time-correlated single-photon counting (TCSPC) with an Edinburgh Instruments OB 920 fluorimeter, using a pulsed-diode laser as the excitation source with 374 nm excitation for iridium and dansyl compounds or 475 nm excitation for the [PtL^n(thiolate)] complexes. The laser repetition rate was selected so that the pulse period was at least 5-10 times longer than the measured lifetime. The emission was detected at 90° to the excitation source, after passage through a monochromator using a Peltier-cooled R928 PMT. The observed photon count at a given time is proportional to the concentration of the excited state and can be expressed by a monoexponential decay of the form shown in Equation 4.

$$C = C_0 e^{-\frac{t}{\tau}}$$

Equation 4

Where C is the counts at time, t, C_0 is the initial count after excitation and τ is the excited state lifetime. τ values were obtained from a least-squares fit to such a monoexponential decay.

5.1.4 Electrochemistry

Cyclic voltammetry was carried out using a μAutolab Type III potentiostat with GPES Manager software. Samples were made to ~1 mM concentration in CH_2Cl_2 with 0.1 M $[Bu_4N][PF_6]$ as the supporting inert electrolyte. A three-electrode assembly was employed, consisting of a glassy-carbon working electrode, and platinum wire counter and reference electrodes. Solutions were purged with solvent-saturated nitrogen gas for 5 minutes with stirring, prior to measurements being taken without stirring. The voltammograms were referenced to the ferrocence-ferrocenium couple ($E_{1/2}$ = 0.42 V versus SCE).

5.1.5 DFT

Calculations were performed with Gaussian03 software using the B3LYP hybrid functional. The platinum and iridium core orbitals were modelled with a relativistic effective core potential (ECP), with the outer core and valence orbitals (5s, 5p and 5d) represented using the LANL2DZ basis set. All other elements were represented using the 6-31G* or 6-31G basis sets. The results from calculations were visualised using Gaussview 4.1 software.

5.1.6 Cellular studies

A Chinese hamster ovary (CHO) adherent cell line was maintained in exponential growth as a monolayer in appropriate F-12 (Ham) medium supplemented with 10% foetal bovine serum (FBS) and 1% penicillin and streptomycin. To prevent overcrowding and build up of toxins (both of which

could cause uncharacteristic behaviour of the cells) the cells were sub-cultured every three-to-four days.

Sub-culturing was performed as follows: in preparation, sterile solutions of pH 7.5 phosphate buffered saline (PBS), trypsin and fresh growth medium were warmed to 37°C. The old medium was removed from the culture flask and the cells were rinsed with PBS followed by addition of 1.5 mL trypsin. The cells were then incubated for 3 min until they became detached from the flask surface. Fresh medium was then added and the suspension of cells was centrifuged at 1500 rpm for 3 min. The medium containing residual trypsin was removed by pipette and the cells were resuspended in 4 mL medium. Approx 0.5 mL of this suspension was transferred to a fresh culture flask containing 10 mL medium while the remaining cells could be transferred to microplates for assays.

5.1.6.1 Cytotoxicity measurements

A suspension containing approximately 1×10^6 cells in media (10 mL) was prepared from the 4 mL stock solution during sub-culturing. This was transferred to a 96-well microplate in 100 µL aliquots giving approximately 1×10^4 cells per well and the cells were incubated at 37 °C and 5% CO_2 overnight, during which time adhesion occurred. The cells were then dosed with a range of concentrations of the test compounds (with each concentration repeated in 3 separate wells) and incubated for a further 24 h. The dosing media was then removed and the cells were rinsed with sterile PBS (pH 7.5, 100 µL), and 100 µL fresh media was added. The cells were incubated for 4 h with a 1.0 mM solution of 3-(4,5-dimethylthiazol-2-yl)-2,5-diphenyltetrazolium bromide (MTT). After this time, the culture medium was removed, and DMSO (150 µL) was added to each well. The plate was shaken for 2 min and the absorbance of each well at 541 nm was measured against a blank microplate containing 150 µL DMSO. Measurement of the absorbance was performed using an Analytic Jena FLASHScan 530, using WinFLASH version 1.5 software. The proportion of live cells in each well was calculated by the average absorbance for a given concentration divided by the average absorbance of wells containing un-dosed cells. The IC_{50} values for the compounds were

obtained graphically from a plot of the proportion of live cells versus log(concentration).

5.1.6.2 Fluorescence microscopy

Cells were seeded into 12 well plates with each well containing a microscope coverslip and allowed to grow to around 70% confluence in an incubator. The old medium was removed and replaced by fresh medium dosed with the test compounds and incubated for 3 h. The coverslips were then removed and mounted on microscope slides. The slides were imaged immediately using Zeiss Axiovert 200M epifluorescence microscope with a digital camera, and were processed using the Zeiss Axiovision software. A × 40 oil-immersion objective lens was used to visualize the image. The filter sets used were G365 (Zeiss) for excitation in all compounds while $FITC_{em}$ and 12803 filters were used for emission with the iridium-based and dansyl-based luminophores respectively.

5.1.6.3 Flow Cytometry

Cells for analysis were seeded in twelve-well plates and grown to around 80% confluence. The old medium was removed and replaced with fresh medium dosed with varying concentrations of compound and the cells were incubated for 3 h at 37 °C and 5% CO_2. The cells were then treated with 200 µL trypsin for 3 min at 37°C and the resulting suspension was centrifuged at 1500 rpm for 3 min. The dosed medium was removed and the cell plug was resuspended in 2 mL sterile PBS and stored on ice. The samples were filtered before measurement to remove cell clumps.

Flow cytometry measurement was conducted using a DakoCytomation Inc. MoFlo multi-laser flow cytometer (Fort Collins, CO, USA) operating with a 70 µM nozzle at 60 Psi. Samples were interrogated with a UV-laser operating at 50 mW. Luminescence signals were detected through interference filters with bandpasses of 530/40 or 630/30 for compounds with dansyl or iridium luminophores respectively. Fluorescence signals were collected in the logarithmic mode and the data was analysed using Summit v4.3 (Beckman Coulter) software.

5.2 Synthesis of compounds

In many cases procedures were repeated several times. In these cases, masses and yields given are from a typical example.

5.2.1 Compounds from Chapter 2

3-(2-Pyridyl)benzonitrile

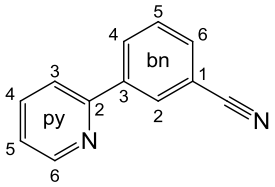

2-(Tri-n-butylstannyl)pyridine (84% purity by mass, 5.24 g, 11.96 mmol), 3-bromobenzonitrile (1.83 g 10.05 mmol), lithium chloride (2.15 g, 50.7 mmol) and bis-(triphenylphosphino)palladium dichloride (150 mg, 0.214 mmol) were placed in toluene (20 mL) and the mixture was degassed using the freeze-pump-thaw method. The reaction was then heated at reflux for 24 h under a nitrogen atmosphere. The reaction was cooled to room temperature, a saturated solution of $KF_{(aq)}$ (10 mL) was added and the mixture was stirred for 1 h. The reaction was filtered and the insoluble material was washed with toluene. The combined filtrate and washings was reduced to dryness under reduced pressure and the residue was taken into 50 mL DCM. The organic phase was washed with 4 × 50 mL 5% $NaHCO_{3\ (aq)}$, separated and dried over K_2CO_3. The solution was filtered and the solvent was removed under reduced pressure to yield the crude product. This was purified by column chromatography on silica with gradient elution from 0% to 20% diethyl ether in hexane. Coincidentally, the required product co-eluted with the by-product 2,2'-bipyridine so the following procedure was adopted for the removal of this impurity: The proportion of by-product was determined by NMR assay and an appropriate amount of $(NH_4)_2Fe(SO_4)_2$ (3:1 mole ratio of bpy to Fe^{2+}) was dissolved in H_2O (25 mL). The impure product was taken into DCM (25 mL) and shaken with the iron (II) solution producing a red pink colour in the aqueous layer indicating the formation of iron(II)-tris-bipyridine. The organic phase was separated and the aqueous part was extracted with DCM (25 mL). The combined organics were

dried over $MgSO_4$ and the solvent was removed under reduced pressure to yield a fluffy white solid (1.75 g, 96%). ^{1}H NMR (400 MHz, $CDCl_3$): δ 8.73 (1H, d, ^{3}J 5.2 Hz, H^6-py), 8.32 (1H, s, H^2-bn), 8.24 (1H, d, ^{3}J 8.0 Hz, H^4-bn), 7.82 (1H, td, ^{3}J 8.0 Hz, ^{4}J 2.0 Hz, H^4-py), 7.74 (1H, d, ^{3}J 7.6 Hz, H^3-py), 7.70 (1H, d, ^{3}J 7.6 Hz, H^6-bn), 7.59 (1H, t, ^{3}J 8.0 Hz, H^5-bn), 7.32 (1H, dd, ^{3}J 7.2 Hz, 4.8 Hz, H^5-py). ^{13}C NMR (125 MHz, $CDCl_3$): δ 155.1 (C^2-py), 150.2 (C^6-py), 140.6 (C^1-bn), 137.3 (C^4-py), 132.4 (C^6-bn), 131.2 (C^4-bn), 130.8 (C^2-bn), 129.7 (C^5-bn), 123.3 (C^5-py), 120.7 (C^3-py), 118.9 (CN), 113.1 (C^3-bn). HRMS (ES+): m/z 181.07621 $(M+H)^+$; calculated for $C_{12}H_9N_2$: 181.07602.

3-(2-Pyridyl)benzylamine

pybzaH

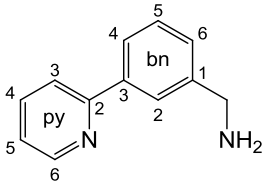

3-(2-Pyridyl)benzonitrile (2.05 g, 11.35 mmol) was placed in a flask under nitrogen. Borane (1M in THF, 32 mL) was added and the solution was refluxed under nitrogen for 48 h. After cooling to room temperature, MeOH (10 mL) was added carefully and the solvent removed under reduced pressure. This was repeated with a further 3 $\times$ 10 mL MeOH. The resulting oil was refluxed in 6M HCl (15 mL) for 6 h. The reaction was made basic by careful addition of 10 mL 20% NaOH forming a white emulsion. This was extracted with 2 $\times$ 25 mL DCM and the combined organic phases were separated and dried over K_2CO_3. The solution was filtered and the solvent was removed under reduced pressure to yield a pale brown oil (1.11 g, 53%). ^{1}H NMR (400 MHz, $CDCl_3$): δ 8.69 (1H, d, ^{3}J 4.4 Hz, H^6-py), 7.97 (1H, s, H^2-bn), 7.83 (1H, d, ^{3}J 6.8 Hz, H^4-bn), 7.75 (2H, m, H^3-py and H^4-py), 7.44 (1H, t, ^{3}J 7.6 Hz, H^5-bn), 7.37 (1H, d, ^{3}J 8.0 Hz, H^6-bn), 7.22 (1H, t, ^{3}J 5.2 Hz, H^5-py), 3.89 (2H, s, CH_2), 1.59 (2H, s, NH_2). ^{13}C NMR (100 MHz, $CDCl_3$): δ 157.5 (C^2-py), 149.8 (C^6-py), 143.7 (C^1-bn), 139.8 (C^3-bn), 136.9 (C^4-py), 129.1 (C^5-bn), 127.9 (C^6-bn), 125.9 (C^2-bn), 125.6 (C^4-bn), 122.3 (C^5-py), 120.8 (C^3-py), 46.6 (CH_2).

N,N-dimethyl-3-(2-pyridyl)benzylamine

dmpybzaH

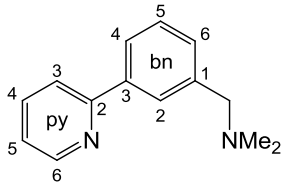

3-(2-Pyridyl)benzylamine (192 mg, 1.04 mmol) was placed in formic acid (0.5 mL) and formaldehyde (37% in H_2O, 0.5 mL) was added. The reaction was stirred for 2 h and then heated at reflux for 2.5 h. The reaction was cooled to room temperature and c.HCl (1 mL) was added. After stirring for 10 min the solvent was removed under reduced pressure then 5 mL H_2O was added followed by 20% $NaOH_{(aq)}$ (20 mL). The resulting emulsion was extracted with 2×20 mL DCM and the combined organic phases were dried over K_2CO_3, filtered and the solvent removed under reduced pressure. The crude product was purified by column chromatography on silica with gradient elution from 0% to 30% diethyl ether in hexane. Yield 132 mg (60%). ^{1}H NMR (400 MHz, $CDCl_3$): δ 8.69 (1H, d, ^{3}J 4.4 Hz, H^6-py), 7.93 (1H, s, H^2-bn), 7.88 (1H, d, ^{3}J 7.6 Hz, H^4-bn), 7.75 (2H, m, H^3-py and H^4-py), 7.44 (1H, t, ^{3}J 7.6 Hz, H^5-bn), 7.38 (1H, d, ^{3}J 7.6 Hz, H^6-bn), 7.23 (1H, m, H^5-py), 3.51 (2H, s, CH_2), 2.27 (6H, s, Me). ^{13}C NMR (125 MHz, $CDCl_3$): δ 157.6 (C^2-py), 149.8 (C^6-py), 139.6 (C^3-bn), 139.2 (C^1-bn), 136.9 (C^4-py), 129.9 (C^6-bn), 128.9 (C^5-bn), 127.8 (C^2-bn), 126.0 (C^4-bn), 122.2 (C^5-py), 120.9 (C^3-py), 64.4 (CH_2), 45.5 (Me).

N-(3-(2-pyridyl)benzyl)benzylimine

pybzbiH

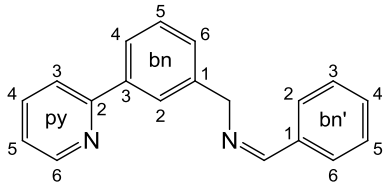

3-(2-Pyridyl)benzylamine (152 mg, 0.825 mmol) and benzaldehyde (81 mg, 0.763 mmol) were placed in ethanol (25 mL) and refluxed for 45 min. The reaction was cooled to room temperature and the solvent was removed under reduced pressure. The crude product was taken into ethyl acetate and filtered rapidly through a short silica plug to remove residual starting materials. The filtrate was reduced to dryness under vacuum. Yield 180 mg (87%). ^{1}H NMR

(400 MHz, $CDCl_3$): δ 8.69 (1H, d, ^3J 4.4 Hz, H^6-py), 8.45 (1H, s, N=C**H**), 7.97 (1H, s, H^2-bn), 7.88 (1H, d, ^3J 7.2 Hz, $H^{4\text{ or }6}$-bn), 7.80 (2H, m, $H^{2/6\text{ or }3/5}$-bn'), 7.74 (2H, m, H^3-py and H^4-py), 7.47 (1H, t, ^3J 7.6 Hz, H^5-bn), 7.43 (4H, m, H^4-bn', $H^{2/6\text{ or }3/5}$-bn' and $H^{4\text{ or }6}$-bn), 7.23 (1H, dd, ^3J 8.8 Hz, 4.8 Hz, H^5-py), 4.92 (2H, s, CH_2).

5-Chloropentanal

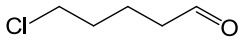

5-Chloropentan-1-ol (4.04 g, 32.9 mmol) was dissolved in dry DCM (10 mL) under nitrogen. This solution was transferred to a suspension of pyridinium chlorochromate (9.35 g, 43.4 mmol) in dry DCM (80 mL) under nitrogen. The mixture was heated at reflux for 1.5 h then allowed to cool to room temperature. Diethyl ether (100 mL) was added and the solution was decanted off. The remaining black gum was extracted with 3×40 mL ether. The combined organics were filtered through celite and the solvent was removed by gentle distillation. The dark brown residue was placed on a short silica plug and washed through rapidly with diethyl ether. The solvent was removed, again by distillation to yield 2.80 g (71%) brown oil. ^{1}H NMR (400 MHz, $CDCl_3$): δ 9.78 (1H, s, C**H**O), 3.55 (2H, t, ^3J 6.4 Hz, C**H**$_2$Cl), 2.49 (2H, t, ^3J 6.4 Hz, C**H**$_2$CHO), 1.80 (4H, m, C^3H_2 and C^4H_2).

Ethyl 7-chloro-2(E)-heptenoate

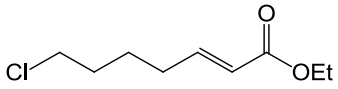

Sodium hydride (0.56 g, 23.3 mmol) was suspended in dry THF (80 mL) under nitrogen. Triethyl phosphonoacetate (4.7 mL, 5.31 g, 23.7 mmol) was added over 5 min with stirring. The solution was stirred for a further 10 min to allow H_2 evolution and then 5-chloropentanal (2.8 g, 23.2 mmol) in dry THF (10 mL) was added. The reaction was stirred at room temperature for 1.5 h then the solvent removed under reduced pressure. H_2O (100 mL) was added to the residue and this was extracted with hexane (100 mL). The organic phase was separated and washed with 2×50 mL H_2O, dried over $MgSO_4$, then the solution was filtered and the solvent removed under reduced pressure yielding a thin oil. NMR showed only approx. 50% conversion so the procedure was repeated with

a further 0.575 g NaH and 4.6 mL triethyl phosphonoacetate yielding 2.35 g (53%) light brown oil. Spectral data are consistent with those reported.[256]

Ethyl 7-iodo-2(E)-heptenoate

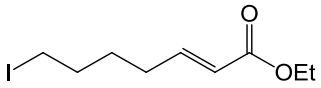

Ethyl 7-chloro-2(E)-heptenoate (2.36 g, 12.4 mmol) and potassium iodide (8.50 g, 56.8 mmol) were placed in acetone (50 mL) and heated at reflux for 24 h. The reaction was cooled to room temperature and the solvent was removed under reduced pressure. H_2O (50 mL) was added to the residue and was extracted with diethyl ether (2 × 50 mL). The ether was separated, washed with 2 × 50 mL H_2O, and dried over $MgSO_4$. The solution was filtered and the solvent removed under reduced pressure to yield a pale red oil (3.00 g, 86%). Spectral data are consistent with those reported.[196]

Ethyl 1-(3-(2-pyridyl)benzyl)piperidin-2-yl acetate
pybzpipH

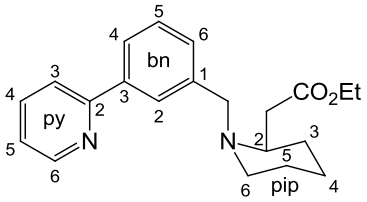

3-(2-Pyridyl)benzylamine (389 mg, 2.11 mmol), ethyl 7-iodo-2(E)-heptenoate (590 mg, 2.09 mmol) and triethylamine (280 mg, 2.27 mmol) were placed in ethanol (100 mL) and heated at reflux. The reaction was monitored by GCMS and after 70 h the conversion was no longer increasing. The reaction was cooled to room temperature and the solvent was removed under reduced pressure. 50 mL H_2O was added to the residue and was extracted with 2 × 50 mL diethyl ether. The combined organics were washed with H_2O (50 mL) and 5% $Na_2SO_{3\,(aq)}$ (50 mL) then dried over $MgSO_4$. After filtration and removal of the solvent under reduced pressure the crude product was purified by column chromatography on silica with gradient elution from 0% to 50% diethyl ether in hexane yielding a colourless oil (111 mg, 16%). ^{1}H NMR (400 MHz, $CDCl_3$): δ 8.69 (1H, td, ^{3}J 4.4 Hz, ^{4}J 1.4 Hz, H^6-py), 7.92 (1H, s, H^2-bn), 7.85 (1H, m, H^4-bn), 7.74 (2H, m, H^3-py and H^4-py), 7.41 (2H, m, H^6-bn and H^5-bn), 7.22 (1H, dd, ^{3}J 8.4 Hz, 4.8 Hz, H^5-py), 4.12 (2H, q, ^{3}J 7.2 Hz,

OC**H**$_2$CH$_3$), 3.88 (1H, d, ^{2}J 13.6 Hz, ArC**H**HN), 3.45 (1H, d, ^{2}J 13.6 Hz, ArCH**H**N), 3.01 (1H, m, H^2-pip), 2.73 (1H, dd, ^{2}J 14.4 Hz, ^{3}J 4.8 Hz, C**H**HCO$_2$Et), 2.65 (1H, m, H^6-pip), 2.45 (1H, dd, ^{2}J 14.4 Hz, ^{3}J 8.0 Hz, CH**H**CO$_2$Et), 2.21 (1H, m, H^6-pip), 1.75 (1H, m, H$^{3,\,4\text{ or }5}$-pip), 1.62 (1H, m, H$^{3,\,4\text{ or }5}$-pip), 1.48 (4H, m, H$^{3,\,4\text{ or }5}$-pip), 1.23 (3H, t, ^{3}J 7.2 Hz, OCH$_2$C**H$_3$**). ^{13}C NMR (125 MHz, CDCl$_3$): δ 173.1 (C=O), 157.8 (C^2-py), 149.8 (C^6-py), 140.4 (C$^{1\text{ or }3}$-bn), 139.5 (C$^{1\text{ or }3}$-bn), 136.9 (C^4-py), 129.6 (C^6-bn), 128.8 (C^5-bn), 127.4 (C^2-bn), 125.6 (C^4-bn), 122.2 (H^5-py), 120.9 (C^3-py), 60.5 (O**C**H$_2$CH$_3$), 58.7 (Ar**C**H$_2$N), 57.8 (C^2-pip), 50.3 (C^6-pip), 36.4 (**C**H$_2$CO$_2$Et), 31.0 (C$^{3,4\text{ or }5}$-pip), 25.3 (C$^{3,4\text{ or }5}$-pip), 22.4 (C$^{3,4\text{ or }5}$-pip), 14.3 (OCH$_2$**C**H$_3$). HRMS (ES+): m/z 339.20658 (M+H)+; calculated for $C_{21}H_{26}N_2O_2$: 339.20670.

(1,3-Di(2-pyridyl)benzene)platinum(II) methanethiolate
[PtL^1(mt)]

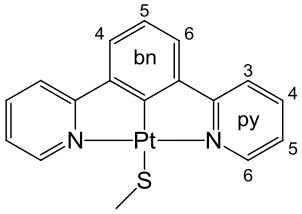

Sodium methanethiolate (50 mg, 0.15 mmol, 21% w/w in H_2O) was dissolved in methanol (5 mL) and the solution degassed via four freeze-pump-thaw cycles prior to back-filling the reaction vessel with nitrogen gas. [PtL^{1}Cl] (63 mg, 0.14 mmol) was added under a flow of nitrogen and the suspension stirred at room temperature for 18 h. The solid was separated using a centrifuge, washed successively with methanol (5 mL), water (3 x 5 mL) and diethyl ether (2 x 5 mL), and finally dried under reduced pressure, giving the desired product as an orange solid (26 mg, 40%). ^{1}H NMR (400 MHz, d_6-DMSO): δ 9.40 (2H, d, ^{3}J 4.8, ^{3}J(^{195}Pt) 21, H^6-py), 8.19 (2H, t, ^{3}J 8.0, H^4-py), 8.11 (2H, d, ^{3}J 6.4, H^3-py), 7.81 (2H, d, ^{3}J 7.6, H$^{4/6}$-bn), 7.53 (2H, t, ^{3}J 6.4, H^5-py), 7.29 (1H, t, ^{3}J 7.6, H^5-bn), 2.23 (3H, s, CH_3). ^{13}C NMR (125 MHz, d_6-DMSO): δ 167.9, 152.2, 140.9, 140.2, 124.8, 124.1, 123.4, 120.5, 12.6. C, H, & N analysis: 42.57% C, 2.90% H, 5.75% N measured; 43.13% C 2.98% H, 5.92% N calculated for $C_{17}H_{14}N_2PtS$.

(1,3-Di(2-pyridyl)benzene)platinum(II) phenylthiolate
[PtL^1(tp)]

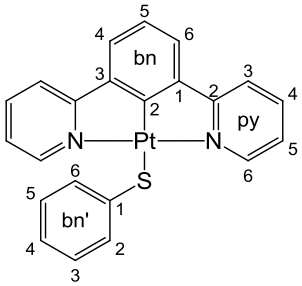

Thiophenol (47 mg, 0.42 mmol) was dissolved in methanol (6 mL) and the solution degassed via four freeze-pump-thaw cycles before being placed under an atmosphere of nitrogen. Potassium *tert*-butoxide (48 mg, 0.43 mmol) was added under a flow of nitrogen gas, and the mixture stirred for 5 min followed by addition of [PtL^{1}Cl] (129 mg, 0.28 mmol). The suspension was stirred at room temperature for 16 h under nitrogen. The solid was then separated using a centrifuge, washed successively with methanol and diethyl ether (3 x 5 mL of each), and dried under vacuum, to give the product as a yellow solid (120 mg, 80%). ^{1}H NMR (500 MHz, d_6-DMSO): δ 9.19 (2H, d, ^{3}J 5.5, ^{3}J(^{195}Pt) 19, H^6-py), 8.14 (4H, overlapping m, H^3-py and H^4-py), 7.81 (2H, d, ^{3}J 7.5, H$^{4/6}$-bn), 7.51 (2H, d, ^{3}J 8.0, H$^{2/6}$-bn'), 7.40 (2H, t, ^{3}J 6.3, H^5-py), 7.31 (1H, t, ^{3}J 7.5, H^5-bn), 6.94 (2H, t, ^{3}J 7.5, H$^{3/5}$-bn'), 6.79 (1H, t, ^{3}J 7.5, H^4-bn'). ^{13}C NMR (125 MHz, d_6-DMSO): δ 169.1 (C^2-bn), 167.8 (C^2-py), 152.7 (C^6-py), 148.8 (C^1-bn'), 141.2 (C$^{1/3}$-bn), 140.3 (C^4-py), 132.2 (C$^{2/6}$-bn'), 127.6 (C$^{3/5}$-bn'), 124.8 (C$^{4/6}$-bn), 124.1 (C5-py), 123.8 (C^5-bn), 121.1 (C^4-bn'), 120.5 (C^3-py). C, H, & N analysis: 48.56% C, 2.95% H, 5.14% N measured; 49.34% C, 3.01% H, 5.23% N calculated for $C_{22}H_{16}N_2PtS$.

(1,3-Di(2-pyridyl)benzene)platinum(II) 4-methylphenylthiolate
[PtL^1(mtp)]

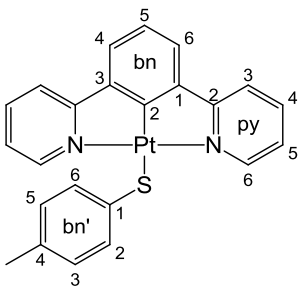

This complex was prepared in a similar manner to [PtL^1(tp)], starting from [PtL^{1}Cl] (128 mg, 0.28 mmol), 4-methylthiophenol (55 mg, 0.44 mmol) and

KO^tBu (60 mg, 0.54 mmol), leading to the product as an orange solid (118 mg, 78%). ^1H NMR (500 MHz, d_6-DMSO): δ 9.19 (2H, d, ^3J 5.5, $^3J(^{195}Pt)$ 15, H^6-py), 8.14 (4H, m, H^3-py and H^4-py), 7.82 (2H, d, ^3J 8.0, $H^{4/6}$-bn), 7.41 (2H, t, ^3J 7.5, H^5-py), 7.39 (2H, d, ^3J 8.0, $H^{2/6}$-bn'), 7.32 (1H, t, ^3J 8.0, H^5-bn), 6.77 (2H, d, ^3J 8.0, $H^{3/5}$-bn') 2.12 (3H, s, CH_3). ^{13}C NMR (125 MHz, d_6-DMSO): δ 170.0 (C^2-bn), 168.5 (C^2-py), 153.3 (C^6py), 145.4 (C^1-bn'), 141.8 ($C^{1/3}$-bn), 141.0 (C^3-py), 132.8 ($C^{2/6}$-bn'), 130.5 (C^4-bn'), 129.1 ($C^{3/5}$-bn'), 125.5 ($C^{4/6}$-bn), 124.8 (C^5-py), 124.4 (C^5-bn), 121.2 (C^4-py), 20.44 (CH_3). C, H, & N analysis: 48.89% C, 3.19% H, 4.92% N measured; 48.98% C, 3.50% H, 4.97% N calculated for $[C_{23}H_{18}N_2PtS].\{0.8H_2O\}$.

(1,3-Di(2-pyridyl)benzene)platinum(II) 4-methoxyphenylthiolate [PtL^1(motp)]

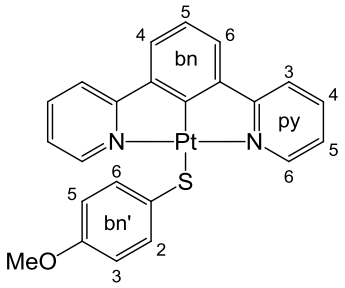

This complex was prepared in a similar manner to [PtL^1(tp)], starting from [PtL^1Cl] (30 mg, 0.065 mmol), 4-methoxythiophenol (23 mg, 0.16 mmol) and KO^tBu (21 mg, 0.19 mmol), giving the product as a red solid (20 mg, 55%). ^1H NMR (400 MHz, d_6-DMSO): δ 9.18 (2H, d, ^3J 4.8, $^3J(^{195}Pt)$ 18, H^6-py), 8.13 (4H, m, H^3-py and H^4-py), 7.82 (2H, d, ^3J 7.6, $H^{4/6}$-bn), 7.40 (2H, t, ^3J = 7.2, H^5-py), 7.39 (2H, d, ^3J 8.8, $H^{2/6}$-bn'), 7.32 (1H, t, ^3J 7.6, H^5-bn), 6.59 (2H, d, ^3J 8.8, $H^{3/5}$-bn'), 3.61 (3H, s, OCH_3). ^{13}C NMR (125 MHz, d_6-DMSO): δ 167.9 (quat), 152.5 (C^6-py), 141.1 (quat), 140.3 (C^3-py or C^4-py), 133.1 (C^5-py or $C^{2/6}$-bn' or $C^{3/5}$-bn'), 124.8 ($C^{4/6}$-bn), 124.0 (C^5-py or $C^{2/6}$-bn' or $C^{3/5}$-bn'), 123.6 (C^5-bn), 120.5 (C^3-py or C^4-py), 113.6 ($C^{2/6}$bn' or $C^{3/5}$-bn'), 54.9 (OCH_3); remaining quaternaries not detected. C, H, & N analysis: 48.54% C, 3.16% H, 4.92% N measured; 48.85% C, 3.21% H, 4.95% N calculated for $C_{23}H_{18}N_2OPtS$.

(1,3-Di(2-pyridyl)benzene)platinum(II) 4-nitrophenylthiolate [PtL^1(ntp)]

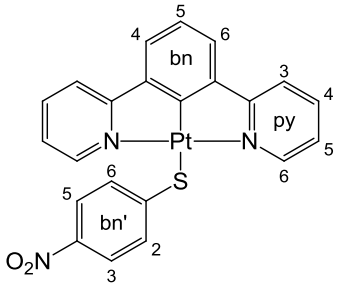

This compound was prepared from [PtL^{1}Cl] (52 mg, 0.13 mmol), 4-nitrothiophenol (36 mg, 0.23 mmol) and KO^{t}Bu (25 mg, 0.23 mmol), using the same procedure as for [PtL^1(tp)], giving the product as a red/orange solid (52 mg, 72%). ^{1}H NMR (400 MHz, d_6-DMSO): δ 9.08 (2H, d, ^{3}J 6.0, ^{3}J(^{195}Pt) 15, H^6-py) 8.17 (4H, m, H^3-py and H^4-py), 7.84 (2H, d, ^{3}J 7.6, H$^{4/6}$-bn) 7.82 (2H, d, ^{3}J 8.8, H$^{2/6 \text{ or } 3/5}$-bn') 7.71 (2H, d, ^{3}J 8.8, H$^{2/6 \text{ or } 3/5}$-bn'), 7.46 (2H, t, ^{3}J 6.4, H^5-py), 7.35 (1H, t, ^{3}J = 7.6, H^5-bn). C, H & N analysis: 44.57% C, 2.58% H, 6.51% N measured; 44.48% C, 2.80% H, 7.07% N calculated for [$C_{22}H_{15}N_3O_2PtS$].{0.75H_2O}.

(Methyl-3,5-di(2-pyridyl)benzoate)platinum(II) methanethiolate [PtL^2(mt)]

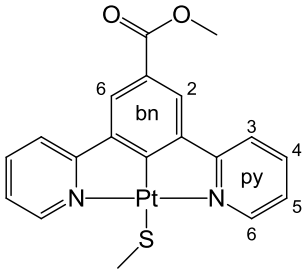

This complex was prepared using the method described for [PtL^1(mt)], starting from [PtL^{2}Cl] (45.8 mg, 0.088 mmol) and sodium methanethiolate (31 mg, 0.092 mmol, 21% w/w in H_2O) in methanol (5 mL), leading to the product as an orange/red solid (24 mg, 51%). ^{1}H NMR (400 MHz, d_6-DMSO): δ 9.39 (2H, d, ^{3}J 4.8, ^{3}J(^{195}Pt) 21, H^6-py), 8.33 (2H, s, H$^{2/6}$-bn), 8.73 (2H, d, ^{3}J 7.2, H^3-py), 8.21 (2H, t, ^{3}J 7.6, H^4-py), 7.58 (2H, t, ^{3}J 6.8, H^5-py), 3.90 (3H, s, OCH_3), 2.26 (3H, s, SCH_3). C, H & N analysis: 42.50% C, 2.98% H, 4.92% N measured; 42.94% C, 3.03% H, 5.27% N calculated for $C_{19}H_{16}N_2O_2PtS$.

(Methyl-3,5-di(2-pyridyl)benzoate)platinum(II) phenylthiolate [PtL^2(tp)]

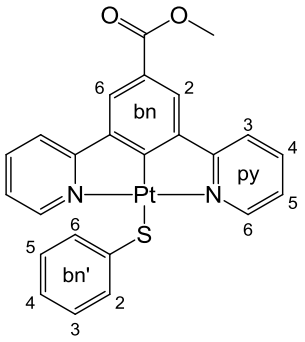

The title compound was prepared using the same procedure as that described for [PtL^1(tp)], starting from [PtL^{2}Cl] (93 mg, 0.18 mmol), thiophenol (41 mg, 0.37 mmol) and KO^{t}Bu (46 mg, 0.41 mmol), leading to the product as a yellow solid (86 mg, 81%). ^{1}H NMR (400 MHz, d_6-DMSO): δ 9.19 (2H, d, ^{3}J 4.8, ^{3}J(^{195}Pt) 8.0, H^6-py), 8.35 (2H, s, H$^{2/6}$-bn), 8.29 (2H, d, ^{3}J 8.0, H^3-py), 8.18 (2H, t, ^{3}J 7.2, H^4-py), 7.51 (2H, d, ^{3}J 7.6, H$^{2/6}$-bn'), 7.45 (2H, t, ^{3}J 7.2, H^5-py), 6.97 (2H, t, ^{3}J 7.6, H$^{3/5}$-bn'), 6.82 (1H, t, ^{3}J 7.2, H^4-bn'), 3.92 (3H, s, OCH_3). ^{13}C NMR (100 MHz, d_6-DMSO): δ 166.7, 152.6, 140.7, 132.3, 127.8, 125.6, 124.85, 121.3, 52.25. MS (EI): m/z 593 (M^+), 484 (M^+-thiolate), 425 (M^+-thiolate-CO_2Me), 110 (thiol$^+$). HRMS (EI): m/z 593.0726 (M^+); calculated for $C_{24}H_{18}N_2O_2PtS$: 593.0731. C, H & N analysis: 48.34% C, 3.03% H, 4.59% N measured; 48.56% C, 3.06% H, 4.72% N calculated for $C_{24}H_{18}N_2O_2PtS$.

(Methyl-3,5-di(2-pyridyl)benzoate)platinum(II) 4-methylphenylthiolate [PtL^2(mtp)]

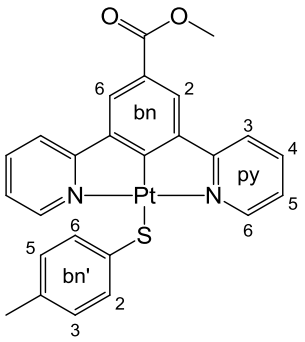

This complex was prepared similarly, from [PtL^{2}Cl] (98 mg, 0.19 mmol), 4-methylthiophenol (50 mg, 0.40 mmol) and KO^{t}Bu (50 mg, 0.045 mmol), leading to the product as a yellow/orange solid (78 mg, 68%). ^{1}H NMR (400 MHz, d_6-DMSO): δ 9.22 (2H, d, ^{3}J 4.0, ^{3}J(^{195}Pt) 14, H^6-py), 8.40 (2H, s, H$^{2/6}$-bn), 8.32 (2H, d, ^{3}J 8.4, H^3-py), 8.20 (2H, t, ^{3}J 8.8, H^4-py), 7.48 (2H, t, ^{3}J 6.0, H^5-py), 7.38

(2H, d, ^3J = 8.4, $H^{2/6}$-bn'), 6.79 (2H, d, ^3J = 8.4, $H^{3/5}$-bn'), 3.92 (3H, s, OCH_3), 2.13 (3H, s, CH_3). MS (EI): m/z 607 (M^+), 484 (M^+-thiolate), 425 (M^+-thiolate-CO_2Me), 124 (thiol$^+$), 91 ($C_7H_7^+$). HRMS (EI): m/z 607.0889 (M^+); calculated for $C_{25}H_{20}N_2O_2PtS$: 607.0888. C, H, & N analysis: 49.20% C, 3.29% H, 4.42% N measured; 49.42% C, 3.32% H, 4.61% N calculated for $C_{25}H_{20}N_2O_2PtS$.

(Methyl-3,5-di(2-pyridyl)benzoate)platinum(II) 4-methoxyphenylthiolate [PtL^2(motp)]

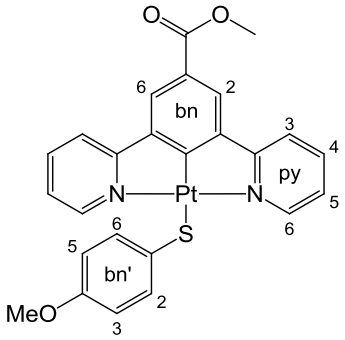

The title complex was prepared in the same way, starting from [PtL^2Cl] (50 mg, 0.096 mmol), 4-methoxythiophenol (28 mg, 0.20 mmol) and KO^{t}Bu (24 mg, 0.21 mmol), leading to the product as a red solid (43 mg, 71%). ^1H NMR (400 MHz, d_6-DMSO): δ 9.19 (2H, d, ^3J 5.6, $^3J(^{195}Pt)$ 19, H^6-py), 8.38 (2H, s, $H^{2/6}$-bn), 8.31 (2H, d, ^3J 8.4, H^3-py), 8.19 (2H, t, ^3J 7.2, H^4-py), 7.47 (2H, t, ^3J 6.8, H^5-py), 7.38 (2H, d, ^3J 8.4, $H^{2/6}$-bn'), 6.61 (2H, d, ^3J 8.4, $H^{3/5}$-bn'), 3.92 (3H, s, $COOCH_3$), 3.62 (3H, s, OCH_3). C, H & N analysis: 48.01% C, 3.17% H, 4.46% N measured; 48.15% C, 3.32% H, 4.49% N calculated for $C_{25}H_{20}N_2O_3PtS$.

(Methyl-3,5-di(2-pyridyl)benzoate)platinum(II) 4-nitrophenylthiolate [PtL^2(ntp)]

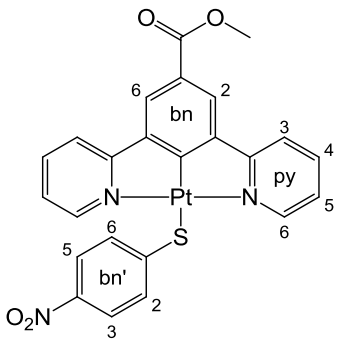

This complex was also prepared using the same general procedure, from [PtL^2Cl] (96 mg, 0.19 mmol), 4-nitrothiophenol (59 mg, 0.38 mmol) and KO^{t}Bu

(44 mg, 0.39 mmol), giving the product as a yellow solid (109 mg, 92%). ^{1}H NMR (300 MHz, d_6-DMSO): δ 9.03 (2H d, ^{3}J 5.1, ^{3}J(^{195}Pt) 17, H^{6}-py), 8.26 (2H, s, H$^{2/6}$-bn), 8.91 (4H, m, H^{3}-py and H^{4}-py), 7.80 (2H, d, ^{3}J 8.1, H$^{2/6\ or\ 3/5}$-bn'), 7.66 (2H, d, ^{3}J 8.1, H$^{2/6\ or\ 3/5}$-bn') 7.47 (2H, t, ^{3}J 5.4, H^{5}-py), 3.92 (3H, s, OCH_3). MS (EI): m/z 640 (M^+), 484 (M^+-thiolate), 425 (M^+-thiolate-CO_2Me), 155 (thiol$^+$). HRMS (EI): m/z 638.0579 (M^+); calculated for $C_{24}H_{17}N_3O_4PtS$: 638.0582. C, H & N analysis: 44.96% C, 2.67% H, 6.43% N measured; 45.14% C, 2.63% H, 6.58% N calculated for $C_{24}H_{17}N_3O_4PtS$.

5.2.2 Compounds from Chapter 3

Bis(2-phenylpyridine)(pyridine)iridium(III) chloride
[Ir(ppy)$_2$(py)Cl]

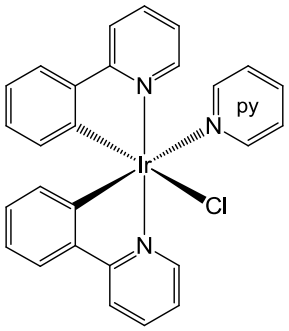

Tetrakis(2-phenylpyridine)(μ-dichloride)diiridium(III) (107 mg, 0.10 mmol) was placed in a flask under nitrogen and dissolved in 10 mL DCM. Pyridine (18 μL, 17.7 mg, 0.22 mmol) was added and the reaction was heated at reflux for 16 h. Removal of the solvent gave 122 mg (99%) yellow solid. ^{1}H NMR (400 MHz, $CDCl_3$): δ 9.92 (1H, d, ^{3}J 6.4 Hz), 9.5-8.4 (v.v. broad signal, H$^{2/6}$-py) 8.07 (1H, d, ^{3}J 6.8 Hz), 7.89 (1H, d, ^{3}J 8.0 Hz), 7.76-7.65 (5H, m*), 7.55 (1H, d, ^{3}J 8.0 Hz), 7.50 (1H, d, ^{3}J 7.6 Hz), 7.19 (1H, s (broad), H^{4}-py), 7.17 (1H, t, ^{3}J 5.6 Hz), 7.00 (1H, t, ^{3}J 7.2 Hz), 6.86 (1H, t, ^{3}J 7.2 Hz), 6.80 (1H, t, ^{3}J 6.4 Hz), 6.78 (1H, t, ^{3}J 6.4 Hz), 6.72 (1H, t, ^{3}J 7.2 Hz), 6.35 (1H, d, ^{3}J 7.6 Hz), 6.19 (1H, d, ^{3}J 7.2 Hz).

* Includes (2H, s (broad), H$^{3/5}$-py).

Bis(2-phenylpyridine)(N,N-dimethyl-4-aminopyridine)iridium(III) chloride [Ir(ppy)$_2$(DMAP)Cl]

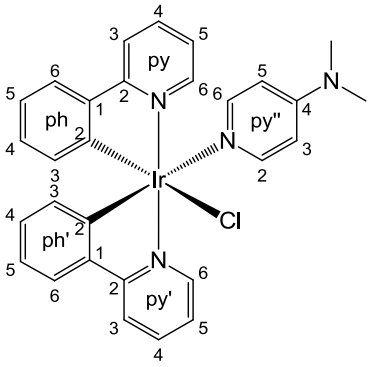

Tetrakis(2-phenylpyridine)(μ-dichloride)diiridium(III) (107 mg, 0.10 mmol) and N,N-dimethyl-4-aminopyridine (25 mg, 0.20 mmol) were placed in a flask under nitrogen and dissolved in 10 mL DCM. The reaction was heated at reflux for 16 h, cooled to RT then the solvent was removed under reduced pressure. The crude product was redissolved in 15 mL fresh DCM and the organic phase was washed with 2×20 mL sat. $NH_4Cl_{(aq)}$, separated and dried over $MgSO_4$. Removal of the solvent under reduced pressure gave 112 mg (85%) yellow solid. ^{1}H NMR (500 MHz , $CDCl_3$): δ 9.92 (1H, d, ^{3}J 6.0 Hz, H^6-py), 8.18 (1H, d, ^{3}J 6.0 Hz, H^6-py'), 7.85 (1H, d, ^{3}J 8.0 Hz, H^3-py'), 7.71 (1H, d, ^{3}J 8.0 Hz, H^3-py), 7.66 (1H, t, ^{3}J 8.0 Hz, H^4-py'), 7.62 (1H, t, ^{3}J 8.0 Hz, H^4-py), 7.53 (1H, d, ^{3}J 8.0 Hz, H^6-ph'), 7.48 (1H, d, ^{3}J 8.0 Hz, H^6-ph), 7.13 (1H, t, ^{3}J 7.5 Hz, H^5-py), 6.98 (1H, t, ^{3}J 8.0 Hz, H^5-py'), 6.82 (1H, t, ^{3}J 8.0 Hz, H^5-ph), 6.76 (1H, t, ^{3}J 7.5 Hz, H^5-ph'), 6.74 (1H, t, ^{3}J 7.5 Hz, H^4-ph), 6.70 (1H, t, ^{3}J 7.5 Hz, H^4-ph'), 6.32 (1H, d, ^{3}J 7.5 Hz, H^3-ph), 6.29 (2H, s (broad), H$^{3/5}$-py''), 6.24 (1H, d, ^{3}J 7.5 Hz, H^3-ph'), 2.89 (6H, s, Me). ^{13}C NMR (125 MHz, $CDCl_3$): δ 168.9 (C^2-py'), 167.9 (C^2-py), 153.7 (C^4-py''), 151.3 (C^2-ph), 151.2 (C^6-py), 150.5 (broad, C$^{2/6}$-py''), 149.8 (C^2-ph'), 149.3 (C^6-py'), 144.2 (C^1-ph'), 144.0 (C^1-ph), 136.6 (C^4-py), 136.4, (C^4-py'), 132.3 (C^3-ph'), 131.4 (C^3-ph), 130.0 (C^4-ph), 129.4 (C^4-ph'), 124.0 (C^6-ph), 123.8 (C^6-ph'), 122.0 (C^5-py), 121.6 (C^5-py'), 120.9 (C^5-ph'), 120.7 (C^5-ph), 119.0 (C^3-py'), 118.0 (C^3-py), 107.5 (C$^{3/5}$-py''), 39.1 (Me). MS (ES+): m/z 623 (M-Cl)$^+$. MS (MALDI+): m/z 658 (M$^+$), 623 (M-Cl)$^+$, 536 (M-DMAP)$^+$.

Tetrakis(2-phenylpyridine)-bis-(μ-toluene-4-thiolate)diiridium(III)

$[Ir(ppy)_2(\mu\text{-}mtp)]_2$

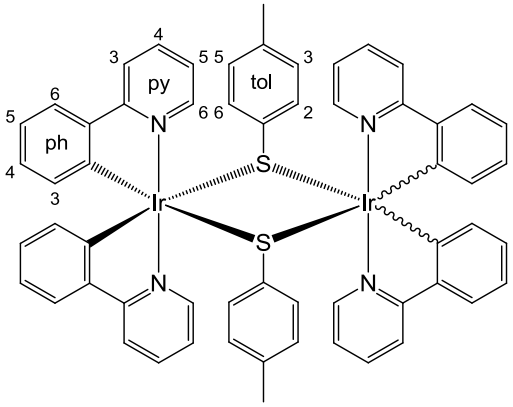

Method 1 (Gives Δ,Δ and Λ,Λ isomers only)

Separate solutions of bis(2-phenylpyridine)(N,N-dimethyl-4-aminopyridine)iridium(III) chloride (33 mg, 0.50 mmol) in 2 mL DCM and 4-methylthiophenol (7 mg, 0.56 mmol) and potassium tert-butoxide (6.3 mg, 0.56 mmol) in 3 mL MeOH were degassed using the freeze-pump-thaw method. The DCM solution was then added to the thiolate solution via cannula and the reaction was stirred for 6 h at RT. The solvents were removed under reduced pressure and the residue was taken into 25 mL DCM. This solution was washed with 2 × 25 mL 5% $NaHCO_{3\ (aq)}$, dried over $MgSO_4$ and then the solvent was removed under reduced pressure giving 35 mg crude product. This was purified by column chromatography on silica with gradient elution from 0% to 2.5% MeOH in DCM giving 2 products. The major component (19 mg, R_f = 0.95 $_{(5\%\ MeOH/DCM)}$) was the product while the minor component (3 mg, R_f 0.35 $_{(5\%\ MeOH/DCM)}$) appeared to be tetrakis(2-phenylpyridine)(μ-dichloro)diiridium(III). The primary product still contained some impurities, so was columned again, yielding 11 mg (35%) yellow solid. ^{1}H NMR (400 MHz, $CDCl_3$): δ 9.47 (4H, d, ^{3}J 6.0 Hz, H^6-py), 7.88 (4H, d, ^{3}J 8.0 Hz, H^3-py), 7.70 (4H, t, ^{3}J 7.6 Hz, H^4-py), 7.56 (4H, d, ^{3}J 8.0 Hz, H^6-ph), 6.82 (4H, t, ^{3}J 8.0 Hz, H^5-ph), 6.71 (4H, t, ^{3}J 7.2 Hz, H^5-py), 6.64 (4H, t, ^{3}J 7.6 Hz, H^4-ph), 6.18 (4H, d, ^{3}J 8.0 Hz, $H^{2/6\ or\ 3/5}$-tol), 5.97 (4H, d, ^{3}J 8.0 Hz, H^3-ph), 5.82 (4H, d, ^{3}J 8.0 Hz, $H^{2/6\ or\ 3/5}$-tol), 1.92 (6H, s, Me). MS (MALDI+): m/z 1246 (M^+), 1123 (M-thiol)$^+$, 624 ($Ir(phpy)_2$(thiol))$^+$, 501 $(Ir(phpy)_2)^+$.

Method 2 (Gives mixtures of diastereoisomers)

A solution of tetrakis(2-phenylpyridine)(μ-dichloro)diirium(III) (53 mg, 0.049 mmol) in 2.5 mL DCM was degassed using the freeze-pump-thaw method. A separate solution of 4-methylthiophenol (13 mg, 0.10 mmol) and potassium tert-butoxide (12 mg, 0.11 mmol) in 3 mL MeOH was degassed by the same method. The solution of dimer was then transferred to the thiolate via cannula under nitrogen and the reaction was heated at reflux for 7 h. The reaction was cooled to RT and the precipitate was collected using a centrifuge and washed with 2 × 8 mL MeOH then dried under vacuum, giving 60 mg (98%) yellow solid. In this case with 4-methylthiophenol, the resulting product was an approx. 1:1 mixture of two distinct diastereoisomers of the product, one of which is identical to the product from method 1. The two isomers were separated by column chromatography with gradient elution from 30% - 100% ether in hexane then 0% - 20% dichloromethane in ether. This yielded 9 mg (15%) isomer from method 1 (Δ,Δ and Λ,Λ) and 41 mg (67%) alternate isomer (Δ,Λ meso), although neither product was entirely isomerically pure. The spectral data for the alternate isomer is given here: ^{1}H NMR (400 MHz, $CDCl_3$): δ 10.49 (4H, d, ^{3}J 6.0 Hz, H^{6}-phpy), 7.65 (4H, t, ^{3}J 8.0 Hz, H^{4}-phpy), 7.49 (4H, d, ^{3}J 7.6 Hz, H^{3}-phpy), 7.30 (4H, t, ^{3}J 7.2 Hz, H^{5}-phpy), 7.08 (4H, m, H^{12}-phpy), 6.58 (8H, m, H$^{10/11}$-phpy), 6.20 (4H, m, H^{9}-phpy), 5.96 (4H, d, ^{3}J 8.0 Hz, H$^{2/6\ or\ 3/5}$-tol), 5.27 (4H, d, ^{3}J 8.0 Hz, H$^{2/6\ or\ 3/5}$-tol), 1.99 (6H, s, Me).

Tetrakis(2-phenylpyridine)-bis-(μ-phenylthiolate)diiridium(III)

$[Ir(ppy)_2(\mu\text{-}tp)]_2$

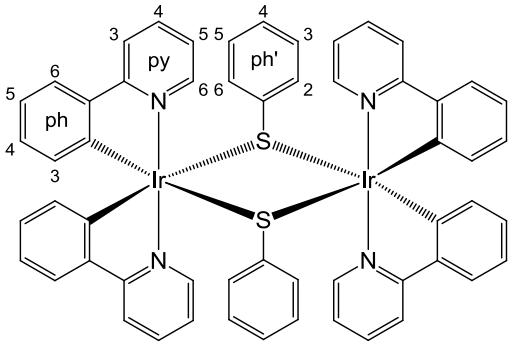

A solution of thiophenol (12 μL, 12.9 mg, 0.117 mmol) and potassium tert-butoxide (13 mg 0.116 mmol) in 3 mL MeOH was degassed using the freeze-pump-thaw method. A separate solution of tetrakis(2-phenylpyridine)(μ-dichloro)diirium(III) (53 mg, 0.049 mmol) in 3 mL DCM was degassed by the

same method and transferred via cannula to the thiolate solution. The reaction was heated at reflux under nitrogen for 16 h. After cooling to RT, the precipitate was collected using a centrifuge and washed with 3 × 8 mL MeOH and 8 mL Et_2O yielding 48 mg (80%) yellow solid. ^{1}H NMR (400 MHz, $CDCl_3$): δ 9.46 (4H, d, ^{3}J 5.2 Hz, H^6-py), 7.89 (4H, d, ^{3}J 7.2 Hz, H^3-py), 7.71 (4H, t, ^{3}J 6.4 Hz, H^4-py), 7.56 (4H, d, ^{3}J 6.4 Hz, H^6-ph), 6.82 (4H, t, ^{3}J 6.4 Hz, H^5-ph), 6.72 (4H, t, ^{3}J 6.0 Hz, H^5-py), 6.64 (4H, t, ^{3}J 6.4 Hz, H^4-ph), 6.53 (2H, t, ^{3}J 5.6 Hz, H^4-ph'), 6.35 (4H, t, ^{3}J 6.0 Hz, $H^{3/5}$-ph'), 5.96 (8H, m, H^3-ph and $H^{2/6}$-ph'). MS (MALDI+): m/z 1220 (M^+), 1109 (M-thiol)$^+$, 610 (Ir(phpy)$_2$(thiol))$^+$.

Tetrakis(2-phenylpyridine)-bis-(μ-4-nitrophenylthiolate)diiridium(III) [Ir(ppy)$_2$(μ-ntp)]$_2$

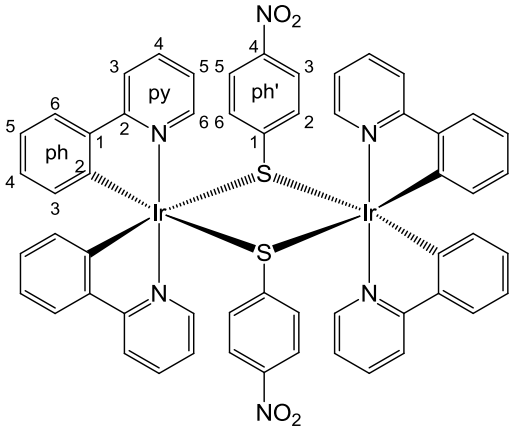

A solution of 4-nitrothiophenol (19 mg, 0.122 mmol) and potassium tert-butoxide (13 mg 0.125 mmol) in 4 mL MeOH was degassed using the freeze-pump-thaw method. A separate solution of tetrakis(2-phenylpyridine)(μ-dichloro)diirium(III) (61 mg, 0.057 mmol) in 3 mL DCM was degassed by the same method and transferred via cannula to the thiolate solution. The reaction was heated at reflux for 16 h under nitrogen, cooled to RT and the precipitate was collected using a centrifuge. The solid was washed with 3 × 8 mL MeOH and 2 × 4 mL Et_2O yielding 40 mg (54%) orange solid*. ^{1}H NMR (400 MHz, $CDCl_3$): δ 9.24 (4H, d, ^{3}J 4.8 Hz, H^6-py), 7.93 (4H, d, ^{3}J 7.6 Hz, H^3-py), 7.81 (4H, t, ^{3}J 7.2 Hz, H^4-py), 7.60 (4H, d, ^{3}J 7.6 Hz, H^6-ph), 7.19 (4H, d, ^{3}J 9.2 Hz, $H^{2/6}$-ph'), 6.91 (4H, t, ^{3}J 7.6 Hz, H^5-ph), 6.80 (4H, t, ^{3}J 6.8 Hz, H^5-py), 6.72 (4H, t, ^{3}J 7.6 Hz, H^4-ph), 6.08 (4H, d, ^{3}J 9.2 Hz, $H^{3/5}$-ph'), 5.98 (4H, d, ^{3}J 8.0 Hz, H^3-ph). ^{13}C NMR

* Solid becomes red in contact with methanol and yellow in contact with diethyl ether. All changes are reversible, with the solid returning to orange upon drying.

(100 MHz, $CDCCl_3$): δ 168.7 (C^2-py), 153.4 (C^6-py), 152.4 (C^4-ph'), 150.8 (C^2-ph), 143.6 (C^1-ph), 143.2 (C^1-ph'), 136.8 (C^4-py), 131.1 (C^4-ph), 130.5 ($C^{3/5}$-ph'), 130.0 (C^3-ph), 124.3 (C^6-ph), 122.7 (C^5-py), 122.3 (C^5-ph), 122.1 ($C^{2/6}$-ph'), 119.3 (C^3-py). MS (MALDI+): m/z 1310 (M^+), 1156 (M-thiol)$^+$, 655 $(Ir(phpy)_2(thiol))^+$.

4,6-Di(2-pyridyl)xylene

dpyxH

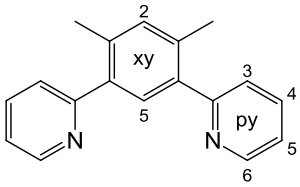

4,6-Dibromoxylene (200 mg, 0.76 mmol), LiCl (257 mg, 6.06 mmol) and 2-(tri-n-butylstannyl)pyridine (918 mg, 76% purity by NMR assay, 1.90 mmol) were placed in 5 mL toluene and degassed using the freeze-pump-thaw method then placed under nitrogen. Bis(triphenylphosphine)palladium(II) dichloride (21 mg, 0.030 mmol) was added through a flow of nitrogen and the reaction was heated at reflux for 16 h. After cooling to RT, 6 mL sat. $KF_{(aq)}$ was added and the mixture was stirred for 30 min. The resulting solid was removed by filtration and washed with toluene. The combined organic filtrate and washings were washed with 3 $\times$ 30 mL 5% $NaHCO_{3\ (aq)}$, dried over $MgSO_4$, filtered and the solvent was removed under reduced pressure. Column chromatography on silica with gradient elution from 30% to 80% Et_2O in hexane yielded 162 mg (82%) white solid. ^{1}H NMR (400 MHz, $CDCl_3$): δ 8.68 (2H, d, ^{3}J 5.6 Hz, H^6-py), 7.72 (2H, t, ^{3}J 7.6 Hz, H^4-py) 7.47 (1H, s, H^2-xy), 7.44 (2H, d, ^{3}J 7.6 Hz, H^3-py), 7.21 (2H, dd, ^{3}J 5.6 Hz, 7.6 Hz, H^6-py), 2.40 (6H, s, Me).

Di-μ-chlorobis(4,6-di(2-pyridyl)xylene)diiridium(III) dichloride

$[Ir(dpyx)(\mu\text{-}Cl)Cl]_2$

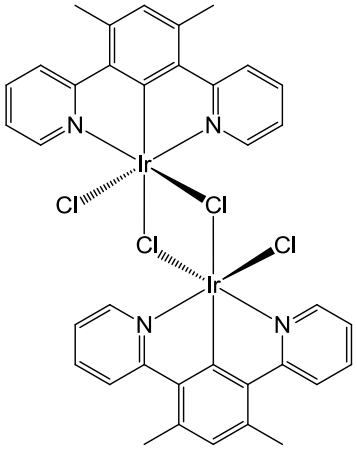

4,6-Di(2-pyridyl)xylene (200 mg, 0.768 mmol) and $IrCl_3.3H_2O$ (265 mg, 0.752 mmol) were placed in 20 mL 7:3 2-ethoxyethanol:water under nitrogen and heated at 80 °C for 16 h. The resulting precipitate was collected using a centrifuge and washed with 2 x 8 mL each of H_2O, EtOH and Et_2O. Yield 269 mg (67%). ^{1}H NMR (400 MHz, d_6-DMSO): δ 9.08 (4H, s (broad)), 8.18 (4H, d, ^{3}J 8.4 Hz), 7.93 (4H, t, ^{3}J 7.4 Hz), 7.41 (4H, t, ^{3}J 6.8 Hz), 6.90 (2H, s(broad)), 2.76 (12H, s, Me).

Di-μ-chlorobis(3,5-di(2-pyridyl)toluene)diiridium(III) dichloride

$[Ir(dpyt)(\mu\text{-}Cl)Cl]_2$

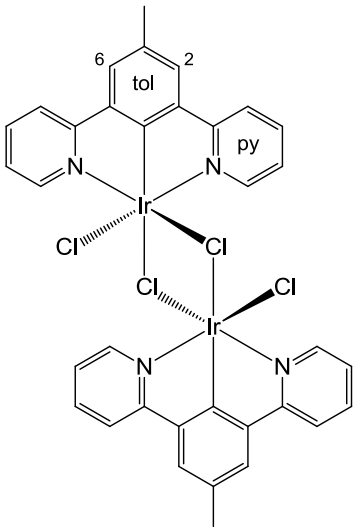

3,5-Di(2-pyridyl)toluene (50 mg, 0.20 mmol) and $IrCl_3.3H_2O$ (70 mg, 0.20 mmol) were placed in 10 mL 7:3 2-ethoxyethanol:water under nitrogen and heated at 80 °C for 16 h. The precipitate was collected and washed with 2 x 8 mL each of H_2O, EtOH and Et_2O yielding 62 mg (30%) of sparingly soluble yellow/orange solid. ^{1}H NMR (400 MHz, d_6-DMSO): δ 9.05 (4H, d, ^{3}J 4.8 Hz, H-py), 8.22 (4H,

d, ^{3}J 8.4 Hz, H-py), 7.95 (4H, t, ^{3}J 8.0 Hz, H-py), 7.83 (4H, s, H$^{2/6}$-tol), 7.38 (4H, t, ^{3}J 7.2 Hz, H-py) 2.57 (6H, s, Me).

(4,6-Di(2-pyridyl)xylene)(2-phenylpyridine)iridium(III) chloride [Ir(dpyx)(ppy)Cl]

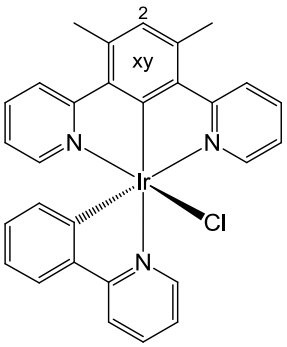

[Ir(dpyx)(μ-Cl)Cl]$_2$ (70 mg, 0.067 mmol) and silver(I) triflate (88 mg, 0.34 mmol) were placed in 2-phenylpyridine (0.5 mL, 0.54 g, 4.7 mmol) under nitrogen and heated at 110 °C for 16 h. The reaction was cooled to RT and diluted with 8 mL DCM. The solution was separated from the residual AgCl using a centrifuge and the solid was extracted with 2 x 6 mL DCM. The combined organics were washed with 3 x 20 mL 1 M HCl, separated and dried over $MgSO_4$. Removal of the solvent under reduced pressure yielded 80 mg (93%) orange solid. The product was identified by ^{1}H NMR, however the sample contained some impurities. ^{1}H NMR (400 MHz, $CDCl_3$): δ 10.13 (1H, d, ^{3}J 5.6 Hz), 8.07 (1H, d, ^{3}J 8.4 Hz), 8.00 (2H, d, ^{3}J 8.4 Hz), 7.96 (1H, t, ^{3}J 6.4 Hz), 7.65 (2H, d, ^{3}J 6.4 Hz), 7.59 (1H, d, ^{3}J 6.4 Hz), 7.56-7.50 (3H, m), 6.89 (1H, s, H^{2}-xy), 6.75 (2H, t, ^{3}J 6.4 Hz), 6.72 (1H, t, ^{3}J 6.4 Hz), 6.54 (1H, t, ^{3}J 7.2 Hz), 6.01 (1H, d, ^{3}J 8.0 Hz), 2.83 (6H, s, Me).

(3,5-Di(2-pyridyl)toluene)(2-phenylpyridine)iridium(III) chloride
[Ir(dpyt)(ppy)Cl]

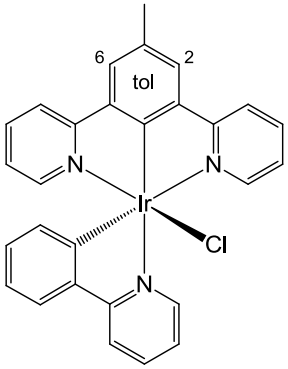

$[Ir(dpyt)(\mu\text{-}Cl)Cl]_2$ (51 mg, 0.50 mmol) and silver(I) triflate (55 mg, 0.21 mmol) were placed in 2-phenyl-pyridine (0.25 mL, 0.27 g, 4.4 mmol) and heated at 110 °C for 16 h. The reaction was cooled to RT and diluted with 8 mL DCM. The solution was separated from the residual AgCl using a centrifuge and the solid was extracted with 2 x 6 mL DCM. The combined organics were washed with 2 x 20 mL 1 M HCl, separated and dried over $MgSO_4$. The solvent was removed under reduced pressure to yield the crude product. This was purified by column chromatography on silica with gradient elution from 0% to 5% MeOH in DCM, yielding 54 mg (70%) yellow solid. ^{1}H NMR (400 MHz, $CDCl_3$): δ 10.14 (1H, d, ^{3}J 5.6 Hz), 8.07 (1H, d, ^{3}J 8.0 Hz), 7.96 (1H, t, ^{3}J 8.0 Hz), 7.81 (2H, d, ^{3}J 7.6 Hz), 7.65 (2H, s, $H^{2/6}$-tol), 7.61-7.51 (6H, m), 6.77 (2H, t, ^{3}J 7.2 Hz), 6.71 (1H, t, ^{3}J 8.0 Hz), 6.53 (1H ,t, ^{3}J 7.2 Hz), 6.01 (1H, d, ^{3}J 7.6 Hz), 2.58 (3H, s, Me).

(4,6-Di(2-pyridyl)xylene)(2,2'-bipyridine)iridium(III) chloride hexafluorophosphate
$[Ir(dpyx)(bpy)Cl]PF_6$

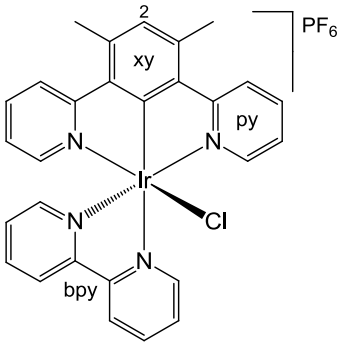

$[Ir(dpyx)(\mu\text{-}Cl)Cl]_2$ (42 mg, 0.040 mmol) and 2,2'-bipyridine (13 mg, 0.083 mmol) were placed under nitrogen and 2 mL ethylene glycol was added via syringe,

then the reaction was heated at reflux for 2.5 h. Once cooled to RT, the solution was added dropwise to 15 mL sat. $KPF_{6\ (aq)}$ and the resulting yellow precipitate was collected using a centrifuge and washed with 2 × 5 mL each of H_2O, EtOH and Et_2O. Yield: 49 mg (77%). ^{1}H NMR (400 MHz, d_6-acetone): δ 9.98 (1H, d, ^{3}J 5.2 Hz, H-bpy), 8.97 (1H, d, ^{3}J 8.4 Hz, H-bpy), 8.70 (1H, d, ^{3}J 7.6 Hz, H-bpy), 8.63 (1H, t, ^{3}J 8.0 Hz, H-bpy), 8.35-8.31 (3H, m, overlapped H-bpy triplet and H-py doublet), 8.00 (1H, t, ^{3}J 8.0 Hz, H-bpy), 7.93 (2H, t, ^{3}J 8.0 Hz, H-py), 7.82 (2H, d, ^{3}J 5.6 Hz, H-py), 7.65 (1H, d, ^{3}J 5.6 Hz, H-bpy), 7.32 (1H, t ^{3}J 7.2 Hz, H-bpy), 7.16 (2H, t, ^{3}J 6.8 Hz, H-py), 7.16 (1H, s, H^2-xy), 2.92 (6H, s, Me). MS (ES+): m/z 643 $(M\text{-}PF_6)^+$.

(3,5-Di(2-pyridyl)toluene)(2,2'-bipyridine)iridium(III) chloride hexafluorophosphate

$[Ir(dpyt)(bpy)Cl]PF_6$

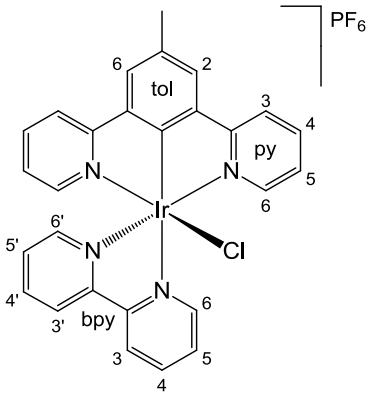

$[Ir(dpyt)(\mu\text{-}Cl)Cl]_2$ (23 mg, 0.023 mL) and 2,2'-bipyridine (8 mg, .051 mmol) were placed in 1.5 mL ethylene glycol and heated to 195 °C for 3 h. The reaction was cooled to RT and the solution was separated from the residual solid. This solid was extracted with 2 × 2 mL MeCN which was combined with the reaction solution. The solution was added dropwise to 5 mL sat. $KPF_{6\ (aq)}$, initially giving a yellow precipitate that redissolved. Reduction of the solvent volume under reduced pressure caused the product to precipitate again and it was collected using a centrifuge and washed with 2 × 5 mL H_2O, a minimum amount of ethanol and 2 × 5 mL Et_2O. Yield 10 mg (29%). ^{1}H NMR (700 MHz, d_6-acetone): δ 10.0 (1H, d, ^{3}J 4.9 Hz, $H^{6\text{ or }6'}$-bpy) 8.98 (1H, d, ^{3}J 8.4 Hz, $H^{3\text{ or }3'}$-bpy), 8.71 (1H, d, ^{3}J 7.7 Hz, $H^{6\text{ or }6'}$-bpy), 8.63 (1H, t, ^{3}J 7.7 Hz, $H^{4\text{ or }4'}$-bpy), 8.33 (1H, t, ^{3}J 5.6 Hz, $H^{5\text{ or }5'}$-bpy), 8.29 (2H, d, ^{3}J 7.7 Hz, H^6-py), 8.00 (1H, t, ^{3}J 7.7 Hz, $H^{5\text{ or }5'}$-bpy), 8.00 (2H, s, $H^{2/5}$-tol), 7.95 (2H, t, ^{3}J 8.4 Hz, H^5-py), 7.80

(2H, d, ^{3}J 7.7 Hz, H^{3}-py), 7.66 (1H, d, ^{3}J 4.9 Hz, H$^{3 \text{ or } 3'}$-bpy), 7.35 (1H, t, ^{3}J 6.3 Hz, H$^{4 \text{ or } 4'}$-py), 7.18 (2H, t, ^{3}J 7.0 Hz, H^{4}-py), 2.67 (3H, s, Me). ^{13}C NMR (175 MHz, d_6-acetone): δ 168.8, 167.3, 158.6, 155.9, 153.5, 152.5, 149.5, 141.5, 140.4, 139.9, 139.4, 133.4, 129.1, 128.2, 124.9, 124.8, 124.0, 121.0, 21.2.

(4,6-Di(2-pyridyl)xylene)(2-phenylpyridine)iridium(III) toluene-4-thiolate [Ir(dpyx)(ppy)(mtp)]

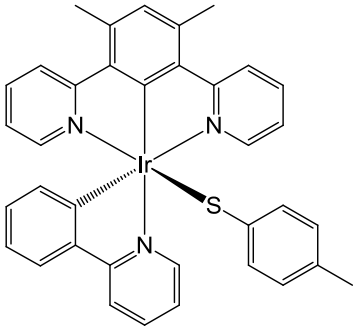

A suspension of (4,6-di(2-pyridyl)xylene)(2-phenylpyridine)iridium(III) chloride (29.5 mg, 0.046 mmol) in 2 mL MeOH was degassed using the freeze-pump-thaw method. In a separate vessel 4-methyl thiophenol (6.2 mg, 0.050 mmol) in 1 mL MeOH was also degassed. Potassium tert-butoxide (6 mg, 0.053 mmol) was added to the thiol solution through a flow of nitrogen. This solution was then tranfered to the suspension of complex via a cannula and the reaction was stirred under nitrogen for 16 h at RT. The precipitate was collected and washed with 2×3 mL each of MeOH and Et_2O yielding 25 mg (75%) yellow/orange solid. Evidence from ^{1}H NMR indicated that the sample was probably the required product, however not at an acceptable level of purity. Full assignment of the ^{1}H NMR was not possible due to the low solubility resulting in a poor spectrum. ^{1}HNMR (400 MHz, $CDCl_3$): δ 10.49 (1H, d), 8.06 (1H, d), 7.95 (1H, t), 7.78 (2H, m), 7.62 (1H, d), 7.54 (3H, m), 7.39 (2H, m), 6.80 (1H, s), 6.71 (1H, t), 6.61 (2H, m), 6.53 (1H, t), 6.23 (2H, d), 6.14 (2H, d), 6.10 (1H, d), 2.75 (6H, s), 2.61 (3H, s).

(4,6-Di(2-pyridyl)xylene)(2-phenylpyridine)iridium(III) 4-nitrophenylthiolate [Ir(dpyx)(ppy)(ntp)]

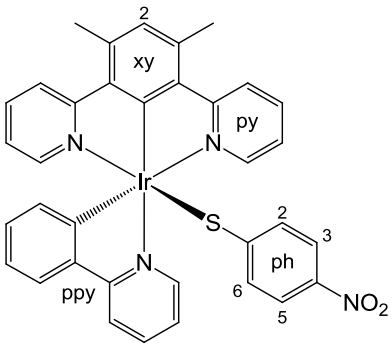

(4,6-Di(2-pyridyl)xylene)(2-phenylpyridine)iridium(III) chloride (32 mg, 0.050 mmol) was suspended in 2 mL MeOH and degassed using the freeze-pump-thaw method and placed under nitrogen. A separate solution of 4-nitrothiophenol (8.5 mg, 0.055 mmol) and potassium tert-butoxide (6.2 mg, 0.55 mmol) in 2 mL MeOH was also degassed then transferred via cannula to the suspension of complex. The reaction was stirred at RT for 16 h and then the solid was collected using a centrifuge. This solid was washed with 2 × 4 mL MeOH and 2 × 4 mL Et_2O giving 27 mg crude product. TLC of this product showed two main components at $R_f = 0.55$ and $R_f = 0.30$ (silica plates, 5% MeOH/DCM). The crude was columned on silica, eluting with 3% MeOH in DCM. Upon loading onto silica for the column, the product changed from yellow to red and the first component eluted from the column was the required product, 6 mg (16%) red solid, but now had $R_f = 0.9$ in 5% MeOH/DCM. 16 mg starting complex was also recovered from the column. ^{1}H NMR (400 MHz, $CDCl_3$): δ 10.21 (1H, d, ^{3}J 6.0 Hz, H-ppy), 8.09 (1H, d ,^{3}J 8.0 Hz, H-ppy), 7.99 (1H, t, ^{3}J 8.0 Hz, H-ppy), 7.84 (2H, d, ^{3}J 8.4 Hz, H-py), 7.62 (1H, d, ^{3}J 7.6 Hz, H-ppy), 7.60-7.55 (3H, m, H-ppy and H-py), 7.44 (2H, t, ^{3}J 8.0 Hz, H-py), 7.28 (2H, d, ^{3}J 7.6 Hz, H$^{2/6 \text{ or } 3/5}$-ph), 6.86 (1H, s, H^2-xy), 6.75-6.68 (3H, m, H-ppy and H-py), 6.52 (1H, t, ^{3}J 7.2 Hz, H-ppy), 6.37 (2H, d, ^{3}J 7.6 Hz, H$^{2/6 \text{ or } 3/5}$-ph), 6.03 (1H, d, ^{3}J 7.6 Hz, H-ppy), 2.76 (6H, s, Me).

Bis(4,6-di(2-pyridyl)xylene)(μ-di(4-nitrophenylthiolate))diiridium(III) di(4-nitrophenylthiolate)

$[Ir(dpyx)(\mu\text{-}ntp)(ntp)]_2$

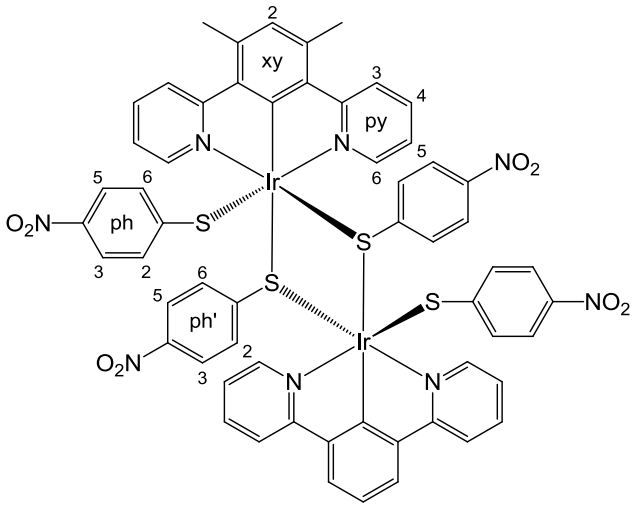

$[Ir(dpyx)(\mu\text{-}Cl)Cl]_2$ dimer (26 mg, 0.025 mmol), 4-nitrothiophenol (16 mg, 0.10 mmol) and potassium *tert*-butoxide (12 mg, 0.11 mmol) were placed in a flask under nitrogen. A mixture of 2 mL DCM and 3 mL MeOH was degassed using the freeze-pump-thaw method in a separate vessel and added to the solids via cannula. The reaction was then heated at reflux for 24 h. The solvents were removed under reduced pressure and the solid was washed with 3×8 mL MeOH. The crude product was purified by column chromatography on silica with gradient elution from 0% to 0.5% MeOH in DCM yielding 23 mg (61%) orange solid. ^{1}H NMR (400 MHz, $CDCl_3$): δ 8.91 (4H, d, ^{3}J 6.8 Hz, H^6-py), 7.99 (4H, d, ^{3}J 8.0 Hz, H^3-py), 7.74 (4H, t, ^{3}J 8.0 Hz, H^4-py), 7.52 (4H, d, 8.8 Hz, H-ph or H-ph'), 7.20 (4H, d, 8.8 Hz, H-ph or H-ph'), 7.00 (2H, s, H^2-xy), 6.94 (4H, d, 8.8 Hz, H-ph or H-ph'), 6.85 (4H, t, ^{3}J 6.8 Hz, H^5-py), 6.28 (4H, d, 8.8 Hz, H-ph or H-ph'), 1.55 (12H, s, Me). MS (MALDI+): m/z 760 $(Ir(NCN)(thiol)_2)^+$.

5.2.3 Compounds from Chapter 4

4-Bromophthalic acid

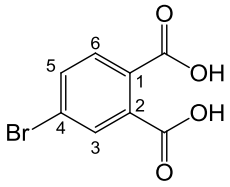

Potassium hydrogen phthalate (12.30 g, 60.2 mmol) and KOH (3.42 g, 61.0 mmol) were placed in 75 mL H_2O. Br_2 (5 mL, 97.1 mmol) was added and the reaction was stirred vigorously for 24 h. The excess bromine was removed by boiling for 30 min and upon cooling the potassium hydrogen salt precipitated from solution. This was collected by filtration, washed with ice cold water and purified by recrystallisation from water. Yield 4.70 g (28%). The final product was obtained by acidification of potassium hydrogen 4-bromophthalate with HCl in water followed by extraction with diethyl ether (4.02 g, 27%). ^{1}H NMR (500 MHz, d_6-DMSO): δ 7.82 (1H, d, ^{4}J 2.0 Hz, H^3), 7.80 (1H, dd, ^{3}J 8.0 Hz, ^{4}J 2.0 Hz, H^5), 7.64 (1H, d, ^{3}J 8.0 Hz, H^6). ^{13}C NMR (125 MHz, d_6-DMSO): δ 167.7 (C^1**C**=O), 167.4 (C^2**C**=O), 135.4 (C^2), 133.6 (C^5), 131.4 (C^1), 130.8 (C^3), 130.7 (C^6), 124.3 (C^4).

4-Bromophthalimide

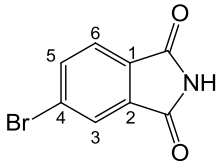

4-Bromophthalic acid (4.02 g, 16.4 mmol) and ammonium thiocyanate (1.27 g, 16.7 mmol) were ground together using a pestle and mortar then heated to 165 ºC for 20 min. The reaction was cooled and the solid broken up and dispersed in water using a sonicator. This was then washed four times with H_2O using a centrifuge. The resulting cream solid was dried under reduced pressure (2.05 g, 55%). ^{1}H NMR (500 MHz, d_6-DMSO): δ 11.48 (1H, s, NH), 8.01 (1H, dd, ^{3}J 8.0 Hz, ^{4}J 1.5 Hz, H^5), 8.00 (1H, d, ^{4}J 2.0 Hz, H^3), 7.75 (1H, d, ^{3}J 8.0 Hz, H^6). ^{13}C NMR (125 MHz, d_6-DMSO): δ 168.5 (C^1-**C**=O), 167.9 (C^2-**C**=O), 137.0 (C^5), 134.7 (C^2), 131.6 (C^1), 127.9 (C^4), 125.9 (C^3), 124.9 (C^6). C, H, & N analysis: 42.26% C, 1.73% H, 6.21% N measured; 42.51% C, 1.78% H, 6.20% N calculated for $C_8H_4NO_2Br$. IR: ν(C=O) 1715 cm^{-1}. Mp 206 – 208 °C.

4-Bromophthalamide

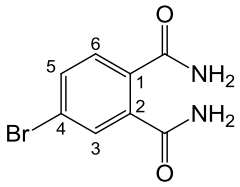

4-Bromophthalimide (3.62 g, 16.0 mmol) was added in portions to 100 mL conc. $NH_{3\ (aq)}$ and stirred for 2 days producing a white precipitate. This was isolated by filtration, washed with H_2O and dried under reduced pressure. Yield 1.74 g (45%). ^{1}H NMR* (400 MHz, d_6-DMSO): δ 7.83 (1H, s (broad), NH), 7.77 (1H, s (broad), NH), 7.65 (1H, dd, ^{3}J 8.0 Hz, ^{4}J 2.0 Hz, H+), 7.60 (1H, d, ^{4}J 2.0 Hz, H^3), 7.43 (1H, s (broad), NH), 7.40 (1H, d, ^{3}J 8.0 Hz, H^6), 7.39 (1H, s (broad), NH). ^{13}C NMR (100 MHz, d_6-DMSO): δ 169.8 (C^1-**C**=O), 169.2 (C^2-**C**=O), 139.1 (C^2), 136.1(C^1), 132.6 (C^5), 130.9 (C^3), 130.4 (C^6), 122.8 (C^4). HRMS (ES+): m/z 242.9764 $(M+H)^+$; calculated for $C_8H_8BrN_2O_2$: 242.9765. C, H, & N analysis: 39.34% C, 1.77% H, 11.50% N measured; 39.53% C, 2.90% H, 11.53% N calculated for $C_8H_7N_2O_2Br$. IR: ν(N-H) 3430, 3320, 3170 cm^{-1}, ν(C=O) 1650 cm^{-1}. Mp 207 – 208 °C.

4-Bromophthalonitrile

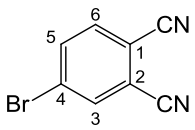

4-Bromophthalamide (2.5 g, 10.3 mmol) was placed under nitrogen and suspended in 90 mL dry THF. DMF (1.75 mL, 22.6 mmol) was added followed dropwise by triphosgene (6.71 g, 22.6 mmol) in 20 mL dry THF. The reaction was heated at reflux for 3 h then, after cooling to RT, the solvent was removed. 50 mL H_2O was added to the residue and this was extracted with 3 x 30 mL DCM. The combined organics were washed with 2 x 50 mL 5% $NaHCO_{3\ (aq)}$, dried over $MgSO_4$ and reduced to dryness. The crude product was purified by column chromatography on silica eluting with 30% diethyl ether in hexane yielding a white solid (1.94 g, 91%). ^{1}H NMR (500 MHz, $CDCl_3$): δ 7.97 (1H, d, ^{4}J 1.5 Hz, H^3), 7.90 (1H, dd, ^{3}J 8.0 Hz, ^{4}J 2.0 Hz, H^5), 7.68 (1H, d, ^{3}J 8.5 Hz, H^6). ^{13}C NMR (125 MHz, $CDCl_3$): δ 136.8 (C^5), 136.6(C^3), 134.6(C^6), 128.3 (C^4),

* Note – Due most likely to H-bond interactions, all amide protons appear as individual peaks in the ^{1}H NMR

117.5, 114.9, 114.8, 114.2. MS (EI): m/z 208 (M^+ (^{81}Br)), 206 (M^+ (^{79}Br)), 127 $(M-Br)^+$. C, H, & N analysis: 46.33% C, 1.58% H, 13.05% N measured; 46.41% C, 1.46% H, 13.53% N calculated for $C_8H_3N_2Br$

(4-(2,2'-Bipyridin-4-yl)phenyl)(neopentyl glycolato)boron

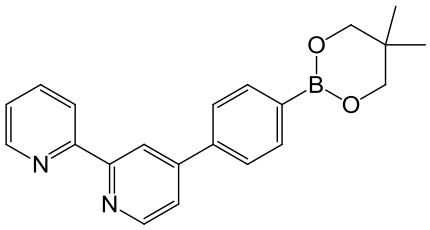

4-(4-Bromophenyl)-2,2'-bipyridine (311 mg, 1.00 mmol), bis(neopentyl glycolato)diboron (245 mg, 1.08 mmol) and potassium acetate (295 mg, 3.00 mmol) were placed in 10 mL dry DMSO and degassed using the freeze-pump-thaw technique. With the reaction maintained under nitrogen (bis-diphenylphosphinoferrocene)palladium dichloride (35 mg, 0.048 mmol) was added then the reaction was heated at 85 ºC for 4 h. After cooling to RT the reaction was diluted with 30 mL DCM and this was washed with 5 x 100 mL H_2O, separated, dried over Na_2SO_3 and reduced to dryness. The crude product (229 mg, 67%) was used without further purification. ^1H NMR (200 MHz, $CDCl_3$): δ 8.71 (3H, m), 8.45 (1H, d, J 8.0 Hz), 7.95-7.75 (5H, m), 7.57 (1H, dd, J 5.2 Hz, 1.8 Hz), 7.35 (1H, dd, J 7.6 Hz, 4.8 Hz), 3.80 (4H, s, CH_2), 1.05 (6H, s, CH_3). MS (EI): m/z 344 (M^+).

4-(3,4-Dicyano-4'-biphenylyl)-2,2'-bipyridine

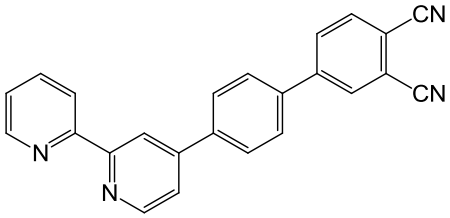

4-Bromophthalonitrile (135 mg, 0.65 mmol) and (4-(2,2'-bipyridin-4-yl)phenyl)(neopentyl glycolato)boron (210 mg, 0.65 mmol) in DME (3 mL) and sodium carbonate (210 mg, 1.98 mmol in 0.5 mL H_2O) were degassed together using the freeze-pump-thaw method. Tetrakis(triphenylphino)palladium(0) (35 mg, 0.03 mmol) was added through a positive flow of nitrogen then the reaction was stirred for 30 min followed by reflux for 16 h under nitrogen. The reaction was then cooled to RT and diluted with 50 mL DCM and the organic

phase was washed with 4 x 50 mL H_2O, dried over $MgSO_4$ and the solvent removed. The crude product was purified by column chromatography on silica with gradient elution from 0 – 15% MeOH in DCM yielding 140 mg (64%) white solid. ^{1}H NMR (500 MHz, $CDCl_3$): δ 8.78 (1H, d, J 5.0 Hz), 8.73 (2H, s), 8.48 (1H, d, J 8.0 Hz), 8.08 (1H, s), 8.00 (1H, d, J 8.0 Hz), 7.95-7.89 (3H, m), 7.87 (1H, t, J 8.0 Hz), 7.73 (2H, d, J 8.0 Hz), 7.59 (1H, d, J 5.0 Hz), 7.36 (1H, t, J 6.0 Hz). ^{13}C NMR* (125 MHz, $CDCl_3$): δ 157.1, 156.0, 150.0, 149.3, 148.0, 145.7, 139.9, 137.6, 137.3, 134.2, 132.0, 131.5, 128.4, 128.0, 124.2, 121.6, 121.5, 119.0, 116.8, 115.5(4), 115.4(8), 114.4. HRMS (ES+): m/z 359.12929 $(M+H)^+$; calculated for $C_{24}H_{15}N_4$: 359.12912. C, H, & N analysis: 78.32% C, 3.89% H, 15.04% N measured; 78.30% C, 3.89% H, 15.13% N calculated for $C_{24}H_{14}N_4.\{0.14(CH_2Cl_2)\}$. Mp 246 – 248 °C.

5-Bromoisophthalic acid

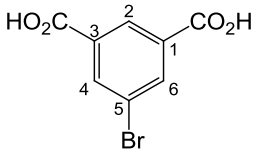

Dimethyl-5-aminoisophthalate (2.5 g, 12.0 mmol) was placed in 50 mL 1:1 MeOH/6M H_2SO_4. Sodium nitrite (2.5 g, 36.2 mmol) in 20 mL H_2O was added slowly while cooling the reaction in an ice bath. The reaction was stirred for 30 min at RT then $CuBr_2$ in 20 mL 48% HBr was added followed by heating for 15 min at reflux. The reaction was then neutralised with 40% $NaOH_{(aq)}$ and filtered while hot. Acidification of the filtrate with HCl gave a precipitate which was collected and dissolved in a minimum amount of 10% $NaOH_{(aq)}$. The product was then precipitated again with HCl, collected by filtration and washed with cold H_2O. Yield 0.98 g (33%). ^{1}H NMR (500 MHz, d_6-DMSO): δ 8.41 (1H, s, H^2), 8.24 (2H, $H^{4/6}$). ^{13}C NMR (125 MHz, d_6-DMSO): δ 165.3 (C=O), 135.5 ($C^{4/6}$), 133.6 ($C^{1/3}$), 128.7 (C^2), 121.8 (C^5). MS (ES-): m/z 245 ($M(^{81}Br)-H)^-$, 243 ($M(^{79}Br)-H)^-$. Mp 279 – 283 °C.

* Weak spectrum, 2 signals not resolved from noise.

Dimethyl-5-iodoisophthalate

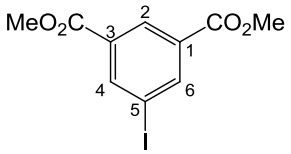

Sodium nitrite (1.00 g, 14.5 mmol) in 15 mL H_2O was added dropwise to dimethyl-5-aminoisophthalate (2.62 g, 12.5 mmol) in 7.5 mL 20% $HCl_{(aq)}$ at – 5 ºC. 20 mL toluene was added followed, dropwise, by potassium iodide (4.2 g, 25.3 mmol) in 10 mL H_2O. The reaction was stirred vigorously overnight at RT then heated to reflux for 1 h. The reaction was then cooled to RT and the organic phase separated. The aqueous part was extracted with 2 x 20 mL toluene and the combined organic phases were washed with 3 x 50 mL H_2O, dried with $MgSO_4$ and the solvent was removed under reduced pressure. Recrystallisation from MeOH gave a light brown solid and further purification by column chromatography on silica eluted with DCM gave 0.593 g (15%) of white solid. ^{1}H NMR (400 MHz, $CDCl_3$): δ 8.63 (1H, t, ^{4}J 1.6 Hz, H^2), 8.54 (2H, d, ^{4}J 1.6 Hz, $H^{4/6}$), 3.95 (6H, s, Me). ^{13}C NMR (125 MHz, $CDCl_3$): δ 164.8 (C=O), 142.5 ($C^{4/6}$), 132.2 ($C^{1/3}$), 129.9 (C^2), 93.5 (C^5), 52.7 (Me). MS (EI): m/z 320 (M^+). Mp 101 – 102 °C.

Di(L-cysteine ethyl ester)-5-bromoisophthalamide

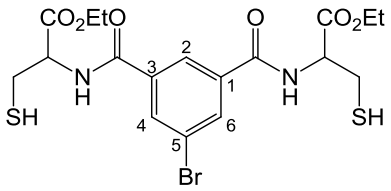

5-Bromoisophthalate (61 mg, 0.25 mmol) was placed under nitrogen in 10 mL dry THF. At 0 ºC, EDCI (105 mg, 0.55 mmol) was added through a positive flow of nitrogen and the reaction was stirred for 15 min. Ethyl-L-cysteine (100 mg, 0.54 mmol) was then added through nitrogen and the reaction was warmed to RT and stirred overnight. The solution was decanted from the white gum and the solvent was removed under reduced pressure. The crude material was then columned under nitrogen on silica with gradient elution 0 – 5% MeOH in DCM. Yield 20 mg (16%). ^{1}H NMR (400 MHz, $CDCl_3$): δ 8.20 (1H, t, ^{4}J 2.0 Hz, H^2), 8.10 (2H, d, ^{4}J 2.0 Hz, $H^{4/6}$), 7.20 (2H, d (broad) or two s (broad), NH), 5.04 (2H, m, *CH), 4.30 (4H, q, ^{3}J 7.2 Hz, C**H$_2$**CH_3), 3.14 (4H, m, C**H$_2$**SH), 1.34 (6H, t, ^{3}J

7.2 Hz, $CH_2C\mathbf{H_3}$). MS (ES+): m/z 507 $(M(^{79}Br)+H)^+$, 509 $(M(^{81}Br)+H)^+$, 1015 $(2M+H)^+$.

Bis(N-dansyl) dimethyl-5-aminoisophthalate

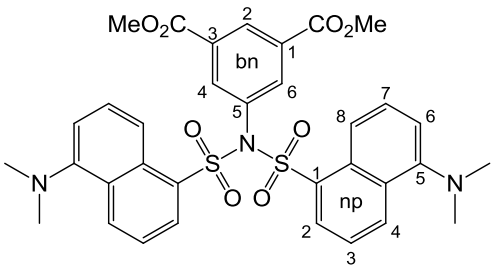

Dansyl chloride (135 mg, 0.500 mmol), dimethyl-5-aminoisophthalate (105 mg, 0.502 mmol) and DMAP (65 mg, 0.532 mmol) were placed in 10 mL dry THF under nitrogen and the reaction was stirred overnight. The solvent was removed under reduced pressure and DCM (25 mL) was added to the residue. The organic phase was washed with 3 × 25 mL H_2O, separated and dried over $MgSO_4$. Removal of the solvent yielded 225 mg crude product. Column chromatography on silica, eluting with 3% MeOH in DCM, gave 79 mg (47%) product (R_f = 0.78) and a mixture of two other components, the main constituent of which was N-dansyl dimethyl-5-aminoisophthalate (R_f = 0.42). ^{1}H NMR (400 MHz, $CDCl_3$): δ 8.64 (1H, t, ^{4}J 1.6 Hz, H^2-bn), 8.60 (2H, d, ^{3}J 8.4 Hz, H-np), 8.31 (2H, d, ^{3}J 8.4 Hz, H-np), 7.85 (2H, d, ^{4}J 1.6 Hz, $H^{4/6}$-bn), 7.72 (2H, d, ^{3}J 8.0 Hz, H-np), 7.49 (2H, t, ^{3}J 8.4 Hz, H-np), 7.14 (2H, t, ^{3}J 8.0 Hz, H-np), 7.10 (2H, d, ^{3}J 8.0 Hz, H-np), 3.85 (6H, s, OMe), 2.89 (12H, s, NMe). ^{13}C NMR (100 MHz, $CDCl_3$): δ 164.9 (C=O), 152.1, 137.7, 134.6, 133.6, 133.1, 132.5, 132.2, 131.7, 130.1, 128.6, 123.2, 118.9, 115.5. MS (ES+): m/z 676 $(M+H)^+$, 1351 $(2M+H)^+$.

N-dansyl dimethyl-5-aminoisophthalate

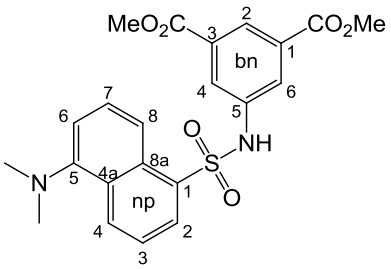

Dimethyl-5-aminoisophthalate (210 mg, 1.00 mmol) and pyridine (0.10 mL, 0.1 g, 1.3 mmol) were placed in 5 mL dry DCM under nitrogen and dansyl chloride (280 mg, 1.04 mmol) in 10 mL dry DCM was added via cannula. The

reaction was heated at reflux for 16 h then the solvent was removed under reduced pressure. The crude product was purified by column chromatography on alumina eluting with 3% MeOH in DCM (R_f = 0.42) yielding 428 mg (96%) white solid. ^{1}H NMR (500 MHz, $CDCl_3$): δ 8.51 (1H, d, ^{3}J 9.0 Hz, H^4-np), 8.31, (1H, s, H^2-bn), 8.30 (1H, d, ^{3}J 9.0 Hz, H^8-np), 8.27 (1H, d, ^{3}J 7.5 Hz, H^2-np), 7.86 (2H, s, H$^{4/6}$-bn), 7.56 (1H, t, ^{3}J 8.5 Hz, H^7-np), 7.47 (1H, t, ^{3}J 9.0 Hz, H^3-np), 7.31 (1H, s (broad), N**H**), 7.17 (1H, d, ^{3}J 7.5 Hz, H^6-np), 3.89 (6H, s, OMe), 2.86 (6H, s, NMe). ^{13}C NMR (125 MHz, $CDCl_3$): δ 165.7 (C=O), 152.4 (C^5-np), 137.7 (C^5-bn), 133.7 (C^1-np), 131.7 (C$^{1/3}$-bn), 131.5 (C^4-np), 130.8 (C^2-np), 130.0 (C^{4a}-np), 129.6 (C^{8a}-np), 129.1 (C^7-np), 126.8 (C^2-bn), 125.4 (C$^{4/6}$-bn), 123.2 (C^3-np), 118.2 (C^8-np), 115.5 (C^6-np), 52.7 (OMe), 45.5 (NMe). HRMS (ES+): m/z 443.12636, 465.10901; calculated for $C_{22}H_{23}N_2O_6S^+$: 443.12714, $C_{22}H_{22}N_2O_6Na^+$: 465.10908.

N-dansyl-5-aminoisophthalic acid

1a

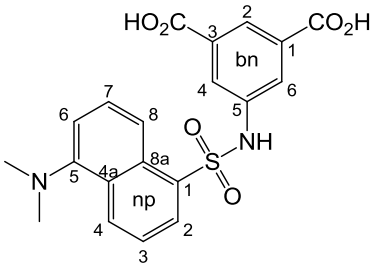

N-dansyl dimethyl-5-aminoisophthalate (88 mg, 0.20 mmol) was dissolved in 5 mL THF and 5 mL 15% NaOH in water was added. The reaction was heated at reflux for 2 h then the THF was removed under reduced pressure. The remaining aqueous solution was diluted to approx 10 mL and brought to approx. neutral pH by dropwise addition of 2M HCl, producing a white precipitate. A saturated aqueous solution of NH_4Cl (20 mL) was added and the product was extracted with 2 $\times$ 25 mL EtOAc. The combined organics were dried over $MgSO_4$ and the solvent was removed under reduced pressure to yield a yellow/green solid (82 mg, 99%). ^{1}H NMR (500 MHz, d_6-acetone): δ 8.57 (1H, d, ^{3}J 8.5 Hz, H^4-np), 8.50 (1H, d, ^{3}J 9.0 Hz, H^8-np), 8.36 (1H, d, ^{3}J 7.5 Hz, H^2-np), 8.32 (1H, t, ^{4}J 1.5 Hz, H^2-bn), 8.01 (2H, d, ^{4}J 1.5 Hz, H$^{4/6}$-bn), 7.63 (1H, t, ^{3}J 9.0 Hz, H^7-np), 7.62 (1H, t, ^{3}J 9.0 Hz, H^3-np), 7.29 (1H, d, ^{3}J 7.5 Hz, H^6-np), 2.86 (6H, s, NMe). ^{13}C NMR (125 MHz, d_6-acetone): δ 166.8 (C=O), 152.9 (C^5-np), 139.3 (C^5-bn), 135.5 (C^1-np), 133.6 (C$^{1/3}$-bn), 131.6 (C^4-np), 131.2 (C^2-np),

130.7 (C^{4a}-np), 130.4 (C^{8a}-np), 129.3 (C^{7}-np), 126.7 (C^{2}-bn), 124.8 ($C^{4/6}$-bn), 124.1 (C^{3}-np), 119.7 (C^{8}-np), 116.3 (C^{6}-np), 45.5 (NMe). MS (ES-): m/z 413 $(M-H)^-$, 827 $(2M-H)^-$. IR: ν(O-H) 3250-2725 cm^{-1} (broad), ν(C=O) 1693 cm^{-1}.

N-dansyl-4-aminobenzoic acid

2a

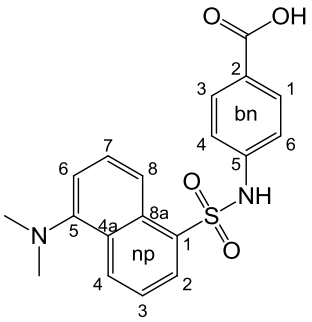

Dansyl chloride (67 mg, 0.25 mmol) and 4-aminobenzoic acid (35 mg, 0.26 mmol) were placed in 8 mL DCM and pyridine (20 mg, 0.25 mmol) in 2 mL DCM was added. The reaction was heated at reflux for 16 h, cooled to RT then diluted to approx. 20 mL with DCM. The organic phase was washed with 2×20 mL sat. $NH_4Cl_{(aq)}$, dried over $MgSO_4$ and the solvent was removed under reduced pressure. The crude product was purified by column chromatography on silica eluting with 4% MeOH in DCM (product R_f = 0.15, 5% MeOH/DCM). Yield 31 mg (34%). ^{1}H NMR (700 MHz, $CDCl_3$): δ 8.52 (1H, d, ^{3}J 8.4 Hz, H^4-np), 8.33 (1H, d, ^{3}J 9.1 Hz, H^2-np), 8.30 (1H, d, 7.0 Hz, H^8-np), 7.85 (2H, d, ^{3}J 9.1 Hz, $H^{1/6 \text{ or } 3/5}$-bn), 7.56 (1H, t, ^{3}J 8.4 Hz, H^7-np), 7.48 (1H, t, ^{3}J 8.4 Hz, H^3-np), 7.17 (1H, d, ^{3}J 7.0 Hz, H^6-np), 7.06 (2H, d, ^{3}J 9.1 Hz, $H^{1/6 \text{ or } 3/5}$-bn), 2.84 (6H, s, NMe). ^{13}C NMR (100 MHz, $CDCl_3$): δ 170.7 (C=O), 152.1, 148.1, 141.9, 134.0, 131.6, 131.4, 130.6, 130.0, 129.6, 128.9, 124.5, 123.2, 118.4, 115.5, 45.5 (Me). MS (ES+): m/z 371 $(M+H)^+$. IR: ν(O-H) 3260-2780 cm^{-1} (broad), ν(C=O) 1705 cm^{-1}.

Bis(2-phenylpyridine)(4'-methyl-2,2'-bipyridine-4-carboxylic acid)iridium(III) hexafluorophosphate

3a

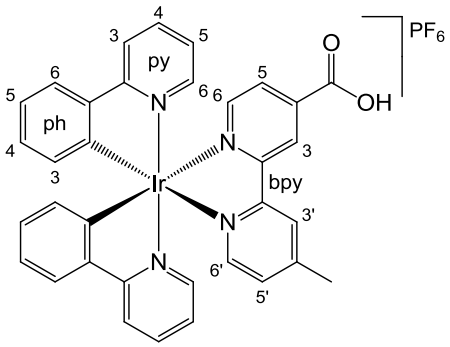

Tetrakis(2-phenylpyridine)(μ-dichloro)diiridium(III) (98 mg, 0.091 mmol) was dissolved in 10 mL DCM and added via cannula to a suspension of 4'-methyl-2,2'-bipyridine-4-carboxylic acid (39 mg, 0.18 mmol) in 10 mL dry MeOH under nitrogen. The reaction was heated at reflux for 16 h. The solvents were removed under reduced pressure and 20 mL 0.5 M HCl and 20 mL DCM were added to the residue. The mixture was shaken and the organic phase was separated and washed with 20 mL sat. $KPF_{6\ (aq)}$, dried over $MgSO_4$, filtered and the solvent removed under reduced pressure yielding 139 mg (90%) red solid. ^{1}H NMR (400 MHz, $CDCl_3$): δ 9.08 (1H, s, $H^{3\ or\ 3'}$-bpy), 8.41 (1H, s, $H^{3\ or\ 3'}$-bpy), 8.02 (1H, d, ^{3}J 5.2 Hz), 7.96 (1H, d, ^{3}J 5.2 Hz), 7.88 (2H, d, ^{3}J 7.2 Hz, H-ph), 7.56-7.71 (3H, m), 7.66 (2H, d, ^{3}J 8.0 Hz, H-ph), 7.54 (1H, d, ^{3}J 6.0 Hz), 7.51 (1H, d, ^{3}J 6.8 Hz), 7.22 (1H, d, ^{3}J 6.0 Hz), 7.09-7.00 (4H, m) 6.90 (2H, t, ^{3}J 7.2 Hz, H-ph), 6.28 (2H, t, ^{3}J 6.8 Hz, H-ph), 2.57 (3H, s, Me). MS (ES+): m/z 715 $(M\text{-}PF_6)^+$.

Bis(2-phenylpyridine)(2,2'-bipyridine-4,4'-dicarboxylic acid)iridium(III) hexafluorophosphate

4a

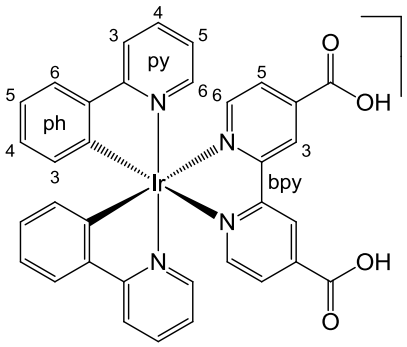

2,2'-Bipyridine-4,4'-dicarboxylic acid (75 mg, 0.33 mmol) was suspended in 20 mL dry MeOH under nitrogen. A solution of tetrakis(2-phenylpyridine)(μ-dichloro)diiridium (166 mg, 0.15 mmol) in 20 mL dry DCM was transferred to the ligand suspension via cannula and the reaction was heated at reflux for 3.5 h. Sodium acetate (220 mg, 2.68 mmol) in 4 mL MeOH was then added and the reaction was refluxed for a further 2 h. The reaction was cooled to RT, the solvents were removed under reduced pressure and 16 mL 1 M HCl was added to the residue. After stirring for 20 min the red solid was collected and washed with H_2O. This solid was extracted with MeOH* and 4 mL sat. NH_4PF_6 in MeOH was added to the extracts. The solvent was removed under reduced pressure and the residue extracted with DCM. Removal of the solvent gave 91 mg (34%) red solid. ^{1}H NMR (400 MHz, d_3-acetonitrile): δ 9.09 (s, 2H, H^3-bpy), 8.14 (2H, d, ^{3}J 5.6 Hz), 8.06 (2H, d, ^{3}J 4.8 Hz), 7.95 (2H, d, ^{3}J 5.6 Hz), 7.87-7.80 (4H, m), 7.56 (2H, d, ^{3}J 4.8 Hz), 7.09-6.99 (4H, m), 6.94 (2H, t, ^{3}J 7.2 Hz), 6.26 (2H, d, ^{3}J 6.4 Hz). MS (ES+): m/z 745 $(M\text{-}PF_6)^+$.

* In several repeats of this prep. a large amount of yellow/orange solid remained after extraction with MeOH. In most cases this was the neutral monohydro-2,2'-bipyridine-4,4'-dicarboxylate complex which is fairly insoluble. Addition of a few drops of 1 M HCl to this solid in MeCN gave a red solution showing a single component LCMS trace with m/z 745. In one particular prep 178 mg (80%) was recovered.

(4,6-Di(2-pyridyl)xylene)(4'-methyl-2,2'-bipyridine-4-carboxylic acid)iridium(III) chloride hexafluorophosphate

5a

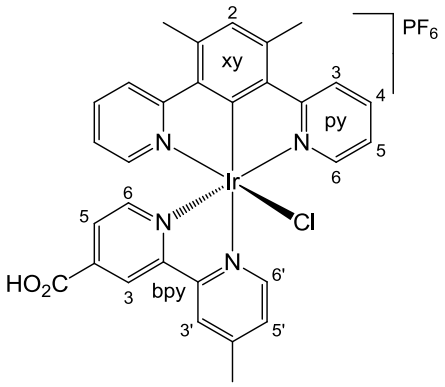

$[Ir(dpyx)(\mu\text{-}Cl)Cl]_2$ (52 mg, 0.050 mmol) and 4'-methyl-2,2'-bipyridine-4-carboxylic acid (22 mg, 0.10 mmol) were placed in 2 mL triglyme under nitrogen and heated at 190 °C for 3 h. No reaction appeared to have occurred so after cooling to a more ambient temperature, silver(I) triflate (25.7 mg, 0.05 mmol) was added then the reaction was heated again at 190 °C for a further 3 h. The solution was collected using a centrifuge and the residual solid was extracted with ~ 5 mL acetonitrile. The combined solution and extracts were added dropwise to 20 mL sat. $KPF_{6\ (aq)}$. This, however, did not precipitate the product as expected so the aqueous mixture was extracted with 2×20 mL DCM. The combined organics were washed with 3×20 mL H_2O, dried over $MgSO_4$, filtered and the solvent was removed under reduced pressure. This left a yellow solid suspended in residual triglyme. This solid was collected using a centrifuge and washed with 3×8 mL H_2O, 4 mL EtOH and 2×8 mL Et_2O giving a yield of 28 mg (33%). ^{1}H NMR (400 MHz, d_3-acetonitrile): δ 9.92 (1H, d, ^{3}J 5.2 Hz, H^6-bpy), 9.13 (1H, s, H^3-bpy), 8.61 (1H, d, ^{3}J 5.2 Hz, H^5-bpy), 8.40 (1H, s, $H^{3'}$-bpy), 8.22 (2H, d, ^{3}J 8.4 Hz, H^6-py), 7.81 (2H, t, ^{3}J 7.6 Hz, H^5-py), 7.65 (2H, d, ^{3}J 5.6 Hz, H^3-py), 7.23 (1H, d, ^{3}J 6.0 Hz, $H^{6'}$-bpy), 7.13 (1H, s, H^2-xy), 7.04 (2H, t, ^{3}J 6.8 Hz, H^4-py), 6.94 (1H, d, ^{3}J 6.0 Hz, $H^{5'}$-bpy), 2.88 (6H, s, xy-Me), 2.42 (3H, s, bpy-Me). MS (ES+): m/z 701 $(M\text{-}PF_6)^+$.

(4,6-Di(2-pyridyl)xylene)(2,2'-bipyridine-4,4'-dicarboxylic acid)iridium(III) chloride hexafluorophosphate

6a

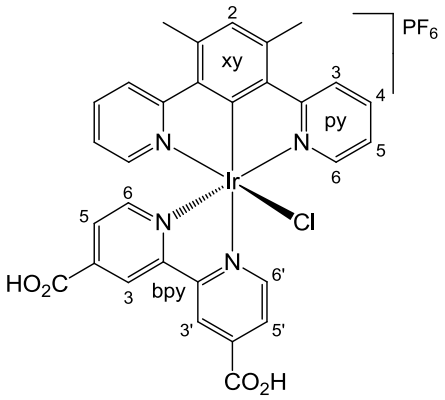

$[Ir(dpyx)(\mu\text{-}Cl)Cl]_2$ (52 mg, 0.050 mmol), 2,2'-bipyridine-4,4'-dicarboxylic acid (25 mg, 0.10 mmol) and silver(I) triflate (25.7 mg, 0.050 mmol) were placed in 2 mL triglyme under nitrogen and heated at 195 °C for 2 h. After this time the solid in the reaction appeared slightly redder in colour but very little had dissolved. Sodium acetate (17 mg, 0.21) was added and the reaction was heated for a further 12 h. After cooling to RT, 1 mL 2 M HCl was added turning the solution red. The solution was separated using a centrifuge and the residual solid was extracted with 3 × 3 mL acetonitrile. The combined reaction solution and extracts were added dropwise to 20 mL sat. $KPF_{6\ (aq)}$ producing a red/orange precipitate. This was collected and washed with 3 ×8 mL H_2O and a small amount of EtOH. Yield: 37 mg (42%). ^1H NMR (400 MHz, d_3-acetonitrile): δ 10.03 (1H, d, ^3J 5.6, H^6-bpy), 9.19 (1H, s, H^3-bpy), 8.88 (1H, s, $H^{3'}$-bpy), 8.61 (1H, d, ^3J 4.0 Hz, H^5-bpy), 8.23 (2H, d, ^3J 7.6 Hz, H^6-py) 7.82 (2H, t, ^3J 7.6 Hz, H^5-py), 7.64 (1H, d, ^3J 6.4 Hz, $H^{6'}$-bpy), 7.58 (2H, d, ^3J 5.6 Hz, H^3-py), 7.52 (1H, d, ^3J 6.4 Hz, $H^{5'}$-bpy), 7.15 (1H, s, H^2-xy), 7.03 (2H, t, ^3J 6.8 Hz, H^4-py), 2.87 (6H, s, Me). MS (ES+): m/z 731 $(M\text{-}PF_6)^+$.

Di-(O-ethyl-L-cysteinyl)-5-(N-dansylamino)isophthalamide

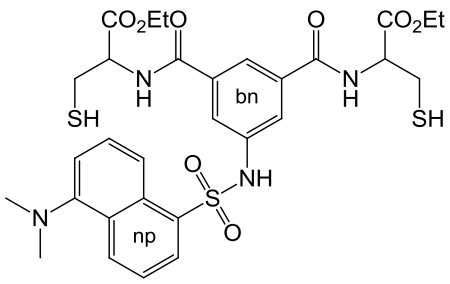

N-dansyl-5-aminoisophthalic acid (96 mg, 0.23 mmol) was placed in 10 mL dry THF under nitrogen and cooled to 0 °C. EDCI (98 mg, 0.51 mmol) was added through a positive flow of nitrogen and the reaction was stirred for 15 min. Ethyl cysteine hydrochloride (95 mg, 0.51 mmol) was then added and the reaction was warmed to RT then stirred for 16 h while maintained under a nitrogen atmosphere. The resulting pale green solution was decanted from the residual white gum and the gum was washed with 2×5 mL THF. The combined supernatant and washings were reduced to dryness under reduced pressure. An attempt to purify the product by flash column chromatography on alumina under nitrogen eluting with 5% MeOH in DCM ramped to 10% MeOH gave a small amount of product which was identified by ^{1}H NMR and mass spectrometry, but not at an acceptable level of purity. Yield (23 mg, 15%). ^{1}H NMR (400 MHz, $CDCl_3$): δ 8.49 (1H, d, ^{3}J 8.4 Hz, H-np), 8.39 (1H, d, ^{3}J 7.6 Hz, H-np), 8.35 (1H, d, ^{3}J 8.8 Hz), 7.88 (1H, s, H^{2}-bn), 7.79 (2H, s, $H^{4/6}$-bn), 7.51 (1H, t, ^{3}J 8.4 Hz, H-np), 7.47 (1H, t, ^{3}J 8.4 Hz, H-np), 7.11 (1H, d, ^{3}J 7.2 Hz, H-np), 5.02 (2H, m, C*H), 4.26 (4H, q, ^{3}J 7.2 Hz, OC**H_2**CH_3), 3.11 (4H, d, ^{3}J 4.4 Hz, C**H_2**SH), 2.83 (6H, s, NMe), 1.31 (6H, t, ^{3}J 7.2 Hz, OCH_2C**H_3**). MS (ES-): m/z 675 $(M-H)^-$.

S-(N-ethylaminocarbonyl)-cysteine ethyl ester hydrochloride

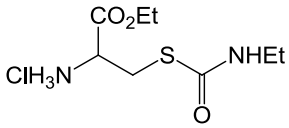

Ethyl cysteine hydrochloride (1.85 g, 9.96 mmol) was dissolved in 15 mL DMF under argon gas and cooled to 0 °C. Ethyl isocyanate (800 µL, 718 mg, 10.1 mmol) was added and the reaction was stirred for 72 h at RT under argon. The DMF solvent was removed using a Genevac leaving a white solid. This solid was washed with diethyl ether and recrystallised from ethanol to give 1.16 g (45%) white crystalline solid. ^{1}H NMR (400 MHz, D_2O): δ 4.42 (1H, t, ^{3}J

4.8 Hz, C*H), 4.29 (2H, q, ^{3}J 7.2 Hz, OC**H$_2$**CH$_3$), 3.54 (1H, dd, ^{2}J 12.8 Hz, ^{3}J 4.8 Hz, SC**H**H), 3.48 (1H, dd, ^{2}J 12.8 Hz, ^{3}J 4.8 Hz, SCH**H**), 3.24 (2H, q, ^{3}J 7.6 Hz, NC**H$_2$**CH$_3$), 1.29 (3H, t, ^{3}J 7.2 Hz, OCH$_2$C**H$_3$**), 1.09 (3H, t, ^{3}J 7.6 Hz, NCH$_2$C**H$_3$**). MS (ES+): m/z 221 $(M\text{-}Cl)^+$.

Di(O-ethyl-S-(N-ethylaminocarbonyl)-cysteinyl)-5-(N-dansylamino)isophthalamide

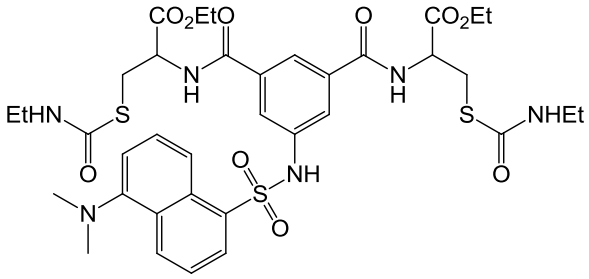

N-dansyl-5-aminoiosphthalic acid (66 mg, 0.16 mmol) was dissolved in 7 mL dry THF under argon and the solution was cooled to 0 °C. EDCI (67 mmol, 0.35 mmol) was added and the reaction was stirred for 30 min at 0 °C before addition of triethylamine (50 µL, 36.3 mg, 0.36 mmol) and ethyl-S-(N-ethylaminocarbonyl)-cysteine hydrochloride (103 mg, 0.40 mmol). The reaction was then warmed to RT and stirred for 16 h. The solution was decanted from the residual gum and the solvent removed under reduced pressure. The crude product was columned on silica, eluting with 5% MeOH in DCM. This yielded 83 mg (64%) product (identified by mass spectrometry), however the purity was poor. HRMS (ES+): m/z 819.24114; calculated for $C_{36}H_{47}N_6O_{10}{}^{32}S_3$: 819.25103

Bis(2-phenylpyridine)(O-ethyl-S-(N-ethylaminocarbonyl)-L-cysteinyl)-4'-methyl-2,2'-bipyridine-4-carboxamide)iridium(III) hexafluorophosphate

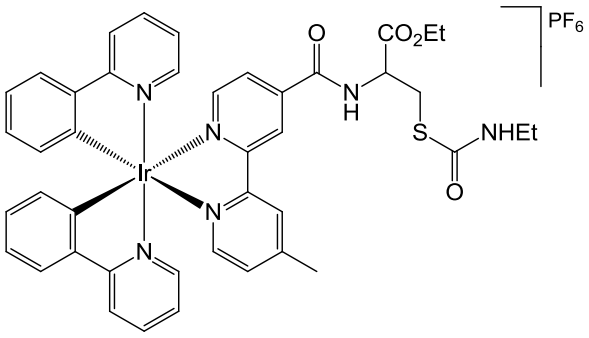

Bis(2-phenylpyridine)(4'-methyl-2,2'-bipyridine-4-carboxylic acid)iridium(III) hexafluorophosphate (100 mg, 0.116 mmol), was placed in 5 mL dry THF under argon and cooled to 0 °C. EDCI (25 mg, 0.13 mmol) was added and the

reaction was stirred for 30 min. Triethylamine (18 µL, 13.1 mg, 0.13 mmol) and ethyl-S-(N-ethylaminocarbonyl)-cysteine hydrochloride (35 mg, 0.14 mmol) were added and the reaction was warmed to RT then stirred for 16 h. The THF solution was decanted from the reaction vessel and the gummy residue was extracted with 2 × 5 mL THF. The combined THF solutions were reduced to dryness on a rotary evaporator and the residue was dissolved in a minimum amount of acetonitrile. This was added dropwise to a saturated solution of $KPF_{6\ (aq)}$. The resulting solid was collected and washed with H_2O using a centrifuge then extracted into DCM. Removal of the DCM under reduced pressure yielded the crude product. Column chromatography on silica eluting with 5% MeOH in DCM gave 55 mg (45%) product, identified by mass spectrometry, however not at an acceptable level of purity. MS(ES+): m/z 917 $(M\text{-}PF_6)^+$.

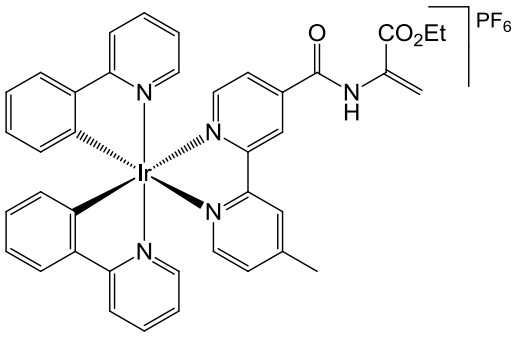

The attempted thiol deprotection of bis(2-phenylpyridine)((S-(N-ethylaminocarbonyl)-cysteine ethyl ester)-4'-methyl-2,2'-bipyridine-4-carboxamide)iridium(III) hexafluorophosphate by the following method instead gave the dethiolated compound shown above, identified by mass spectrometry:
The starting material was dissolved in 5 mL THF and degassed using the freeze-pump-thaw method. 5 mL 1 M $NaOH_{(aq)}$ was degassed separately then transferred to the reaction vessel via a cannula. The reaction was then stirred at RT for 25 min. The reaction was then quenched by addition of 5 mL 2 M HCl and 10 mL DCM was also added. After stirring for 5 min the organic layer was separated and the solvent was removed under reduced pressure. A saturated solution of NH_4PF_6 in methanol (2 mL) was added to the residue and stirred for 5 min. The methanol was removed under reduced pressure and the resulting solid was extracted with DCM. The DCM solution was reduced to dryness yielding 12 mg red solid. HRMS (ES+): m/z 810.21810; calculated for $C_{39}H_{33}O_3N_5{}^{191}Ir$: 810.21839.

S-(*tert*-butylmercapto)-L-cysteine methyl ester

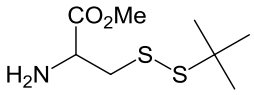

Acetyl chloride (1.0 mL, 1.10 g, 14.1 mmol) was added dropwise to 15 mL dry MeOH under nitrogen at -4 °C. S-(tert-butylmercapto)-L-cysteine (2.6 g, 12.4 mmol) was added to the reaction which was then stirred at 0 °C for 2 h, then for a further 16 h at RT. The solvent was removed under reduced pressure and the residue was taken into 10 mL H_2O and 20 mL 10% $NaHCO_{3\ (aq)}$ was added producing a white precipitate. 30 mL Et_2O was added to the suspension and the mixture was shaken vigorously. Any remaining undissolved solid was removed by filtration (1.27 g starting material) then the organic phase was separated. The aqueous phase was extracted with a further 30 mL Et_2O and the combined organics were dried over $MgSO_4$ and the solvent was removed under reduced giving a clear, thin oil* (837 mg, 30%). ^{1}H NMR (400 Hz, d_4-methanol): δ 3.76 (1H, dd, ^{3}J 5.2 Hz, 6.8 Hz, C*H), 3.74 (3H, s, Me), 3.08 (1H, dd, ^{2}J 13.2 Hz, ^{3}J 5.2 Hz, SC**H**H), 2.95 (1H, dd, ^{2}J 13.2 Hz, ^{3}J 6.8 Hz, SCH**H**), 1.34 (9H, s, ^{t}Bu). MS (ES+): m/z 224 $(M+H)^+$.

(O-methyl-S-*tert*-butylmercapto-L-cysteinyl)-4-(N-dansylamino)benzamide 1b

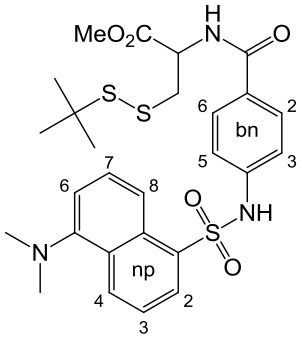

N-dansyl-5-amino benzoic acid (75 mg, 0.20 mmol) and methyl-S-(tert-butylmercapto)-L-cysteine (67 mg, 0.30 mmol) were placed in a flask under nitrogen and dissolved in 5 mL dry THF. The solution was cooled to 0 °C and EDCI (45 mg, 0.23 mmol) was added through a flow of nitrogen. The reaction was stirred for 15 min at 0 °C then warmed to RT and stirred for a further 16 h. The solvent was removed under reduced pressure and the residue was

* Avoid prolonged exposure to vacuum as this product is fairly volatile in the free-base form.

dissolved in 20 mL EtOAc. This solution was washed with 20 mL each of 1 M HCl, 10% $NaHCO_{3\ (aq)}$ and H_2O, dried over $MgSO_4$, fitered and the solvent was removed under reduced pressure. The crude product was purified by column chromatography on silica with gradient elution from 70% to 90% Et_2O in hexane (product R_f = 0.34 in 90% Et_2O/hexane) yielding 56 mg (49%) green solid. ^1H NMR (400 MHz, $CDCl_3$): δ 8.50 (1H, d, ^3J 8.8 Hz, H^4-np), 8.33 (1H, d, ^3J 8.8 Hz, H^8-np), 8.25 (1H, d, ^3J 7.6 Hz, H^2-np), 7.59 (2H, d, ^3J 8.8 Hz, $H^{2/6\ or\ 3/5}$-bn), 7.52 (1H, t, ^3J 8.0 Hz, H^7-np), 7.45 (1H, t, ^3J 8.0 Hz, H^3-np), 7.15 (1H, d, ^3J 7.6 Hz, H^6-np), 7.04 (2H, d, ^3J 8.8 Hz, $H^{2/6\ or\ 3/5}$-bn), 6.97 (1H, d, ^3J 7.6 Hz, NH), 5.03 (1H, m, C*H), 3.77 (3H, s, OMe), 3.25 (2H, m, SC**H**$_2$C*), 2.85 (6H, s, NMe), 1.28 (9H, s, ^{t}Bu). ^{13}C NMR* (100 MHz, $CDCl_3$): δ 171.2 (C=O), 166.3 (C=O), 140.3, 134.0, 131.2, 130.6, 129.6, 129.4, 128.8, 128.6, 123.4, 119.5, 118.7, 115.6, 52.9, 52.7, 48.5, 42.1, 29.8 (C(**C**$H_3)_3$). HRMS (ES+): m/z 576.16545; calculated for $C_{27}H_{34}N_3O_5S_3$: 576.16551. IR: ν(C=O) 1739, 1644 cm^{-1}. C, H & N analysis: 53.56% C, 6.06% H, 6.83% N measured; 53.40% C, 6.06% H, 6.92% N calculated for $C_{27}H_{33}N_3O_5S_3$.{1.75(H_2O)}.

Di-(O-methyl-S-*tert*-butylmercapto-L-cysteinyl)-5-(N-dansylamino)phthalamide

2b

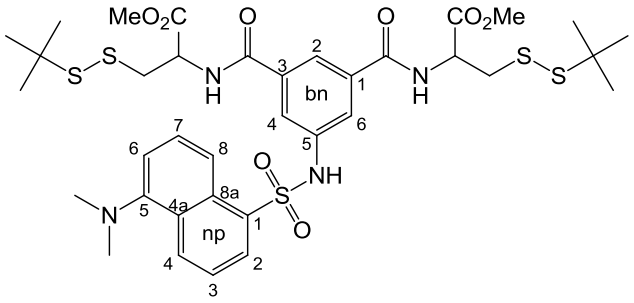

N-dansyl-5-aminoiosphthalic acid (41 mg, .099 mmol) and O-methyl-S-(tert-butylmercapto)-L-cysteine (78 mg, 0.35 mmol) were placed in 5 mL dry THF under nitrogen and cooled to 0 °C. EDCI (48 mg, 0.25 mmol) was added through a flow of nitrogen and the reaction was stirred for 30 min at 0 °C then warmed to RT and stirred for a further 16 h. The solvent was removed under reduced pressure and the residue was taken into 20 mL EtOAc and washed with 20 mL each of 1 M $HCl_{(aq)}$, 10% $NaHCO_{3\ (aq)}$ and H_2O. The solution was then dried over $MgSO_4$, filtered and the solvent was removed under reduced

* Weak spectrum, 2 signals not resolved from noise.

pressure giving 57 mg (70%) green solid. ^{1}H NMR (700 MHz, $CDCl_3$): δ 8.48 (1H, d, ^{3}J 8.4 Hz, H^{4}-np), 8.41 (1H, d, ^{3}J 7.0 Hz, H^{2}-np), 8.29 (1H, d, ^{3}J 8.4 Hz, H^{8}-np), 7.87 (1H, s, H^{4}-bn), 7.80 (2H, s, $H^{2/6}$-bn), 7.51 (1H, t, ^{3}J 7.7 Hz, H^{3}-np), 7.41 (1H, t, ^{3}J 8.4 Hz, H^{7}-np), 7.31 (2H, d (broad), ^{3}J 7.7 Hz, CON**H**), 7.08 (1H, d, ^{3}J 7.7 Hz, H^{6}-np), 5.14 (2H, m, C*H), 3.78 (6H, s, OMe), 3.32 (2H, dd, ^{2}J 14.0 Hz, ^{3}J 4.9 Hz, SC**H**H), 3.27 (2H, dd, ^{2}J 14.0 Hz, ^{3}J 5.6 Hz, SCH**H**), 2.82 (6H, s, NMe), 1.30 (18H, s, ^{t}Bu). ^{13}C NMR (175 MHz, $CDCl_3$): δ 171.0 (O**C**=O), 166.0, (NH**C**=O), 152.0 (C^{5}-np), 138.7 ($C^{3/5}$-bn), 135.0 (C^{1}-bn), 133.8 (C^{1}-np), 131.3 (C^{4}-np), 131.0 (C^{2}-np), 130.0 (C^{4a}-np), 129.6 (C^{8a}-np), 128.7 (C^{7}-np), 123.4 (C^{3}-np), 120.8 ($C^{2/6}$-bn), 120.7 (C^{4}-bn), 118.6 (C^{8}-np), 115.4 (C^{6}-np), 52.9(2) and 52.9(1) (C* and O**C**H_3), 48.4 (**C**Me_3), 45.5 (N**C**H_3), 41.9 (C***C**H_2S), 29.9 (C(**C**$H_3)_3$). HRMS (ES+): m/z 825.51492; calculated for $C_{36}H_{49}N_4O_8S_5$: 825.21485. IR: ν(C=O) 1698, 1651 cm^{-1}. C, H & N analysis: 52.19% C, 6.02% H, 6.34% N measured; 52.40% C, 5.86% H, 6.79% N calculated for $C_{36}H_{48}N_4O_8S_5$.

Bis(2-phenylpyridine)(O-methyl-S-*tert*-butylmercapto-L-cysteinyl)-4'-methyl-2,2'-bipyridine-4-carboxamide)iridium(III) hexafluorophosphate 3b

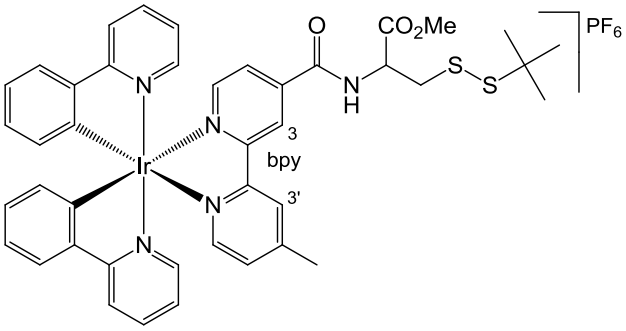

Bis(2-phenylpyridine)(4'-methyl-2,2'-bipyridine-4-carboxylic acid)iridium(III) hexafluorophosphate (138 mg, 0.16 mmol) and O-methyl-S-*tert*-butylmercapto-L-cysteine (60 mg, 0.27 mmol) were placed in 5 mL 1:1 dry THF:dry DCM under nitrogen. The solution was cooled to 0 °C then EDCI (40 mg, 0.21 mmol) was added and the reaction stirred for 15 min. The reaction was warmed to RT and stirred for a further 16 h. The solvents were removed under reduced pressure and 20 mL sat. $NH_4Cl_{(aq)}$ was added to the residue. The resulting solution was extracted with 2 × 15 mL DCM. The combined organics were washed with 20 mL sat. $KPF_{6\ (aq)}$, dried over $MgSO_4$, filtered and the solvent removed under

reduced pressure. The crude product was purified by column chromatography on silica, eluting with 7.5% MeOH in DCM to yield 128 mg (74%) red solid. ^{1}H NMR (400 MHz, $CDCl_3$): δ 10.59 (1H, s (broad), NH), 10.29 (1H, s, $H^{3\text{ or }3'}$-bpy), 9.67 (1H, s, $H^{3\text{ or }3'}$-bpy), 8.05 (1H, d, ^{3}J 5.2 Hz), 7.97 (1H, d, ^{3}J 5.6 Hz), 7.91 (2H, d, ^{3}J 8.0 Hz), 7.78-7.67 (5H, m), 7.48 (1H, d, ^{3}J 6.0 Hz), 4.44 (1H, d, ^{3}J 6.0 Hz), 7.17 (1H, d, ^{3}J 6.0 Hz), 7.06-6.88 (6H, m), 6.29 (2H, t, ^{3}J 6.8 Hz), 5.10 (1H, m, C*H), 3.73 (1H, m, SC**H**H), 3.73 (3H, d*, OMe), 3.37 (1H, mm SCH**H**), 2.61 (3H, s, bpy-Me), 1.33 (9H, d*, ^{t}Bu). HRMS (ES+): m/z 918.22533; calculated for $C_{42}H_{41}{}^{191}IrN_5O_3S_2$: 918.22514. IR: ν(C=O) 1720, 1666 cm^{-1}. C, H & N analysis: 46.17% C, 4.53% H, 5.87% N measured; 46.04% C, 4.00% H, 6.39% N calculated for $C_{42}H_{42}IrN_5O_3S_2PF_6.\{1.75(H_2O)\}$.

Bis(2-phenylpyridine)(Di-(O-methyl-S-*tert*-butylmercapto-L-cysteinyl)-2,2'-bipyridine-4-4'-dicarboxamide)iridium(III) hexafluorophosphate

4b

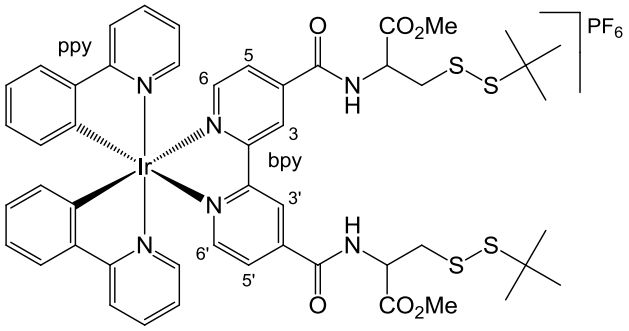

Bis(2-phenylpyridine)(hydro-2,2'-bipyridine-4,4'-dicarboxylate)iridium(III) (117 mg, 0.157 mmol) and O-methyl-S-*tert*-butylmercapto-L-cysteine (106 mg, 0.475 mmol) were placed under nitrogen and 5 mL MeCN was added. 2 M HCl was added dropwise until the iridium complex dissolved (~0.1 mL). The solution was then cooled to 0 °C and EDCI (70 mg, 0.355 mmol) was added through a flow of nitrogen. The reaction was stirred for 15 min at 0 °C, warmed to RT and stirred for a further 16 h. The solvent was removed under reduced pressure and 20 mL DCM was added to the residue. 20 mL sat. $NH_4Cl_{(aq)}$ was also added and the mixture shaken vigorously. The organic phase was separated and washed with a further 20 mL sat. $NH_4Cl_{(aq)}$ and then 2 × 10 mL sat. $KPF_{6\ (aq)}$, dried over $MgSO_4$, filtered and the solvent removed under

* Methyl and tert-Butyl signals are both split into 2 equal integral signals. Unlikely to be J coupling (~15 Hz for Me, ~7 Hz for ^{t}Bu). Possibly a result of diastereoisomers.

reduced pressure. The product was purified by column chromatography on silica with gradient elution from 0% to 5% MeOH in DCM (Product R_f = 0.59 in 5% MeOH) yielding 120 mg (59%) red solid. ^{1}H NMR (400 MHz, $CDCl_3$): 8.89 (2H, s (broad), $H^{3/3'}$-bpy), 8.07 (2H, d, ^{3}J 6.0 Hz, $H^{6/6'}$-bpy), 7.93 (2H, d, ^{3}J 8.0 Hz, H-ppy), 7.88 (2H, d, ^{3}J 5.6 Hz, $H^{5/5'}$-bpy), 7.78 (2H, t, ^{3}J 8.0 Hz, H-ppy), 7.70 (2H, d, ^{3}J 8.0 Hz, H-ppy), 7.67 (2H, s (broad), NH), 7.48 (2H, d, ^{3}J 5.6 Hz, H-ppy), 7.09-7.02 (4H, m, 2H-ppy), 6.94 (2H, t, ^{3}J 7.2 Hz, H-ppy), 6.28 (2H, d, ^{3}J 7.6 Hz, H-ppy), 5.12, (2H, m, C*H), 3.80 (3H, s, Me), 3.78 (3H, s, Me), 3.35 (2H, dd, ^{2}J 13.6 Hz, ^{3}J 4.8 Hz, SC**H**H), 3.20 (2H, dd, ^{2}J 13.6 Hz, ^{3}J 8.8 Hz, SCH**H**), 1.34 (9H, s, ^{t}Bu), 1.33 (9H, s, ^{t}Bu). ^{13}C NMR (100 MHz, $CDCl_3$): δ 170.3, 167.6, 164.1, 156.0, 151.0, 149.4, 148.6, 144.6, 143.3, 138.4, 131.7, 131.0, 127.3, 124.9, 123.6, 123.0, 122.5, 119.8, 53.5, 52.8, 48.2, 40.8, 29.9. HRMS (ES+): m/z 1153.26075; calculated for $C_{50}H_{54}{}^{191}IrN_6O_6S_4$: 1153.25883. IR: ν(C=O) 1725, 1675 cm^{-1}. C, H & N analysis: 45.44% C, 4.20% H, 6.30% N measured; 45.43% C, 4.23% H, 6.36% N calculated for $C_{50}H_{53}IrN_6O_6S_4PF_6.\{1.25(H_2O)\}$.

General procedure for deprotection of S-^{t}butylmercapto cysteines

Between 0.01 mmol and 0.04 mmol protected mimic was dissolved in 2 mL acetonitrile and degassed using the freeze-pump-thaw method. In a separate flask, a solution of DTT in H_2O (200 mM for singly functionalised mimics or 400 mM for doubly functionalised) was degassed. 2 mL of the DTT solution was then transferred to the mimic solution via cannula and the reaction was heated at reflux for 1 h under nitrogen. After cooling to RT, 6 mL organic solvent (EtOAc for Dansyl mimics and DCM for Iridium mimics) was added to the residue and then washed with 2 $\times$ 6 mL sat. $Na_2S_2O_{3\ (aq)}$. The organic phase was separated and dried over $MgSO_4$, filtered and the solvent was removed under reduced pressure yielding the deprotected product. Deprotection was confirmed by mass spectrometry and by the loss of ^{t}Bu signals in the ^{1}H NMR spectrum.

Chapter 6

References

6 References

[1] A. P. de Silva, H. Q. N. Gunaratne, T. Gunnlaugsson, A. J. M. Huxley, C. P. McCoy, J. T. Rademacher and Terence E. Rice, *Chem. Rev*. 1997, **97**, 1515

[2] L. Basabe-Desmonts, D. N. Reinhoudt and M. Crego-Calama, *Chem. Soc. Rev.*, 2007, **36**, 993

[3] J. G. Vosa and J. M. Kelly, *Dalton Trans*., 2006, 4869

[4] E. C. Constable, *Chem. Soc. Rev*., 2007, **36**, 246

[5] J. A. G. Williams, *Chem. Soc. Rev.*, 2009, **38**, 1783

[6] V. Fernández-Moreira, F. L. Thorp-Greenwood and M. P. Coogan, *Chem. Commun.*, 2010, **46**, 186

[7] Q. Zhao, C. Huang an F. Li, *Chem. Soc. Rev.*, 2010, DOI: 10.1039/c0cs00114g

[8] A. Gilbert and J. Baggot, *'Principles of Fluorescence Spectroscopy'*, Blackwell Scientific Publications, 1991

[9] A. Juris, V. Balzani, F. Barigelletti, S. Campagna, P. Belser and, A. von Zelewsky, *Coordin. Chem. Rev.*, 1988, **84**, 85

[10] P. D. Rillema, D. S. Jones and H. A. Levey, *J. Chem. Soc., Chem. Commun.*, 1979, 849

[11] I. M. Dixon, J.-P. Collin, J.-P. Sauvage, L. Flamigni, S. Encinas and F. Barigelletti, *Chem. Soc. Rev.*, 2000, **29**, 385

[12] C. M. Flynn, Jr. and J. N. Demas, *J. Am. Chem. Soc.*, 1974, **96**, 1959

[13] R. J. Watts, S. Efrima and H. Metiu, *J. Am. Chem. Soc.*, 1979, **101**, 2742

[14] M. K. DeArmond, W. L. Huang and C. M. Carlin, *Inorg. Chem.*, 1979, **18**, 3388

[15] B. Davisia, P. C. Ford and R. J. Watts, *J. Am. Chem. Soc*., 1980, **102**, 7264

[16] S. C. Rasmussen, M. M. Richter, E. Yi, H. Place and K. J. Brewer, *Inorg. Chem.*, 1990, **29**, 3926

[17] R. J. Watts, J. S. Harrington and J. van Houten, *J. Am. Chem. Soc.*, 1977, **99**, 2179

[18] W. A. Wickramasinghe, B. H. Bird and N. Serpone, *J. Chem. Soc. Chem. Commun.*, 1981, 1284

[19] S. Sprouse, K. A. King, P. J. Spellane and R. J. Watts, *J. Am. Chem. Soc.*, 1984, **106**, 6647

[20] R. J. Hoare and O. S. Mills, *J. Chem. Soc., Dalton Trans.*, 1972, 2138

[21] R. J. Hoare and O. S. Mills, *J. Chem. Soc., Dalton Trans.*, 1972, 2141

[22] F. O. Garces, K. Dedeian, N. L. Keder and R. J. Watts, *Acta Crystallogr. Sect. C*, 1993, **49**, 1117

[23] K. A. McGee and K. R. Mann, *Inorg. Chem.*, 2007, **46**, 7800

[24] M. Nonoyama, *Bull. Chem. Soc. Jpn.*, 1974, **47**, 767

[25] Y. Ohsawa, S. Sprouse, K. A. King, M. K. DeArmond, K. W. Hanck and R. J. Watts, *J. Phys. Chem.*, 1987, **91**, 1047

[26] S. Lamansky, P. Djurovich, D. Murphy, F. Abdel-Razzaq, H.-E Lee, C. Adachi, P. E. Burrows, S. R. Forrest and M. E. Thompson, *J. Am. Chem. Soc.*, 2001, **123**, 4304

[27] K. A. King, P. J. Spellane and R. J .Watts, *J. Am .Chem. Soc.*, 1985, **107**, 1431

[28] A. B. Tamayo, B. D. Alleyne, P. I. Djurovich, S. Lamansky, I. Tsyba, N. N. Ho, R. Bau and M. E. Thompson, *J. Am. Chem. Soc.*, 2003, **125**, 7377

[29] R. Gao, D. G. Ho, B. Hernandez, M. Selke, D. Murphy, P. I. Djurovich, and M. E. Thompson, *J. Am. Chem. Soc.*, 2002, **124**, 14828

[30] M. C. DeRosa, D. J. Hodgson, G. D. Enright, B. Dawson, C. E. B. Evans and R. J. Crutchley, *J. Am. Chem. Soc.*, 2004, **126**, 7619.

[31] B. W. D'Andrade, M. A. Baldo, C. Adachi, J. Brooks, M. E. Thompson and S. R. Forrest, *Appl. Phys. Lett.*, 2001, **79**, 1045

[32] S. Okada, K. Okinaka, H. Iwawaki, M. Furugori, M. Hashimoto, T. Mukaide, J. Kamatani, S. Igawa, A. Tsuboyama, T. Takiguchi and K. Ueno, *Dalton Trans.*, 2005, 1583

[33] R. Ragni, E. A. Plummer, K. Brunner, J. W. Hofstraat, F. Babudri, G. M. Farinola, F. Naso and L. De Cola, *J Mater. Chem.*, 2006, **16**, 1161

[34] H. Kanno, N. C. Giebink, Y. Sun and S. R. Forrest, *Appl. Phys. Lett.,* 2006, **89**, 023503

[35] N. P. Ayala, C. M. Flynn, L. Sacksteder Jr., J. N. Demas and B. A. De Graff, *J. Am. Chem. Soc.*, 1990, **112**, 3837

[36] J.-P. Collin, I. M. Dixon, J.-P. Sauvage, J. A. G. Williams, F. Barigelletti and L. Flamigni, *J. Am. Chem. Soc.*, 1999, **121**, 5009

[37] M. Licini and J. A. G. Williams, *Chem. Commun.*, 1999, 1943

[38] K. J. Arm, W. Leslie and J. A. G. Williams, *Inorg. Chim. Acta*, 2006, **359**, 1222

[39] W. Goodall and J. A. G. Williams, *J. Chem. Soc., Dalton Trans.*, 2000, 2893

[40] E. C. Constable, R. P. G. Henney, T. A. Leese and D. A. Tocher, *J. Chem. Soc., Chem. Commun.*, 1990, 513.

[41] J.-P. Collin, M. Beley and J.-P. Sauvage, *Inorg. Chim. Acta*, 1991, **186**, 91

[42] M. Beley, J.-P. Collin, R. Louis, B. Metz and J.-P. Sauvage, *J. Am. Chem. Soc.*, 1991, **113**, 8521

[43] A. Mamo, I. Stefio, M. F. Parisi, A. Credi, M. Venturi, C. Di Pietro and Sebastiano Campagna, *Inorg. Chem.*, 1997, **36**, 5947

[44] M. Polson, S. Fracasso, V. Bertolasi, M. Ravaglia and F. Scandola, *Inorg. Chem.*, 2004, **43**, 1950

[45] M. Polson, M. Ravaglia, S. Fracasso, M. Garavelli and F. Scandola, *Inorg. Chem.*, 2005, **44**, 1282

[46] A. J. Wilkinson, A. E. Goeta, C. E. Foster and J. A. G. Williams, *Inorg. Chem.*, 2004, **43**, 6513

[47] A. J. Wilkinson, H. Puschmann, J. A. K. Howard, C. E. Foster and J. A. G. Williams, *Inorg. Chem.*, 2006, **45**, 8685

[48] V. L. Whittle and J. A. G. Williams, *Inorg. Chem.*, 2008, **47**, 6596

[49] J. A. G. Williams, A. J. Wilkinson and V. L. Whittle, *Dalton Trans.*, 2008, 2081

[50] J.-P. Sauvage, J.-P. Collin, J.-C. Chambron, S. Guillerez, C. Coudret, V. Balzani, F. Barigelletti, L. De Cola and L. Flamigni, *Chem. Rev.*, 1994, **94**, 993

[51] H. Hofmeiera and U. S. Schubert, *Chem. Soc. Rev.*, 2004, **33**, 373

[52] L. Chassot and A. von Zelewsky, *Helv. Chim. Acta*, 1983, **66**, 2443

[53] L. Chassot, E. Muller and A. von Zelewsky, *Inorg. Chem.*, 1984, **23**, 4249

[54] M. M. Mdleleni, J. S. Bridgewater, R. J. Watts and P. C. Ford, *Inorg. Chem.*, 1995, **34**, 2334

[55] E. C. Constable, R. P. G. Henney, T. A. Leese and D. A. Tocher, *J. Chem. Soc., Dalton Trans.*, 1990, 443

[56] E. C. Constable, R. P. G. Henney, T. A. Leese and D. A. Tocher, *J. Chem. Soc., Chem. Commun.*, 1990, 513

[57] T.-C. Cheung, K.-K. Cheung, S.-M. Peng and C.-M. Che, *J. Chem. Soc., Dalton Trans.*, 1996, 1645

[58] C. Cornioley-Deuschel, T. Ward and A. von Zelewsky, *Helv. Chim. Acta,* 1988, **71**, 130

[59] G. W. V. Cave, N. W. Alcock and J. P. Rourke, *Organometallics*, 1999, **18**, 1801

[60] W. Lu, M. C. W. Chan, K.-K. Cheung and C.-M. Che, *Organometallics*, 2001, **20**, 2477

[61] D. J. Cardenas and A. M. Echavarren, *Organometallics*, 1999, **18**, 3337

[62] J. A. G. Williams, A. Beeby, E. S. Davies, J. A. Weinstein and C. Wilson, *Inorg. Chem*., 2003, **42**, 8609

[63] S. J. Farley, D. L. Rochester, A. L. Thompson, J. A. K. Howard and J. A. G. Williams, *Inorg. Chem*., 2005, **44**, 9690

[64] W. Sotoyama, T. Satoh, H. Sato, A. Matsuura and N. Sawatari, *J. Phys. Chem. A*, 2005, **109**, 9760

[65] J. A. G. Williams, S. Develay, D. L. Rochester and L. Murphy, *Coord. Chem. Rev.*, 2008, **252**, 2596

[66] V. N. Kozhevnikov, B. Donnio and D. W. Bruce, *Angew. Chem. Int. Ed.*, 2008, **47**, 6286

[67] S. W. Botchway, M. Charnley, J. W. Haycock, A. W. Parker, D. L. Rochester, J. A. Weinstein and J. A. G. Williams, *Proc. Natl. Acad. Sci. U. S. A*., 2008, **105**, 16071

[68] http://www.ebi.ac.uk/microarray/biology_intro.html

[69] C. B. Anfinsen and E. Haber, *J. Biol. Chem.*, 1961, **236**, 1361

[70] F. H. White, Jr., *J. Biol. Chem.*, 1961, **236**, 1353

[71] R. F. Goldberger, C. J. Epstein and C. B. Anfinsen, *J. Biol. Chem.*, 1963, **238**, 628

[72] D. Givol, R. F. Goldberger and C. B. Anfinsen, *J. Biol. Chem.*, 1964, **239**, PC3114

[73] F. De Lorenzo, R. F. Goldberger, E. Steers, Jr., D. Givol and C. B. Anfinsen, *J. Biol. Chem.*, 1966, **241**, 1562

[74] N. Lambert and R. B. Freedman, *Biochem. J.*, 1983, **213**, 225

[75] J. C. Edman, L. Ellos, R. W. Blacher, R. A. Roth and W. J. Rutter, *Nature*, 1985, **317**, 267

[76] R. B. Freedman, H. C. Hawkins, S. J. Murant and L. Reid, *Biochem. Soc. Trans.*, 1987, **16**, 96

[77] H. Tachikawa, T. Miura, Y. Katakura and T. Mizunaga, *J. Biochem.*, 1991, **110**, 306

[78] M. M. Lyles and H. F. Gilbert, *J. Biol. Chem.*, 1994, **269**, 30946

[79] K. W. Walker, M. M. Lyles and H. F. Gilbert, *Biochemistry*, 1996, **35**, 1972

[80] M. C. A. Laboissière, S. L. Sturley and R. T. Raines, *J. Biol. Chem.*, 1995, **270**, 28006

[81] R. Xiao, A. Solovyov, H. F. Gilbert, A. Holmgren and J. Lundström-Ljung, *J. Biol. Chem.*, 2001, **276**, 27975

[82] A. Solovyov, R. Xiao and H. F. Gilbert, *J. Biol. Chem.*, 2004, **279**, 34095

[83] R. Xiao, B. Wilkinson, A. Solovyov, J. R. Winther, A. Holmgren and J. Lundström-Ljung and H. F. Gilbert, *J. Biol. Chem.*, 2004, **279**, 49780

[84] E. A. Kersteen, S. R. Barrows and R. T. Raines, *Biochemistry*, 2005, **44**, 12168

[85] J. Kemmink, N. J. Darby, K. Dijkstra, M. Nilges and T. E. Creighton, *Biochemistry*, 1996, **35**, 7684

[86] J. Kemmink, N. J. Darby, K. Dijkstra, M. Nilges and T. E. Creighton, *Curr. Biol.*, 1997, **7**, 239

[87] N. J. Darby, M. van Straaten, E. Penke, R. Vincentelli and J. Kemmink, *FEBS Lett.*, 1999, **448**, 167

[88] S. Munro and H. R. B. Pelham, *Cell*, 1987, **48**, 899

[89] E. A. Kersteen and R. T. Raines, *Antioxid. Redox Signalling*, 2003, **5**, 413

[90] T. Pihlajaniemi, T. Helaakoski, K. Tasanen, R. Myllyla, M.-L. Huhtala, J. Koivu and K. I. Kivirriko, *EMBO J.*, 1987, **6**, 643

[91] D. A. Gordon, J. R. Wetterau and R. E Gregg, *Trends Cell Biol.*, 1995, **5**, 317

[92] H. Cai, C. C. Wang and C. L. Tsou, *J. Biol. Chem.*, 1994, **269**, 24550

[93] A. Holmgren, *Annu. Rev. Biochem.*, 1985, **54**, 237

[94] B. B. Buchanan, P. Schürmann, P. Decottignies and R. M. Lozano, *Arch. Biochem. Biophys.*, 1994, **314**, 257

[95] K. J. Woycechowsky, K. D. Wittrup and R. T .Raines, *Chem. Biol.*, 1999, **6**, 871

[96] P. T. Chivers, M. C. A. Laboissière and R. T. Raines, *EMBO J.*, 1996, **15**, 2659

[97] K. J. Woycechowsky and R. T .Raines, *Biochemistry*, 2003, **42**, 5387

[98] S. Kasina, A. R. Fritzberg, D. L. Johnson and D. Eshima, *J. Med. Chem.*, 1986, **29**, 1933

[99] G. V. Lamoureux and G. M. Whitesides, *J. Org. Chem.*, 1993, **58**, 633

[100] V. P. Saxena and D. B. Wetlaufer, *Biochemistry*, 1970, **9**, 5015

[101] J. D. Gough, R. H. Williams, Jr, A. E. Donofrio and W. J. Lees, *J. Am. Chem. Soc.*, 2002, **124**, 3885

[102] K. J. Woycechowsky, B. A. Hook and R. T .Raines, *Biotechnol. Prog.*, 2003, **19**, 1307

[103] A. R. Frand and C. A. Kaiser, *Mol. Cell*, 1998, **1**, 161

[104] M G. Pollard, K.J. Travers and J. S. Weissman, *Mol. Cell*, 1998, **1**, 171

[105] A. Cabibbo, M. Pagani, M. Fabbri, M. Rocchi, M. R. Farmery, N. J. Bulleid and R. Sitia, *J. Biol. Chem.*, 2000, **275**, 4827

[106] M. Pagani, M. Fabbri, C. Benedetti, A. Fassio, S. Pilati, N. J. Bulleid, A. Cabibbo and R. Sitia, *J. Biol. Chem.*, 2000, **275**, 23685

[107] B. T. Tu, S. C. Ho-Schleyer, K. J. Travers and J. S. Weissman, *Science*, 2000, **290**, 1571

[108] S. N. Molteni, A. Fassio, M. R. Circolo, G. Filomeni, E. Pasqualetto, C. Fagioli and R. Sitia, *J. Biol. Chem.*, 2004, **279**, 32667

[109] S. Chakravarthi and N. J. Bulleid, *J. Biol. Chem.*, 2004, **279**, 39872

[110] B. P. Tu and J. S. Weissman, *Mol. Cell*, 2002, **10**, 983

[111] A. R. Frand and C. A. Kaiser, *Mol. Cell*, 1999, **4**, 469

[112] A. Mezghrani, A. Fassio, A. Benham, T. Simmen, I. Braakman and R. Sitia, *EMBO J.*, 2001, **20**, 6288

[113] J. S. Cox, C. E. Shamu and P. Walter, *Cell*, 1993, **73**, 1197

[114] K. Mori, W. Ma, M.-J. Gething and J. Sambrook, *Cell*, 2003, **74**, 743

[115] B. Gess, K.-H. Hofbauer, R. H. Wenger, C. Lohaus, H. E. Meyer and A. Kurzt, *Eur. J. Biochem.*, 2003, **270**, 2228

[116] S. Dias-Gunasekara, J. Gubbens, M. van Lith, C. Dunne, J. A. G. Williams, R. Kataky, D. Scoones, A. Lapthorn, N. J. Bulleid and A. M. Benham, *J. Biol. Chem.*, 2005, **280**, 33066

[117] A. M. Benham, A. Cabibbo, A. Fassio, N. Bulleid, R. Sitia and I. Braakman, *EMBO J.*, 2000, **19**, 4493

[118] A. R. Frand and C. A. Kaiser, *Mol. Biol. Cell*, 2000, **11**, 2833

[119] E. Gross, D. B. Kastner, C. A. Kaiser and D. Fass, *Cell*, 2004, **117**, 601

[120] O. Nekrassoa, N. S. Lawrence and R. G. Copton, *Talanta*, 2003, **60**, 1085

[121] H. Refsum, P. M. Ueland, O. Nygard and S. E .Vollset, *Annu. Rev. Med.*, 1998, **49**, 31

[122] S. Seshadri, A. Beiser, J. Selhub, P. F. Jacques, I. H. Rosenberg, R. B. D'Agostino and P. W. F. Wilson, *New Engl. J. Med.*, 2002, **346**, 476

[123] S. Shahrokhian, *Anal Chem.*, 2001, **73**, 5972

[124] S. L. Whiskur, H. Aït-Haddou, J. J. Lavigne and E. V. Anslyn, *Acc. Chem. Res.*, 2001, **34**, 963

[125] O. Rusin, N. N. St. Luce, R. A. Agbaria, J. O. Escobedo, S. Jiang, I. M. Warner, F. B. Dawan, K. Lian and R. M. Strongin, *J. Am. Chem. Soc.*, 2004, **126**, 438

[126] Z. G. Zhao, J. S. Im, K. S. Lam and D. F. Lake, *Bioconjugate Chem.*, 1999, **10**, 424

[127] T. J. Tolberg and C.-H. Wong, *Angew. Chem. Int. Ed.*, 2002, **41**, 2171

[128] J. V. Ros-Lis, B. García, D. Jiménez, R. Martínez-Máñez, F. Sancenón, J. Soto, F. Gonzalvo and M. C. Valldecabres, *J. Am. Chem. Soc.*, 2004, **126**, 4064

[129] J. E. T. Corrie, *J. Chem. Soc. Perkin Trans. 1*, 1994, 2975

[130] D. J. Pouchnik, L. E. Laverman, F. Janiak-Spens, D. M. Jameson, G. D. Reinhart and C. R. Cremo, *Anal. Biochem.*, 1996, **235**, 26

[131] M. Brune, J. L. Hunter, J. E. T. Corrie and M. R. Webb, *Biochemistry*, 1994, **33**, 8262

[132] M. A. Hortalá, L. Fabbrizzi, N. Marcotte, F. Stomeo and A. Taglietti, *J. Am. Chem. Soc.*, 2003, **125**, 20

[133] Y. Fu, H. Li, W. Hu and D. Zhu, *Chem. Commun.*, 2005, 3189

[134] C.-F. Chow, B. K. Chiu, M. H. W. Lam and W.-Y. Wong, *J. Am. Chem. Soc.*, 2003, **125**, 7802

[135] F. N. Castellano, J. D. Dattelbaum and J. R. Lakowicz, *Anal. Biochem.*, 1998, **255**, 165

[136] J. D. Dattelbaum, O. O. Abugo and J. R. Lakowicz, *Bioconjugate Chem.*, 2000, **11**, 533

[137] K. K.-W. Lo, W.-K. Hui, D. C.-M. Ng and K.-K. Cheung, *Inorg. Chem.*, 2002, **41**, 40

[138] M. Wrighton and D. L. Morse, *J. Am. Chem. Soc.*, 1974, **96**, 998

[139] G. A. Crosby and W. H. Elfring, Jr., *J. Phys. Chem.*, 1976, **80**, 2206

[140] W. H. Elfring, Jr. and G. A. Crosby, *J. Am. Chem. Soc.*, 1981, **103**, 2683

[141] J. N. Demas and G. A. Crosby, *J. Am. Chem. Soc.*, 1971, **93**, 2841

[142] Z. Murtaza, P. Herman and J. R. Lakowicz, *Biophys. Chem.*, 1999, **80** 143

[143] C. Garino, S. Ghiani, R. Gobetto, C. Nervi, L. Salassa, V. Ancarani, P. Neyroz, L. Franklin, J. B. A. Ross and E. Seibert, *Inorg. Chem.*, 2005, **44**, 3875

[144] K. R. Wunschel, Jr. and W. E. Ohnesorge, *J. Am. Chem. Soc.*, 1967, **89**, 2777

[145] C. M. Flynn, Jr. and J. N. Demas, *J. Am .Chem. Soc.*, 1974, **96**, 1959

[146] F. O. Garces, K. A. King and R. J. Watts, *Inorg. Chem.*, 1988, **27**, 3464

[147] N. P. Ayala, C. M. Flynn, Jr., L. Sacksteder, J. N. Demas and B. A. DeGraff, *J. Am .Chem. Soc.*, 1990, **112**, 3837

[148] K. K.-W. Lo, D. C.-M. Ng and C.-K. Chung, *Organometallics*, 2001, **20**, 4999

[149] K. K.-W. Lo, C.-K. Chung, D. C.-M. Ng and N. Zhu, *New J. Chem.*, 2002, **26**, 81

[150] K. K.-W. Lo, C.-K. Chung, T. K.-M. Lee, L.-H. Lui, K. H.-K. Tsang and N. Zhu, *Inorg. Chem.*, 2003, **42**, 6886

[151] H. Chen, Q. Zhao, Y. Wu, F. Li, H. Yang, T. Yi and C. Huang, *Inorg. Chem.*, 2007, **46**, 11075

[152] L. Xiong, Q. Zhao, H. Chen, Y. Wu, Z. Dong, Z. Zhou and F. Li, *Inorg. Chem.*, 2010, **49**, 6402

[153] L. Prodi, F. Bolletta, M. Montalti and N. Zaccheroni, *Coord. Chem. Rev.*, 2000, **205**, 59

[154] D. Parker, *Coord. Chem. Rev.*, 2000, **205**, 109

[155] M .H. Keefe, K. D. Benkstein and J. T. Hupp, *Coord. Chem. Rev.*, 2000, **205**, 201

[156] J. Matsui, Y. Tachibana and T. Takeuchi, *Anal. Commun.*, 1998, **35**, 225

[157] S. Röösli, E. Pretsch, W. E. Morf, E. Tsuchida and H. Nishade, *Anal. Chim. Acta*, 1997, **338**, 119

[158] S. Lee and I. Okura, *Anal. Chim. Acta*, 1998, **342**, 181

[159] J. Bedlek-Anslow, J. Hubner, B. Carroll and K. Schanze, *Langmuir*, 2000, **16**, 9137

[160] A. Robertson and S. Shinkai, *Coord. Chem. Rev.*, 2000, **205**, 157

[161] S. Mizukami, T. Nagano, Y. Urano, A. Odani and K. Kikuchi, *J. Am. Chem. Soc.*, 2002, **124**, 3920

[162] J. I. Dulebohn, S. C. Haefner, K. A. Bergelund and K. R. Dunbar, *Chem. Mater.*, 1992, **4**, 506

[163] C. W. Rogers and M. O. Wolf, *Chem. Commun.*, 1999, 2297

[164] J. Terheijden, G. van Koten, W. P. Mul and D. J. Stufkens, *Organometallics*, 1986, **5**, 519

[165] M. Albrecht, M. Schlupp, J. Bargon and G. van Koten, *Chem. Commun.*, 2001, 1874

[166] H. Nikol, H.-B. Bürgi, K. I. Hardcastle and H. B. Gray, *Inorg. Chem.*, 1995, **34**, 6319

[167] T. W. Green, R. Lieberman, N. Mitchell, J. A. Krause Bauer and W. B. Connick, *Inorg. Chem.*, 2005, **44**, 1955

[168] http://en.wikipedia.org/wiki/File:FluorescenceFilters_2008-09-28.svg

[169] R. P. Haugland, H*andbook of Fluorescent Probes and Research Chemicals*, Molecular Probes Inc., Eugene, OR, 9th ed., 1996

[170] R. Y. Tsien, *Angew. Chem. Int. Ed.*, 2009, **48**, 5612

[171] X. Michalet, F. F. Pinaud, L. A. Bentolila, J. M. Tsay, S. Doose, J. J. Li, G. Sundaresan, A. M. Wu, S. S. Gambhir and S. Weiss, *Science,* 2005, **307**, 538

[172] S. Faulkner, S. J. A. Pope, B. P. Burton-Pye, *Appl. Spectrosc. Rev.*, 2005, **40**, 1

[173] C. P. Montgomery, B. S. Murray, E. J. New, R. Pal and D. Parker, *Acc. Chem. Res.*, 2009, **42**, 925

[174] E. G. Moore, A. P. S. Samuel and K. N. Raymond, *Acc. Chem. Res.*, 2009, **42**, 542

[175] K. K.-W. Lo, M.-W. Louie, K.-S. Sze, J. S.-Y. Lau, *Inorg. Chem.*, 2008, **47**, 602

[176] K. Y. Zhang, K. K.-W. Lo, *Inorg. Chem.*, 2009, **48**, 6011

[177] K. K.-W. Lo, T. K.-M. Lee, J. S.-Y. Lau, W.-L. Poon, S.-H. Cheng, *Inorg. Chem.*, 2008, **47**, 200

[178] M. Wilchek and E. A. Bayer, *Anal. Biochem*., 1988, **171**, 1

[179] N. M. Green, *Methods Enzymol.*, 1990, **184**, 51

[180] M. Wilchek and E. A. Bayer, *Methods Enzymol.*, 1990, **184**, 123

[181] C. A. Puckett and J. K. Barton, *J. Am. Chem. Soc.*, 2007, **129**, 46

[182] Q. Zhao, M. X. Yu, L. X. Shi, S. J. Liu, C. Y. Li, M. Shi, Z. G. Zhou, C. H. Huang and F. Y. Li, *Organometallics*, 2010, **29**, 1085

[183] S. K. Leung, K. Y. Kwok, K. Y. Zhang and K. K.-W. Lo, *Inorg. Chem.*, 2010, **49**, 4984

[184] A. J. Ameroso, M. P. Coogan, J. E. Dunne, V. Fernández-Moreira, J. B. Hess, A. J. Hayes, D. Lloyd, C. Millet, S. J. A. Pope and C. Williams, *Chem. Commun.*, 2007, 3066

[185] P. Wu, E. L. M. Wong, D. L. Ma, G. S. M. Tong, K. M. Ng and C. M. Che, *Chem.–Eur. J*., 2009, **15**, 3652

[186] C. K. Koo, K. L. Wong, C. W. Y. Man, Y. W. Lam, L. K. Y. So, H. L. Tam, S. W. Tsao, K. W. Cheah, K. C. Lau, Y. Y. Yang, J. C. Chen and M. H. W. Lam, *Inorg. Chem*., 2009, **48**, 872

[187] C. K. Koo, K. Y. Leo, K. L. Wong, Y. M. Ho, Y. W. Lam, M. H. W. Lam, K. W. Cheah, C. W. Cheng and W. M. Kwok, *Chem.–Eur. J.*, 2010, **16**, 3942

[188] K. Suhling, P. M. W. French and D. Phillips, *Photochem. Photobiol. Sci.*, 2005, **4**, 13

[189] A. H. A. Clayton, Q. S. Hanley, D. J. Arndt-Jovin, V. Subramaniam and T. M. Jovin, *Biophys. J.*, 2002, **83**, 1631

[190] Y. Chen and M. D. Barkley, *Biochemistry*, 1998, **37**, 9976

[191] B. Treanor, P. M. P. Lanigan, K. Suhling, T. Schreiber, I. Munro, M. A. A. Neil, D. Phillips, D. M. Davis and P. M. W. French, *J. Microsc.*, 2005, **217**, 36

[192] A. Beeby, S. W. Botchway, I. M. Clarkson, S. Faulkner, A. W. Parker, D. Parker and J. A. G. Williams, *J. Photochem. Photobiol. B*, 2000, **57**, 83

[193] J.-C. Shi, H.-Y. Chao, W.-F. Fu, S.-M. Peng and C.-M. Che, *J. Chem. Soc., Dalton Trans.*, 2000, 3128

[194] J. Brooks, Y. Babayan, S. Lamansky, P. I. Djurovich, I. Tsyba, R. Bau and M. E. Thompson, *Inorg. Chem.*, 2002, **41**, 3055

[195] H. T. Clarke, H. B. Gillespie and S. Z. Weisshaus, *J. Am .Chem. Soc.*, 1933, **55**, 4571

[196] R. A. Bunce, C. J. Peeples and P. B. Jones, *J. Org. Chem.*, 1992, **57**, 1727

[197] S. Develay and J. A. G. Williams, *Dalton Trans.*, 2008, 4562

[198] S. W. Thomas III, K. Venkatesan, P. Müller and T. M. Swager, *J. Am. Chem. Soc.*, 2006, **128**, 16641

[199] B. Soro, S. Stoccoro, G. Mighetti, A. Zucca, M. A. Cinellu, S. Gladiali, M. Manassero and M. Sansoni, *Organometallics*, 2005, **24**, 53

[200] G. Lowe, S. A. Ross, M. Probert and A. Cowley, *Chem. Commun.*, 2001, 1288

[201] A. Vogler and H. Kunkely, *J. Am. Chem. Soc.*, 1981, **103**, 1559

[202] B.-C. Tzeng, W.-F. Fu, C.-M. Che, H.-Y. Chao, K.-K. Cheung and S.-M. Peng, *J. Chem. Soc., Dalton Trans.*, 1999, 1017

[203] J. A. Zuleta, M. S. Burberry and R. Eisenberg, *Coord. Chem. Rev.*, 1990, **97**, 47

[204] S. D. Cummings and R. Eisenberg, *J. Am. Chem. Soc.*, 1996, **118**, 1949

[205] S. D. Cummings and R. Eisenberg, *Inorg. Chem.*, 1995, **34**, 2007

[206] E. M. Kober, J. V. Caspar, R. S. Lumpkin and T. J. Meyer, *J. Phys. Chem.*, 1986, **90**, 3722

[207] E. Whittle, J. A. Weinstein, M. W. George and K. S. Schanze, *Inorg. Chem.*, 2001, **40**, 4053

[208] G. Freeman, *personal communication*

[209] C. S. Chin, M.-S. Eum, S. yi Kim, C. Kim and S. K. Kang, *Eur. J. Inorg. Chem*., 2007, 372

[210] M. Kotera and T. Suzuki, *Inorg. Chim. Acta.*, 2010, **363**, 3602

[211] L. Carlton, Z. N. Tetana and M. A. Fernandes, *Polyhedron*, 2008, **27**, 1959

[212] K.-W. Chan, Y.-K. Sau, Q.-F. Zhang, W.-Y. Wong, I. D. Williams and W.-H. Leung, *Eur. J. Inorg. Chem.*, 2008, 4353

[213] *Knovel Critical Tables (2nd Ed.)*, Knovel, 2008

[214] T. Ishiyama, M. Murata, N. Miyaura, *J. Org. Chem*., 1995, **60**, 7508

[215] S. Bodige and F. M. MacDonnel, *Tet. Lett.*, 1997, **38**, 8159

[216] I. B. Berlman, *Handbook of Fluorescence Spectra of Aromatic Molecules,* Academic Press, 1971

[217] J. L. Sessler, T. D. Mody, D. A. Ford and V. Lynch, *Angew. Chem. Int. Ed.*, 1992, **31**, 452

[218] R. Miao, Q.-Y. Zheng, C.-F. Chen and Z.-T. Huang, *Tet. Lett.*, 2005, **46**, 2155

[219] G. Märkl, K. Gschwendner, I. Rötzer and P. Ktreitmeier, *Helv. Chim. Acta.*, 2004, **87**, 825

[220] A. S. B. Prasad, J. V. B. Kanth and M. Periasamy, *Tetrahedron*, 1992, **48**, 4623

[221] G. K. Walkup, S. C. Burdette, S. J. Lippard and R. Y. Tsien, *J. Am. Chem. Soc.*, 2000, **122**, 5644

[222] E. J. Jun, J. A. Kim, M. K. Swamy, S. Park and J. Yoon, *Tet. Lett.*, 2006, **47**, 1051

[223] C. A. G. N. Montalbetti and V. Falque, *Tetrahedron*, 2005, **61**, 10827

[224] W. J. Thompson and J. Gaudino, *J. Org. Chem.*, 1984, **49**, 5237

[225] Y. Fukuyama,Y. Kiriyama and M. Kodama, *Tetrahedron Lett*., 1993, **34**, 7637

[226] T. Watanabe, N. Miyaura and A. Suzuki, *Synlett*, 1992, 207

[227] H. Chaumeil, S. Signorella and C. Le Drian, *Tetrahedron*, 2000, **56**, 9655

[228] C. J. O'Brien, E. A. B. Kantchev, C. Valente, N. Hadei, G. A. Chass, A. Lough, A. C. Hopkinson and M. G. Organ, *Chem.-Eur. J.*, 2006, **12**, 4743

[229] M. G. Organ, S. Avola, I. Dubovyk, N. Hadei, E. A. B. Kantchev, C. J. O'Brien, and C. Valente, *Chem.-Eur. J.*, 2006, **12**, 4749

[230] B. S. Hartley and V. Massey, *Biochem. Biophys. Acta*, 1956, **21**, 58

[231] J. M. Walker, *Methods Mol. Biol.*, 1995, **32**, 321

[232] S. Smanmoo, W, Nasomphan, P, Tangboriboonrat, *Inorg. Chem. Commun.*, 2011, **14**, 351

[233] J. B. Waern, C. Desmarets, L.-M. Chamoreau, H. Amouri, A. Barbieri, C. Sabatini, B. Ventura and F. Barigelletti, *Inorg. Chem.*, 2008, **47**, 3340

[234] S. Guttmann, *Helv. Chim. Acta*, 1966, **49**, 83

[235] W. W. Cleland, *Biochemistry,* 1964, **3**, 480

[236] J. A. Burns, J. C. Butler, J.Moran and G. M. Whitesides, *J. Org. Chem.*, 1991, **56**, 2648

[237] J. Bramhall, *Biochemistry*, 1986, **25**, 3479

[238] L. F. Gradchenko, A. F. Lobazov, V. A. Mostovnikov and S. V. Nechaev, *J. Appl. Spectrosc.*, 1987, **47**, 905

[239] R. F. Chen and J. C. Kernohan, *J. Biol. Chem.*, 1967, **242**, 5813

[240] H. Brown, F. Sanger and R. Kitai, *Biochem. J.*, 1955, **60**, 556

[241] A. P. Ryle, F. Sanger, L. F. Smith and R. Kitai, *Biochem. J.*, 1955, **60**, 541

[242] Z. T. Farahkbakhsh, Q.-L. Huang, L.-L. Ding, C. Altenbach, H.-J. Steinhoff, J. Horwitz and W. L. Hubbell, *Biochemistry*, 1995, **34**, 509

[243] J. Bhattacharyya and K. P. Das, *Biochem. Pharm.*, 2001, **62**, 1293

[244] T. Mosmann, *J. Immunol. Methods*, 1983, **65**, 55

[245] S. Fuchs, T. Kapp, H. Otto, T. Schöneberg, P. Franke, R. Gust and A. D. Schlüter, *Chem.-Eur. J.*, 2004, **10**, 1167

[246] M. Yu, Q. Zhao, L. Shi, F. Li, Z. Zhou, H. Yang, T. Yi and C. Huang, *Chem. Commun.*, 2008, 2115

[247] K. K.-W. Lo, P.-K. Lee, J. S.-Y. Lau, *Organometallics*, 2008, **27**, 2998

[248] J. S.-Y. Lau, P.-K. Lee, K. H.-K. Tsang, C. H.-C. Ng, Y.-W. Lam, S.-H. Cheng, K. K.-W. Lo, *Inorg. Chem.*, 2009, **48**, 708

[249] Z. Diwu, Y. Lu, C. Zhang, D. H. Klaubert and R. P. Haugland, *Photochem. Photobiol.*, 1997, **66**, 424

[250] C. Mueller, M. A. H. Capelle, T. Arvinte, E. Seyrek and G. Borchard, *J. Pharm. Sci.*, DOI 10.1002/jps.22401

[251] S. P. Y. Li, H. W. Liu, K. Y. Zhang and K. K.-W. Lo, *Chem.-Eur. J.*, 2010, **16**, 8329

[252] J. Beld, K. J. Woycechowsky and D. Hilvert, *ACS Chem. Biol.*, 2010, **5**, 177

[253] J. Beld, K. J. Woycechowsky and D. Hilvert, *J. Biotechnol.*, 2010, **150**, 481

[254] J. R. Lackowicz, '*Principles of Fluorescence Spectroiscopy'*, Plenum Press, 1999

[255] K. Nakamaru, *Bull. Chem. Soc. Jpn.*, 1982, **55**, 2697

[256] M. P. Cooke, Jr. and R. K. Widener, *J. Org. Chem.*, 1987, **52**, 1381